Fabrication and Characterisation of DNA-templated Copper Nanowires

By

Jonathan Pate

A thesis submitted in partial fulfilment of the requirements of the degree of Doctor of Philosophy

School of Chemistry

Newcastle University

Newcastle upon-Tyne, UK

July 2013

Abstract

This thesis describes four approaches developed towards the fabrication of conductive 1-dimensional copper nanostructures, or nanowires, using a DNA-templating strategy. Cu-DNA nanowires are of interest for miniaturised interconnects in microprocessors. The chemical identity of the nanowires was characterised using X-ray Photoelectron Spectroscopy (XPS) and powder X-ray Diffraction (XRD) methods. Structural investigations were performed using Fourier-Transform Infra-Red (FTIR) Spectroscopy and Atomic Force Microscopy (AFM) to study the Cu^{n+}-DNA interaction mode(s) and nanowire size/morphologies, respectively. The electrical properties of nanowires were elucidated using Electrostatic Force Microscopy (EFM), Conductive-AFM (C-AFM) and a two-probe semiconductor device analyser for recording current-voltage (i-V) relationships.

One method describes a non-aqueous route to the formation of 1-D Cu nanostructures. This was achieved by doping of surface-immobilised DNA (the template) with Cu^{+} ions from $Cu(CH_3CN)_4.PF_6$ followed by chemical reduction to the zero-valent metal using phenylsilane and organic solvent, under inert conditions. Metallic copper was confirmed to have formed on DNA and copper hydroxide ($Cu(OH)_2$) was also identified as a surface overlayer on this material. The final structures were ~6 nm in height and show complete coverage of the template. The material was polycrystalline due to observations of a densely packed series of Cu nanoparticles along the template axis. However, electrical studies indicated these structures to be highly resistive. Thermal annealing of the templated material resulted in a considerable structural transformation, from tightly packed particles to the formation of a sporadic array of larger clusters well separated along the structure length.

Another approach involved an aqueous solution-based synthesis, whereby Cu^{2+} from $Cu(NO_3)_2$ and ascorbic acid were added to a solution of DNA. This resulted in nanowires, ~7 nm in height, which were mostly continuous in morphology and noticeably absent of inter-particle boundaries. The Cu^{2+}:DNA(phosphate) ratio (n) was found to be critical for the formation of smooth nanowires (n= 0.05) as opposed to aggregated assemblies of material (n> 0.1). Chemical characterisation of the reaction product confirmed the presence of metallic copper as well as a surface layer of $Cu(OH)_2$. Nanowires were confirmed to be conductive and i-V measurements gave a

conductivity value of 0.94 Scm^{-1}; the first recorded conductance for copper templated on DNA, over micron length scales.

Attempts were made to passivate the nanowires formed in solution by attachment of thiol molecules (p-mercaptobenzoic acid) onto the copper surface. This modification resulted in the formation of a Cu(I)-thiolate layer on Cu^0 and significantly protected the nanowires from oxidation, resulting in the formation of almost pure metallic Cu nanowires. The electrical conductivity (1.01 Scm^{-1}) was similar to that obtained for the unprotected wires (0.94 Scm^{-1}). This suggested that, although the degree of oxidation was minimised significantly, other factors must be more accountable for causing resistance in these wires such as surface and/or grain boundary scattering.

Finally, a physical-based approach towards metallisation of DNA was performed using a vacuum deposition method. This was achieved by suspending single molecules of DNA between two electrodes, across a trench etched into the substrate. This was followed by metallisation of the sample by evaporation of copper in a sealed vacuum chamber. Electron Microscopy data showed that nanowires lay taut across the trench and were highly continuous in coverage. This process resulted in a working two-terminal nanowire device which was conductive due to nanowire(s) bridging between insulating gaps.

Dedication

To my family

“Science may set limits to knowledge, but should not set limits to imagination.”

-Bertrand Russell-

“There are some ideas so wrong that only a very intelligent person could believe in them.”

-George Orwell-

Acknowledgements

I would like to express great appreciation to my supervisor Professor Andrew Houlton for his valuable advice, knowledge and constructive suggestions throughout this research work. I am particularly grateful for the assistance provided by Dr Scott Watson for his invaluable day to day assistance in all manners of my work. Gratitude is also directed to Scott for his talent and kindness in the production of several illustrations for this thesis. I would also like to thank my secondary supervisors, Dr Benjamin Horrocks and Professor Nick Wright, for their guidance and expertise provided to me during my PhD.

I would also like to thank Intel for partially funding the project, and particular mention to Bernie Capraro for sharing his useful insights and ideas during my research. Special thanks are also extended to people within my own research group for their advice, humour and morale support throughout the project. I wish to acknowledge the contributions provided by the XPS service at Newcastle University for their help in the analysis of data. Technical assistance offered by members of the department, both past and present, is also deeply appreciated. Special mention also goes to Dr Félix Zamora for his much appreciated support during our collaboration and the productive work carried out at the Universidad Autónoma de Madrid.

Finally I would like to offer my appreciation to my friends and family, particularly my parents, for their indispensable morale support and for giving me the confidence and determination to progress in my academic work.

Abbreviations

σ	Conductivity
λ	Mean free path
λ-DNA	Lambda DNA
µL	Microlitre
µm	Micrometre
µM	Micromolar
Ω	Ohm
%T	Percentage transmittance
Δθ	Phase shift
ρ	Resistivity
λ	Wavelength
ϕ	Work function
0-D	Zero-dimensional
1-D	One-dimensional
2-D	Two-dimensional
3-D	Three-dimensional
A	Adenine
Å	Angstrom
AAO	Anodic aluminium oxide
AFM	Atomic Force Microscopy
C	Cytosine
c-AFM	Conductive-AFM
CNT	Carbon nanotube
CTAB	Cetyl trimethylammonium bromide
CT-DNA	Calf-thymus DNA
CuNW	Copper nanowire
CVD	Chemical Vapour Deposition

d	Diameter
dc	Direct current
DCM	Dichloromethane
DMSO	Dimethylsulfoxide
DNA	Deoxyribonucleic acid
E_b	Binding Energy
ECD	Electrochemical deposition
EDA	Ethylenediamine
EDTA	Ethylenediaminetetraacetic acid
EDX	Energy Dispersive X-ray
EFM	Electrostatic Force Microscopy
E_g	Band-gap energy
EG	Ethylene glycol
E_k	Kinetic energy
ESCA	Electron Spectroscopy for Chemical Analysis
EUV	Extreme Ultra-violet
eV	Electron Volt
f_0	Resonance frequency
fcc	Face-centred cubic
FTIR	Fourier-Transform Infra-Red
FWHM	Full-width half-maximum
G	Guanine
HDA	Hexadecylamine
HOMO	Highest Occupied Molecular Orbital
IC	Integrated Circuit
ITRS	International Technology Roadmap for Semiconductors
i-V	Current-Voltage
K	Kelvin

k	Cantilever spring constant
L	Length
LUMO	Lowest Unoccupied Molecular Orbital
mg	Milligram
mL	Millilitre
mM	Millimolar
nm	Nanometre
Q-dot	Quantum dot
R	Resistance
RC	Resistance-Capacitance
RNA	Ribonucleic acid
S	Siemens
SAM	Self-assembled monolayer
SCM	Scanned Conductance Microscopy
SE	Secondary electron
SEM	Scanning Electron Microscopy
SPM	Scanning Probe Microscopy
SQUID	Superconducting quantum interference device
STM	Scanning Tunnelling Microscopy
SWNT	Single-walled (carbon) nanotube
T	Thymine
TEM	Transmission Electron Microscopy
T_m	Melting temperature
TMS	Trimethylsilane
TMV	Tobacco Mosaic Virus
UHV	Ultra-high vacuum
XPS	X-ray Photoelectron Spectroscopy
XRD	X-ray Diffraction

Table of contents

List of Figures and Tables

Chapter 1: Introduction

1.1. Nanochemistry & Nanotechnology

Nanochemistry is related to the reaction and assembly of molecules, atoms or clusters of atoms as a synthetically driven approach towards the synthesis of nanoscale materials. Thus, the field of nanochemistry is interwoven with the concept of bottom-up self-assembly, whereby the organisation of matter on a molecular level can lead to the production of matter on a larger-scale in one, two or three dimensions.[1] The field of nanochemistry is more widely concerned with the study and control of the chemical and physical properties of nanoscale materials.

Nanoscale materials are defined on the basis that their size is 1-100 nm (1 nm= $1x10^{-9}$ m) in in at least one spatial direction.[2, 3] This size range includes atoms and molecules which places chemistry as a central theme of nanostructure formation. Nanoscale materials can be further defined based on the number of dimensions which exist within this size regime. Figure 1.1 attempts to classify the three types of nanoscale structures. Materials constrained to the nanoscale in one, two or three spatial directions are known as nanofilms, nanowires and nanodots (also known as quantum dots or Q-dots), respectively. Alternatively, these materials are named based on the number of bulk dimensions within the structure. Nanofilms are therefore considered as 2-dimensional materials as they possess two bulk dimensions and one nanoscale dimension. Nanowires are considered 1-dimensional structures (one bulk dimension, two nanoscale dimensions) and nanodots are 0-dimensional (zero bulk dimensions, three nanoscale dimensions). This thesis is concerned with the bottom-up synthesis of 1-dimensional conducting nanomaterials, or nanowires.

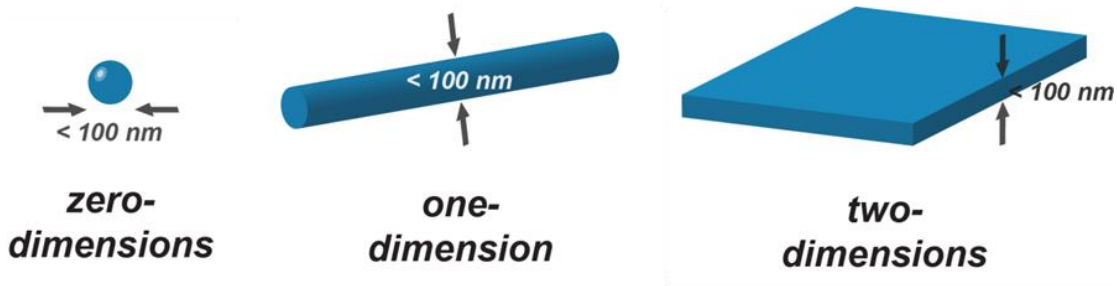

Figure 1.1: Scheme showing the classification of the three types of nanostructured materials

The distinct field of nanochemistry emerged in the early 1990s following G.M. Whiteside's early work on molecular self-assembly as a chemical strategy for synthesis of nanostructures.[4] Self-assembly is a process whereby molecules or atoms (as building blocks), spontaneously assemble, organise and grow in a controlled manner to form well-ordered aggregates. Based on this principle, the general approach in nanochemistry is to utilise established synthetic procedures and methods, primarily reserved for molecular synthesis, for building nanostructured materials. For this purpose the chemical synthetic approach to nanostructure formation has been compared with the "self-organisation of matter." Geoffrey Ozin's leading article "Nanochemistry: Synthesis in diminishing dimensions,"[5] also describes the approach of self-assembly of molecular species for highly controlled growth of nanostructures of a defined shape, size and composition, based upon known chemical principles. Nanochemistry is a challenging area which lies at the interface between molecular synthesis and the growth of large-scale structures in the bulk phase. There is often a thermodynamic driving force for the assembly of nanoscale materials in order to compensate for the decrease in entropy of forming ordered systems.[1] Therefore, formation of nanostructured materials requires high precision of assembly (of the building blocks) and careful consideration of the growth conditions.[6]

As a more general appreciation of this approach, Richard Feynman is widely credited as *the* most inspirational figure within the field. The conceptual basis of bottom-up strategy for the generation of structural complexity was first alluded to by Feynman in 1959 during his popularised lecture, "There's Plenty of Room at the Bottom."[7] Feynman envisaged an atom by atom approach for the creation of sophisticated and complex structural designs on a very small level. This was considered a radical idea at the time. Advancements in chemical engineering, synthesis and understanding of fundamental physical principles have allowed this concept to flourish and have since shaped the field of nanochemistry and nanotechnology as it stands today. The term nanotechnology refers to the application of nanomaterials at these dimensions. The invention of the Scanning Tunnelling Microscope (STM) in 1981 by Binning and Rohrer made it possible to visualise individual atoms at a surface. It was since used by Don Eligler and Erhard Schweizer to strategically position atoms on a nickel surface to spell out the letters "IBM" (see figure 1.2).[8]

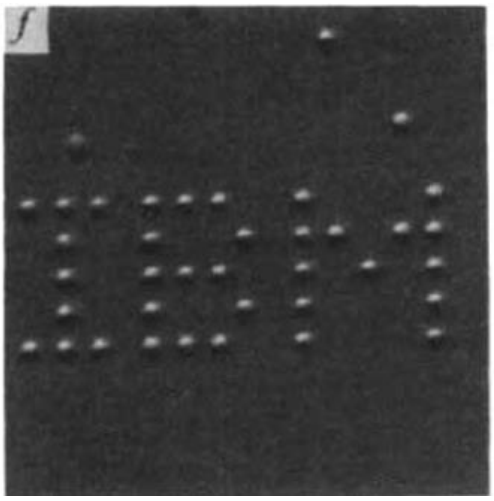

Figure 1.2: Scanning Tunnelling Microscopy (STM) images of 35 Xe atoms arranged on a Ni(110) surface using the STM tip, to spell the letters "IBM." Adapted from reference [8]

Strategic manipulation of chemical properties such as molecular function/recognition, bonding characteristics and crystallinity can lead to the development of nanoscale assemblies with well-defined physical features and properties.[1] Exploitation of these molecular properties has led to nanostructures of a pre-defined complexity via the self-assembly of simple building blocks.[9] Figure 1.3 shows an example of how spontaneous formation of simple building blocks can lead to ordered structures. Polymer coated gold nanoparticles were aligned on the surface via self-assembly leading to the stripy pattern shown in the image.[10] The ability to control the size and composition of such materials and management over their properties for the desired application is becoming an increasingly sophisticated and reproducible feat.

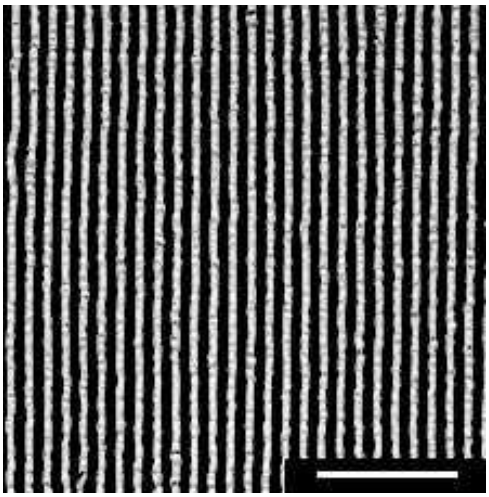

Figure 1.3: SEM image of a striped gold nanoparticle array (ref. [10]). Scale bar= 100 μM

The properties of materials on the nanoscale often behave remarkably differently to their bulk-like counterparts. This change occurs during the transition from solid-state structure to isolated molecular structure.[11] If a bulk material is reduced in size to the nanometre regime it commonly exhibits 'unexpected' properties for a range of 0-D,[11-13] 1-D[6, 14, 15] and 2-D[16] nanomaterials. For example, a bulk material has similar properties irrespective of how 'bulky' it is. However, within the nano size regime (1-100 nm) there exists a size-dependent 'window' for tuning of the material properties. Hence it is possible to alter the chemical,[11] electrical,[14, 17] optical,[12, 17] and magnetic properties[18] of a material, simply by varying its size on the nanoscale. One can therefore tailor the size of the structure for use in a particular application and this has led to the emergence of materials based on quantum wells,[19, 20] nanowires[21] and quantum dots,[13] with a wide range of potential applications from quantum lasers[20, 22] to molecular switches.[23, 24] The potential to produce materials which display these unusual and unique properties is what drives the field of nanochemistry.

There are two size-dependent factors which are responsible for the properties of nanoscale materials; (i) the surface/volume ratio,[11, 18] which is related to the fraction of atoms residing at the surface and (ii) quantisation of the electronic band structure.[12, 17, 18] Both the surface/volume ratio and the quantisation of the electronic structure increase as size is reduced.

The surface effects relate to the fact that atoms residing at the surface of a material are chemically inequivalent to atoms residing in the bulk of the material. As the size is reduced further the surface/volume ratio increases also. Hence the physio-chemical properties of the nanostructure change with size. By way of an explanation, surface atoms have a lower coordination number than bulk atoms and are less tightly bound to the lattice. Therefore atoms at the surface are more energetic than atoms in the bulk. The surface effect therefore governs the physio-chemical properties of the material and the way it functions on the nanoscale.

As an example, the size-dependence of melting temperature (T_m) for Au particles has been reported.[25] Particle sizes above 40 nm exhibit melting temperatures around 1337 K, typical of bulk gold. As Au particle size is scaled down, a melting point depression is observed; with the bulk T_m depressed by ~50% to 700K for 20 nm particles. Figure 1.4 shows a graph of melting temperature against particle size and it highlights the abrupt drop in T_m (depression) at small sizes (<40 nm). This effect is explained as follows; the

surface tension caused by the presence of high energy surface atoms becomes increasingly high as surface/volume ratio increases and can be minimised by converting the solid into the liquid phase. The lowering of T_m therefore becomes more energetically favourable as particle size decreases.

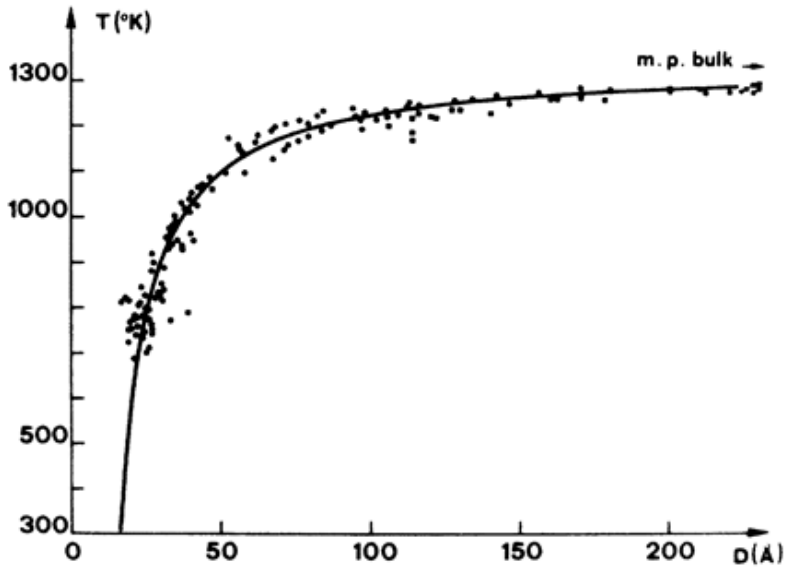

Figure 1.4: Graph of melting temperature (T_m) of Au particles as a function of size. Figure from ref. [25]

The second type of size-dependent effect is the quantisation of the electronic band structure, otherwise known as quantum confinement. In order to describe this, it is necessary to classify the electronic structures of bulk metals, semiconductors and insulators. Figure 1.5 is a schematic illustration of this. In a bulk metal there is a continuous range of energy levels available for an electron to access. In such materials there is no band gap for the electron to overcome. The electron may move freely through the lattice and act as an electrical conductor. The band gap can be defined as the energy difference between the filled valence band and the empty conduction band (E_g), between which there are no electronic states for an electron to occupy. The valence band is the highest occupied electronic state of a structure; much like the HOMO (Highest Occupied Molecular Orbital) of a molecule. The conduction band is the next available state that an electron can occupy if the valence band is filled; akin to the LUMO (Lowest Unoccupied Molecular Orbital) of a molecule. If E_g is too high for the electron to overcome then the material is an insulator as electrons do not populate the conduction band. If E_g is small enough in energy then electrons may enter the conduction band and conduct electricity. Hence, the size of E_g distinguishes between

conducting and insulating materials. Semiconductors have an E_g between that of a conductor and an insulator. The distinction is somewhat arbitrary and a value of 3.1 eV is chosen here.

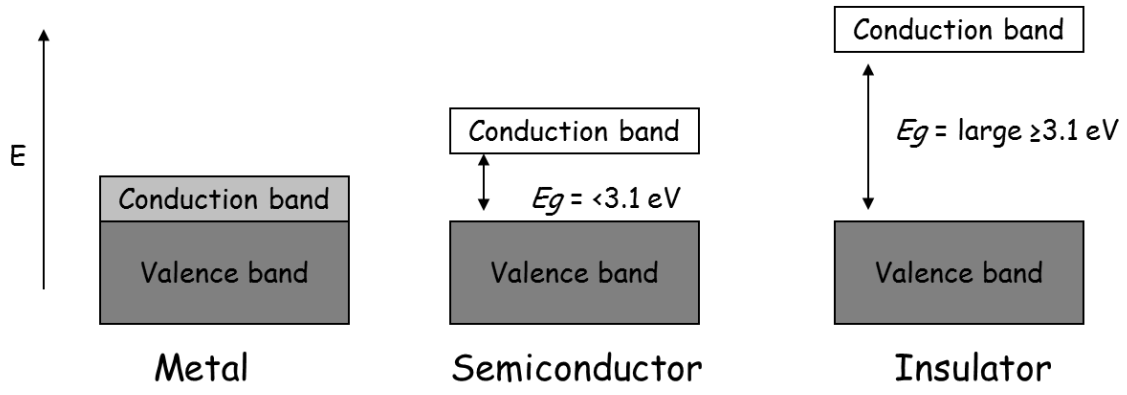

Figure 1.5: Schematic showing the electronic structure of solids. The valence band is populated and the conduction band may be partially filled for metals and semiconductors. For insulators the conduction band remains empty due to the large band gap (E_g)

The size of the band gap, E_g, in a semiconductor restricts the intrinsic population of electrons in the conduction band. Such transitions may be aided by light to provide the energy needed for electrons to excite into the conduction band.[26] Electrical conduction generated in this way is called photoconductivity. For metals, the absence of a band gap means there is little change in the electronic structure down to very small sizes. Therefore the quantum confinement phenomenon is mainly discussed in relation to semiconductors, as semiconductors have a band gap which can be easily manipulated by varying the size of the structure.

As a microcrystalline material is scaled down in size to the molecular level there is a corresponding change in the spacing of electronic energy levels within the structure (see figure 1.6). The electronic structure of the material is determined by the number, type, strength and symmetry of bonding orbitals formed between individual atoms. These factors govern the distribution (density) of electronic states and the size/location of band gaps. For a molecule, there are a set number of energy levels which are quantised in energy. Here the HOMO-LUMO band gap is the most important factor in determining the electronic properties of the structure. Nanoscale structures have an electronic structure which corresponds to somewhere between the bulk and molecular band structures. On the nanoscale, the band structure is no longer continuous (as in the bulk) and discrete energy levels begin to emerge (as a molecule); the system is said to be

quantised and the electrons are confined to discrete energy levels with defined band gaps. Nanoscale materials may be quantised in one, two or three dimensions.

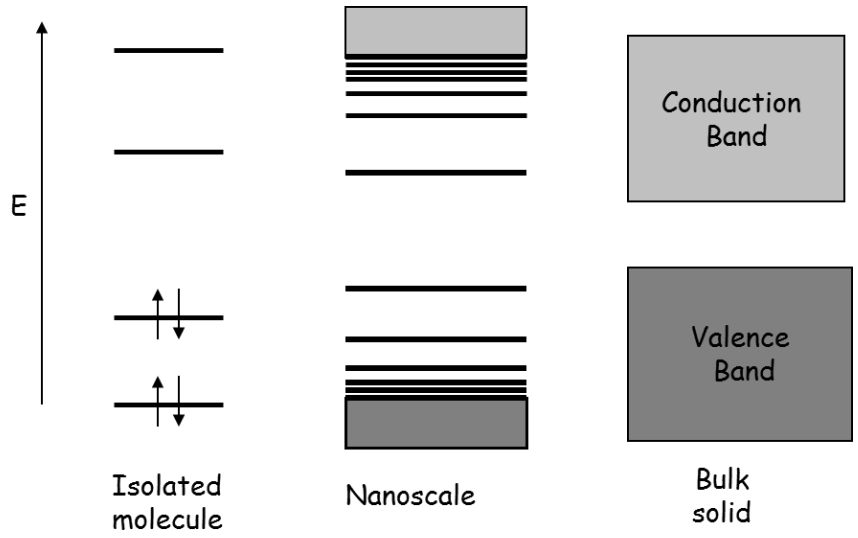

Figure 1.6: Schematic showing the change in band structure from bulk solids to the nanoscale, compared to the electronic structure of an isolated molecule. The band gap increases as size is scaled down. Formation of discrete energy levels indicates that the structure is quantised

The size of the band gap increases as size is scaled down (i.e. the structure becomes more 'molecular-like') and thus reduces the probability of exciting an electron from the valence band into the conduction band at a given temperature.

A demonstration of how size-dependent quantisation, which can also be applied in a functional way, is the case of Q-Dots. These are nanoscale particles which are quantised in three dimensions. CdSe-ZnS core-shell nanoparticles can emit light (luminesce) efficiently via photoexcitation of electrons at specific energies, depending on the size of the band gap, E_g.[17] Since E_g depends on the physical size of the material, there is the remarkable ability to tune the optical properties through physical/size-dependent or chemical manipulation. Figure 1.7 shows the change in colour of solutions containing CdSe-ZnS nanoparticles from blue to red as the size is increased.

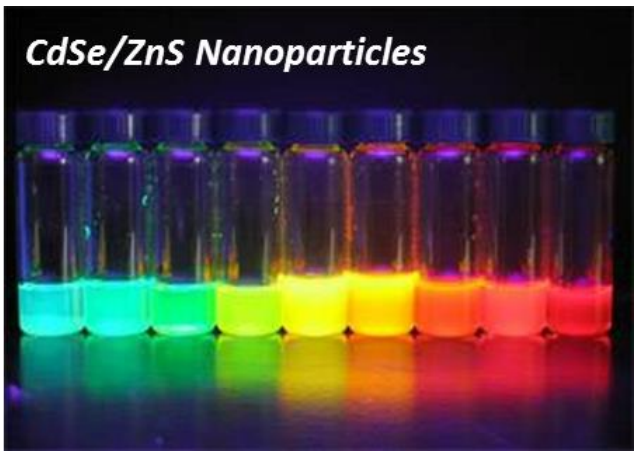

Figure 1.7: Solutions containing CdSe-ZnS core-shell nanoparticles. The particle size increases in each solution from left to right and so the wavelength of emitted light also increases. Figure adapted from reference [17]

For a nanowire, electron mobility is confined to the two nanoscale dimensions and the electron is free only to traverse along the wire in the one bulk direction. Size effects may therefore dramatically affect the electronic properties of nanowires.[14, 15] We have so far discussed how such size-dependent effects emerge and can be useful. However, for the purpose of preparing *conductive* metal nanowires, size scaling may become prohibitive beyond a certain limit, as the number of mobile carriers within the band structure is reduced, thus reducing conductivity. In some critical application areas, notably integrated electronics, there is a drive to miniaturisation on the nanoscale, whereby bulk-like properties are desirable. As this thesis is concerned with the formation of conductive copper nanowires, the alternative challenge is to actually retain the bulk-like properties of the metal on the nanoscale and overcome the problems that quantisation and surface effects may present as we access deeper into the nanoscale. The next part of the introduction aims to address the reason why size-scaling remains very important, for other reasons than those mentioned thus far.

To summarise, the ability to organise matter on this scale makes the potential for new functional materials immense. Nanochemistry has the potential to fulfil some of the most important technological challenges modern society is confronted with. In particular the demand for reduced component size in integrated devices, as set out by the International Technology Roadmap for Semiconductors (ITRS),[27] has been made achievable by Nanoscience. We need to continue working in this field in order to sustain society's increasing technological demands.

1.2. Drive to Miniaturised Electronics

Since the invention of the integrated circuit (IC) in 1959 the microprocessor industry has dramatically improved upon computing performance on a yearly basis, increasing both processing power and efficiency.[28] ICs are now used in the vast majority of electronic devices in operation today. These comprise an array of electronic circuits integrated onto a single semiconductor chip (usually Si) which, in turn, consist of several components; transistors, resistors, capacitors, diodes and inductors etc. Interconnections (or interconnects) are required to provide electrical connections between these components. An interconnection is a conductive metal wire used to link two otherwise isolated components on a chip. For example as a line in a series of transistors, or as a VIA (vertical interconnect access) that act to electrically connect multiple layers of components on a single chip. These conductive lines are essential to device operation in terms of distributing clock signals and maintaining signal levels during processing, as well as providing power to various circuits in the microprocessor.

In order to increase device performance, it is necessary to fit more components onto the circuit in a given area.[29] This will lead to an increased density of transistors. Current state of the art technology is able to manufacture billions of transistors on a single 300 mm semiconductor wafer. In order to increase the density of components on a circuit, a reduction in the size of the transistor (defined by the gate length, also known as feature size) is essential. This reduction in feature size must also be accompanied by a reduction of the interconnect line width. Ideally this should be achieved without incurring significant increase to the resistance-capacitance (RC, resistance x capacitance) time delay of signal propagation in a circuit. The signal time delay increases as the resistance of the metal interconnect increases, which is inevitable as the line width is reduced. However, as distances between transistors scale with decreasing feature sizes the increase in line resistance may not lead to an overall increase in signal delay.[28] Thus, miniaturisation of all device components is considered beneficial for enhanced circuit performance, providing the electrical conductance of metal interconnect is not compromised significantly as size is reduced.[14]

Efforts to maintain device scaling have been met by increased interest in nanotechnology. This has influenced a rapid surge in computing power over the past five decades. The trend of down scaling within integrated circuits was predicted by Gordon. E. Moore at Intel Corporation in 1965 and is often expressed as ‘Moore’s

Law.'[30] 'Moore's Law' predicts an approximate doubling of information density every 18 months,[29] which has been sustained up to the present time. The 'law' may also be expressed as the doubling of the number of transistors on a chip every two years. Figure 1.8 is a graph of 'Moore's Law' showing the trend for reduction in transistor size, since its invention, to its projected size reduction in the future. In order to aid the industry in continuing to meet this trend, the International Technology Roadmap for Semiconductors (ITRS)[27] was initiated in 1999. This organisation aims to give a 15 year estimate as to the industries current development and research needs. The current consensus suggests that device scaling at the current rate cannot be sustained beyond the next decade as the downsizing of silicon chips is limited by current conventional manufacturing methods.[31]

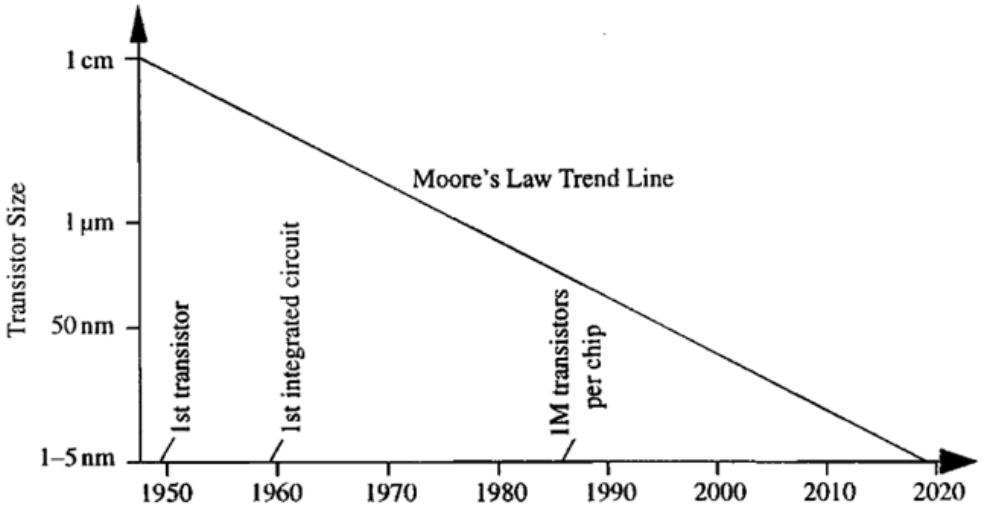

Figure 1.8: **'**Moore's Law' plot of transistor size reduction over time. From reference [3]

Copper is currently the material of choice as interconnect due to the materials low electrical resistivity ($\rho = 1.7 \times 10^{-8} - 1.9 \times 10^{-8}$ Ωm) and relatively high resistance to electromigration, compared to the previous material of choice, aluminium.[32, 33] Electromigration is a physical phenomenon experienced in interconnects, which can lead to circuit damage and failure. This occurs when the current density is high and transfers a large amount of momentum from electrons to copper ions. As a result mass diffusion of ions can occur within the conductor, causing build-up of copper to give unintended connections (hillock failure). Electromigration can also lead to the occurrence of voids in the conductor (open circuit). These effects become more

significant when the line width is reduced and therefore poses a major issue for continued miniaturisation of circuit components.

The resistance in a metal is attributable to the scattering of electrons off lattice vibrations within the structure. The application of a voltage causes electrons to accelerate, which then scatter off a lattice vibration causing a change in velocity. After a certain amount of time (the relaxation time) they reach a steady speed. For a true metal, the effect of raising the temperature leads to an increase in the resistance of the metal. This is due to there being more lattice vibrations available to scatter electrons off course. This lowers the steady speed of electrons and causes an increase in the resistance of the metal.

There are an additional two factors responsible for the increase in metal resistance which become highly significant as the size/width of the metal (*d*) is reduced on the nanoscale. These are (i) grain boundary scattering and (ii) surface scattering.[14, 34, 35] Grain boundary scattering is the scattering of electrons at the interface between two grains in a metal (i.e. when the metal is not a single crystal, as is usually the case for copper interconnect) and thus contributes to electrical resistance. This effect becomes highly pronounced at diameters (d) comparable to the mean-free path of the electron.[35, 36] For copper this is 30 nm (at 27°C).[37] Surface scattering depends on how many and how often electrons transfer near to the surface. This depends on the surface: volume ratio and becomes more significant as the metal becomes thin.[38] Figure 1.9 shows a schematic diagram to illustrate these effects. The scheme shows that for a thinner metal, surface scattering becomes more significant. Scattering of electrons at lattice vibrations still occurs in both cases.

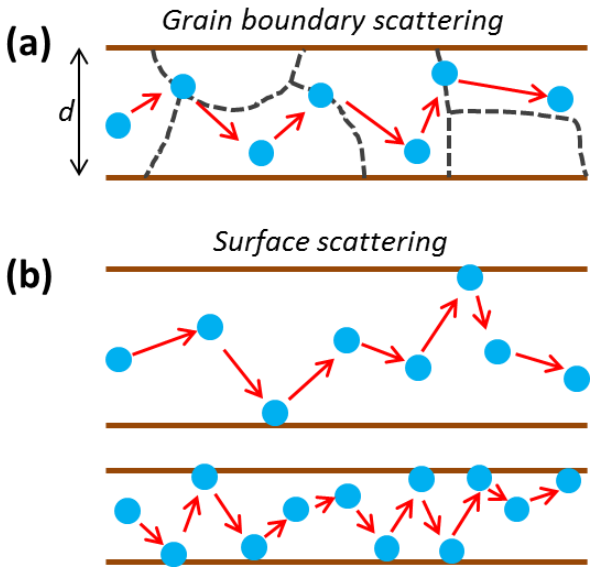

Figure 1.9: Schematic illustration of the effects of electron scattering at (a) grain boundaries and (b) surface boundaries. The latter effect becomes more pronounced as the metal diameter (*d*) is reduced

Figure 1.10 shows how copper interconnect resistivity changes as a function of linewidth (d). Resistivity abruptly increases at diameters smaller than ~100 nm. One of the challenges in nanotechnology for the fabrication of copper nanowires (for application as interconnects) is to retain conductivity values as close to that of bulk copper (5.96×10^7 Sm^{-1} at 20°C) on the nanoscale.

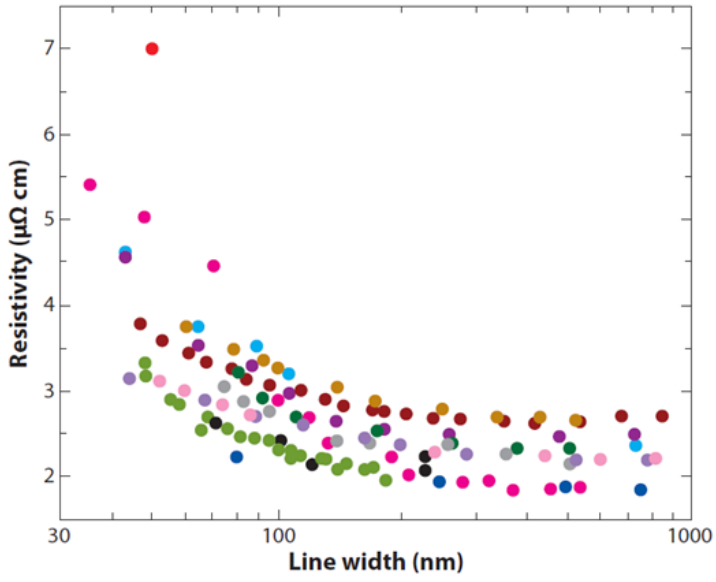

Figure 1.10: Resistivity of copper interconnects as a function of line width (diameter). The data was collated from various different sources as denoted by different coloured points in the figure. Figure adapted from reference [14]. Data originally extracted from reference [37]

Current methods for the fabrication of miniaturised electronics utilise 'top-down' processes, such as lithography. Lithography is a technique used to etch small features into a bulk substrate in order to create a patterned surface for subsequent processing towards a working device. Photolithography, which utilises light, and electron beam lithography, are two primary examples of the techniques implemented to create these patterned surfaces.

An important top-down procedure in the electronics industry is concerned with the fabrication of copper interconnect. Fabrication of these structures is currently achieved via a three step process, known as the "Dual Damascene" process,[39, 40] whereby (i) initial dry etching of the lithographically-patterned silicon oxide substrate to create narrow trenches, is followed by (ii) electroplating of copper to fill the trenches and finally (iii) chemical mechanical polishing (CMP) for planarization of the substrate surface and to remove excess material.[41, 42] Figure 1.11 shows a schematic illustration of the manufacturing process. Electroplating (also referred to as Electrochemical Deposition) is a process used to deposit metal layers onto a conductive surface, and therefore requires a metal seed layer on top of the wafer prior to deposition. In the damascene process this is made of copper which improves the adhesion and uniformity of the subsequent electroplated copper.[42] The process of electrochemistry involves the transfer between electrical energy and chemical energy. In the damascene process, metal deposition takes place in an electrolytic cell containing an anode (usually copper), a cathode (e.g. the metal surface) and a solution of electrolyte containing copper ions (e.g. copper sulphate).[43] When a current is passed through the cell, deposition of the metal takes place at the cathode (negative) by reduction of copper ions, whilst oxidation at the anode (which may also be comprised of copper) occurs to generate copper ions and maintain the flow of electrical current.

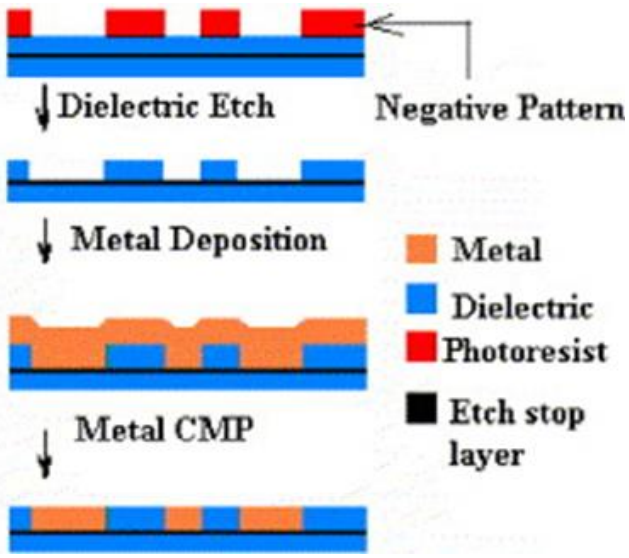

Figure 1.11: Schematic of the "Damascene" process used to fabricate metal interconnects embedded within the substrate. One or more masks are used to pattern the surface with photoresist before the channels are etched to create lines and/or vias. The pattern is then removed. Copper is deposited in the open trench by electroplating and is overfilled. Finally CMP is used to planarise the substrate surface. Image reprinted from reference [44].

However, such top-down routes will carry severe limitations in terms of reproducibility at the low end nanometre regime (sub 10 nm) and an overall lowering of the economic benefit that such methods generate. Importantly, photolithography, a technique which has been heavily employed in the past to create patterned substrates, has resolution limitations dictated by the wavelength of the light used. As of 2012 the lowest reproducibly achievable target was the 22 nm node (defined as half the distance between individual features), based on Intel's 3-D Tri-gate technology (see figure 1.12). This is expected to extend to 14 nm node technology by 2014, according to Moore's Law. It is worth noting that a reduction in the node size (nm) also requires a reduction in interconnect width (nm). These two sizes are generally very similar and are projected to remain so.[39]

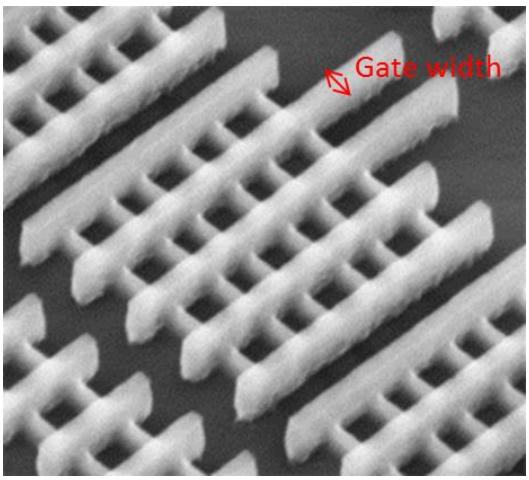

Figure 1.12: Intel's 22 nm Tri-gate transistor. Credit: Intel

In order to continue meeting these size demands by 'top-down' methods it will become necessary to utilise shorter wavelength radiation to etch the minimum feature size. Extreme Ultra-Violet Lithography (EUV) is now becoming the favoured manufacturing process by the industry,[45] as opposed to conventional photolithography (longer wavelength than EUV), which has served well up to current limits. Indeed, EUV also commands a fundamental limit to the lowest accessible feature size, as dictated by its wavelength (124 nm – 10 nm), and so will have major difficulty in accessing sub 10 nm structures on a reproducible level. Other associated issues include increased cost and material damage due to the high energy impact of EUV radiation. At present we are approaching the limits of miniaturisation using current 'top-down' methods and this may limit the progress in the development of integrated circuit (IC) design in the future.

As mentioned, the top-down fabrication of interconnects beyond the current limits is proving difficult. The main reasons for this are due to the optical limitations of creating the patterned substrates, the procedural difficulty of depositing metal into ever decreasing trench widths and the subsequent increasing fabrication costs of sub-20 nm structures. Therefore, as size scaling via top down procedures into the future generations of microprocessor (requiring sub-10 nm feature sizes) becomes prohibitively challenging, there is a drive for a fundamental change of thinking in the way devices are fabricated. The alternative is to utilise so-called 'bottom-up' methods, as opposed to 'top-down,' for device fabrication. These 'bottom up' approaches are currently being investigated at research level for the development of nanoelectronic technology.[46-48] These involve self-assembly methods, chemical reactions, and a general synthetic route

to the fabrication of molecular level electronic components such as nanowires. Figure 1.13 illustrates Intel's technology pipeline from 2009 to 2015+ and how future fabrication techniques rely heavily on research at the bottom-up level.

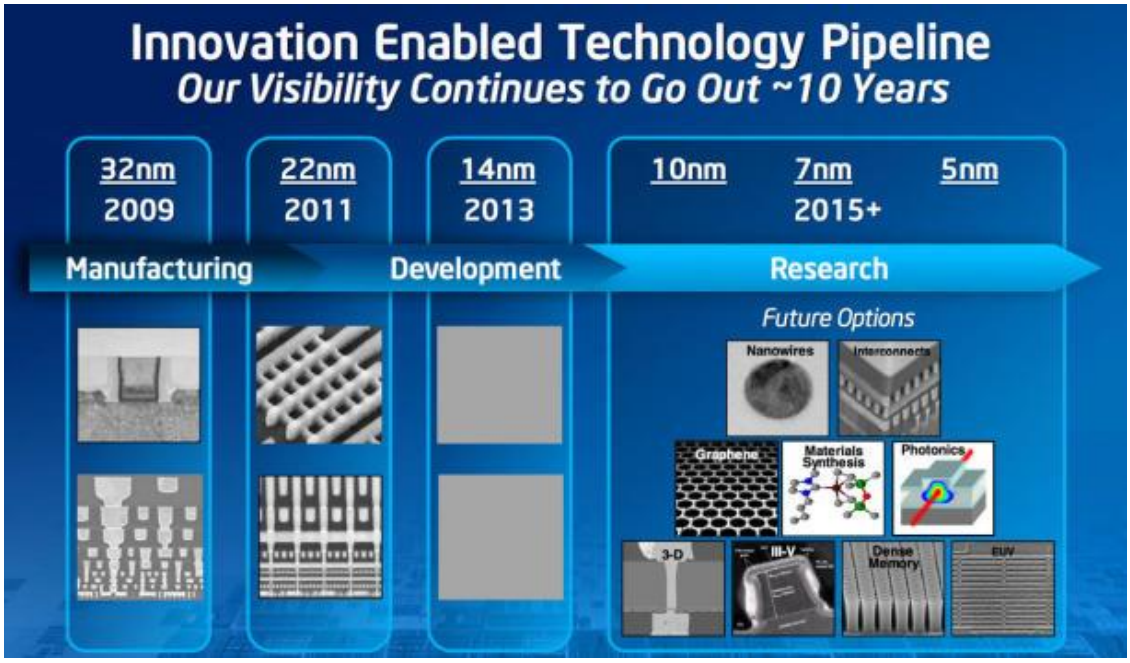

Figure 1.13: Image showing Intel's developmental pipeline for microprocessor technology. Research is being funded by the industry for the development of nanowires for use as electronic components. Credit: Intel

'Bottom-up' methods offer considerable potential for construction at the nanoscale. The benefits of adopting such an approach are numerous, including reduced cost, higher control over metal growth and potential access into sub-10 nm feature sizes. In particular, the integration of copper interconnect as a material using bottom up routes will ease the transition from top-down to bottom-up methods and this has attracted much interest from researchers. The work contained in this thesis is concerned with the development of bottom up methods for construction of copper nanowires (CuNWs), which could have potential use as interconnections.

1.3. Bottom-up Routes to Copper Nanowires

Bottom-up fabricated nanoscale structures are currently of huge importance and interest to the electronics industry for the construction of ever better-performing devices.[48-50] The fabrication of such components and the drive to make them electrically conductive has dominated the field of nanotechnology in recent years. The aim is set out to develop nanodevices that are capable of functioning more efficiently than current state of the art technology can deliver, by way of higher switching speed or reduced power consumption.[48] The ability to fine tune the electrical properties of bottom-up constructed components to give the desired properties has led to the engineering of materials with ever smaller dimensions.

Nanowires are widely anticipated to play a major role in future nano-scale devices and are particularly applicable to the electronics industry for wiring-up circuits.[51, 52] The high interest in nanowires is due to these being the smallest structure for efficient transport of electrons. In many cases, the low dimensionality and high aspect ratio (length: width ratio) of these materials proffers potential for them to replace current technology in ICs. Therefore, these one-dimensional conducting structures are considered useful for application as interconnects. There are numerous examples of bottom-up strategies to nanowire formation. Indeed metal nanowires consisting of Au,[53] Ag[54] and Pd[55] have already been fabricated as interconnections within 2-terminal devices and exhibit electrical conductance. However, as copper is the material of choice for interconnect material in the current state of the art technology, the majority of this introduction is concerned with the strategies involved in the bottom-up fabrication of copper nanowires.[56]

It is generally agreed that the intrinsic properties of metal nanowires, such as electrical conductivity, are mostly determined by their shape, size, composition, structure and crystallinity.[57] Intensive efforts are therefore being made from the bottom-up perspective to demonstrate precise control over such factors as size and crystallinity. In this manner one is able to attain the desired chemical and physical properties of the material for a particular application, such as for miniaturised interconnect. Investment in this field could therefore lead to reduced line widths affording higher density transistor lay outs.

However, before we discuss copper-based strategies in detail, we first outline an example of a material which demonstrates the remarkable (and rare) ability of self-

assembly into 1-dimensional nanostructures, as is the case with trigonal-selenium (t-Se). As mentioned previously the ability for molecules, atoms or clusters of atoms to spontaneously self-assemble can be useful for the controlled growth of nanowires with defined sizes and crystallinity. Nanowires consisting of t-Se have been shown to grow via self-assembly from single seeds of t-Se in solution.[58] This material has a number of interesting properties such as its high photoconductivity (~0.8 x 10^5 S cm^{-1}) and catalytic activity. These t-Se nanostructures form by the spontaneous epitaxial growth of selenium into single-crystalline 1-dimensional strands and thus do not require a physical external guide to control their growth. This method is classed as a non-templated approach to nanowire synthesis. Figure 1.14 shows a proposed mechanism for the formation of t-Se nanowires based on a solid-solution-solid pathway. Reduction of selenious acid with excess hydrazine is followed by nucleation and growth of t-Se particles in one dimension. Nanowires did not grow from amorphous selenium (a-Se) as these particles tended to aggregate in solution. Rapid cooling of the reaction mixture is required to generate the t-Se seeds to drive the growth of nanowires, which is consistent with a nucleation and growth pathway. This process is accompanied by the dissolution of a-Se. These nanowires were grown with controllable lateral dimensions in the range ~10 to ~800 nm and have lengths up to hundreds of micrometres (see figure 1.15).

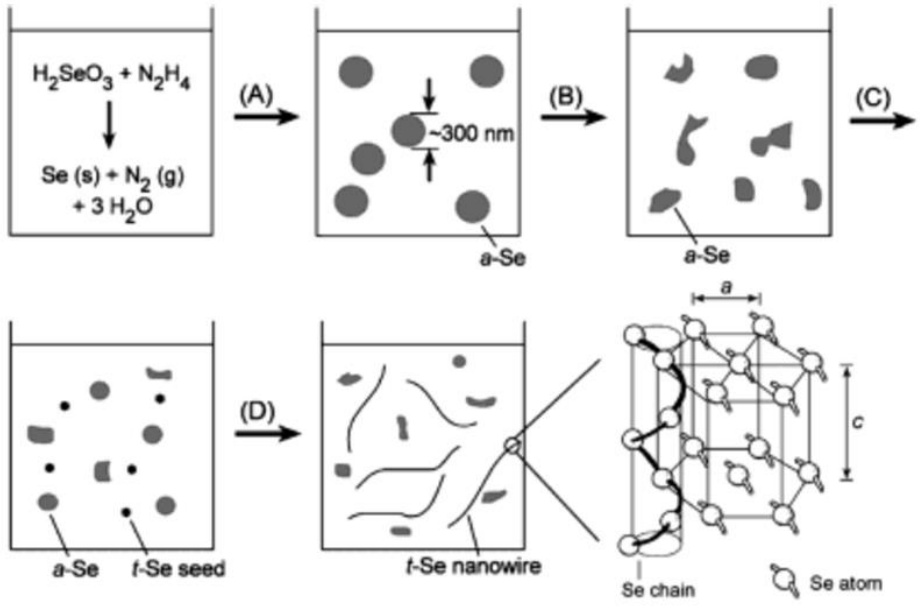

Figure 1.14: Schematic illustration of the nanowire growth mechanism. Chemical reduction of selenium salt generates a-Se colloidal particles (a) which aggregate in solution (b). Trigonal-Se seeds are formed upon rapid cooling of the reaction mixture to RT, and nanowires grow from these seeds (d) in the form of hexagonally packed spiral chains of Se atoms. Image taken from ref. [58]

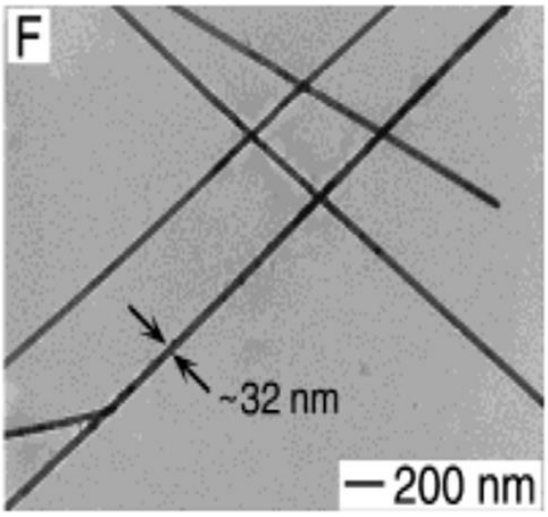

Figure 1.15: Transmission Electron Microscopy (TEM) image of t-Se nanowires. Image adapted from ref. [58]

There are also a few examples of non-templated chemical synthetic routes to copper nanowires.[59, 60] The following non-templated methods require a chemical(s) in the reaction solution such as surfactant, in addition to the source of copper and reductant, in order to aid the anisotropic growth of copper in one dimension. Such structures have been shown to have a single-crystalline morphology. It is ideally desirable to form single-crystalline nanowires as these are intrinsically free of grain boundaries (i.e. mismatches in the crystal lattice are not present) and should therefore not exhibit effects of resistance which are attributed to electron scattering at these interfaces.

The current techniques for CuNW synthesis mainly rely on aqueous-media reduction of copper salts, such as those synthesised by the reduction of $Cu(NO_3)_2$ with hydrazine in the presence of ethylenediamine (EDA).[61] These were formed as films of nanowires (~90 nm diameter, ~ 10 μm lengths) for transparent conducting electrodes. A similar method has been performed in nonaqueous media.[62] Zhang *et.al* have demonstrated the self-catalytic growth of CuNWs from $Cu(acac)_2$ in a liquid crystalline medium consisting of hexadecylamine (HDA) and cetyl trimethylammonium bromide (CTAB) to form hexagonal-shaped single-crystalline CuNWs.[62] In this method, a heated mixture of HDA and CTAB form a tubular liquid-crystalline structure. Copper ions can then coordinate within this tube-like medium. Figure 1.16 shows the proposed formation mechanism. This process occurs at a Pt surface which acts to catalyse the reduction of Cu ions to form metallic particles. The initially formed particles act as seeds for crystallisation to occur along a single crystalline axis. This generated ultra-long

nanowires (10-100s μm's) that are ~78 nm in width (see figure 1.17) and consist of copper metal, as suggested by X-ray Diffraction (XRD) data. These types of syntheses require surfactants/capping agents in order to control the growth. The surfactant acts as a structure directing agent, and thus, these methods are considered as a scaffold-based synthesis.

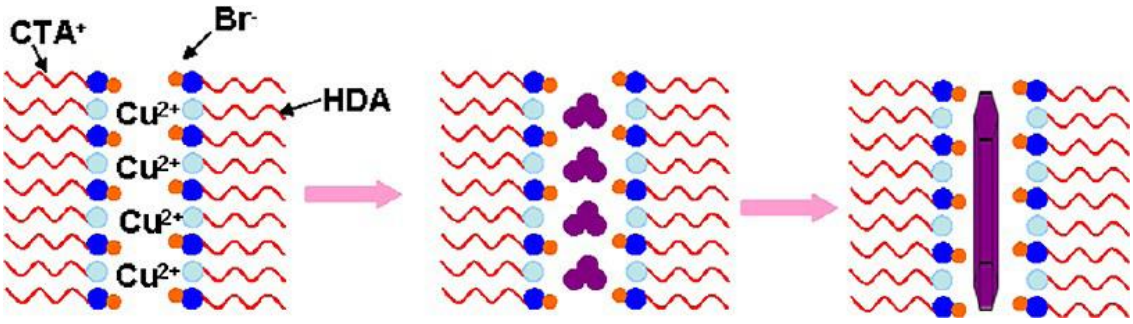

Figure 1.16: Scheme showing the growth of CuNWs directed by the liquid-crystalline medium [62]

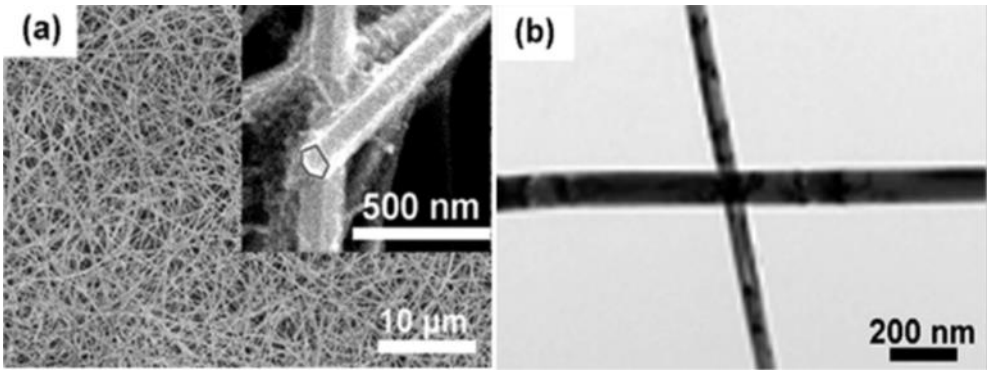

Figure 1.17: (a) Scanning Electron Microscopy (SEM) image of a film of CuNWs and inset showing the hexagonal shape of a wire, (b) Transmission Electron Microscopy (TEM) image of single wires. Figure adapted from reference [62]

Hydrothermal/solvothermal methods are also commonly used for the controlled growth of nanowires.[60, 63] These techniques are used for precipitating solids from solution into crystalline materials including noble metal, ceramic, and polymer nanoparticles.[64] In the presence of a synthetic growth-directing agent (i.e. surfactants) the crystallisation can take place along a single axis to afford 1-dimensional nanocrystals, as previously discussed. In the solvothermal method, the reaction mixture is heated above the boiling point of the solvent, often in an autoclave, at high pressure (when water is used as the solvent, the process is described as the hydrothermal method). These conditions present accelerated crystal growth, narrow structure size distribution and smoother structure

morphologies than synthetic routes can afford. Such methods can lead to structures of varying morphology/homogeneity and size, which is tailorable by varying the reaction conditions.

Zhao *et.al* demonstrated what is described as a "soft synthesis" of single-crystal CuNWs based on various hydrothermal/solvothermal methods.[65] These preparations were carried out in a Teflon-lined stainless steel autoclave at temperatures of ~160 °C, at atmospheric pressure for over 24 hours. The authors describe this approach as an alternative to various "hard" approaches such as chemical vapour deposition (CVD) and organometallic CVD (MOCVD), which require higher temperatures, higher cost and complex reaction processes. Figure 1.18 is a schematic of the solvothermal method for growing nanocrystals in one dimension.

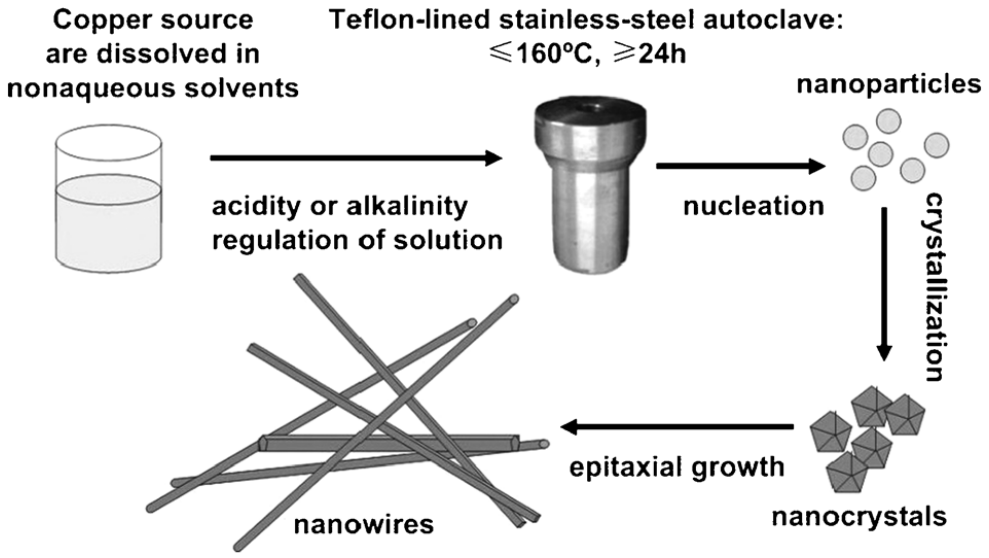

Figure 1.18: Solvothermal synthetic route to single-crystal CuNW formation [65]

One such method employed was the solvothermal reduction of $Cu(NO_3)_2.H_2O$ solution using ethylene glycol (EG) in the presence of polyvinyl pyrrolidone (PVD) for 24 hours, whereby the latter acts as the crystal capping agent.[65] The capping agent is necessary to control the growth rate, to afford good nanowire dispersibility and restrict the growth of copper to a single crystalline face. This process led to very straight nanowires with an average diameter between 30-50 nm and lengths between 5-20 µm. Figure 1.19 shows SEM data of a network of copper nanowires and a TEM image of a single wire, indicating their smooth surface morphology. The composition of the product was examined by Energy Dispersive X-ray Analysis (EDX) which indicated the

presence of copper. These nanowires were found to be stable to oxidation when protected with n-hexane. Further X-ray analysis confirmed that these nanowires are single-crystals and grow along the [110] axis with a face centred cubic (fcc) symmetry. The shape of the nanowires was found to be tuneable by varying the PVP concentration and reaction time and temperature. However, the electrical properties of this material were not investigated.

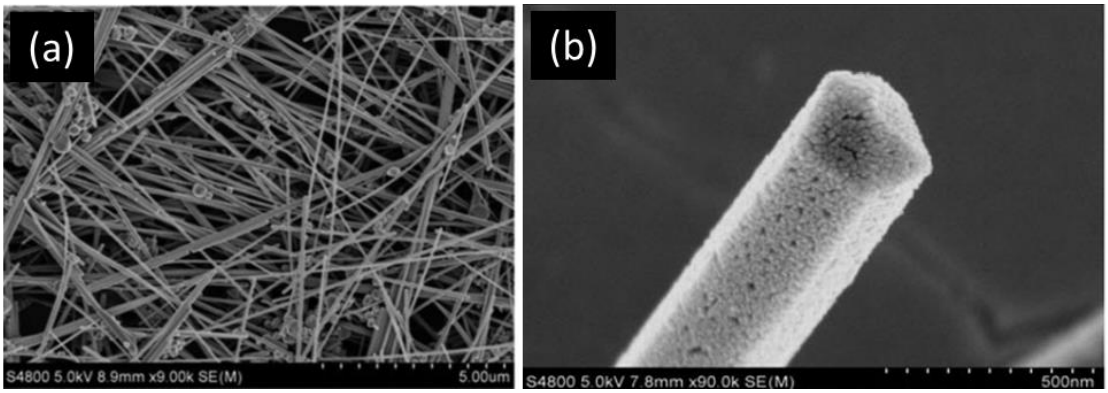

Figure 1.19: (a) SEM image of CuNWs obtained by a solvothermal process with PVD and (b) TEM image of a loose end of a nanowire. Figure adapted from reference [65]

Mohl *et.al* utilised a simple hydrothermal method employing glucose to reduce copper ions and HDA as the surfactant.[57] These formed straight, single-crystalline copper nanowires ~68 ± 8 nm diameter and a few micrometres in length. Electrical analysis was carried out upon networks of this material by recording current-voltage curves (i-V) at the surface of the nanowires. These results confirmed their conductive properties. Resistance was shown to increase with temperature, which is typical for true metals. However, upon heating the sample in an inert atmosphere up to 360 K the sample was easily oxidised and the resistance rose dramatically. This effect was found to be irreversible despite further changes in temperature. The authors also claimed that cluster formation was evident along the nanowires upon heating them to 550 K.

Other non-templated methods to the synthesis of copper nanowires include ink-jet printing,[66] vacuum-vapour deposition,[67] and direct electrochemical AFM (Atomic Force Microscopy) lithography.[68] In the case of direct AFM lithography, Kwon *et.al* demonstrated precise control over copper nanowire formation in terms of structure size, shape and alignment, simply by controlling the movement of an electrically biased AFM tip on the surface. The silicon surface was first modified with SAM, before spin coating of a Cu(II) acetate resist layer on top.[68] Application of a negative bias resulted

in the localised reduction of copper ions beneath the tip, decomposition of the SAM, and formation of copper lines in the direction of the electrical field (see AFM and SEM images in figure 1.20). i-V analysis was performed using conductive-AFM (C-AFM) (see figure 1.21) on a single wire (34 nm height, 20 µm length). This gave a resistivity value of 44 µΩ.cm, which is ~25 times higher than that of pure copper. This was ascribed to oxidation of copper and grain boundary scattering effects. The polycrystalline nature of the material is clearly evident in the magnified SEM image in figure 1.20b where particle-particle boundaries are present along the line and thus may partly explain the higher resistivity.

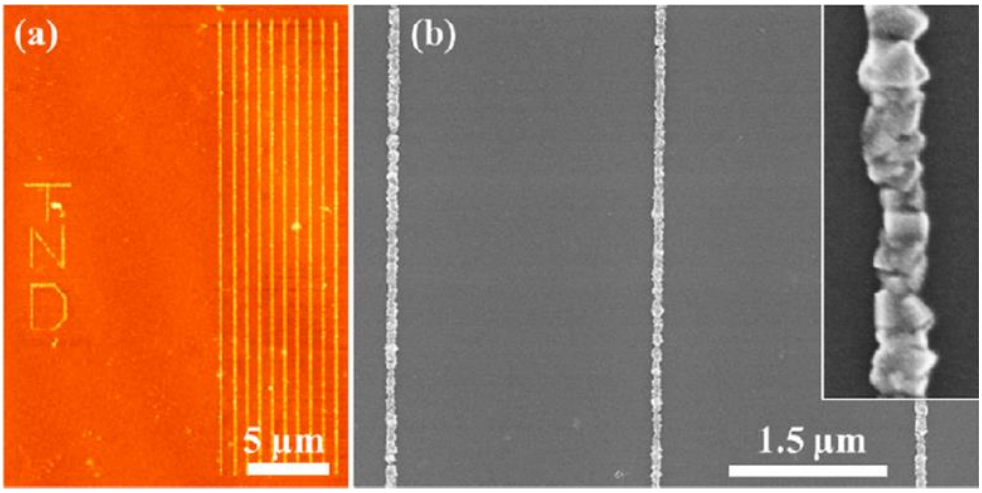

Figure 1.20: AFM image (a) and SEM image (b) of copper lines formed on a silicon surface by reduction of copper ions using an AFM tip. Figure from reference [68]

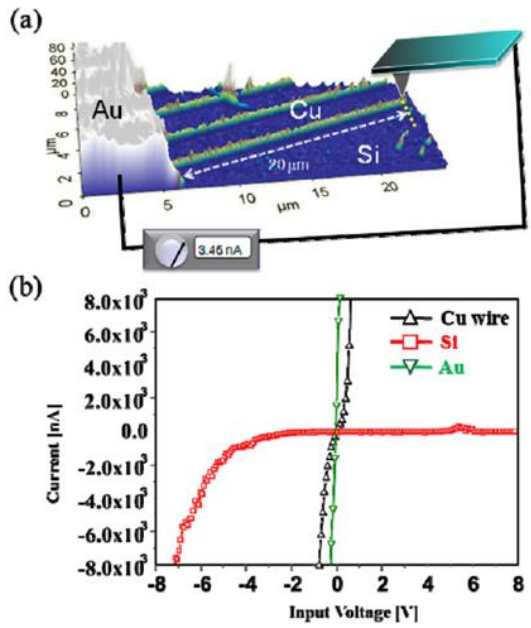

Figure 1.21: (a) scheme of C-AFM set-up to measure wire resistivity and (b) i-V plots recorded of Cu wire which exhibits ohmic behaviour compared to Si surface which is non-conductive. Figure from reference [68]

Generally, the non-templated construction of nanowires is a relatively rare case. Most of the routes described thus far have led to the formation of copper nanowires with diameters ≥50 nm and thus cannot be considered as plausible alternatives to the top-down fabrication of copper interconnect, which can be manufactured to sub-50 nm widths using current top-down technology.[69] There is also the added difficulty in isolating single nanowires for two-terminal device purposes where many of the reported procedures result in dense networks of material. However, in many of these syntheses the copper nanowires is not for the solution of interconnect technology. Copper nanowires are also known to be suitable for transparent electrodes (which require dense networks of nanowires) as candidates to replace ITO (indium tin oxide): the currently used material for thin solar cells. The interest in CuNWs for such an application is due to their better transparency, mechanical flexibility and conductive behaviour.

Additionally, non-templated methods usually require precise and/or rigorous processing conditions such as elevated temperature and/or pressure and may be considered tedious to perform. Indeed, the spontaneously assembled growth of nanowires as in the case of t-Se does not occur for the majority of materials. For most materials, a physical template is required to control the growth of the building blocks in a single uniform direction to construct nanowires of a defined size.

Template synthesis of nanowires has become a popular approach since the pioneering work of Martin's group.[70, 71] There are a range of templates available for construction of copper nanowires in particular.[70, 72] The most widely used approach is the porous templating procedure. Some of the most common porous-templates used are track ion etch membranes,[73, 74] porous alumina membrane (Al_2O_3),[75-79] polycarbonate membrane,[35] and porous silica (SiO_2).[56, 65, 80, 81] The pores are usually created by anodic oxidation of the solid substrate, except for the case of ion etch membranes. Formation of copper nanowires within these templates has been achieved by electrochemical deposition (ECD),[35, 56, 76, 77, 82] chemical vapour deposition (CVD),[6, 56, 81] hydrothermal/solvothermal processes,[57, 60, 63] solid-state reduction,[75] or solution-phase chemical reduction.[61, 83]

These templated methods have led to copper nanowires of varying morphologies, sizes and properties, whereby the size of the nanowires are defined by the diameter of the pores within the substrate, whereby the pores themselves be tailored to defined sizes. One of the most common methods for the preparation of CuNWs is via the porous

template-directed electrochemical method. Figure 1.22 shows a schematic illustration of the porous templating procedure for the formation of metal nanowires using electrochemical deposition (ECD). Based on this approach, Gao *et.al* fabricated copper nanowires with diameters of ~60 nm and lengths of 30 μm.[82] The template used was porous anodic alumina (PAA) prepared by anodic oxidation of aluminium in 0.3 M oxalic acid solution. ECD was used to generate metallic copper within the pores of the template. The process takes place in a three-electrode bath containing the cathode (template substrate), the reference electrode (standard calomel electrode, SCE), the counter electrode and an electrolytic solution containing $CuSO_4.5H_2O$. A gold layer was deposited onto the back of the PAA template to act as one electrode. The copper ions infiltrate the pores of the substrate by capillary action. A fixed potential was applied (-0.15 V) to drive the reduction of copper ions at the cathode (or working electrode), which in this case is the PAA substrate, and copper nanowires are grown. Electron microscopy data revealed these to be dense and continuous along their entire lengths (see figure 1.23). However, no electrical characterisation was carried out on these nanostructures.

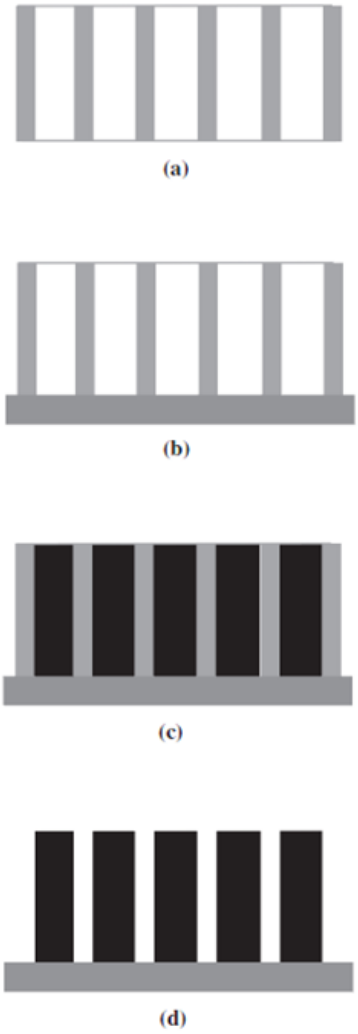

Figure 1.22: A schematic diagram of the template synthetic process. (a) The porous template, (b) evaporation of conductor layers on one side of the template, (c) the metal ECD process, and (d) metal nanowires after removing the template. Figure and caption adapted from reference [82]

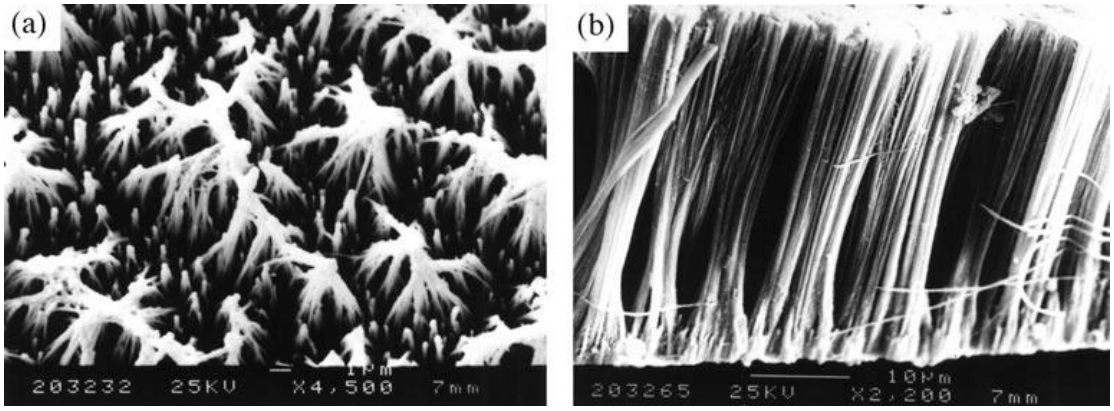

Figure 1.23: SEM images of CuNWs grown by ECD in PAA template, (a) top-down view and (b) lateral view. Figure taken from reference [82]

A similar strategy was performed by Bid *et.al*. except that a porous polycarbonate template was used.[84] Also, the ECD setup was slightly different to Gao's, as the counter electrode used was a microtip (~100 µm diameter) fitted to a micropositioner which enables site specific growth of copper within the template. Figure 1.24 shows a schematic of this setup. After growth of the copper wires the template was removed by dissolving the substrate in dichloromethane (DCM), and then the wires were characterised. The smallest wires observed by TEM were 15 nm. These were shown to be single-crystalline and conductive. The metallic nature of the wires was confirmed by temperature dependent resistivity measurements, which gave a positive temperature coefficient (i.e. resistance increases with temperature). To the best of our knowledge these are the smallest conductive bottom-up grown CuNWs reported in the literature. The electrical measurements were performed on arrays of wires (between 2-50 wires). The estimated resistivity (ρ) obtained for 15 nm copper wire ranged from ~2.0 $x10^{-6}$ – ~5.0 $x10^{-6}$ Ω.cm between 0 – 350 K. For larger wires (~30 nm diameter) the resistivity was found to be lower, which was suggested to be a result of reduced surface scattering.

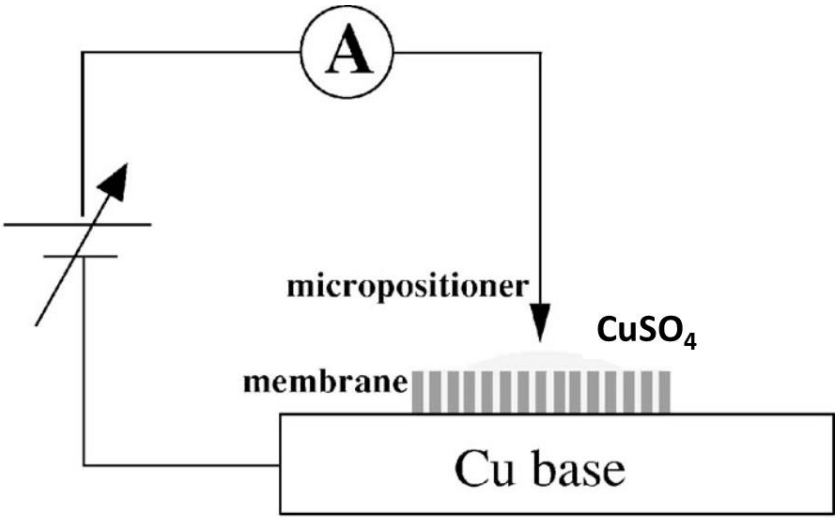

Figure 1.24: Schematic of the ECD set-up using a microtip for site-specific growth of copper within the porous membrane. Figure taken from reference [84]

Another example of electrodeposited CuNWs was demonstrated by Toimil Molares *et.al*. using polycarbonate etched ion-track membranes as the template.[73] Electrodeposition was carried out again in a three-electrode bath with electrolyte containing $CuSO_4.5H_2O$. Variation of the deposition parameters such as temperature and applied voltage, resulted in both polycrystalline and single-crystalline NWs. The

membrane was dissolved in DCM and the wires were detached from the support by sonication. Gold electrodes were deposited onto a single wire (60 nm diameter) by means of optical lithography and the i-V characteristics of the wire were plotted (see figure 1.25a). This demonstrated clear ohmic behaviour with increasing resistance as a function of temperature, indicating metallic behaviour. The resistivity of the wire (ρ) was calculated as 1.71 x 10^{-5} Ω.cm, which is ~10 times higher than that of bulk copper at 300 K. This was ascribed to the effects of oxidation, high contact resistance and surface scattering. The increased resistance of a wire over a 12 hour time period ($t_1 - t_5$) (see figure 1.25b) highlights the ageing process due to oxidation.

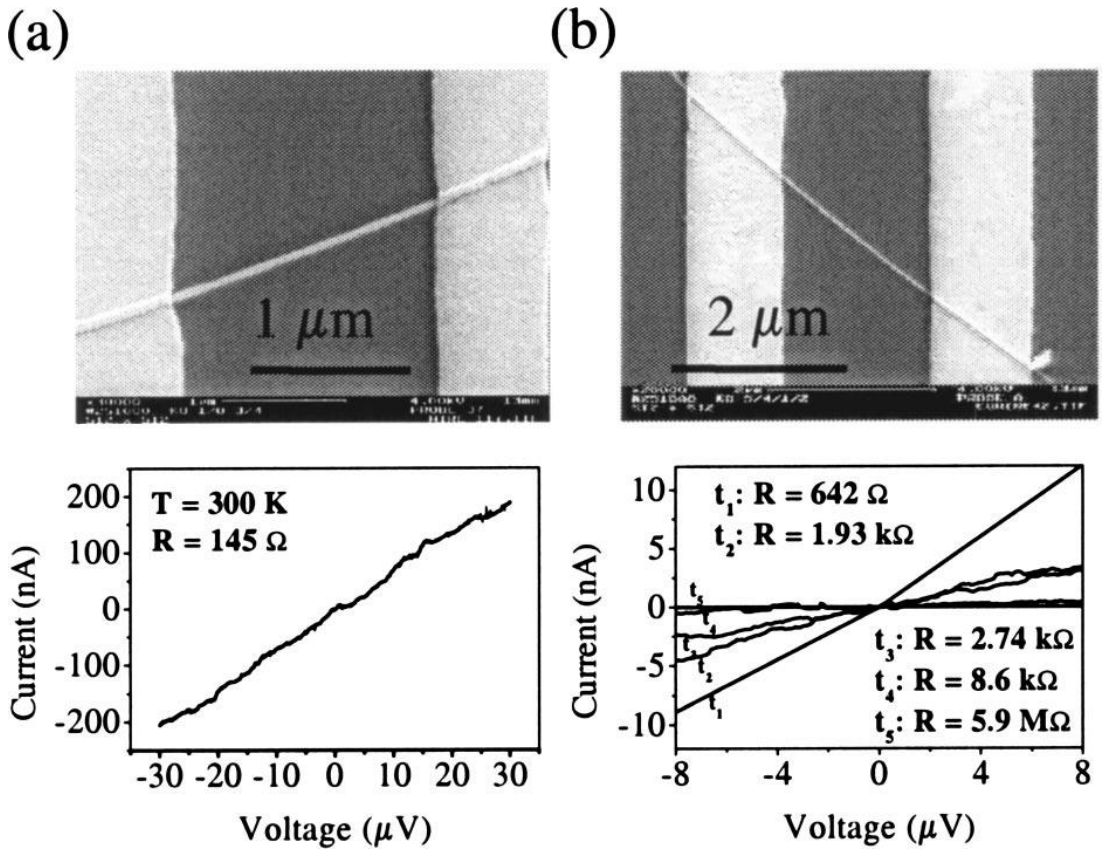

Figure 1.25: (a) i-V characteristics of a single 60 nm CuNW and (b) i-V measurements of another wire showing resistance drops as a function of time; indicating ageing by oxidation. Figure from reference [73]

However, these porous-directed growth procedures present an issue for removal of the auxiliary template following nanowire formation, which often require rigorous processing conditions. Additional processing steps such as centrifugation are sometimes required in order to obtain isolated nanowires rather than films, networks or aggregates. For example, in Feliciano's preparation of copper nanowires in anodic alumina

membranes, the template was removed by dissolution in 20 M NaOH and agitation for 1 day.[75] Traces of the membrane were also found in the final characterised product.

Other metal templating procedures involving the use of molecular-based templates have been investigated which afford considerably smaller structure sizes.[9, 85, 86] These are comparable to the order of the molecular diameter (i.e. often <10 nm) and smaller than those obtained by all of the previously described methods. Molecular-templating also presents great potential for generation of structures with precisely controlled and well-defined sizes on a reproducible basis. Molecular-templating methods are often relatively simple to perform and can be carried out at room temperature under standard laboratory conditions (i.e. bench-top preparations), unlike most of the previously described methods which require higher temperature and high pressure. Another advantage of using a molecular-based template is that the templates can be deposited on to a flat surface prior to metallisation and there is therefore no requirement to remove the template subsequent to metal growth. Moreover, the possibility of aligning single molecules onto a surface in a predefined arrangement may offer considerable potential to create templated circuit-like features on the surface.[51, 87]

By far the most widely explored molecular templates are biological macromolecules, which are highly promising candidates for the growth of conductive materials.[53, 88-90] Proteins, viruses and biopolymers such as cellulose,[86] can provide a solution to the construction of wires on the nanoscale as they naturally exist within this size regime. However the poor physical stability and poor electrical characteristics of these molecules have prevented their direct use in electrical devices. However, as mentioned, they can be used to direct the growth of conductive material such as metals into the form of nanowires. The first example of a biomolecular template used in this way were phospholipid tubules.[91] Other examples include proteins such as the use of self-assembling amyloid protein fibres for the covalent attachment of colloidal gold particles via the readily accessible cysteine residues.[53]

Another example of a widely used bio-template is the tobacco mosaic virus (TMV). The cylindrical shape, hollow interior, high aspect ratio and self-assembling properties of this molecule, as well as the ability to coat metals onto its interior surface make it attractive for forming nano-sized electronic components. The external width of the structure is 18 nm, with a 4 nm interior. Both cobalt and nickel have been crystallised within the central channel of TMV to afford nanowires ~3 nm thick and lengths up to

several micrometres.[92] However, despite this method being categorised as a molecular-templating approach, it is also reminiscent of the previously described porous-templating. The same group also showed how the external surface of the TMV can be metallised with nickel and cobalt clusters following a Pd(II) activation step.[93] The Pd is required to provide nucleation sites for the self-catalytic growth of metal along the external surface of the structure. This was found to occur at site-specific locations on the surface, which has a variety of functional groups available to bind metal ions. The metal ions are reduced on the surface of TMV by electroless chemical reduction. By varying the chemical parameters of the reaction procedure, such as pH and duration of treatment, the specificity of metal ion interaction with certain functional groups can be controlled. Figure 1.26 shows TEM images of TMV metallised with Ni (a) and Co (b). The metal structures were found to be not smooth as revealed by metal cluster formation along the surface.

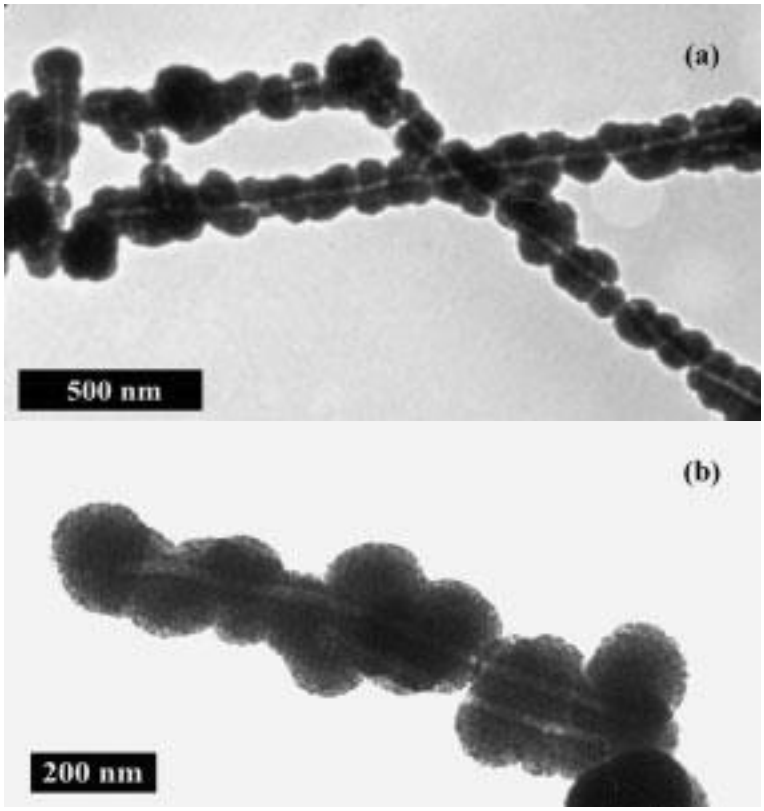

Figure 1.26: TEM images of TMV coated with Ni (a) and Co (b) following activation with Pd(II). Figure from reference [93]

Another bio-polymer template, which has received considerable interest for growth of metal nano-architectures, is DNA.[94, 95] DNA is an ideal shape and size for the construction of nanowires. It is ~2 nm wide and available in precise lengths over the

nanometre to millimetre range in 3.5 Å increments. Other notable properties of DNA that add to its growing interest within this field, for the growth of nanostructures, are the highly sophisticated structure building aspects. This is based on the self-assembling properties of DNA resulting from the complementary hydrogen bonding of the nucleobases. The highly predictable base-pairing rules of duplex DNA, known as Watson-Crick base-pairs (adenine-thymine and cytosine-guanine), can afford higher order DNA-based architectures.[96, 97] The recently developed "origami" approach demonstrates the ability to design precise patterns based on these properties.[98] This could lend an extension to the growth of more complex nanoscale systems in one, two or three dimensions for the construction of more sophisticated device components.[99-102] However as DNA is not sufficiently conductive for use in electrical components,[103] despite contention in the scientific community to prove otherwise,[104] it is necessary to modify the structure with conductive material.

For the context of this thesis, the interest lies in the ability of DNA to bind metals and control their growth in a single dimension. DNA-templated methods for nanomaterials fabrication offer a highly sophisticated method for control over the assembly of metal ions. DNA emerged as a highly desirable agent for the templating of conductive species since the early work by Braun in 1998.[54] Braun was able to fabricate a conductive DNA-templated silver nanowire device by metallisation of a single DNA strand stretched between two electrodes. Since then, a range of different nanoparticles and nanoclusters have been assembled onto DNA.[95, 105] In a general sense, the attention that DNA has received for building nanosized components stem from its highly sophisticated structure-building properties. This aspect of DNA will be discussed only briefly in the proceeding section. More specifically however, the high interest in DNA for templating metallic species stems from its remarkable ability to bind metal ions. Therefore, in order to understand how DNA can be used as a template for metallisation, it is necessary to develop an understanding of the fundamental principles of DNA-metal ion complexation.

1.4. DNA-Metal Ion Binding

DNA structure

Deoxyribonucleic Acid (DNA) is a macromolecular biopolymer responsible for encoding the genetic information of living organisms. The structure of DNA was elucidated by James Watson and Francis Crick in 1953, based on X-ray Diffraction data.[106] DNA is a double helix structure, made up of two polymeric strands running in opposite directions. Each strand consists of a series of nucleotide units comprising a 2-deoxyribose sugar unit, a phosphate group, and one of the four nucleobases: adenine (A), thymine (T), cytosine (C) or guanine (G). Figure 1.27a shows the chemical structure of a single strand of DNA. Each base is bound to the deoxyribose ring at the 1' –carbon position. The nucleotide units are connected by phosphodiester linkages between the 3'-hydroxyl group of the sugar moiety and oxygen of the phosphate group of the preceding nucleotide. This comprises the backbone of DNA and is polyanionic owing to the presence of the negatively charged phosphate groups (one negative charge per phosphodiester entity).

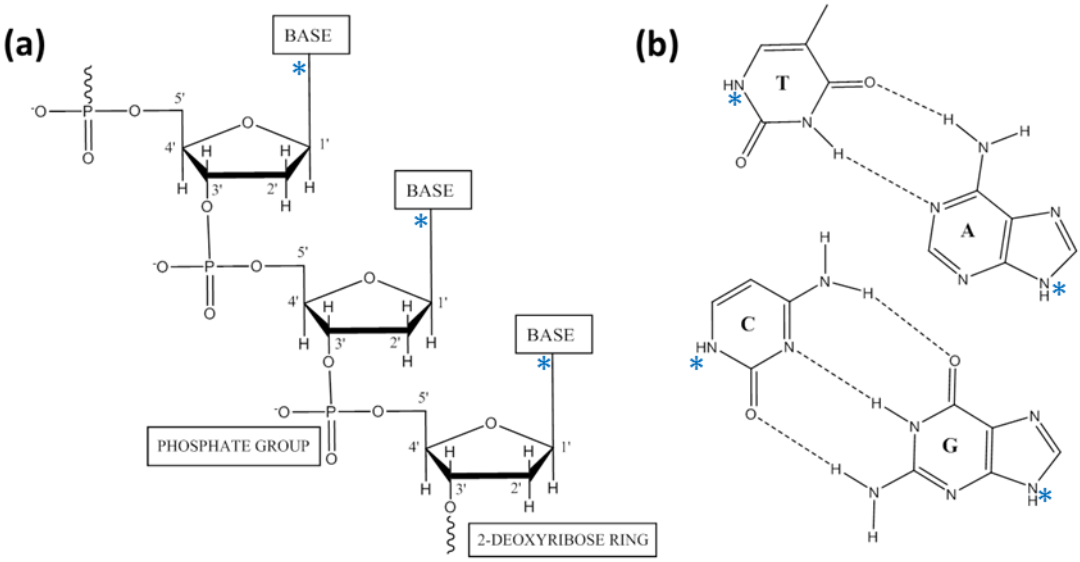

Figure 1.27: (a) Structure of a single DNA strand, (b) structure of the bases and their complementary binding through H-bonds. Atoms denoted with '*' indicate where on the base where the sugar is attached

The bases can be categorised into two distinct groups: purines (G and A) consisting of a bicyclic framework with one 5-membered ring and one 6-membered ring; and pyrimidines (C and T) consisting of a single 6-membered ring framework. The bases are

complementary to one another and pair up on opposite strands via intermolecular H-bonding, known as Watson-Crick base pairs, in the manner A-T and G-C, as shown in figure 1.27b. It is this predictable nature of DNA which makes it such a sophisticated tool for structure building.[97, 98] Isolated fragments of DNA containing the nucleobase bound to the sugar group (no phosphate attached) are termed nucleosides. The DNA structure is approximately 2 nm in diameter and can range in length from nanometres to millimetres. The length can be readily controlled based on the number of base pairs within the strand. The spacing between each base pair is 3.5 Å.

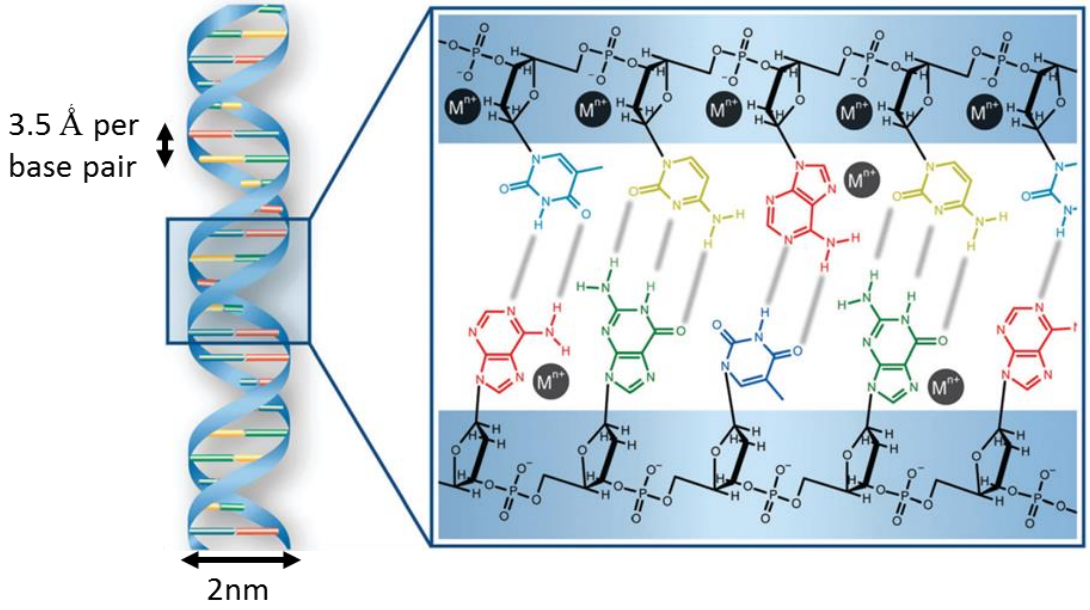

Figure 1.28: Scheme showing the DNA double helix structure and 'zoomed' in region showing the chemical structure of the backbone and complementary base pairs. Regions of metal ion binding to the phosphate groups and nucleobase sites are indicated. Binding at the N7 position of guanine (coloured in green) and adenine (red) is particularly common

The DNA structure provides ideal binding sites for metal-ions.[107] Metal binding can take place at the phosphate groups, the sugar entity, at various donor positions on the nucleobases, or a combination thereof via inter-strand (between two individual strands) or intra-strand (between neighbouring sites on the same strand) complexation.[108] Metal chelate formation via complexation to multiple nucleobase binding sites, simultaneously, is also known to occur, but is relatively rare.[107, 109] One such study provides evidence of a possible guanine (N7)-chromium-phosphate chelate complex.[109] Binding of metal ions to the ribose oxygen atoms is possible,[110] but this type of bonding is not general and is only applicable to RNA. Figure 1.28 shows a schematic of the DNA double helix, indicating regions of where metal ion complexation can occur at

local sites within the structure (as denoted by the positions of M^{n+}). The basic modes of DNA-metal ion interaction can be divided into two types; non-covalent interactions and coordinate bonding.

Phosphate vs. base binding affinity

Firstly, non-covalent, electrostatic attraction of positive metal ions at the negatively charged phosphate groups is a major mode of interaction. This can be enhanced by additional interactions involving potential H-bonding between coordinated ligand molecules and phosphate groups, as for example, with the amine groups of cobalt(III)hexammine.[110] The phosphate interaction is probably the most important mode for coordination of metal ions, particularly for alkali and alkaline earth metals, as these represent natural counterions of nucleic acids in cells.[107] Thus, metal ions such as Mg^{2+} for example, tend to bind non-covalently with the backbone of DNA due to their low affinity for the bases, compared to other metal ions such as the late transition metals. Generally, phosphate binding to positive metal ions is highly favourable as this results in charge neutralisation of the polyanionic backbone.[111] In this perspective, metal ions can condense around DNA in a cylindrical manner which is known to stabilise the duplex.[112] The increase in stability is attributable to a lessening of repulsive forces between individual charged molecules. This charge compensation can lead to condensation of DNA and result in the formation of folded DNA assemblies or aggregates of many strands. It is considered that metal ions of +3 charge are required to trigger DNA condensation, such as that induced by Co^{3+}.[113] However divalent metal ions (+2 charge) are also known to induce DNA condensation at higher metal ion concentration.[114, 115]

The second mode of interaction is coordinate bonding with the DNA bases. The bases can form coordinate bonds with metal ions through their electron donor sites (primarily through ring N atoms) to suitable vacant orbitals on the metal atom.[116, 117] Most commonly the donor sites are provided through the endocyclic nitrogen atoms which comprise part of the heterocyclic rings. Exocyclic amino groups of C, A and G can only become metal binding sites following deprotonation of the amine group.[107] This is because there is no available lone electron pair to permit metal complexation, but rather this is delocalised into the aromatic ring. DNA base sites can also H-bond to metal ligands, as the phosphates do.

Direct metal-base binding is considered to destabilise the DNA double helix and accelerate DNA denaturation.[118] This is thought to result from disruption to base-pairing interactions, which is partly responsible for holding together the helical shape of DNA (along with base-stacking interactions). The effect of denaturation of the double helix, after being treated with metal ions, can be examined by recording the DNA melting temperature (T_m) as a function of metal ion concentration. The melting temperature is defined as the temperature at which half of the DNA molecules are in the single-stranded state (i.e. when the double helix unravels). Consequently, a reduction in T_m would be indicative of a destabilising effect on the DNA structure. A classic study by Eichorn and Shin revealed that a range of metal ions, including Mg(II), Co(II), Ni(II), Mn(II), Zn(II), Cd(II) and Zn(II), can be placed into a series (as written) that indicates, qualitatively, their relative phosphate to base binding affinities (decreasing from left to right) based on rationalisation of melting temperature data.[119] In this study the T_m of DNA was recorded as a function of metal ion concentration. The resulting graph is shown in figure 1.29. The sequence was elucidated by determining at what metal ion concentration the T_m is at a maximum for each metal ion. The metal for which the maximum T_m occurs at the lowest concentration, was Cu(II). This suggests that Cu(II) has a particularly high binding affinity for the nucleobases relative to the phosphates. On the contrary, it was found that hard metal ions such as Mg(II) favour direct binding to oxygen of the phosphate groups, whereby the T_m continues to increase in the range of concentrations studies, implying increasing stability of the DNA helix attributable to further charge neutralisation of the DNA backbone.

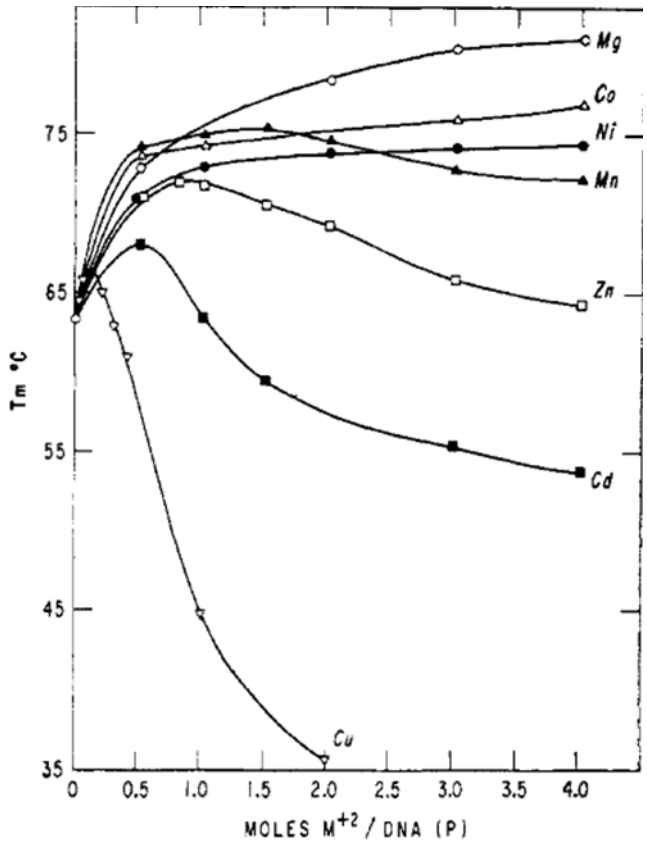

Figure 1.29: "Variations of T_m of solutions of DNA as a function of divalent metal ion concentration."[119]

Given the importance of Cu^{n+}-DNA interactions in this thesis, an overview of the interactions that have been well characterised for known crystallised compounds was undertaken, using the Cambridge Structural Database (CSD). More specifically, this review was to deduce where the most prominent binding sites are on DNA for Cu^{n+} (for the nucleobases in particular). The search was constrained to copper ions complexed with any of the four nucleobase substructures, so as to encompass single nucleobases, nucleosides and nucleotides. In all reported crystal structures, copper was in the +2 oxidation state. There was no literature precedent for crystal structures of the univalent copper ion, Cu(I), bound to DNA. This is presumably due to the high likelihood of Cu(I) salts oxidising to the more stable Cu(II) state, in air, or aqueous DNA solution.

In the following reports copper ions are coordinated to single nucleotide units or dimers.

Phosphate binding

In the majority of crystal structures reported, the divalent copper ions bind to the phosphate groups in *preference* to the bases.[108, 120-122]. In most cases, Cu(II) ions were

deduced to bind two oxygens of a phosphate group, as these both carry a negative charge in a single nucleotide. Figure 1.30 shows one example of a Cu(II) phenanthroline complex coordinated to one oxygen of one phosphate group and to another oxygen of a phosphate group on a second nucleotide (adenine) unit. This affords a dimeric Cu(II) nucleotide complex. There was no evidence of metal binding to the nucleobase sites in this example. Thus it is considered that although Cu^{2+} has a particularly high base to phosphate binding ratio, comparative to other metal ions, binding to the phosphate group remains the primary mode of interaction. This can be better understood when considering the stabilising effect metal ion phosphate binding has on the DNA double helix.

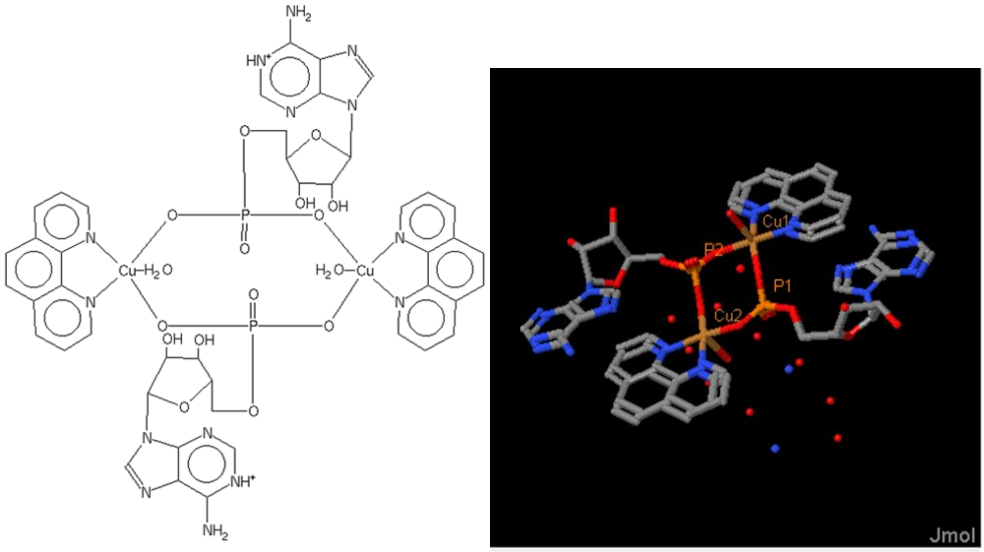

Figure 1.30: Crystal structure of copper(II)-1,10-phenanthroline complex bound to the phosphate groups of N(1)-protonated adenosine 5'-monophosphate [120]

However, as has been proven in the literature, the phosphate vs. base binding is metal ion concentration dependent.[118, 119, 123] Andruschenko *et.al*. investigated the effect of Cu^{2+} binding to DNA as a function of the Cu^{2+}:DNA(phosphate) ratio (or [Cu]/[P]), using vibrational spectroscopy.[123] These studies revealed that at low metal ion concentrations (with respect to a constant DNA concentration), in the range 0.2-0.4 [Cu]/[P] ratio, Cu^{2+} binding at the phosphate groups is the only detectable interaction. Upon increasing the concentration of Cu^{2+} (0.7 [Cu]/[P]) the base pairs become significantly distorted indicating strong interaction at nucleobase sites. Furthermore, according the Eichorn and Shin experiments, Cu^{2+} in particular has a comparatively large destabilising effect on DNA even at low metal ion concentration (~0.1

[Cu]/[P]).[119] Hence it is clear that Cu^{2+} has high base-binding affinity, especially when compared to other transition metal ions such as Co^{2+} or Cd^{2+}. However, as suggested, phosphate binding is still the major mode of interaction of metal ions with DNA, even for Cu^{2+}. Thus, one of the challenges in this thesis will be to prevent major conformational change to the DNA structure when binding copper ions. Based on the reported evidence, this can be facilitated by controlling the [Cu]/[P] ratio and appreciating these competing modes of interaction (phosphate vs. base).

Base binding

Various structures have been crystallised based upon Cu^{2+} binding to thymine, guanine, cytosine and adenine with or without the sugar/phosphate attached. Figure 1.31 shows where the most prominent binding sites are on the nucleobases (denoted with '*'), following a review of the CSD for copper-nucleobase related compounds

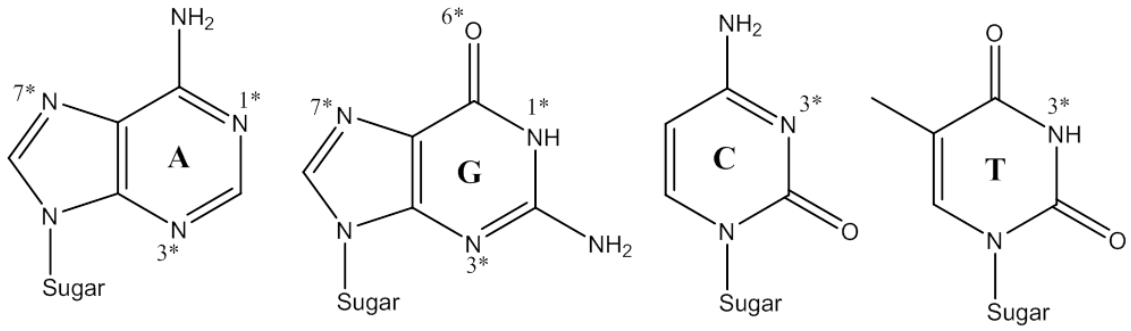

Figure 1.31: Structure of the nucleobases with common metal ion binding sites indicated

By far the most common and predominant binding site for metal complexation with the purines, guanine and adenine, is at the N7 position,[107, 111, 124, 125] Cu^{2+} coordinated to each of the N7 positions of guanine within a duplex DNA hexamer (six base pairs long) has been characterised.[126] This is perhaps unsurprising considering N7 is readily accessible within the major groove of the double helix and is not involved in base-pairing interactions.[127] Another example is the Cu(II) hydrate complex bound to two guanines at the N7 position (the crystal structure is shown in figure 1.32). Binding at the N1 position of adenine,[128] is also possible. For guanine, deprotonation of the N1 hydrogen is necessary for this interaction to occur. Binding of Cu^{2+} at the N3 of adenine is also relatively common.[129] A complex of Cu^{2+} bound at the N3 position of guanine

has also been crystallised where the N7 position is also coordinated to another Cu^{2+} ion on the same nucleobase.[130] In this example, binding at the N7 position is presumably the initial and predominant interaction. Additionally, metal binding can also take place at the O6 position of guanine,[131] but is less common. Deprotonation at the N9 position (no sugar) opens up many more possibilities for metal complex formation, including those of metal chelates.[107] However these examples are not relevant to DNA *strands* (where the sugar moieties are present) and will not be discussed here. In the case of the pyrimidines, thymine and cytosine, interactions at the N3 position can occur (following deprotonation for thymine).[132, 133]

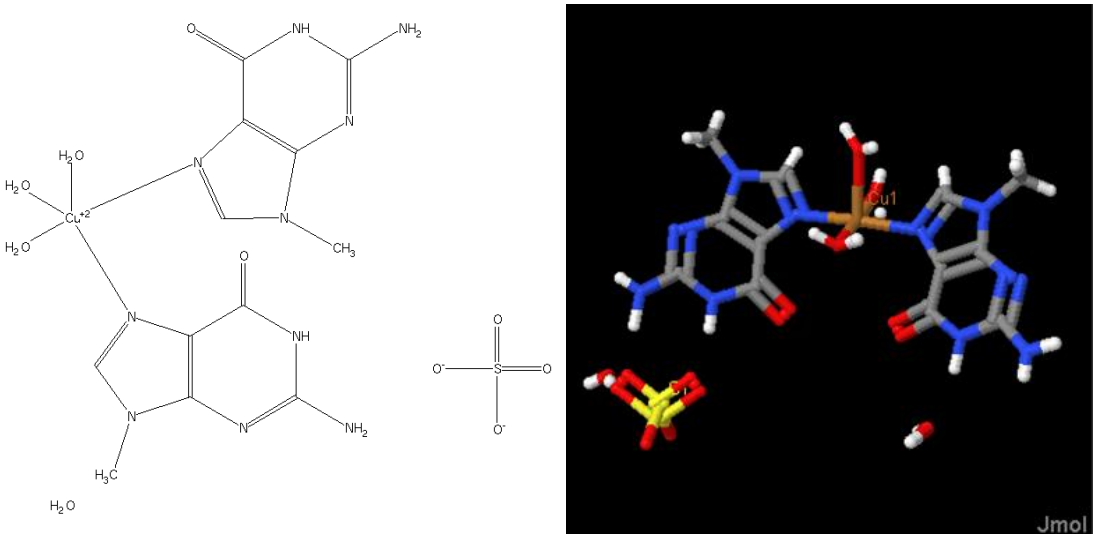

Figure 1.32: Crystal structure of a Cu(II) complex bound to two guanines at the N7 position [125]

Other situations involving mixed chelates have been verified by X-ray analysis, including Cu(II) binding at the N3 position of guanine and simultaneously at the N7 position of a neighbouring guanine (an example of an intrastrand cross-link).[130] Complex formation between two neighbouring guanines at the N7 and O6 positions, respectively, is also known to occur.[131] Additionally it is not uncommon for phosphate oxygen to become involved in coordinating to metal ions as is the case when Cu(II) is bound at the phosphate group as well as at the N7 position of guanine.[134] This was also identified as a possible complex in Andruschenko's study of Cu(II)-DNA binding.[123]

Importantly, in the context of templating, DNA metal binding sites are sufficiently close to permit metal-metal interactions; an aspect that will become important for metallisation of DNA and the growth of conductive 1-dimensional nanostructures.

1.5. Templating Metals on DNA

DNA has been a key building block in nanotechnology within the distinct field of DNA-templated self-assembly since the earliest work by Alivisatos,[101] Mirkin,[135] and Braun.[54] A wide range of metals have since been deposited on single DNA molecules or arrays of DNA-based nanostructures, including Pd,[55, 136] Ag,[54, 102, 137, 138] Cu,[139, 140] Ni,[141] Pt,[142] and Au.[101, 143] This has resulted in the formation of nanowires, in some cases with sizes at the low-end of the nanometre regime (<10 nm), which have potential for use in nanoelectronic devices.[144] Although DNA-based nanowire fabrication is most extensively applied in the case of metals, binary materials such as compound semiconductors (e.g. CdS) have been used,[145] as well as organic conductive polymers.[105, 146]

The general approach towards DNA-templated metal nanowires is based on an electroless two-step procedure. The first step exploits the metal-ion binding properties of DNA, as discussed in the previous section, by incubating the DNA structure with metal salt. This serves to extensively 'dope' the template with the positive metal ions of interest, such as Cu^{2+}, as shown in figure 1.33. The initial doping entails either (i) mixing the appropriate metal cations with a solution of DNA (*solution-based approach*) or more commonly (ii) immobilisation of DNA onto a solid support before incubation with metal ions (*surface-based approach*).

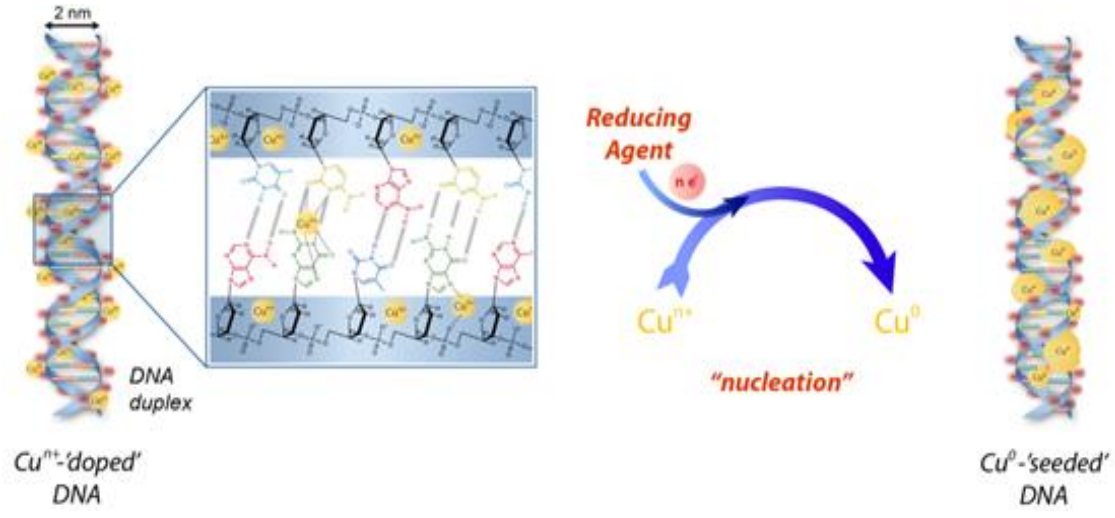

Figure 1.33: Schematic of the two-step 'doping/reduction' procedure for templating metal at DNA

Following doping of the template, DNA-bound metal cations are reduced to the zero-valent metal, by use of a suitable reducing agent (as illustrated in figure 1.33). Chemical

reductants such as dimethylaminoborane (DMAB),[136] or ascorbic acid,[139] are commonly used for this step. Other reducing agents have also been utilised such as H_2 gas,[147] or even reduction induced by photo-irradiation of metal ions such as the UV initiated reduction of Pt^{2+} bound to DNA.[148] The two-step 'doping/reduction' procedure results in metal seed particles bound along the length of DNA strands. Upon extended incubation with metallising agents, further deposition proceeds autocatalytically at the surface of these DNA-bound seed particles (so-called nucleation sites) and can lead to dense metal coverage of the template (as illustrated in figure 1.34). Thus the growth mechanism is via a 'nucleation and growth' pathway.

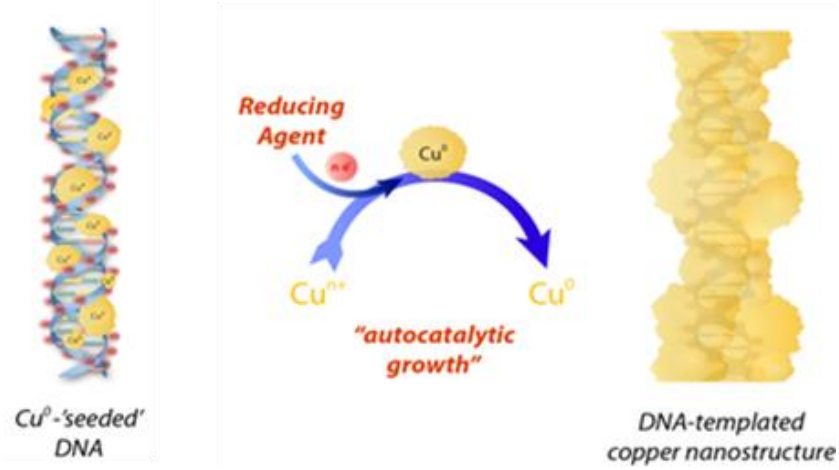

Figure 1.34: Schematic of the 'nucleation and growth' mechanism. Autocatalytic growth of copper takes place at the surface of nuclei bound to specific sites on DNA, affording the desired metallic nanostructure

For the surface-based approach to DNA-templating it is necessary to immobilise the template on a solid support, prior to metallisation. This step is enabled by the ability to separate and stretch out individual molecules of DNA onto a flat surface (e.g. Si/SiO_2). This is important for the purpose of obtaining linear strands of DNA for the subsequent formation of nanowires. Furthermore, manipulation of the template in this manner is useful for the precise positioning of nanoscale components in circuit-based devices. Surface-alignment of DNA can be achieved by a variety of methods including electrophoretic stretching,[149] and molecular combing.[150] The latter technique is the one utilised in our work due its simplicity and effectiveness for obtaining parallel arrays of isolated molecules of DNA on a surface. Molecular combing was first developed by Bensimon *et.al.*,[151] whereby individual DNA molecules are stretched across the surface by way of a receding meniscus. In this process, one end of DNA anchors to the surface, whilst the surface tension created by the moving air/solution interface, perpendicular to

the direction of withdrawal, is enough to stretch out molecules onto the surface. The motion of the droplet can be abetted by air flow, suction, or physical movement with a pipette tip, for example. Figure 1.35 illustrates how the molecular combing technique is implemented in this work. A single droplet of DNA solution is pipetted onto the surface and is combed in a raster pattern across it using a micropipette tip. Afterwards the solution is withdrawn and the sample is briefly washed with Nanopure water.

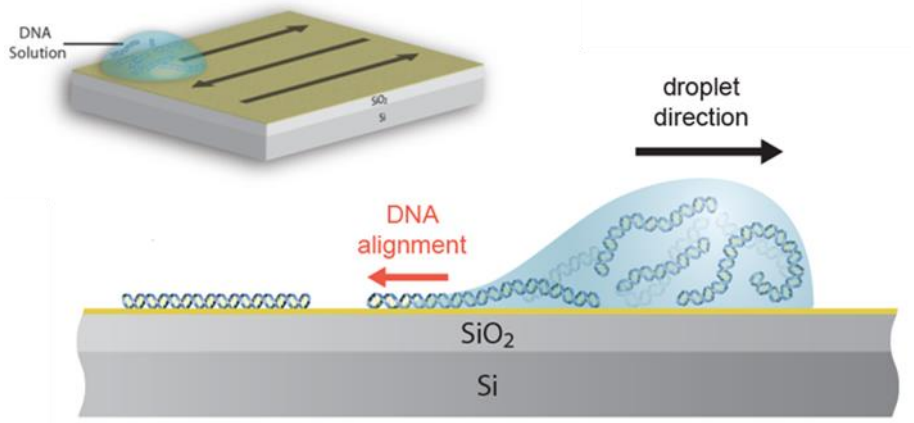

Figure 1.35: Schematic showing the molecular combing technique used to align DNA on a Si/SiO_2 surface. In this illustration the surface is modified with an organic monolayer (yellow layer) in order aid the combing motion and control the density of DNA bound to the substrate

Prior to the combing process, modification of the surface with an organic self-assembled monolayer (SAM) (e.g. trimethylsilane (TMS)),[152] is required to make the surface hydrophobic and enable a fluid combing motion. Surface modification with TMS is achieved by exposure of the bare silicon surface to a vapour of chloro-trimethylsilane. The time of exposure can be used to tailor the wetting properties of the surface. Higher surface hydrophobicity favours the deposition of low density material and isolated molecules. In all Scanning Probe Microscopy (SPM) studies carried out in this thesis, the surface was pre-modified with TMS. This modification step is omitted in the case of sample preparations for chemical analysis, as these experiments require a higher density of surface bound material, and thus a hydrophilic surface. The hydrophobicity of the surface can be monitored by recording static contact angle measurements on the solution-surface interface.

As mentioned, a variety of metal nanowires have been grown using the two-step DNA-templating strategy. Most notably, electrically conductive silver[54] and palladium[147] nanowires have been fabricated based on this approach, specifically for the development

of interconnections. One of the earliest examples of metal templating on DNA was demonstrated by Braun *et.al*. for the fabrication of silver nanowires. In this study a 16 μm length λ-DNA molecule was attached between two gold electrodes.[54] To facilitate the positioning of DNA between the electrodes the authors used a process known as "sticky end synthesis." Two different 12-base oligonucleotides (oligo A and oligo B) modified with a disulfide at one end were attached to each set of electrodes by thiol-gold interaction. λ-DNA molecules with the complementary base sequences at both ends (A' and B': sticky ends) then hybridised between oligos A and B, forming a DNA bridge between the electrodes. The DNA immobilised substrate was then treated with $AgNO_3$. The Ag^+ doped DNA was then reduced with a solution of hydroquinone. This resulted in the formation of a series of Ag nanoclusters along the template. A further "developing" step (more extensive metallisation) was required to transform the morphology of the structure into a continuous metal wire consisting of closely packed grains (~30-50 nm dia.) and wires ~100 nm in diameter, as analysed using AFM (see figure 1.36). Current-voltage (i-V) measurements initially indicated non-ohmic behaviour around zero bias, as well as dependency of the current on the scan direction, which is not characteristic of metallic behaviour. Ohmic behaviour was observed for wires after more extensive metal coverage and/or application of >50 V bias to eliminate the zero-current plateau. Control experiments were carried out in order to show that deposition of metal without DNA to act as a template does not result in a conductive bridge. This result clearly shows that the metal is selective for the DNA template.

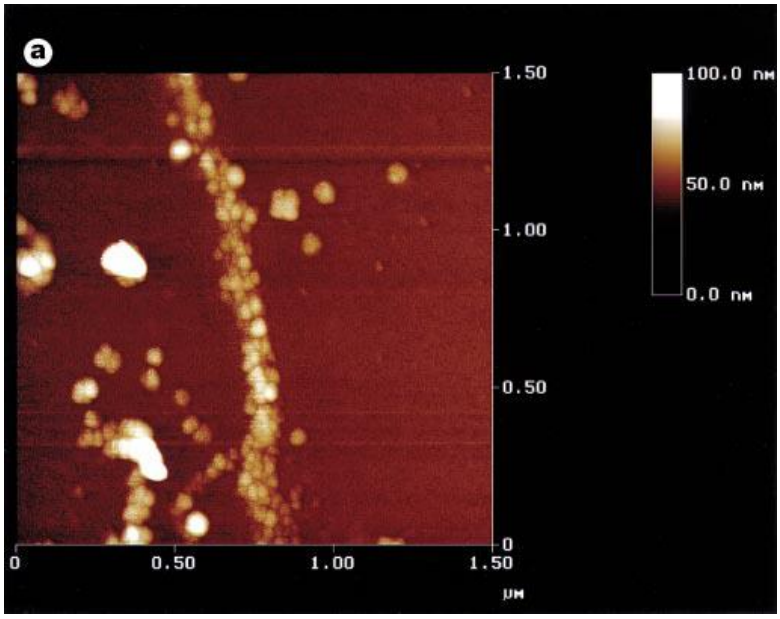

Figure 1.36: AFM image of a DNA-templated silver wire with granular morphology, connecting two gold electrodes (12 μm separation). Image area= 1.5 μm^2. Figure adapted from reference [54]

Recent attempts to extend these two-step DNA-templating methods to copper metal-based materials have not been *as* straightforward as for other metals such as Ag, Pd and Au.[153] *There are currently no examples of conductive DNA-templated copper wires*. There has been keen interest towards the growth of copper-based nanostructures, largely due to this material being the current choice for interconnect within the semiconductor industry.[34] Moreover, the interest in copper-based nano-devices stems from coppers high resistance to electromigration and high electrical conductivity, which is second only to silver.

The first such report for templating of copper on DNA was made Woolley *et.al.*[139] These studies utilised AFM to investigate the deposition of copper on surface-immobilised DNA using an aqueous solution of $Cu(NO_3)_2$ as the source of Cu^{2+} and ascorbic acid as the chemical reductant. This process led to granular structures of ~3 nm in height with incomplete coatings due to metallisation taking place at differing extents along the template (see AFM image, figure 1.37). A repeat metallisation process on these as-formed nanostructures yielded increased structure heights up to 10 nm. However, excessive non-specific deposition on the substrate surface (i.e. non-DNA-templated copper) limited this process to two cycles.

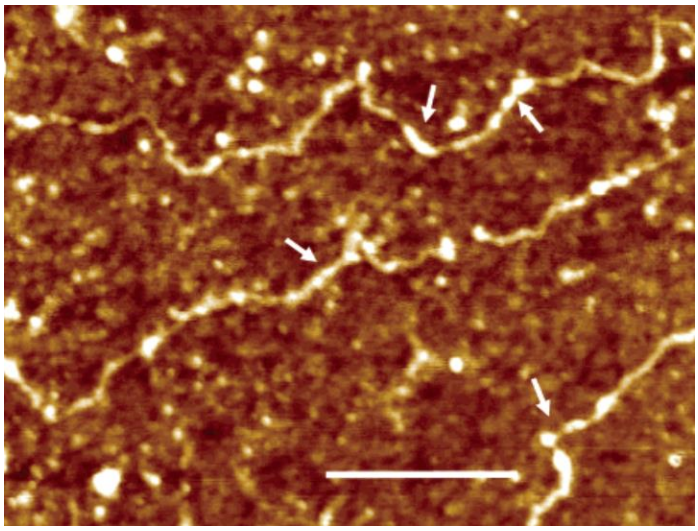

Figure 1.37: AFM height image of λ-DNA treated once with $Cu(NO_3)_2$ and ascorbic acid. Arrows point to raised area along the template where specific copper deposition has taken place. Scale bar= 1 μM, height scale= 5 nm. Figure adapted from reference [139]

A slight alteration to this method involved the use of dimethylsulfoxide (DMSO) as the solvent in replace of water.[140] It is reasoned that polar solvent molecules may actually compete with DNA donor sites for complexation of metal ions. This refinement led to

enhanced interaction of copper ions and the DNA template, which is thought to result from more competitive interaction of positively charged copper ions for negative phosphate groups of DNA, in the absence of a higher dielectric solvent such as water (compared to DMSO). The resulting metallised structures exhibited more extensive coverage of the template after a single doping/reduction treatment (~7 nm structure height), as shown in the AFM image below (figure 1.38), but still exhibit a non-uniform structure morphology due to appearance of irregular sized clumps of material along the template. Although the structural morphologies of the nanomaterial were analysed extensively by AFM, there were no chemical or electrical data to support these studies.

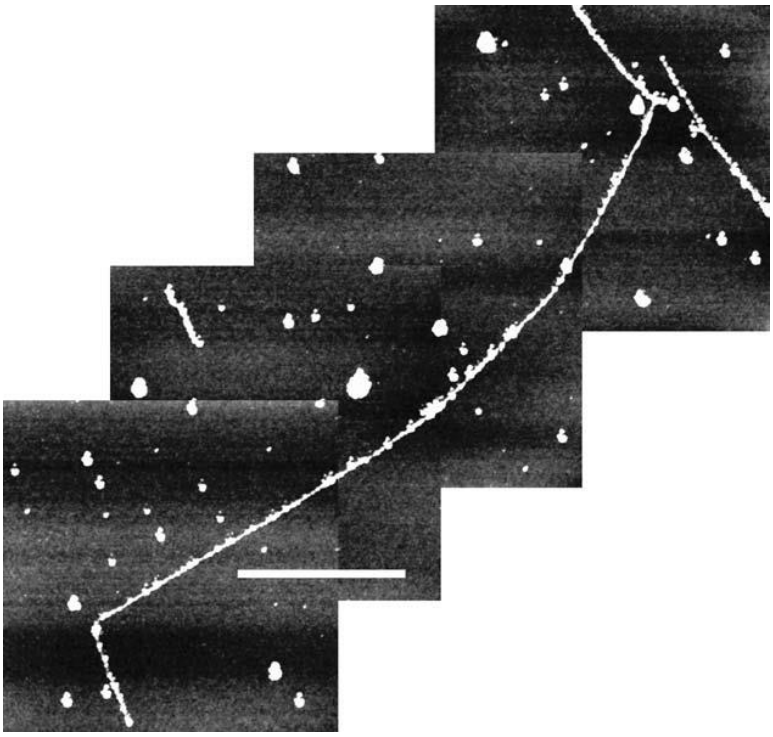

Figure 1.38: AFM height image of a DNA-templated copper nanostructure after a single $Cu(NO_3)_2$/ascorbic acid treatment, whereby Cu^{2+} was dissolved in DMSO. Scale bar= 1 µm, height scale= 5 nm. Figure from reference [140]

The 'nucleation and growth' mechanism by which metallisation of DNA occurs has been exploited by other groups as an alternative approach to metal nanowire formation. These routes specifically take advantage of the 'seeding' aspect of the mechanism whereby the growth of metal particles on the template act to catalyse the further growth of a second metal; so-called heteroatom seeding. Kudo et al[154] developed a heteroatom seeding approach for DNA-templating, analogous to that of the Damascene process used for growing copper interconnect. In Kudo's method, DNA was first 'activated' by growth of a palladium seed layer, followed by metallisation with copper in an

electroless plating bath containing $CuSO_4$, sodium potassium tartrate, NaOH and HCHO. In this method the use of a seeded surface was thought to encourage increased copper deposition. Indeed this process led to extensive deposition of copper along the DNA/Pd nanostructure. Figure 1.39 shows an AFM image of a single copper metallised DNA/Pd nanostructure. Individual metal clusters are clearly discernible and are continuous in coverage along the template. Furthermore Kudo's group was able to demonstrate precise control over structure size by variation of the plating-time. An average plating rate of ~0.75 nm/s for 30 seconds gave nanostructure diameters of ~30 nm. Again however, these studies lack chemical and electrical analysis. Such data may provide crucial evidence for progress in this field and the subsequent implementation of these methods in future electronics manufacturing.

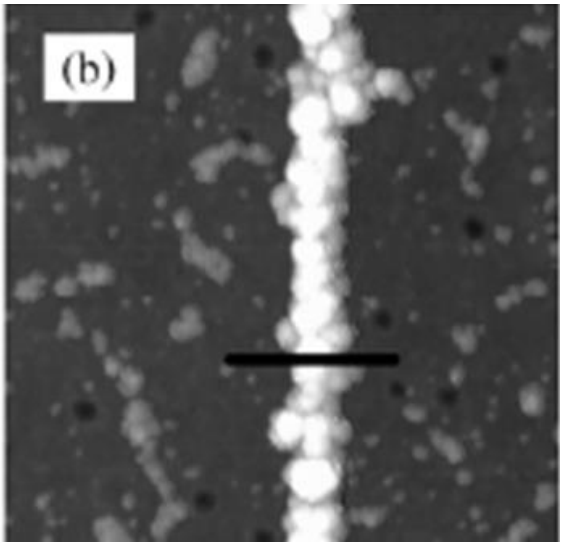

Figure 1.39: AFM height image of a DNA molecule after palladium activation/copper electroless deposition. Image area= 500 nm^2, Height scale= 22.6 nm. Figure from reference [154]

More recently, our group has reported on a similar method to Woolley's, for investigations into the fabrication of highly conductive DNA-templated copper nanowires.[152] In this method, DNA was immobilised onto a TMS-modified Si/SiO_2 substrate by means of molecular combing. $Cu(NO_3)_2$ was used to dope the template with Cu^{2+} ions and ascorbic acid to reduce these to the zero-valent metal. Figure 1.40 shows a scheme for this process. These studies provide comprehensive structural, chemical and electrical characterisations of the resulting material. The coatings consisted of pure metallic copper and showed no signs of oxidation as revealed by X-ray Photoelectron Spectroscopy (XPS) and powder X-ray Diffraction (XRD) studies.

Although the coverage can be described as continuous by means of AFM, the morphology was highly granular in appearance (see AFM image, figure 1.41). It was determined that the resulting structures resembled a so-called 'beads-on-a-string' motif as opposed to a single copper coating on DNA. A detailed statistical analysis of the materials' size revealed a peak modal range of 3.0-5.5 nm. An additional issue associated with this method is the extensive amount of non-specific deposition. Evidence for this is seen in figure 1.41, where metal particles are observed to deposit of on the substrate background.

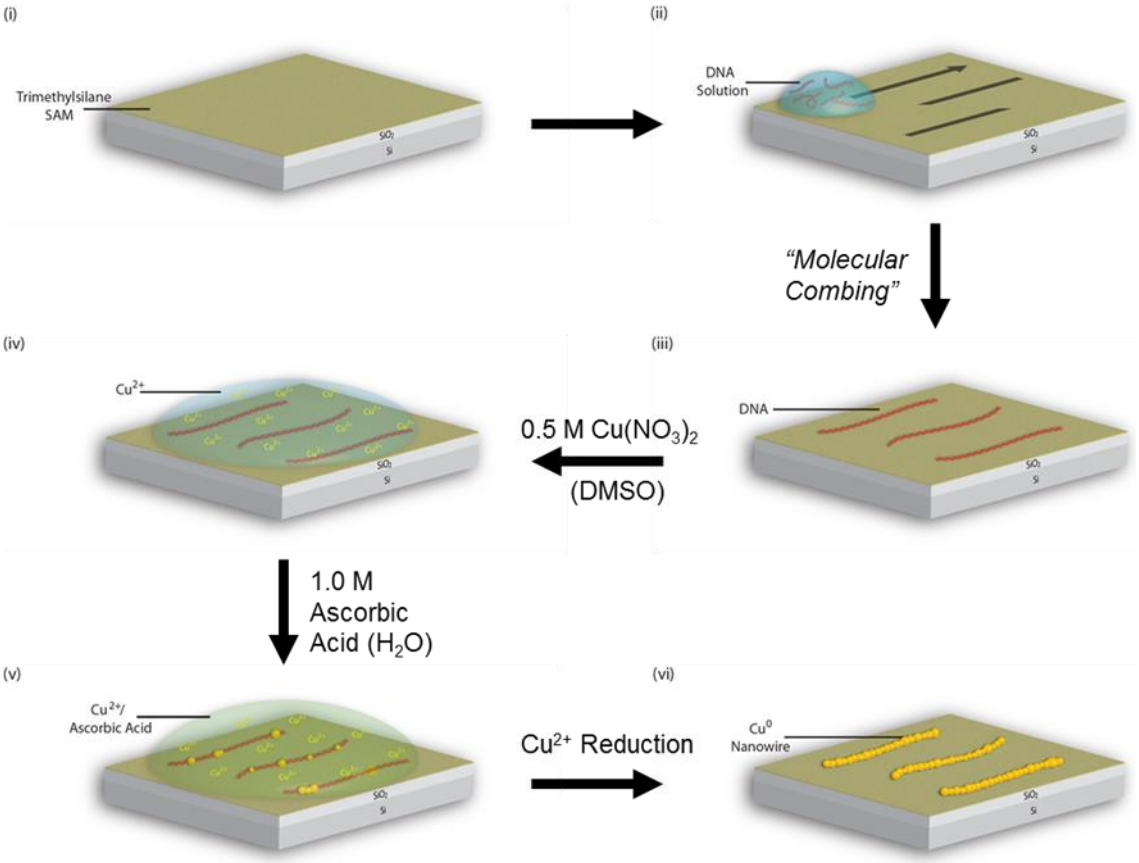

Figure 1.40: Schematic illustrating the procedure for preparing DNA-copper nanowires on silicon wafers: (i) Si/SiO_2 surface is modified with trimethylsilane SAM, (ii) a solution of DNA is pipetted onto the substrate and combed across the surface, (iii) DNA molecules are immobilised and aligned on the substrate, (iv) the DNA-immobilised substrate is treated with Cu^{2+} ions, (v) DNA/Cu^{2+} is reduced to the zero-valent metal with ascorbic acid and finally (vi) copper nanowires are formed following incubation

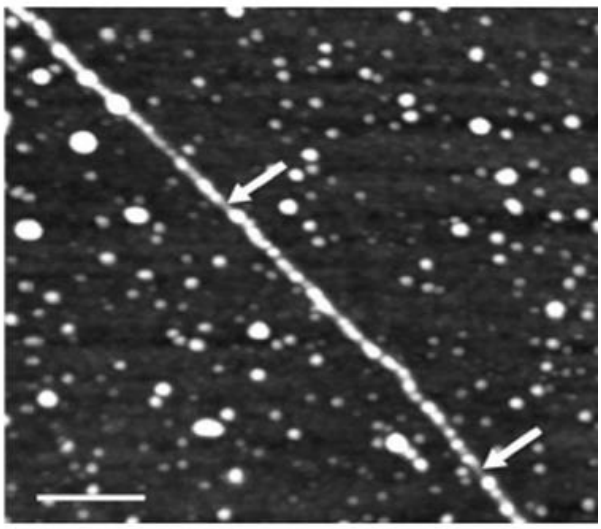

Figure 1.41: AFM height image of a copper nanostructure formed by the reduction of $Cu(NO_3)_2$/DMSO with ascorbic acid on surface immobilised-DNA. The image reveals an extended chain of particles deposited along the template. The arrows highlight regions on the DNA where less substantial Cu^0 deposition has taken place. Scale bar = 200 nm, height scale = 8 nm. Figure from reference [152]

Most significantly however, investigation of the electrical properties, using Electrostatic Force Microscopy (EFM), a non-contact method for mapping electrostatic interactions- explained in chapter 2, revealed that these structures carry negligible current and are highly resistive. This was attributed to the small lateral dimensions of the nanostructures and significant electron scattering at interparticle boundaries.

1.6. Challenges and Project Aims

In light of these previous studies it is apparent that a number of issues need to be addressed, with regards to the formation of smooth and conductive DNA-Cu nanowires. Namely, an improvement in the morphology of the copper coatings is paramount. As has been highlighted in this introduction, many of these molecular-templating methods for the growth of copper nanostructures produce granular coatings akin to a 'beads-on-a-string' appearance. The granular nature of the copper coatings may cause reduction in nanowire conductivity, where the effects of grain boundary electron scattering are likely to become significant, causing high resistance along these structures.[38] In fact the DNA-templating of metals in a general sense has proved problematic in this field of study, especially when compared to those of DNA-templated polymers, which afford much smoother morphologies and are often conductive.[155, 156] The prospect of producing highly continuous and smooth metal structures, via the DNA-templating approach, is an on-going challenge.

It is reasoned here that the 'beads on a string' composite may be in part due to the choice of solvent system adopted for metallisation. Despite the use of DMSO for solubilisation of Cu^{2+} in Woolley's and Watson respective methods, the reducing agent (ascorbic acid) is dissolved in water. Therefore, the reaction scheme employed in those studies is not entirely non-aqueous. By way of utilising non-aqueous reaction conditions, an enhancement of interaction of copper ions with DNA may result, and lead to denser populations of metal particles along the template. Moreover, selective metallisation of the DNA template needs to be enhanced so that the non-specific deposition of copper is minimised. The use of non-aqueous reaction conditions during metallisation of DNA may therefore facilitate more extensive metal coverage of the DNA template and smoother structure morphologies. This thesis attempts to develop such an approach by exploiting organic-based reaction conditions, for the fabrication of smooth DNA-Cu nanowires.

Another aim of this project is to explore the alternative, solution-phase, two-step chemical approach to metallisation of DNA. To the best of our knowledge the solution-phase synthesis of DNA-templated copper nanowires has not yet been attempted. The results from these studies could give insight into the fundamental differences between surface and solution based syntheses in terms of the principles of metal growth at DNA-templates and their resulting properties.

This project is also dedicated to the chemical passivation of DNA-Cu nanowires based on thiol self-assembly. It is well known that copper is easily oxidised under ambient atmospheric conditions,[73] and so passivation of these nanostructures against atmospheric corrosion may become a necessity for future nanoelectronic manufacturing.

If the problems mentioned above can be suitably addressed, namely by optimisation of the reaction conditions, then the DNA-templating of metal nanowires could be better suited to replacing current top-down methods for copper interconnect fabrication than the, other, competing methods described in section 1.3. This thesis is concerned with the development of new approaches towards the formation of smooth and conductive DNA-templated copper nanowires. We aim to demonstrate these electrical properties by integration of a DNA-Cu nanowire in a working two-terminal device.

We also aim to provide comprehensive structural, chemical and electrical analysis of these products, which has been somewhat lacking in previous reports. Each chapter in this thesis describes a unique approach to copper nanowires based on a DNA-templating strategy. Throughout this project a range of techniques were used to characterise the nanostructures. In each separate study we first describe how these structures are formed before the chemical composition of the material is elucidated using X-ray Photoelectron Spectroscopy (XPS) and powder X-ray Diffraction (XRD). An in-depth structural analysis is then carried out using AFM for examination of the structure morphology. FTIR was used to study the interaction of copper with DNA. And lastly the electrical properties of the nanostructures were examined using Scanning Conductance Microscopy (SCM).

1.7. References

1. D. Philp and J. Fraser Stoddart, Self-Assembly in natural and unnatural systems. *Angewandte Chemie (International Edition in English)*, 1996, **35**, 1154-1196.
2. ISO/TS27687:2008, Nanotechnologies-Terminology and definitions for nano-objects-Nanoparticle, nanofibre and nanoplate. available at http://www.iso.org/iso/catalogue_detail?csnumber=44278.
3. G. Cao, Nanostructures and Nanomaterials- Synthesis, Properties and Applications (book). 2006.
4. G. M. Whitesides, J. P. Mathias and C. T. Seto, Molecular self-assembly and nanochemistry: A chemical strategy for the synthesis of nanostructures. *Science*, 1991, **254**, 1312-1319.
5. G. A. Ozin, Nanochemistry: Synthesis in diminishing dimensions. *Advanced Materials*, 1992, **4**, 612-649.
6. N. Wang, Y. Cai and R. Q. Zhang, Growth of nanowires. *Materials Science and Engineering R: Reports*, 2008, **60**, 1-51.
7. R. P. Feynman, There's plenty of room at the bottom. *Journal of Microelectromechanical Systems*, 1992, **1**, 60-66.
8. D. M. Eigler and E. K. Schweizer, Positioning single atoms with a scanning tunnelling microscope. *Nature*, 1990, **344**, 524-526.
9. G. H. Woehrle, M. G. Warner and J. E. Hutchison, Molecular-level control of feature separation in one-dimensional nanostructure assemblies formed by biomolecular nanolithography. *Langmuir*, 2004, **20**, 5982-5988.
10. J. Huang, F. Kim, A. R. Tao, S. Connor and P. Yang, Spontaneous formation of nanoparticle stripe patterns through dewetting. *Nature materials.*, 2005, **4**, 896-900.
11. H. Weller, Colloidal semiconductor Q-particles: Chemistry in the transition region between solid state and molecules. *Angewandte Chemie (International Edition in English)*, 1993, **32**, 41-53.
12. M. G. Bawendi, M. L. Steigerwald and L. E. Brus, The quantum mechanics of larger semiconductor clusters ("Quantum dots"). *Annual Review of Physical Chemistry*, 1990, **41**, 477-496.
13. X. Peng, L. Manna, W. Yang, J. Wickham, E. Scher, A. Kadavanich and A. P. Alivisatos, Shape control of CdSe nanocrystals. *Nature*, 2000, **404**, 59-61.
14. D. Josell, S. H. Brongersma and Z. Tokei, Editon edn., 2009, vol. 39, pp. 231-254.
15. X. Zhao, C. M. Wei, L. Yang and M. Y. Chou, Quantum confinement and electronic properties of silicon nanowires. *Physical Review Letters*, 2004, **92**, 236805-1.
16. W. Cheng, M. J. Campolongo, S. J. Tan and D. Luo, Freestanding ultrathin nano-membranes via self-assembly. *Nano Today*, 2009, **4**, 482-493.
17. A. P. Alivisatos, Semiconductor clusters, nanocrystals, and quantum dots. *Science*, 1996, **271**, 933-937.
18. E. Roduner, Size matters: Why nanomaterials are different. *Chemical Society Reviews*, 2006, **35**, 583-592.
19. S. C. Jain, M. Willander, J. Narayan and R. Van Overstraeten, III-nitrides: Growth, characterization, and properties. *Journal of Applied Physics*, 2000, **87**, 965-1006.
20. F. Qian, Y. Li, S. Gradečak, H. G. Park, Y. Dong, Y. Ding, Z. L. Wang and C. M. Lieber, Multi-quantum-well nanowire heterostructures for wavelength-controlled lasers. *Nature Materials*, 2008, **7**, 701-706.
21. J. Heremans, C. M. Thrush, Y. M. Lin, S. Cronin, Z. Zhang, M. S. Dresselhaus and J. F. Mansfield, Bismuth nanowire arrays: Synthesis and galvanomagnetic properties. *Physical Review B - Condensed Matter and Materials Physics*, 2000, **61**, 2921-2930.
22. Iii, B. Xu, Z. G. Wang, Y. H. Chen, P. Jin, X. L. Ye and F. Q. Liu, in *Materials Science Forum*, eds. Z. Zhong, H. Saka, T. H. Kim, E. A. Holm, Y. Han and X. Xie, Beijing, Editon edn., 2005, vol. 475-479, pp. 1783-1786.

23. D. I. Gittins, D. Bethell, D. J. Schiffrin and R. J. Nichols, A nanometre-scale electronic switch consisting of a metal cluster and redox-addressable groups. *Nature*, 2000, **408**, 67-69.
24. Y. Chen, G. Y. Jung, D. A. A. Ohlberg, X. Li, D. R. Stewart, J. O. Jeppesen, K. A. Nielsen, J. F. Stoddart and R. S. Williams, Nanoscale molecular-switch crossbar circuits. *Nanotechnology*, 2003, **14**, 462-468.
25. P. Buffat and J. P. Borel, Size effect on the melting temperature of gold particles. *Physical Review A*, 1976, **13**, 2287-2298.
26. C. B. Murray, C. R. Kagan and M. G. Bawendi, Synthesis and characterization of monodisperse nanocrystals and close-packed nanocrystal assemblies. *Annual Review of Materials Science*, 2000, **30**, 545-610.
27. *http://www.itrs.net/, ITRS Roadmap*, http://www.itrs.net/.
28. P. S. Peercy, The drive to miniaturization. *Nature*, 2000, **406**, 1023-1026.
29. G. E. Moore, Cramming more components onto integrated circuits. *Proceedings of the IEEE*, 1998, **86**, 82-85.
30. R. R. Schaller, Moore's law: past, present, and future. *IEEE Spectrum*, 1997, **34**, 52-55, 57.
31. R. W. Keyes, Fundamental limits of silicon technology. *Proceedings of the IEEE*, 2001, **89**, 227-239.
32. M. Lane, R. H. Dauskardt, N. Krishna and I. Hashim, Adhesion and reliability of copper interconnects with Ta and TaN barrier layers. *Journal of Materials Research*, 2000, **15**, 203-211.
33. S. Strehle, J. W. Bartha and K. Wetzig, Electrical properties of electroplated Cu(Ag) thin films. *Thin Solid Films*, 2009, **517**, 3320-3325.
34. T. H. Kim, X. G. Zhang, D. M. Nicholson, B. M. Evans, N. S. Kulkarni, B. Radhakrishnan, E. A. Kenik and A. P. Li, Large discrete resistance jump at grain boundary in copper nanowire. *Nano Letters*, 2010, **10**, 3096-3100.
35. A. Bid, A. Bora and A. K. Raychaudhuri, Temperature dependence of the resistance of metallic nanowires of diameter $\geqslant$15nm: Applicability of Bloch-Grüneisen theorem. *Physical Review B*, 2006, **74**, 035426.
36. W. C. Thomas and M. E. Toimil-Molares, *Finite- and Quantum-Size Effects of Bismuth Nanowires*, 2010.
37. L. M. Gignac, C. K. Hu, B. Herbst and B. C. Baker-O'Neal, Tokyo, 2008.
38. R. L. Graham, G. B. Alers, T. Mountsier, N. Shamma, S. Dhuey, S. Cabrini, R. H. Geiss, D. T. Read and S. Peddeti, Resistivity dominated by surface scattering in sub-50 nm Cu wires. *Applied Physics Letters*, **96**.
39. G. Schindler, G. Steinlesberger, M. Engelhardt and W. Steinhögl, Electrical characterization of copper interconnects with end-of-roadmap feature sizes. *Solid-State Electronics*, 2003, **47**, 1233-1236.
40. S. R. Wilson, C. J. Tracy and J. L. Freeman, Jr., William Andrew Publishing/Noyes, Editon edn., 1993.
41. D. Edelstein, J. Heidenreich, R. Goldblatt, W. Cote, C. Uzoh, N. Lustig, P. Roper, T. McDevitt, W. Motsiff, A. Simon, J. Dukovic, R. Wachnik, H. Rathore, R. Schulz and L. Su, *Proceedings of the IEEE Hong Kong Electron Devices Meeting*, Washington, DC, USA, 1997.
42. P. C. Andricacos, C. Uzoh, J. O. Dukovic, J. Horkans and H. Deligianni, Damascene copper electroplating for chip interconnections. *IBM Journal of Research and Development*, 1998, **42**, 567-573.
43. S. Miura and H. Honma, Advanced copper electroplating for application of electronics. *Surface and Coatings Technology*, 2003, **169–170**, 91-95.
44. P. B. Zantye, A. Kumar and A. K. Sikder, Chemical mechanical planarization for microelectronics applications. *Materials Science and Engineering: R: Reports*, 2004, **45**, 89-220.

45. B. Päivänranta, A. Langner, E. Kirk, C. David and Y. Ekinci, Sub-10 nm patterning using EUV interference lithography. *Nanotechnology*, 2011, **22**.
46. Y. Cui and C. M. Lieber, Functional nanoscale electronic devices assembled using silicon nanowire building blocks. *Science*, 2001, **291**, 851-853.
47. C. M. Lieber, Nanoscale science and technology: Building a big future from small things. *MRS Bulletin*, 2003, **28**, 486-491.
48. W. Lu and C. M. Lieber, Nanoelectronics from the bottom up. *Nature Materials*, 2007, **6**, 841-850.
49. Y. Huang, X. Duan, Y. Cui, L. J. Lauhon, K. H. Kim and C. M. Lieber, Logic gates and computation from assembled nanowire building blocks. *Science*, 2001, **294**, 1313-1317.
50. G. Yu and C. M. Lieber, Assembly and integration of semiconductor nanowires for functional nanosystems. *Pure and Applied Chemistry*, 2010, **82**, 2295-2314.
51. Z. Deng and C. Mao, DNA-Templated Fabrication of 1D Parallel and 2D Crossed Metallic Nanowire Arrays. *Nano Letters*, 2003, **3**, 1545-1548.
52. Y. Wu, J. Xiang, C. Yang, W. Lu and C. M. Lieber, Single-crystal metallic nanowires and metal/semiconductor nanowire heterostructures. *Nature*, 2004, **430**, 61-65.
53. T. Scheibel, R. Parthasarathy, G. Sawicki, X. M. Lin, H. Jaeger and S. L. Lindquist, Conducting nanowires built by controlled self-assembly of amyloid fibers and selective metal deposition. *Proceedings of the National Academy of Sciences of the United States of America*, 2003, **100**, 4527-4532.
54. E. Braun, Y. Eichen, U. Sivan and G. Ben-Yoseph, DNA-templated assembly and electrode attachment of a conducting silver wire. *Nature*, 1998, **391**, 775-778.
55. J. Richter, M. Mertig, W. Pompe, I. MÃ¶nch and H. K. Schackert, Construction of highly conductive nanowires on a DNA template. *Applied Physics Letters*, 2001, **78**, 536-538.
56. Y. Zhang and Z. Yan, Synthesis, properties and applications of copper nanowires. *Shiyou Huagong/Petrochemical Technology*, 2009, **38**, 1031-1037.
57. M. Mohl, P. Pusztai, A. Kukovecz, Z. Konya, J. Kukkola, K. Kordas, R. Vajtai and P. M. Ajayan, Low-temperature large-scale synthesis and electrical testing of ultralong copper nanowires. *Langmuir*, 2010, **26**, 16496-16502.
58. B. Gates, B. Mayers, B. Cattle and Y. Xia, Synthesis and characterization of uniform nanowires of trigonal selenium. *Advanced Functional Materials*, 2002, **12**, 219-227.
59. Y. Asano, K. Nakaoka, K. Murashiro, T. Komatsu and K. Hoshino, Template-free electrochemical preparation of dendritic copper nanowire and its capacitor properties. *Materials Letters*, 2012, **81**, 162-164.
60. Q. C. Chen, Preparation of copper nanorods and nanowires by hydrothermal reduction. *Xiandai Huagong/Modern Chemical Industry*, 2005, **25**, 43-44.
61. A. R. Rathmell, S. M. Bergin, Y. L. Hua, Z. Y. Li and B. J. Wiley, The growth mechanism of copper nanowires and their properties in flexible, transparent conducting films. *Advanced Materials*, 2010, **22**, 3558-3563.
62. D. Zhang, R. Wang, M. Wen, D. Weng, X. Cui, J. Sun, H. Li and Y. Lu, Synthesis of ultralong copper nanowires for high-performance transparent electrodes. *Journal of the American Chemical Society*, 2012, **134**, 14283-14286.
63. Y. Zhao, Y. Zhang, Y. Li, Z. He and Z. Yan, Rapid and large-scale synthesis of Cu nanowires via a continuous flow solvothermal process and its application in dye-sensitized solar cells (DSSCs). *RSC Advances*, 2012, **2**, 11544-11551.
64. C. C. Koch, William Andrew Publishing, Editon edn., pp. 18-19.
65. Y. Zhao, Y. Zhang, Y. Li and Z. Yan, Soft synthesis of single-crystal copper nanowires of various scales. *New Journal of Chemistry*, 2012, **36**, 130-138.
66. H. K. Kim, J. A. Jeong, I. K. Yoo, J. B. Koo, H. H. Lee, K. H. Hur, D. H. Kim, S. E. Kim and B. H. Jun, Rapid thermal reduction of inkjet printed Cu interconnects on glass substrate. *Electrochemical and Solid-State Letters*, 2011, **14**, J65-J68.

67. Z. Liu and Y. Bando, A novel method for preparing copper nanorods and nanowires. *Advanced Materials*, 2003, **15**, 303-305.
68. G. Kwon, H. Chu, J. Yoo, H. Kim, C. Han, C. Chung, J. Lee and H. Lee, Fabrication of uniform and high resolution copper nanowire using intermediate self-assembled monolayers through direct AFM lithography. *Nanotechnology*, 2012, **23**.
69. G. Steinlesberger, M. Engelhardt, G. Schindler, W. Steinhögl, A. Von Glasow, K. Mosig and E. Bertagnolli, Electrical assessment of copper damascene interconnects down to sub-50 nm feature sizes. *Microelectronic Engineering*, 2002, **64**, 409-416.
70. C. R. Martin, Nanomaterials: A membrane-based synthetic approach. *Science*, 1994, **266**, 1961-1966.
71. C. J. Brumlik, V. P. Menon and C. R. Martin, Template synthesis of metal microtubule ensembles utilizing chemical, electrochemical, and vacuum deposition techniques. *Journal of Materials Research*, 1994, **9**, 1174-1183.
72. T. R. Kline, M. Tian, J. Wang, A. Sen, M. W. H. Chan and T. E. Mallouk, Template-grown metal nanowires. *Inorganic Chemistry*, 2006, **45**, 7555-7565.
73. M. E. Toimil Molares, E. M. Höhberger, C. Schaeflein, R. H. Blick, R. Neumann and C. Trautmann, Electrical characterization of electrochemically grown single copper nanowires. *Applied Physics Letters*, 2003, **82**, 2139-2141.
74. M. E. Toimil Molares, V. Buschmann, D. Dobrev, R. Neumann, R. Scholz, I. U. Schuchert and J. Vetter, Single-crystalline copper nanowires produced by electrochemical deposition in polymeric ion track membranes. *Advanced Materials*, 2001, **13**, 62-65.
75. J. Feliciano and M. M. Martínez-Iñesta, Synthesis and characterization of Pd, Cu, and Ag nanowires in anodic alumina membranes using solid state reduction. *Materials Letters*, 2012, **82**, 211-213.
76. T. Gao, G. W. Meng, J. Zhang, Y. W. Wang, C. H. Liang, J. C. Fan and L. D. Zhang, Template synthesis of single-crystal Cu nanowire arrays by electrodeposition. *Applied Physics A: Materials Science and Processing*, 2001, **73**, 251-254.
77. L. Zhou, K. Du, J. Xiao, W. Zhang, X. B. Wan and Y. Fang, Synthesis of Cu nanowire array by DC electrodeposition. *Yuanzineng Kexue Jishu/Atomic Energy Science and Technology*, 2008, **42**, 769-772.
78. G. Sharma, V. Kripesh, M. C. Sim and C. H. Sow, Synthesis and characterization of patterned and nonpatterned copper and nickel nanowire arrays on silicon substrate. *Sensors and Actuators, A: Physical*, 2007, **139**, 272-280.
79. H. S. Virk, K. Kishore and V. Balouria, Fabrication of copper nanowires by electrodeposition using Anodic Alumina and polymer templates. *Journal of Nano Research*, 2010, **10**, 63-67.
80. K. J. Ziegler, P. A. Harrington, K. M. Ryan, T. Crowley, J. D. Holmes and M. A. Morris, Supercritical fluid preparation of copper nanotubes and nanowires using mesoporous templates. *Journal of Physics Condensed Matter*, 2003, **15**, 8303-8314.
81. Y. Zhang, F. L. Y. Lam, X. Hu, Z. Yan and P. Sheng, Fabrication of copper nanowire encapsulated in the pore channels of SBA-15 by metal organic chemical vapor deposition. *Journal of Physical Chemistry C*, 2007, **111**, 12536-12541.
82. T. Gao, G. Meng, Y. Wang, S. Sun and L. Zhang, Electrochemical synthesis of copper nanowires. *Journal of Physics Condensed Matter*, 2002, **14**, 355-363.
83. G. Cao and D. Liu, Template-based synthesis of nanorod, nanowire, and nanotube arrays. *Advances in Colloid and Interface Science*, 2008, **136**, 45-64.
84. A. Bid, A. Bora and A. K. Raychaudhuri, Temperature dependence of the resistance of metallic nanowires of diameter >= 15 nm: Applicability of Bloch-Gruneisen theorem (vol 74, pg 035426, 2006). *Physical Review B*, 2006, **74**.
85. G. G. Wildgoose, C. E. Banks and R. G. Compton, Metal nanoparticles and related materials supported on Carbon nanotubes: Methods and applications. *Small*, 2006, **2**, 182-193.

86. S. Padalkar, J. R. Capadona, S. J. Rowan, C. Weder, Y. H. Won, L. A. Stanciu and R. J. Moon, Natural biopolymers: Novel templates for the synthesis of nanostructures. *Langmuir*, 2010, **26**, 8497-8502.
87. K. Keren, R. S. Berman, E. Buchstab, U. Sivan and E. Braun, DNA-Templated Carbon Nanotube Field-Effect Transistor. *Science*, 2003, **302**, 1380-1382.
88. E. Gazit, Use of biomolecular templates for the fabrication of metal nanowires. *FEBS Journal*, 2007, **274**, 317-322.
89. Y. Zhou, Recent progress in biomolecule-templated nanomaterials. *Current Nanoscience*, 2006, **2**, 123-134.
90. A. A. Zinchenko, Templating of inorganic nanomaterials by biomacromolecules and their assemblies. *Polymer Science - Series C*, 2012, **54**, 80-87.
91. J. M. Schnur, R. Price, P. Schoen, P. Yager, J. M. Calvert, J. Georger and A. Singh, Lipid-based tubule microstructures. *Thin Solid Films*, 1987, **152**, 181-206.
92. M. Knez, A. M. Bittner, F. Boes, C. Wege, H. Jeske, E. Maiß and K. Kern, Biotemplate synthesis of 3-nm nickel and cobalt nanowires. *Nano Letters*, 2003, **3**, 1079-1082.
93. M. Knez, M. Sumser, A. M. Bittner, C. Wege, H. Jeske, T. P. Martin and K. Kern, Spatially Selective Nucleation of Metal Clusters on the Tobacco Mosaic Virus. *Advanced Functional Materials*, 2004, **14**, 116-124.
94. F. A. Aldaye, A. L. Palmer and H. F. Sleiman, Assembling materials with DNA as the guide. *Science*, 2008, **321**, 1795-1799.
95. Q. Gu, C. Cheng, R. Gonela, S. Suryanarayanan, S. Anabathula, K. Dai and D. T. Haynie, DNA nanowire fabrication. *Nanotechnology*, 2006, **17**.
96. N. C. Seeman, DNA in a material world. *Nature*, 2003, **421**, 427-431.
97. N. C. Seeman, Editon edn., 2010, vol. 79, pp. 65-87.
98. P. W. K. Rothemund, Folding DNA to create nanoscale shapes and patterns. *Nature*, 2006, **440**, 297-302.
99. H. A. Becerril, R. M. Stoltenberg, D. R. Wheeler, R. C. Davis, J. N. Harb and A. T. Woolley, DNA-templated three-branched nanostructures for nanoelectronic devices. *Journal of the American Chemical Society*, 2005, **127**, 2828-2829.
100. J. Liu, Y. Geng, E. Pound, S. Gyawali, J. R. Ashton, J. Hickey, A. T. Woolley and J. N. Harb, Metallization of branched DNA origami for nanoelectronic circuit fabrication. *ACS Nano*, 2011, **5**, 2240-2247.
101. A. P. Alivisatos, K. P. Johnsson, X. Peng, T. E. Wilson, C. J. Loweth, M. P. Bruchez Jr and P. G. Schultz, Organization of 'nanocrystal molecules' using DNA. *Nature*, 1996, **382**, 609-611.
102. S. H. Park, H. Yan, J. H. Reif, T. H. LaBean and G. Finkelstein, Electronic nanostructures templated on self-assembled DNA scaffolds. *Nanotechnology*, 2004, **15**, S525-S527.
103. D. Porath, A. Bezryadin, S. De Vries and C. Dekker, Direct measurement of electrical transport through DNA molecules. *Nature*, 2000, **403**, 635-638.
104. H. W. Fink and C. Schönenberger, Electrical conduction through DNA molecules. *Nature*, 1999, **398**, 407-410.
105. A. Houlton and S. M. D. Watson, DNA-based nanowires. Towards bottom-up nanoscale electronics. *Annual Reports on the Progress of Chemistry - Section A*, 2011, **107**, 21-42.
106. J. D. Watson and F. H. C. Crick, Molecular structure of nucleic acids: A structure for deoxyribose nucleic acid. *Nature*, 1953, **171**, 737-738.
107. B. Lippert, Multiplicity of metal ion binding patterns to nucleobases. *Coordination Chemistry Reviews*, 2000, **200–202**, 487-516.
108. K. Aoki, X-ray evidence for the metal ion bridged intra- and intermolecular stacking interactions between nucleotide bases and aromatic heterocyclic rings within the ternary complex [Cu(5'-AMP)(bpy)(H2O)]2.(NO3)2.6H2O. *Journal of the American Chemical Society*, 1978, **100**, 7106-7108.

109. H. Arakawa, R. Ahmad, M. Naoui and H. A. Tajmir-Riahi, A comparative study of calf thymus DNA binding to Cr(III) and Cr(VI) ions. Evidence for the guanine N-7-chromium-phosphate chelate formation. *Journal of Biological Chemistry*, 2000, **275**, 10150-10153.
110. I. Bertini, Bioinorganic chemistry. *University Science Books*, 1994.
111. R. K. O. Sigel and B. Lippert, PtII coordination to guanine-N7: enhancement of the stability of the Watson-Crick base pair with cytosine. *Chemical Communications*, 1999, **0**, 2167-2168.
112. V. A. Bloomfield, Condensation of DNA by multivalent cations: Considerations on mechanism. *Biopolymers*, 1991, **31**, 1471-1481.
113. J. Widom and R. L. Baldwin, Cation-induced toroidal condensation of DNA: Studies with Co3+(NH3)6. *Journal of Molecular Biology*, 1980, **144**, 431-453.
114. J. Duguid, V. A. Bloomfield, J. Benevides and G. J. Thomas Jr, Raman spectroscopy of DNA-metal complexes. I. Interactions and conformational effects of the divalent cations: Mg, Ca, Sr, Ba, Mn, Co, Ni, Cu, Pd, and Cd. *Biophysical Journal*, 1993, **65**, 1916-1928.
115. J. G. Duguid and V. A. Bloomfield, Aggregation of melted DNA by divalent metal ion-mediated cross-linking. *Biophysical Journal*, 1995, **69**, 2642-2648.
116. C. Price, Metal-nucleobase complexes : building blocks for supramolecular chemistry (thesis). *University of Newcastle upon-Tyne*, 1998.
117. T. G. Spiro, Nucleic acid—metal ion interactions *Biochemical Education*, 1982, **10**, 36-36.
118. H. A. Tajmir-Riahi, M. Naoui and R. Ahmad, The effects of Cu 2+ and Pb 2+ on the solution structure of calf thymus DNA: DNA condensation and denaturation studied by Fourier Transform ir difference spectroscopy. *Biopolymers*, 1993, **33**, 1819-1827.
119. G. L. Eichhorn and Y. A. Shin, Interaction of metal ions with polynucleotides and related compounds. XII. The relative effect of various metal ions on DNA helicity. *Journal of the American Chemical Society*, 1968, **90**, 7323-7328.
120. K. Aoki and H. Yamazaki, Crystal Structures of Aromatic Diamine-Cu(II)-Nucleotide Ternary Complexes, Bis[(adenosine 51-monophosphate)(1, 10-phenanthroline)aquacopper(II)] Nitrate Octahydrate, Bis[(aguanosine 5'-monophosphate)(di-2pyridylamine)aquacopper(II)] Trihydrate, and Bis[(uridine 2'deoxy-5'-monophosphate)(di-2-pyridylamine)-aquacopper(II)] Pentahydrate, as a Model for Enzyme-Metal Ion-Nucleotide Interac tions. *NIPPON KAGAKU KAISHI*, 1988, **1988**, 611-620.
121. N. S. Begum and H. Manohar, Unusual ribose conformation in a ternary copper(II) 2[prime or minute]deoxyribonucleotide complex. *Journal of the Chemical Society, Dalton Transactions*, 1992, **0**, 2277-2281.
122. K. Aoki, X-Ray crystal structures of the ternary complexes [Cd(5[prime or minute]-UMP)(dpa)(H2O)2](5[prime or minute]-UMP[double bond, length as m-dash]uridine 5[prime or minute]-phosphate, dpa[double bond, length as m-dash]2,2[prime or minute]-dipyridylamine): metal ion bridged stacking between nucleotide bases and aromatic amine rings, and [Cu(5[prime or minute]-CMP)(dpa)(H2O)]2(5[prime or minute]-CMP[double bond, length as m-dash]cytidine 5[prime or minute]-phosphate): phosphate only metal bonding. *Journal of the Chemical Society, Chemical Communications*, 1979, **0**, 589-591.
123. V. Andrushchenko, J. H. Van De Sande and H. Wieser, Vibrational circular dichroism and IR absorption of DNA complexes with Cu2+ ions. *Biopolymers - Biospectroscopy Section*, 2003, **72**, 374-390.
124. B. de Castro, T. J. Kistenmacher and L. G. Marzilli, Platinum interactions with nucleic acids: insights from model compounds. *Agents and Actions Supplements*, 1981, **8**, 435-464.

125. E. Sletten and N. Flogstad, Crystallographic studies on metal-nucleotide base complexes. VII. Di-9-methylguaninetriaquacopper(II) sulphate trihydrate. *Acta Crystallographica Section B*, 1976, **32**, 461-466.
126. T. F. Kagawa, B. H. Geierstanger, A. H. J. Wang and P. Shing Ho, Covalent modification of guanine bases in double-stranded DNA: The 1.2-Å Z-DNA structure of d(CGCGCG) in the presence of CuC12. *Journal of Biological Chemistry*, 1991, **266**, 20175-20184.
127. J. M. Malinge and M. Leng, *B. Lippert (Ed.), Cisplatin: Chemistry and Biochemistry of a Leading Anticancer Drug, VHCA Zurich and Wiley-VCH Weinheim*, 1999.
128. S. Das, C. Madhavaiah, S. Verma and P. K. Bharadwaj, A reusable zigzag copper(II) coordination polymer with bio-essential constituents as a facile DNA scission agent. *Inorganica Chimica Acta*, 2005, **358**, 3236-3240.
129. M. J. Sánchez-Moreno, D. Choquesillo-Lazarte, J. M. González-Pérez, R. Carballo, A. Castiñeiras and J. Niclós-Gutiérrez, Inter-ligand interactions and the selective formation of the unusual metal–N3(adenine) bond in ternary copper(II) complexes with N-benzyliminodiacetato(2−) ligands. *Inorganic Chemistry Communications*, 2002, **5**, 800-802.
130. T. F. Mastropietro, D. Armentano, E. Grisolia, C. Zanchini, F. Lloret, M. Julve and G. De Munno, Guanine-containing copper(ii) complexes: synthesis, X-ray structures and magnetic properties. *Dalton Transactions*, 2008, **0**, 514-520.
131. L. Li, N. N. Murthy, J. Telser, L. N. Zakharov, G. P. A. Yap, A. L. Rheingold, K. D. Karlin and S. E. Rokita, Targeted Guanine Oxidation by a Dinuclear Copper(II) Complex at Single Stranded/Double Stranded DNA Junctions. *Inorganic Chemistry*, 2006, **45**, 7144-7159.
132. D. J. Szalda, L. G. Marzilli and T. J. Kistenmacher, Dipeptide-metal-nucleoside complexes as models for enzyme-metal-nucleic acid ternary species. synthesis and molecular structure of the cytidine complex of glycylglycinatocopper(II). *Biochemical and Biophysical Research Communications*, 1975, **63**, 601-605.
133. J. Anastassopoulou, Metal-DNA interactions. *Journal of Molecular Structure*, 2003, **651-653**, 19-26.
134. W. S. Sheldrick, *Z. Naturforsch., B:Chem.Sci*, 1983, **38**, 16.
135. C. A. Mirkin, R. L. Letsinger, R. C. Mucic and J. J. Storhoff, A DNA-based method for rationally assembling nanoparticles into macroscopic materials. *Nature*, 1996, **382**, 607-609.
136. J. Richter, R. Seidel, R. Kirsch, M. Mertig, W. Pompe, J. Plaschke and H. K. Schackert, Nanoscale palladium metallization of DNA. *Advanced Materials*, 2000, **12**, 507-510.
137. K. Keren, M. Krueger, R. Gilad, G. Ben-Yoseph, U. Sivan and E. Braun, Sequence-specific molecular lithography on single DNA molecules. *Science*, 2002, **297**, 72-75.
138. L. Berti, A. Alessandrini and P. Facci, DNA-templated photoinduced silver deposition. *Journal of the American Chemical Society*, 2005, **127**, 11216-11217.
139. C. F. Monson and A. T. Woolley, DNA-templated construction of copper nanowires. *Nano Letters*, 2003, **3**, 359-363.
140. R. M. Stoltenberg and A. T. Woolley, DNA-templated nanowire fabrication. *Biomedical Microdevices*, 2004, **6**, 105-111.
141. H. A. Becerril, P. Ludtke, B. M. Willardson and A. T. Woolley, DNA-templated nickel nanostructures and protein assemblies. *Langmuir*, 2006, **22**, 10140-10144.
142. R. Seidel, L. C. Ciacchi, M. Weigel, W. Pompe and M. Mertig, Synthesis of platinum cluster chains on DNA templates: Conditions for a template-controlled cluster growth. *Journal of Physical Chemistry B*, 2004, **108**, 10801-10811.
143. T. Yonezawa, S. Y. Onoue and T. Kunitake, Formation of one-dimensional arrays of gold nanoparticles with DNA. *Kobunshi Ronbunshu*, 1999, **56**, 855-859.
144. Q. Gu, C. Cheng, R. Gonela, S. Suryanarayanan, S. Anabathula, K. Dai and D. T. Haynie, DNA nanowire fabrication. *Nanotechnology*, 2006, **17**, R14-R25.

145. L. Dong, T. Hollis, B. A. Connolly, N. G. Wright, B. R. Horrocks and A. Houlton, DNA-templated semiconductor nanoparticle chains and wires. *Advanced Materials*, 2007, **19**, 1748-1751.
146. D. Liqin, T. Hollis, S. Fishwick, B. A. Connolly, N. G. Wright, B. R. Horrocks and A. Houlton, Synthesis, manipulation and conductivity of supramolecular polymer nanowires. *Chemistry - A European Journal*, 2007, **13**, 822-828.
147. K. Nguyen, M. Monteverde, A. Filoramo, L. Goux-Capes, S. Lyonnais, P. Jegou, P. Viel, M. Goffman and J. P. Bourgoin, Synthesis of thin and highly conductive DNA-based palladium nanowires. *Advanced Materials*, 2008, **20**, 1099-1104.
148. S. Kundu, K. Wang, D. Huitink and H. Liang, Photoinduced formation of electrically conductive thin palladium nanowires on DNA scaffolds. *Langmuir*, 2009, **25**, 10146-10152.
149. J. M. Schurr and S. B. Smith, Theory for the extension of a linear polyelectrolyte attached at one end in an electric field. *Biopolymers*, 1990, **29**, 1161-1165.
150. D. Bensimon, A. J. Simon, V. Croquette and A. Bensimon, Stretching DNA with a Receding Meniscus: Experiments and Models. *Physical Review Letters*, 1995, **74**, 4754-4757.
151. A. Bensimon, A. Simon, A. Chiffaudel, V. Croquette, F. Heslot and D. Bensimon, Alignment and sensitive detection of DNA by a moving interface. *Science*, 1994, **265**, 2096-2098.
152. S. M. D. Watson, N. G. Wright, B. R. Horrocks and A. Houlton, Preparation, Characterization and Scanned Conductance Microscopy Studies of DNA-Templated One-Dimensional Copper Nanostructures *Langmuir*, 2009.
153. J. Timper, K. Gutsmiedl, C. Wirges, J. Broda, M. Noyong, J. Mayer, T. Carell and U. Simon, Surface "click" reaction of DNA followed by directed metalization for the construction of contactable conducting nanostructures. *Angewandte Chemie - International Edition*, 2012, **51**, 7586-7588.
154. H. Kudo and M. Fujihira, DNA-templated copper nanowire fabrication by a two-step process involving electroless metallization. *IEEE Transactions on Nanotechnology*, 2006, **5**, 90-92.
155. S. Pruneanu, S. A. F. Al-Said, L. Dong, T. A. Hollis, M. A. Galindo, N. G. Wright, A. Houlton and B. R. Horrocks, Self-assembly of DNA-templated polypyrrole nanowires: Spontaneous formation of conductive nanoropes. *Advanced Functional Materials*, 2008, **18**, 2444-2454.
156. J. Hannant, J. H. Hedley, J. Pate, A. Walli, S. A. Farha Al-Said, M. A. Galindo, B. A. Connolly, B. R. Horrocks, A. Houlton and A. R. Pike, Modification of DNA-templated conductive polymer nanowires via click chemistry. *Chemical Communications*, 2010, **46**, 5870-5872.

Chapter 2: Analysis Techniques and Theory

This chapter describes some of the main techniques used for DNA-templated nanomaterials characterisation.

2.1. Scanning Probe Microscopy (SPM)

Scanning Probe Microscopy is a method used to acquire an image of a sample surface, by scanning a physical probe across it. SPM has contributed a large proportion of the experimental results presented in this research. These studies have been mainly concerned with the morphology and electrical characterization of nanowires. SPM encompasses a wide variety of specialised techniques for these purposes, such as Atomic Force Microscopy (AFM) for the analysis of structure morphology and sizes, Electrostatic Force Microscopy (EFM) for qualitative assessment of the conductive properties of nanowires and Conductive-AFM (c-AFM) for quantitative analysis of the conductance. This section provides an introduction to the principles of these techniques.

Processing of data acquired from SPM experiments was carried out using both Nanoscope version 7.00b19 (Veeco Inc., Digital Instruments) and WSxM4.0 Develop 12.6 (Nanotech Electronica S. L., Madrid, Spain) software.

2.1.1. Atomic Force Microscopy (AFM) [1]

The Atomic Force Microscope invented by Gerd Binnig, Christoph Gerber, and Calvin Quate in 1986,[2] provided a method for mapping topographical surface features at atomic resolution (typically 2-10 nm lateral resolution (x-y) and 0.1 nm height resolution (z)). Principally this involves the use of a cantilever with a tip (typically 10-20 nm in radius) at the end, which is used to track across the sample surface by scanning in a raster pattern across it. Control over the movement of the tip in the x-, y- and z-directions is enabled by the use of x-, y- and z-piezoceramic elements, with an appropriately applied voltage across them. The distance between the tip and the sample surface is modulated by the voltage applied to the z-piezoceramic element, which is termed the “set-point” value. This is regulated so as to maintain a constant vertical force of the probe during imaging. Figure 2.1 illustrates the main components of the atomic force microscope.

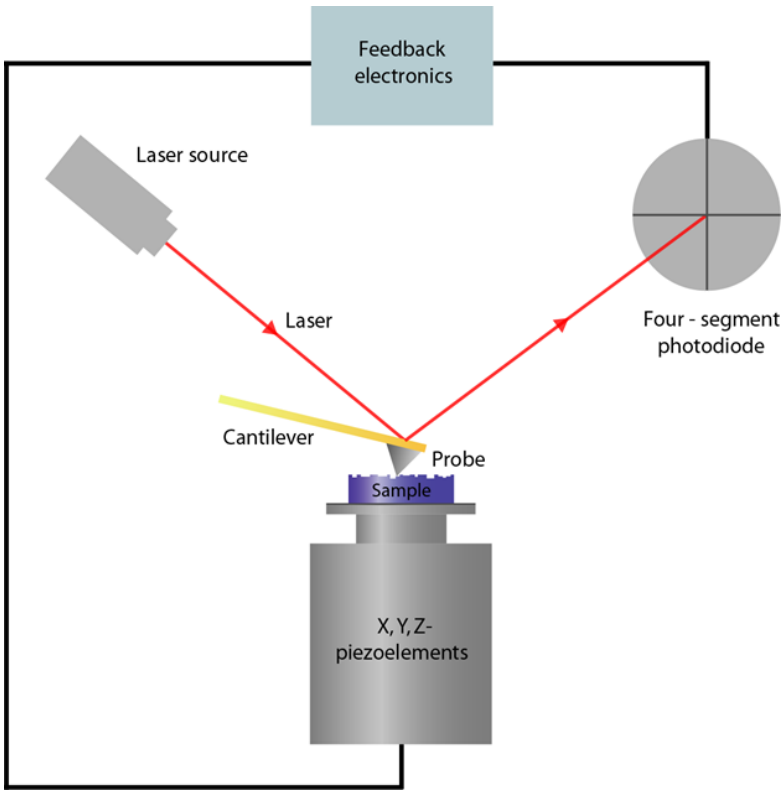

Figure 2.1: Schematic diagram showing the principle components and operation of an AFM

Deflections of the cantilever in the z-direction, caused as the tip encounters features on the surface during scanning, are detected by a laser that is reflected off the back of the cantilever onto a four-segment, position sensitive photodetector. Changes in the position of the laser along the detectors y-axis as the cantilever is deflected, with respect to the x-y coordinate of the tip at the surface, is used to construct a 3-dimensional image of the sample surface. Fluctuations in the height of the tip relative to the surface, as it interacts with surface features, is compensated by a change in the probe's z-position by use of a feedback loop, to maintain a constant vertical force. The interactions of the tip with the sample surface include attractive (van der Waals interactions) and repulsive (atomic) forces, which are due to long range and short range interactions, respectively.

AFM can be operated in a variety of modes, each with its own benefits. The most well established modes of imaging include "contact," "non-contact," and "TappingMode^{TM}" AFM.

2.1.1.1. Contact mode

In contact mode, the AFM tip remains in constant contact with the surface at a defined set-point value, figure 2.2. Set-points used are typically low (compared to the other modes of AFM operation) corresponding to a higher vertical contact force, on the order of nano Newtons (nN). For this reason, contact mode probes are usually flexible (low spring constant, k) and fabricated from hard, robust materials such as silicon nitride (Si_3N_4) to limit tip damage during imaging. The high forces experienced during contact mode are one of the primary drawbacks of the technique, especially for the imaging of soft samples such as biological materials, where the potential to cause damage to the sample is greater.

Contact AFM is the mode of operation used in Conductive-AFM, which is used to map surface topography and current. In this experiment, a bias is applied to the tip during imaging and an additional feedback loop is used to detect current, simultaneously with the surface topography.

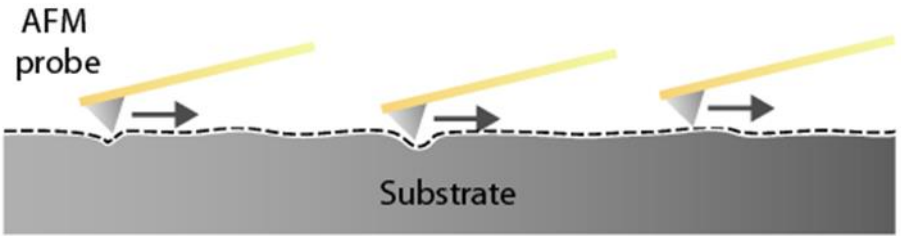

Figure 2.2: Principle of contact mode AFM

2.1.1.2. Non-contact mode and TappingMode™

Non-contact mode is an alternative means to image surface topography. In contrast to contact mode, where repulsive forces cause cantilever deflections, non-contact mode operates within a set distance of the sample surface where attractive forces (van der Waals) dominate the tip-sample interaction. In this technique, a cantilever of high spring constant (k) is oscillated close to its resonant frequency (f_0) (typically at 100 – 400 kHz) at low amplitude near to the sample surface through application of an appropriate set-point voltage, as illustrated in figure 2.3. The forces exerted on the tip as it encounters surface features are measured by monitoring the corresponding variations in the resonant frequency or vibrational amplitude of the tip. In an analogous fashion to maintaining a constant vertical force during contact mode, a feedback mechanism is

used to maintain a constant frequency and/or amplitude for regulating a constant tip-sample distance.

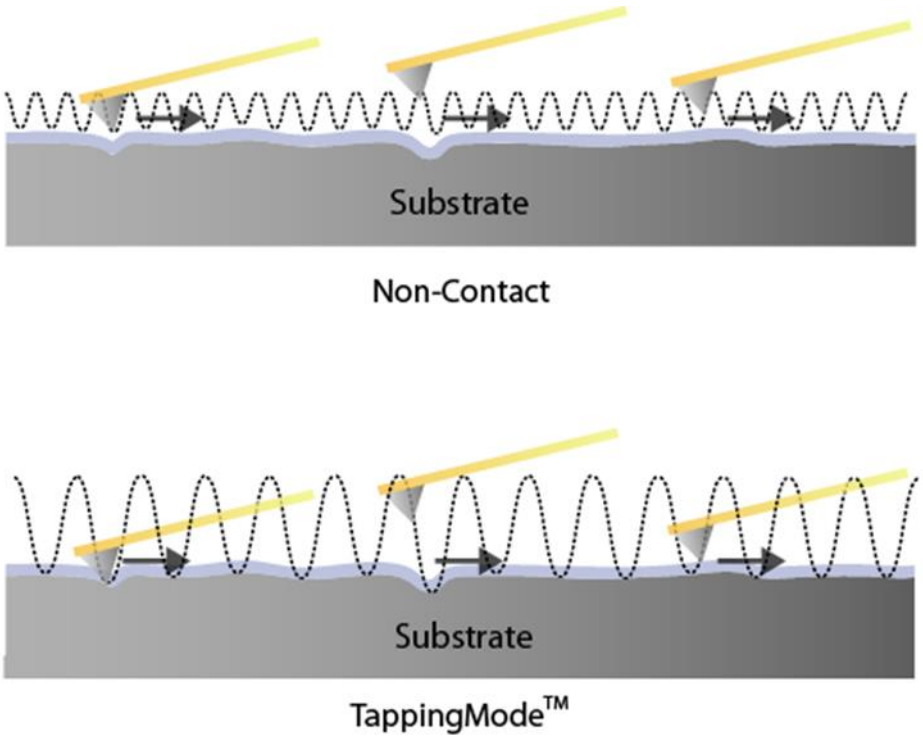

Figure 2.3: Principles of non-contact and TappingMode™ AFM. The thin liquid layer on the surface is represented in blue

The nature of the non-contact mechanism makes it more suitable for imaging of soft organic or biological materials. This is primarily due to the low force exerted on the sample in comparison to contact mode. Additionally, lateral forces (such as drag), which are commonly experienced in contact mode and can lead to surface damage, are virtually eliminated in non-contact mode. A potential disadvantage of this technique however is the result of the tip "sticking" to the surface after coming into accidental contact with the thin liquid film present upon the sample. In such circumstances, the z-scanner must retract the tip far enough away from the surface to overcome the adhesive meniscus force. Such events can result in anomalies in the acquired image.

TappingMode™ AFM, arguably one of the most common forms of AFM microscopy today, circumvents such issues by oscillating the tip at higher amplitude above the sample surface (shown in figure 2.3).[3] The tip, which is usually made of silicon, oscillates at a frequency of 50-500 kHz. In TappingMode™ AFM (also known as intermittent contact mode), the tip comes into brief contact with the surface at the end of

its oscillation period. Over time, this can lead to gradual blunting of the tip and result in reduced resolutions.

Throughout this thesis, AFM imaging of surface topography was performed in air in TappingMode operation on both a Multimode Nanoscope IIIa and Dimension Nanoscope V instruments (Veeco Instruments Inc., Metrology Group, Santa Barbara, CA) using 'TAP300Al-G' or 'TESP7' probes (n-doped Si cantilevers, Veeco Instruments Inc., Metrology Group), with a resonant frequency of 234-287 kHz, and a spring constant of 20-80 Nm^{-1}. Data acquisition was carried out using Nanoscope version 5.12b36 (Multimode IIIA) and Nanoscope version 7.00b19 (Dimension Nanoscope V) software (Veeco Instruments Inc., Digital Instruments).

2.1.1.3. Force curves

Information can be extracted about the tip-sample interactions by generation of a "force curve," in which the deflection of the cantilever is monitored with respect to the set-point (i.e. its displacement in the z-direction). The cantilever deflection is plotted as the probe contacts and withdraws from the surface (at a single point) during z-piezo extension and retraction. A typical "force-distance" plot, as shown in figure 2.4, can be interpreted based upon the attractive, repulsive and adhesive tip-sample interactions.

Quantitative data about the vertical forces generated by the tip can be elucidated by observation of the measured maximum displacement of the tip (x) prior to tip retraction, relative to the set-point value. Using "Hookes Law" where "k" represents the cantilever spring constant and "x" represents the displacement of the spring (the cantilever) the vertical force (F) can be calculated:

$$F = -k.x \qquad \textbf{(equation 2.1)}$$

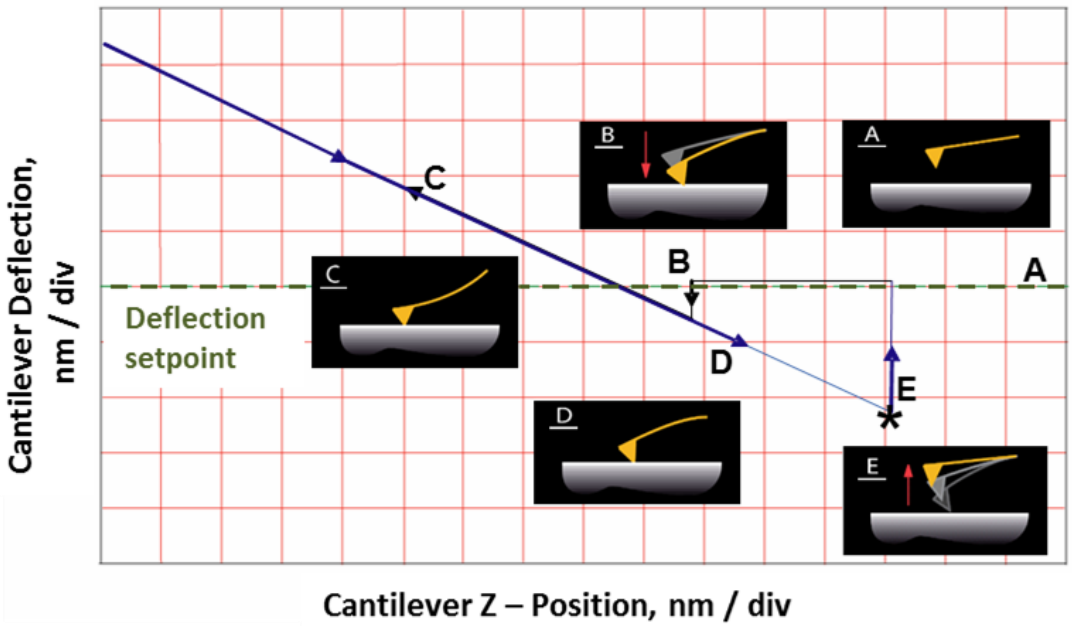

Figure 2.4: Typical "force-distance" curve obtained upon the one cycle of tip extension and retraction. Firstly the tip begins at large distance from the sample surface, at the deflection set-point, where no interactions are experienced(A). As the probe approached the surface and the cantilever z-position is lowered, a slight deflection is observed (B). As the probe continues in extension, the short-range repulsive forces begin to take effect and the cantilever is deflected well beyond the deflection set-point (C). After reaching maximum vertical force, the tip begins to retract causing a decrease in the deflection (D) until a minimum is obtained (E*) which is due to attractive forces between the tip and surface. Finally the tip pulls away from the surface completely when these forces are overcome and the deflection set-point is reached

Such information is also useful for attempting to make deliberate contact between the AFM tip and a nanowire, for example. The force curve can be used to confirm when contact has been made. This is specifically useful for the recording of i-V (current-voltage) plots.

2.1.2. Electrostatic Force Microscopy (EFM)

EFM provides a qualitative, quick and contactless means to elucidate conduction pathways in nanostructured materials.[4-6] In this experiment a sample of nanowires are immobilised upon an insulating, dielectric surface (SiO_2); a thermally grown polarisable layer sandwiched between a conductive silicon substrate and a conductive AFM tip. An applied potential to this set-up results in a capacitance acting between the tip and the substrate where an electric field is stored. As electrons within the nanowire move in the same electric field, the effect of the nanowire is to perturb the tip-substrate capacitance and affect the amount of charge stored. Fluctuations in this capacitance, with respect to

the applied voltage, can be monitored to obtain data relating to the electrical properties of the nanowire. Data collection is made by use of a 'two-pass' technique, as illustrated in figure 2.5. The first pass involves acquiring the sample topography, in standard TappingMode™ AFM. The second pass involves collection of the EFM signal, at a set-raised height above the sample surface (typically 40-100 nm), which correlates spatially with the topography of the sample.

The role of the AFM tip in the second pass is to detect changes in the electrostatic force gradient as it tracks over the sample. The force gradient is mapped by application of a DC voltage and observing the phase angle (ϕ) of the tip in response to the force gradient (with respect to the driving force applied to the cantilever). Essentially, a change in the electrostatic field gradient, due to variations in the tip-substrate capacitance, causes a phase lag in the AFM tip, also known as a phase shift ($\Delta\phi$). Typically the tip is held 40-100 nm above the nanowire, where topographical related information does not affect the phase angle, and long range electrostatic forces dominate the tip-sample interaction. Thus the EFM technique is highly sensitive to surface charges and can be used to qualitatively determine the polarisability of electrons within the sample directly beneath the tip (i.e. whether electrons are insulating or conducting).

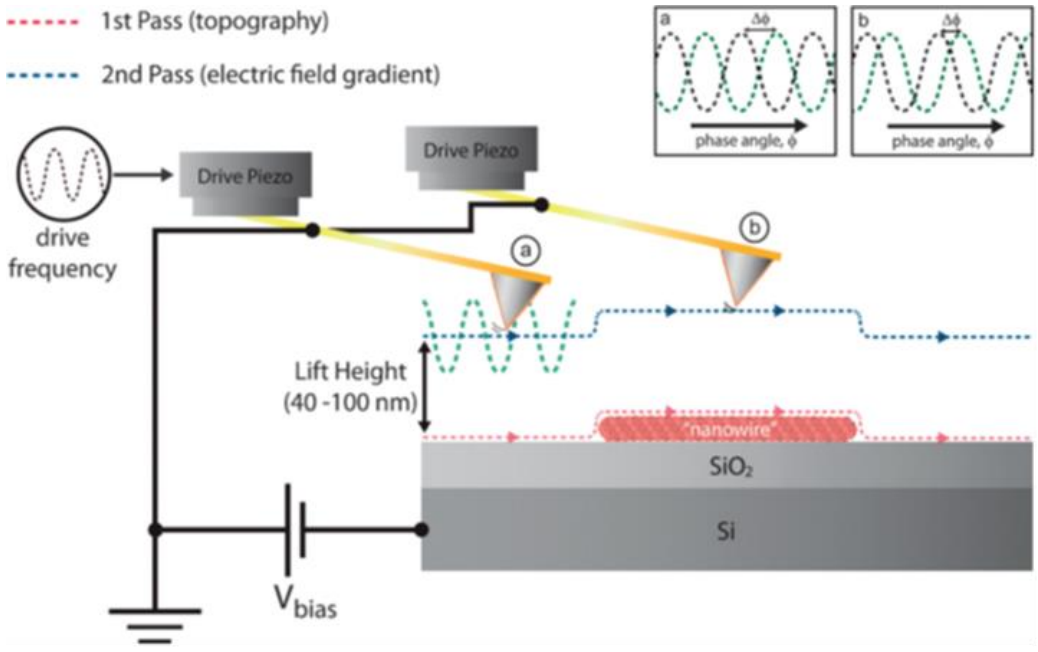

Figure 2.5: Schematic diagram showing the two-pass EFM method for mapping conductance in a nanowire

In practice, the phase shift is measured by changes to the cantilever spring constant (k). Principally there are two contributions to the total energy (*E*) stored in the tip; electrical and mechanical. As stated, the electrical energy created upon application of a bias can perturb the resonance of the tip and cause a phase shift ($\Delta\phi$). When the capacitance of the system changes (i.e. due to the presence of a conductive wire) the electrical energy stored in the tip changes and this causes the tip to deflect by Δx and the phase of the cantilever shifts accordingly. However, as the mechanical energy (the second contribution to the total energy of the tip) stored in the tip *also* changes with respect to 'x' one can monitor the phase shift ($\Delta\phi$) by altering the spring constant (k) of the cantilever. This will change the stiffness of the cantilever in response to the electric field, effectively mimicking changes to the tip/substrate capacitance. Finally, because the capacitance (C) is sensitive to the presence of a conductive nanowire one can use $\Delta\phi$ to determine if the wire is conductive. When a wire is modelled as a thin dielectric strip lying under a tip of defined radius (R_{tip}) the phase shift can be estimated by:[5]

$$\tan(\Delta\phi) = \frac{Q}{2k} V_{tip}^2 \left[\frac{2\pi R_{tip}^2 \varepsilon_0}{(h + t/\varepsilon_{Ox})^3} - \frac{2\pi R_{tip}^2 \varepsilon_0}{(h + t/\varepsilon_{Ox} + d/\varepsilon)^3} \right] \qquad \text{(equation 2.2)}$$

Where Q is the quality factor, k= cantilever spring constant, V is the applied voltage, t= oxide thickness, d= nanowire diameter, and ε and ε_o are the relative permittivity of the nanowire and oxide. The important term in the equation above is the tip radius (R_{tip}). For an insulator, the electric charges are polarised under bias, and are therefore confined to regions directly beneath the tip and the part of material it is probing. Therefore changes in the capacitance are due to polarisation effects (i.e. an insulator). This makes the second term in the equation small, resulting in a *positive phase shift* (bright contrast in phase image with respect to background) that tends to infinity as the electrons become decreasingly responsive to the electric field.

On the other hand, for a conductive wire, electrons not tied to their nuclei are free to travel the full length of the wire (L). Therefore the capacitance is now determined by L rather than R_{tip}, making the second term in the equation large. This results in a *negative phase shift* (dark contrast in phase image).

Hence the sign of the phase shift can be used as a qualitative assessment of whether a structure is insulating or conducting. In principle, for a conductor, a plot of the phase shift against bias should result in a parabolic curve due to the second order relationship of electric field to potential ($E= 1/2CV^2$). The data for this experiment is presented as a correlation between the phase shift and the bias applied to the surface (usually from -10V to +10V). The resulting data, where the phase shift correlates with the nanowire under scrutiny, provides a useful, practical, and straightforward means for indicating whether a structure is conducting or not.

EFM measurements were carried out in air on a Dimension Nanoscope V system in TappingMode operation, using MESP probes (n-doped Si cantilevers, with a metallic Co/Cr coating, Veeco Instruments Inc., Metrology Group), with a resonant frequency of ca. 70 kHz, a quality factor of 200-260, scan rate of 0.3 Hz and a spring constant of 1-5 Nm^{-1}. Data acquisition was carried out using Nanoscope version 7.00b19 software.

2.1.3. Conductive Atomic Force Microscopy (C-AFM)

C-AFM is a secondary imaging mode of contact mode AFM which allows for conductivity variations across a sample surface to be mapped.[6-8] This is achieved by contact scanning a metal coated AFM tip (consisting of a Co/Cr alloy) with low spring constant (0.1-1.0 N/m) across it. In our experiments, a 5 µL solution of nanowires is deposited onto the surface and allowed to dry in the form of a dense macrodeposit on top of an insulating layer of SiO_2. Typically, individual nanowires can be located from the edge of the macrodeposit using contact mode AFM. It is important during imaging in contact mode that the vertical contact force is lowered to an appropriate value (by adjustment of the set-point) so as to prevent damage to the nanostructures, such as cutting. This is especially important for thin nanowires, where the contact force can cause displacement of the nanowire across the surface.

The C-AFM technique is carried out under application of a direct current (dc) bias between the AFM probe and the sample. Then as the tip scans in a raster pattern across the surface, it simultaneously detects current in the sample whilst acquiring topographical data.[6] For a conductive 1-dimensionial structure, the current signals acquired are expected to match the topography of the structure along its entire length. Figure 2.6 shows a schematic of C-AFM in operation. C-AFM is capable of detecting

currents as low as ~10 pA; and so has considerably less sensitivity than EFM. However, due to the contact nature of the technique, C-AFM is quantitative and can be used to acquire i-V curves, whereas EFM cannot (non-contact).

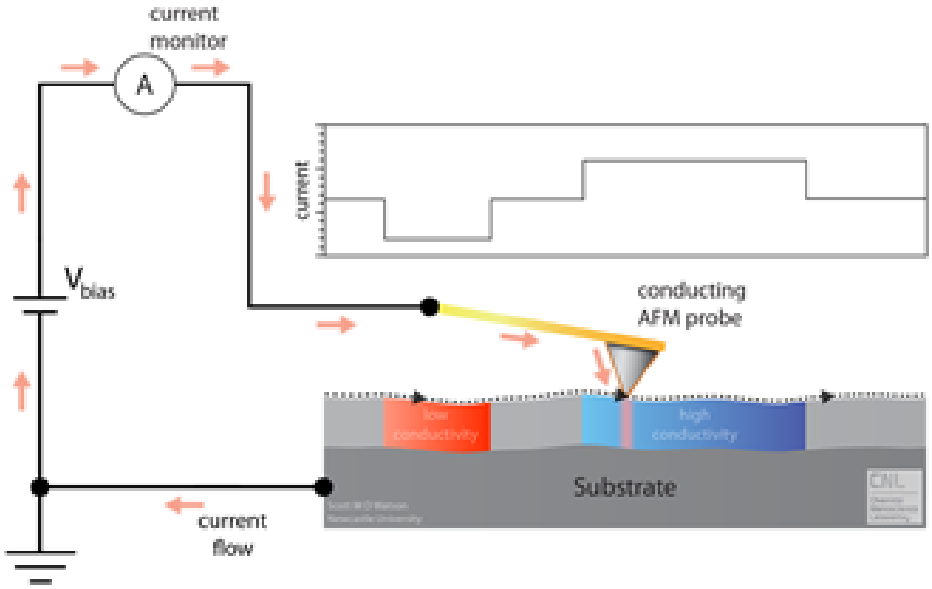

Figure 2.6: Schematic illustration of C-AFM in operation. An increase in the current signal is detected as the tip scans over regions of high conductivity, in contact with the surface

The general C-AFM set-up (as illustrated in figure 2.7) is comprised of a nanowire connected between two electrodes. One macro contact is made directly to the sample using a drop of conductive paste (Ga/In eutectic). This acts to electrically connect the macrodeposit to the AFM chuck. A conductive AFM tip is then used to probe the topography of the surface and contact the nanowire at a single point of interest, thus acting as the second, mobile electrode.

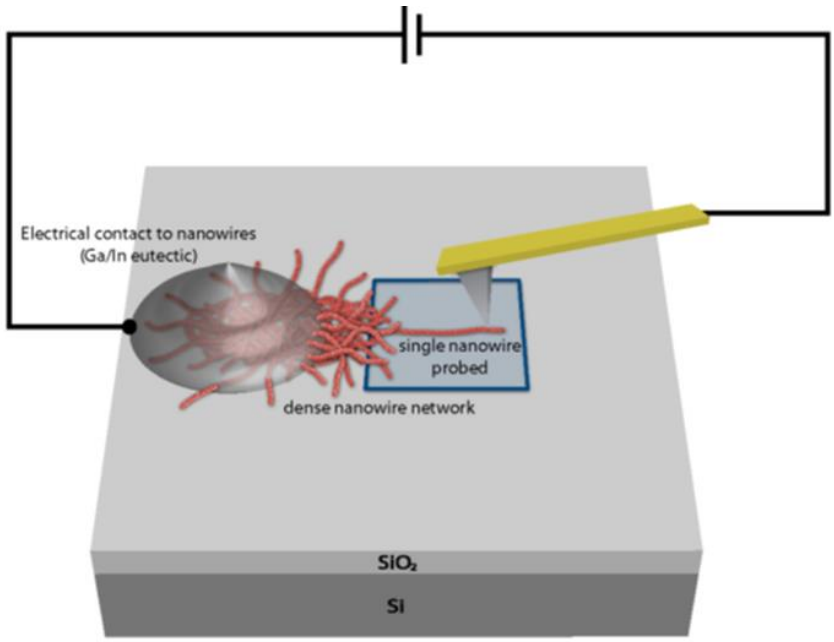

Figure 2.7: Schematic of the C-AFM experimental set-up. A conductive paste is applied to a dense macrodeposit of nanowires, acting as one electrode. A second, mobile, electrode is provided by the AFM tip in contact with a single nanowire

The acquired data is interpreted in terms of a simple series circuit consisting of three separate resistances: R_{tip}, R_{ext} and R_{wire}, where R_{tip} is the tip-nanowire contact resistance, R_{ext} is the resistance between the nanowire and the external circuit and R_{wire} is the resistance along the length of the wire from the edge of the macrodeposit contact to the AFM tip. In order to calculate the resistivity of the wire, it is necessary to measure the value of R_{wire}. However due to the additional contributions from R_{tip} and R_{ext} to the overall resistance, it is not possible to obtain an exclusive measurement of $R_{wire,}$ directly. In order to isolate this value from the overall resistance, one can assume that all of the distance dependence (d) to resistance lies in R_{wire}. Hence a plot of resistance as a function of distance (d) should contain information relating only to the wire resistivity (R_{wire}).

The closed-loop feedback mechanism capabilities of the Dimension V AFM, used in this work, enables accurate "point-and-click" positioning of the AFM probe on a sample surface to allow for distance-dependent current-voltage (i-V) measurements to be carried out. In this experiment a series of i-V plots are recorded as a function of distance (d) along the nanowire (i.e. points 1, 2 and 3), as shown in figure 2.8a. The resistance is expected to increase linearly as the current flows though increasing lengths of the wire. Figure 2.8b shows a plot of resistance vs. relative distance (d) from the tip (following

the course of a wire) to the edge of the macrodeposit.[9] The inset shows an image of the nanowire under investigation, where the red crosses mark the position of tip contact, for generation of an i-V plot. For different applied contact forces the measured resistance is different at each point. The general trend shows that higher contact forces lead to a decrease in resistance; presumably due to a reduction in contact resistance. However, the gradients of the plots match closely, indicating similar resistivity values.

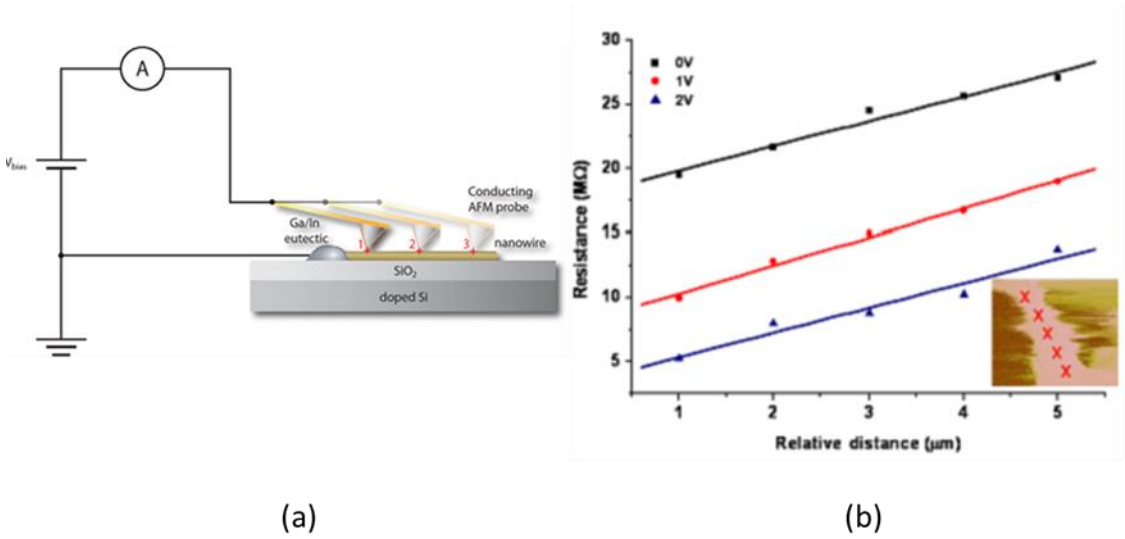

Figure 2.8: Schematic diagram of the C-AFM technique used in a series of distance-dependence i-V measurements. Each measurement is recorded at a different point along the nanowire of interest (a). Plots showing resistance as a function of relative distance along the nanowire for different applied forces (b), inset shows a current map of the nanowire and red crosses indicate the position of the tip for recording i-V plots [9]

2.2. Two-probe semiconductor device analyser [10]

Two-probe i-V measurements can be carried out for more accurate determination of nanowire conductivity with fA-level measurement capability. This is achieved with use of a Microtech probe station situated on a vibrational isolation system and fitted to a semiconductor device analyser and thermal chuck apparatus (see figure 2.9a). In this method a nanowire is alignment, typically by molecular combing, between two microfabricated metal electrodes (e.g. Au) on a thermally oxidised Si chip (figure 2.9c). The sample is then placed inside the chamber of the probe station where two needles (made of tungsten, 10 μm radius) are positioned onto each of the electrode pads for recording i-V plots, as in figure 2.9b.

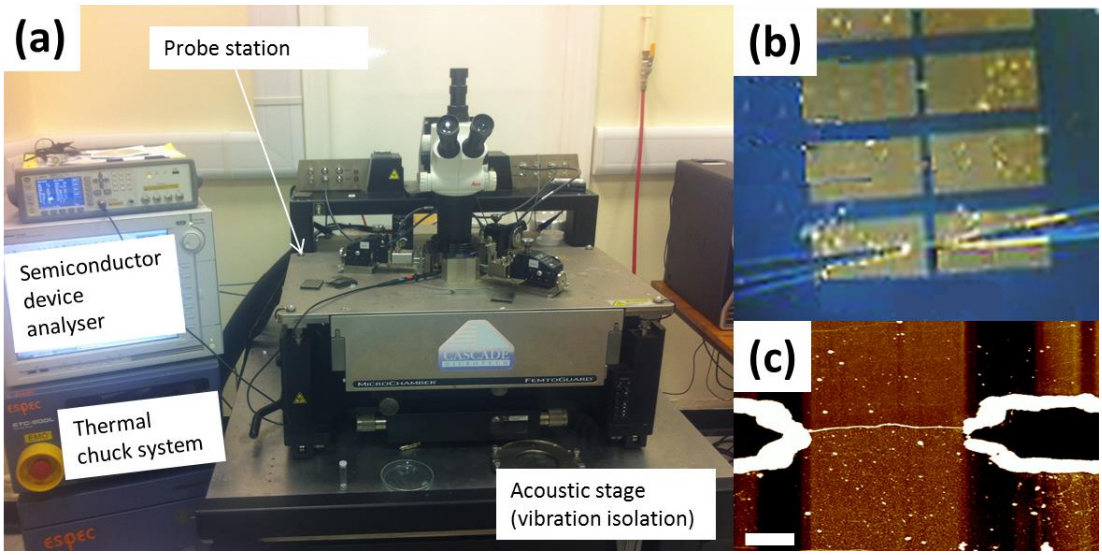

Figure 2.9: Photograph showing the probe station and various fitted components (a), inside the probe station: gold electrodes with probe needles in contact (b), and an AFM image showing a nanowire bridging between the two electrodes, scale bar= 1 µm (c)

The resistance (Ω, VA^{-1}) between the two electrodes can be determined from the i-V plot, given by the reciprocal of the gradient (AV^{-1}) around zero bias. For an ideal conductor, this relationship would be expected to be linear. In the case of a metal, the resistance would also be expected to increase with temperature, due to the increased electron scattering events at lattice vibrations. Whereas, for a semiconductor the resistance is expected to decrease with rising temperature due to further population of the conduction band.[11] Thus, it is possible to distinguish between the physical nature of a conductive material using temperature. The probe station used here is able to perform temperature-dependent i-V analysis for this purpose. From the measured resistance, the conductivity (σ, Scm^{-1}) of a nanowire with defined length and cross-sectional area is calculated from the equation:

$$\sigma = l / R.A \qquad \textbf{(equation 2.3)}$$

In this work, the length and diameter of the structure is estimated based on the AFM data. The cross-sectional area is calculated based on the assumption that the shape of the structure is a perfect cylinder.

2.3. X-ray Photoelectron Spectroscopy (XPS) [12, 13]

X-ray Photoelectron Spectroscopy (XPS), or more traditionally, Electron Spectroscopy for Chemical Analysis (ESCA), is a surface sensitive chemical analysis technique used to obtain elemental information and the chemical state of elements within a sample. The technique is quantitative and can be used to garner information relating to sample composition. For instance, the relative area of an XPS peak is directly related to the number of atoms in the sample giving rise to that peak. XPS is able to identify all elements with an atomic number (Z) of 3 and upwards. The principles of XPS are based on the photoelectric effect, whereby the interaction of photons with matter results in ionisation and the emissions of 'photoelectrons.' The associated energy of an emitted electron contains all of the relevant chemical information about the sample for identification of the elements present within. Samples for XPS analysis are usually required to be solid as XPS requires ultra-high vacuum (UHV).

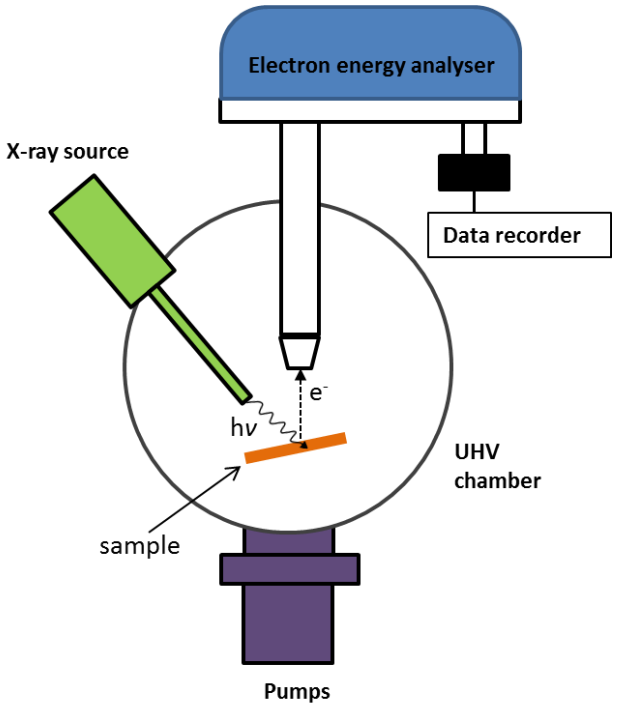

Figure 2.10: Basic components of an X-ray Spectrometer. The sample is irradiated with X-rays from the X-ray source. A photoelectron is ejected from the irradiated specimen and collected by a lens system which focuses the electron into an energy analyser. An electron detector is then used to count the number of electrons as a function of energy

As illustrated in figure 2.10, an X-ray Photoelectron Spectrometer typically consists of a monochromatic X-ray Source (typically MgKα (1253.6 eV) or AlKα (1486.6 eV)) focused onto the sample surface, an electron detector and a photoelectron energy

analyser. Penetration of the X-rays occurs to within 10 micrometres of the sample surface. The interaction of X-rays with the atoms in the sample causes an electron from a core orbital (e.g. 1s, 2s, 2p) to be ejected (as illustrated in figure 2.11). As the electron is pulled away from the nucleus, upon excitation with an X-ray photon, the attraction between the two decreases until the electron reaches the Fermi level (highest occupied state by an electron) enters the ionisation continuum.

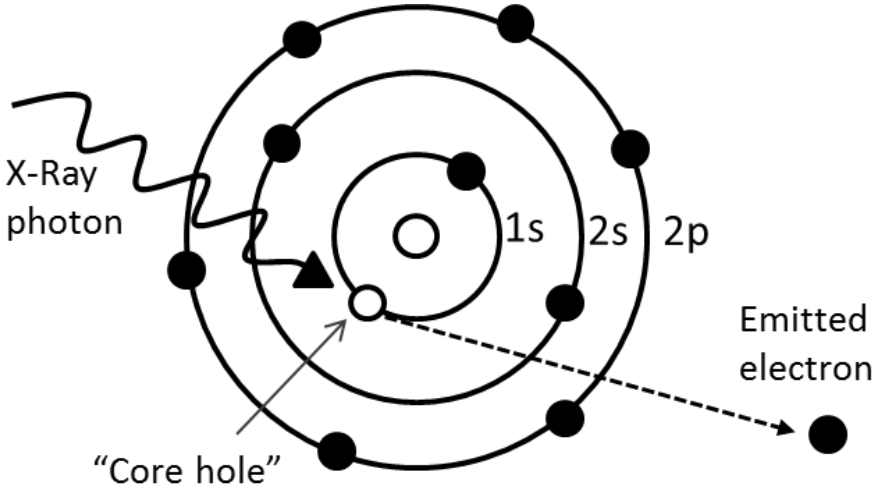

Figure 2.11: Illustration of the photoelectric event. An X-ray photon interacts with a core orbital and causes emission of a photoelectron leaving behind a core hole

Given that the mean free path (λ) of electrons is considerably smaller than that of photons; only those electrons that originate from the top 1-10 nm of the sample surface leave the surface without energy loss. This makes XPS a highly surface sensitive technique. The emitted electrons produce the peaks in the spectrum, where each peak (or set of peaks) correspond to a different chemical species, and provide the most useful information for chemical analysis. Those detected electrons which have undergone inelastic collisions upon interacting with matter, before escaping from the surface, have reduced kinetic energies and form the background of XPS spectra.

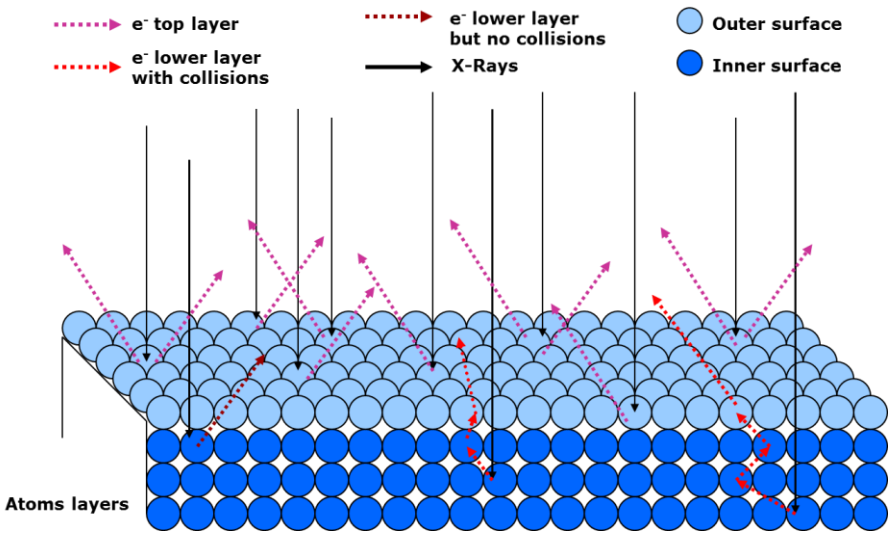

Figure 2.12: Schematic illustration of the surface sensitivity of XPS. Electrons from deep atomic layers (>10 nm) undergo inelastic scattering with electrons from other atoms leading to a reduced kinetic energy. Electrons from the top layer easily escape without undergoing energy loss [14]

Information relating to the chemical identity of a compound, from where the emitted electron escaped, is conveyed by the respective electron binding energy (E_b). The binding energy is the energy required to remove an electron from its ground state level to vacuum level. The binding energy for each core electron is highly specific and is therefore characteristic to every element. The XPS spectrum is a plot of the electron binding energy (E_b) relative to the number of electron counts. E_b can be determined based on the kinetic energy of the escaping electron (E_k) and the energy of the incoming X-ray (or photon energy, E_{photon}), using the equation below, where φ is the spectrometer work function:

$$E_b = E_{photon} - (E_k + \varphi) \qquad \textbf{(equation 2.4)}$$

One of the most important aspects about XPS is that the binding energy depends on the chemical state of the element under investigation. This includes the nature of the bound atoms or ligands and the oxidation state of the element. For example a core electron of an element in +3 oxidation state will generally have a higher binding energy than it would if that element was in a +2 oxidation state, due to the higher attraction from the nucleus. Here XPS not only provides information about the elements present, but also give information about their chemical state.

2.4. References

1. G. J. Leggett, Scanning Probe Microscopy. in *Surface Analysis – The Principal Techniques*, John Wiley & Sons, Ltd, Editon edn., 2009, pp. 479-562.
2. G. Binnig, C. F. Quate and C. Gerber, Atomic force microscope. *Physical Review Letters*, 1986, **56**, 930-933.
3. Q. Zhong, D. Inniss, K. Kjoller and V. B. Elings, Fractured polymer/silica fiber surface studied by tapping mode atomic force microscopy. *Surface Science*, 1993, **290**, L688-L692.
4. M. Bockrath, N. Markovic, A. Shepard, M. Tinkham, L. Gurevich, L. P. Kouwenhoven, M. W. Wu and L. L. Sohn, Scanned Conductance Microscopy of Carbon Nanotubes and Î»-DNA. *Nano Letters*, 2002, **2**, 187-190.
5. C. Staii, A. T. Johnson Jr and N. J. Pinto, Quantitative analysis of scanning conductance microscopy. *Nano Letters*, 2004, **4**, 859-862.
6. A. Houlton and S. M. D. Watson, DNA-based nanowires. Towards bottom-up nanoscale electronics. *Annual Reports on the Progress of Chemistry - Section A*, 2011, **107**, 21-42.
7. R. Hassanien, S. A. F. Al-Said, L. Šiller, R. Little, N. G. Wright, A. Houlton and B. R. Horrocks, Smooth and conductive DNA-templated Cu 2O nanowires: Growth morphology, spectroscopic and electrical characterization. *Nanotechnology*, 2012, **23**.
8. S. M. D. Watson, J. H. Hedley, M. A. Galindo, S. A. F. Al-Said, N. G. Wright, B. A. Connolly, B. R. Horrocks and A. Houlton, Synthesis, characterisation and electrical properties of supramolecular DNA-templated polymer nanowires of 2,5-(bis-2-thienyl)-pyrrole. *Chemistry - A European Journal*, 2012, **18**, 12008-12019.
9. M. A. Hinai, Self-assembly of conductive nanowires using DNA as a template. *Newcastle University*, 2012.
10. D. K. Schroder, Frontmatter. in *Semiconductor Material and Device Characterization*, John Wiley & Sons, Inc., Editon edn., 2005, pp. i-xv.
11. A. B. Kaiser, Systematic conductivity behavior in conducting polymers: Effects of heterogeneous disorder. *Advanced Materials*, 2001, **13**, 927-941.
12. C.D.Wagner, W.M.Rigg, L.E.Davis, J.F.Moulder and G.E.Mullenberg, Handbook of X-ray Photoelectron Spectroscopy. 1979.
13. B. D. Ratner and D. G. Castner, Electron Spectroscopy for Chemical Analysis. in *Surface Analysis – The Principal Techniques*, John Wiley & Sons, Ltd, Editon edn., 2009, pp. 47-112.
14. D. E. Torres, X-Ray Photoelectron Spectrsocopy (XPS). *https://nanohub.org/resources/2109*, 2006.

Chapter 3: A Non-aqueous route to Cu-DNA nanostructures

3.1. Introduction

This chapter describes a 'non-aqueous' route to the fabrication of DNA-templated copper nanostructures via electroless metallisation of surface-immobilised DNA templates.

Due to the difficulties encountered in previously described 'wet' solution based approaches towards the preparation of smooth and conductive DNA-templated copper nanowires,[1-5] a new 'dry' solution based DNA-templating approach is explored here. This approach is based on the use of a Cu(I) coordination complex, tetrakis(acetonitrile)copper(I) hexafluorophosphate ($Cu(CH_3CN)_4.PF_6$) for 'doping' of surface bound DNA with Cu^+ ions and phenylsilane ($PhSiH_3$) as the chemical reductant. Figure 3.1 illustrates the reaction scheme employed. The two-step 'doping/reduction' procedure on surface-immobilised DNA templates was adopted in this work. For convenience, tetrakis(acetonitrile)copper(I) hexafluorophosphate is referred to simply as 'Cu(I).'

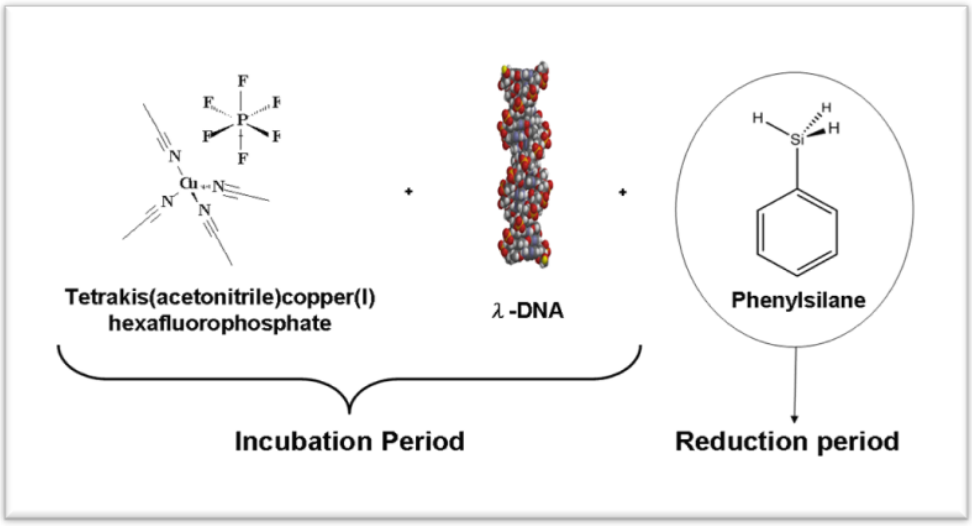

Figure 3.1: Schematic showing the order of addition of reaction components. The reaction is split into two steps; incubation of Cu(I) salt with DNA and then reduction to metallic copper using phenylsilane

To date, all methods for the fabrication of Cu-DNA nanostructures are reliant on the use of Cu(II) complexes for coordination to the DNA duplex as part of a two-step 'doping/reduction' procedure.[1, 2, 5-7] This is primarily because Cu(II) is the most stable and common oxidation state for copper and that Cu(II) salts, such as $Cu(NO_3)_2$ and $Cu(SO_4)$, are easily solubilised in water. Furthermore, the coordination chemistry of Cu^{2+}/DNA interaction has been studied in depth over the years (as has the chemical reduction of Cu^{2+}).[8-10] Significantly however, the preparation of electrically conductive Cu-DNA nanostructures based on Cu(II) complexes has thus far proved elusive.[4]

Divalent Cu(II) salts typically require strongly coordinating (polar) solvents for solubilisation and supply of the divalent copper to the DNA structure. These strongly coordinating solvent molecules may actually compete with DNA donor sites for coordination of copper ions, and may result in copper nanostructures which are structurally irregular. Previous studies have sought to replace water, for a solvent which has a lower dielectric constant, such as DMSO.[2, 5] The use of a lower polarity solvent for the delivery of copper ions is understood to enhance the binding efficiency of copper for the DNA template resulting in more 'intimate' interaction of the copper ion to DNA. However, in both cases where DMSO was used as a solvent instead of water, the resulting morphologies of copper coating on DNA remained irregular (see introduction, section 1.5). Such structures are perhaps best described as a 'beads on a string' type assembly.

The aim of these current studies is to develop a new non-aqueous route for the fabrication of Cu-DNA nanowires using a univalent Cu(I) coordination complex. To the best of our knowledge, attempts to prepare DNA-templated copper nanostructures using Cu(I) salts have not been carried out. Use of a low oxidation state copper salt and a weakly coordinating solvent used for delivery of these ions, may result in the generation of more extensive copper coverage along the DNA template, affording smoother nanostructures. In this sense, Cu(I) salts are considered desirable candidates for templating on DNA, as they can be more easily solubilised in non-polar solvents (lower dielectric values) compared to Cu(II) salts due to the lower charge density on the copper ion.

Equally importantly, many Cu(I) complexes have better compatibility with organo-soluble reducing agents than Cu(II) complexes, negating the need to use aqueous solvents during the metallisation process. The method described in this chapter is based

on a single solvent system with both Cu(I) ions and reducing agent (phenylsilane) in the same solvent phase (acetonitrile), in which the DNA-immobilised substrate is submerged (see figure 3.2). The reaction is carried out in a N_2-filled Schlenk flask in order to prevent oxidation of Cu(I) to Cu(II) and to ensure moisture is excluded from the system. All solvents used were dry and de-gassed in an ultrasound bath and/or bubbling N_2 through the solution.

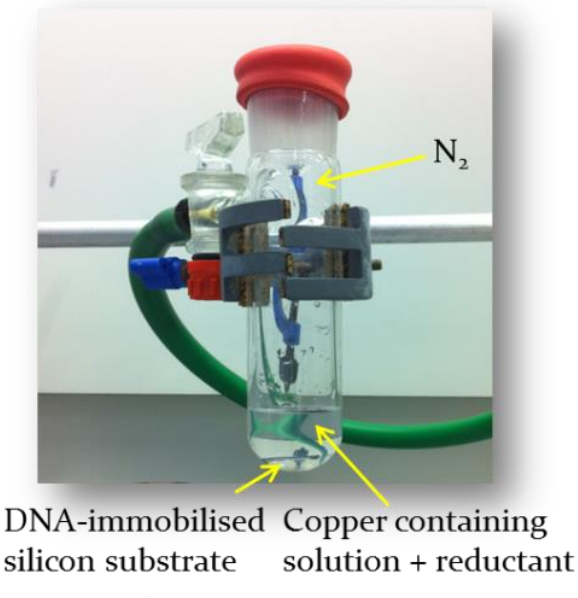

Figure 3.2: Photograph of a DNA-immobilised silicon substrate under treatment with the copper/silane solution

The copper complex chosen for these studies, tetrakis(acetonitrile)copper(I) hexafluorophosphate ($Cu(CH_3CN)_4.PF_6$), is relatively air-stable compared to other Cu(I) salts such as CuCl, Cu(OAc) and CuI. This is largely attributed to the bulky counterion, hexafluorophosphate (PF_6^-), which stabilises the metal ion complex by sterically hindering access, of solvent molecules for example, to the metal centre.[11] Hexafluorophosphate is also a weakly coordinating counterion which is beneficial for the interaction of Cu^+ ions with DNA.

In addition, the oxidation state of this Cu(I) complex is stabilised by the acetonitrile ligands, which prevent rapid oxidation to the Cu(II) state.[11] Upon their removal the complex is readily oxidised to Cu(II). However, in a solution of acetonitrile, the salt is

stable to oxidation for several weeks.* A previous report describes the use of acetonitrile as solvent for the synthesis of copper nanoparticles (CuNPs), which acts as a protective agent against oxidation, as well as stabilising the nanoparticle colloid.[12] Also, copper nitrile ligands are reasonably labile,[13] allowing for better coordination of Cu(I) with DNA.

Takahashi *et.al*. sought to investigate a range of chemical reducing agents for reduction of Cu(I) complexes to form metallic copper nanoparticles.[14] Hydrosilanes were shown to be suitable candidates for the reduction of Cu(I) salts under mild conditions. A series of reactions were carried out with various hydrosilanes and Cu(I) salts such as Cu($OCOCH_3$), CuCl and CuBr using a range of solvents at room temperature. It was found that phenylsilane ($PhSiH_3$) was the most successful candidate for the preparation of high purity CuNPs.

Based upon Takahashis' series of experiments and some of our own, phenylsilane ($PhSiH_3$) will be used as a reductant for $[Cu(CH_3CN)_4][PF_6]$ at DNA-immobilised surface templates to drive CuNP formation; where DNA can act to restrict growth to a single axis. Acetonitrile was chosen as the solvent, primarily because it can solubilise both components of the reaction, but also as the solvent increases the stability of the Cu(I) complex, as previously discussed. It is speculated that this method will lead to formation of a regular and densely packed array of copper nanoparticles along the DNA template, resulting in little or no exposed regions of bare DNA.

This work describes a novel 'water free' approach to the fabrication of DNA-templated copper nanostructures via a two-step 'doping/reduction' approach on surface-immobilised DNA. The ultimate aim is to develop a reproducible method for the fabrication of conductive copper nanowires using DNA templates. These could have potential use for interconnect material in integrated circuitry.

* It was indicated through a simple experiment that the Cu(I) complex is more stable to air when in a solution of acetonitrile. A portion of the pure salt was placed on a watch glass, and then left exposed to air for 24 hours. The solid changed colour from white to green (indicating oxidation to Cu(II)) whereas the Cu(I) solution remained colourless.

3.2. Experimental

All general chemical reagents were obtained from Sigma-Aldrich unless otherwise stated, and were Analytical grade or equivalent. Lambda (λ) DNA was from New England Biolabs, cat no. N3011S (New England Biolabs (UK) Ltd. Hitchin, Herts, United Kingdom). Silicon <p-100> wafers, boron doped 100 mm. diameter, 525 ± 50 µm thickness, 1-10 Ω cm resistance were purchased from Compart Technology LTD. (Peterborough, Cambridgeshire, United Kingdom). Silicon <n-100> wafers with 200 nm SiO_2 layer, Arsenic doped, 100mm. diameter, 500 ± 25 µm thickness, ≤ 0.005 Ω cm were purchased from Virginia Semiconductor (1501 Powhatan St., Fredericksburg VA 22401). All water used was Nanopure with resistance 18.2 Ω.cm.

To ensure consistent and comparative results, all sample preparations were performed on surface immobilised DNA. ***NOTE:*** For control experiments the preparation and method of deposition was carried out in the same way, as described below, but in the absence of DNA.

Two types of DNA were used throughout this work. For the puposes of SPM analysis lambda DNA was used (see details below) and for chemical characterisations (except where stated otherwise) calf-thymus DNA was used.

Lambda DNA (purchased from New England Biolabs, 500 $\mu g mL^{-1}$) is a duplex DNA solution isolated from bacteriophage lamda and is 48,502 base pairs in length. The DNA is isolated by phenol extraction and dialyzed against 10 mM Tris-HCL (pH 8.0), 1 mM EDTA and stored in the same solution.

Calf-thymus DNA (purchased from Sigma-Aldrich) sodium salt is a fibrous material isolated from calf-thymus tissue. DNA from calf-thymus is 41.9 mole % G-C and 58.1 mole % A-T. Fibres were dissolved in nanopure water and concentrations were measured using a BioPhotometer and standard rectangular plastic cuvettes. The BioPhotometer is an absorption single-beam photometer with reference beam and several fixed wavelengths. The absorbance at 230 nm, 280 nm and 320 nm are measured, as well as the ratios A_{260}/A_{280} and A_{260}/A_{230} and the absorbance at 260 nm. The resulting concentration of DNA is calculated is calculated from these measurements. λ_{max} for calf-thymus DNA is 259 nm (100 mM phosphate buffer, pH 7.0). The molar extinction coefficient at 260 nm (ε_{260}) is 13,200 bp cm^{-1} M^{-1} (base pair).

3.2.1. Cleaning of substrates and alignment of λ-DNA

Silicon <p-100> wafers were cut into 1cm^2 pieces with a diamond tip pen. The wafers were then sequentially swabbed in high purity acetone, propanol and Nanopure water using a cotton bud. The surface was then further cleaned by treatment with a sodium dodecyl sulphate (SDS) solution, heated to 50°C (0.01g SDS per 100mL H_2O) for 20 minutes. This was followed by thorough washing with copious amounts of Nanopure water. The wafers were treated in "piranha" solution (4:1 H_2SO_4:H_2O_2) for 45 minutes which serves to oxidise the surface and remove any residual organics. After washing with Nanopure water and drying in an oven for 30 minutes the wafers were modified by treatment with chlorotrimethylsilane ($SiMe_3Cl$) vapour to produce a self-assembled monolayer of trimethylsilane (TMS) on the wafer surface. This involved the wafers being placed on top of a small sample tube contained in a larger sealed sample tube with 200µL of Me_3SiCl and left to stand in the vapour for 8 minutes. Static contact angle measurements, using Nanopure water as the probe liquid, carried out upon the TMS-modified surfaces, revealed them to have contact angles of 65° (typically).

Molecular combing was used to align DNA molecules on the TMS-modified substrate for AFM/EFM analysis; 5 µL of λ-DNA solution (stock 500 µgmL^{-1} diluted to 300 µg mL^{-1}) was placed on the substrate surface and the droplet combed in a uniform direction across the surface using a micropipette tip. This procedure was repeated 20 times.

Wafers used for EFM analysis were silicon <p-100> n++ with a 200 nm thick thermally grown oxide layer on top. Before cleaning and alignment of DNA, one side of the wafer was treated with HF solution (10% aq.) to remove the oxide layer and provide an electrical contact for future measurements.

3.2.2. Metallisation of surface immobilised DNA

DNA metallisation was performed under an inert N_2 atmosphere using Schlenk apparatus at room temperature. The copper salt solution was sonicated for several minutes prior to use in order to achieve the best solubilisation possible. The DNA-aligned substrates were incubated with a solution of tetrakis(acetonitrile)copper(I) hexafluorophosphate ($[Cu(CH_3CN)_4][PF_6]$) (10 mM, 1 mL, dry CH_3CN) in a Schlenk flask for 20 minutes to afford Cu(I) doped DNA. This was then treated with the dropwise addition of phenylsilane ($PhSiH_3$) (20 mM, 1 mL, dry CH_3CN). The substrate

was left to incubate in the solution for 4 minutes, after which a colour change in the solution from colourless to a pale golden brown was observed. Finally, the sample was removed from the metallising solution, washed with dry acetonitrile and finally dried under a flow of nitrogen.

The final DNA-templated copper nanostructures were characterised using powder-XRD, XPS, FTIR and AFM. The electrical properties were tested using EFM and C-AFM.

3.2.3. X-ray Diffraction (XRD)

For analysis of DNA-templated copper nanomaterial, two samples were prepared. The first sample was prepared using *surface*-immobilised DNA and the second sample prepared in *solutions* of DNA in order for the product material to precipitate as a powder. Both preparations follow the 'doping/reduction' approach described in section 3.2.2.

The surface based sample was prepared in the same manner to samples prepared for AFM/EFM studies (see section 3.2.2.2) with the exception of using porous silicon as opposed to flat silicon wafers. The high surface area of the porous Si yields a higher density of material on the substrate, sufficient enough to afford adequate signal to noise ratio in the powder spectrum. The type of DNA used was calf-thymus DNA (0.5 mg mL^{-1}).

Porous silicon was prepared by electrochemical etching. Firstly, the silicon wafer was washed with high purity acetone before loading into an electrochemical cell. HF:EtOH (1:1 v/v) was added to the cell and a current (10 mA) was applied to the set-up for 10 minutes, after which the sample was removed, washed with copious amounts of Nanopure water and dried under a flow of nitrogen. Deposition of DNA was carried out by drop casting the solution into the pores of the substrate and leaving to dry for 2-3 hours in a laminar flow cabinet. The process was repeated to ensure a high quantity of DNA deposited. The sample was then transferred into a N_2-filled Schlenk flask and metallisation was carried out as described in section 3.2.2. The concentration of Cu(I) salt and phenylsilane used were 25 mM and 50 mM, respectively.

The second sample was prepared in a solution of calf-thymus DNA (0.5 mg mL^{-1}, 10 mL) dispersed in equal volumes of Nanopure water and acetonitrile. The solution was

briefly sonicated using an ultrasound bath (60 Hz, Sonomatic, Langford Ultrasonics) in order to achieve good dispersion. The Cu(I) reagent was then added to the DNA solution and magnetically stirred for 20 minutes before addition of two equivalents of phenylsilane. The reaction mixture was continuously stirred until the solution turned from colourless to light golden brown and a dark brown precipitate had formed. The powder was collected by decanting off the solution and filtering using a Buchner funnel and dried (99.1 mg, 62% yield). The supernatant was kept and centrifuged at 5000 rpm for 5 minutes and the colourless liquid containing Cu-DNA nanostructures were aligned onto a clean silicon substrate for AFM analysis. The powder was washed with ethanol, Nanopure water, dried and then submitted for XRD analysis.

Powder X-ray diffraction data was obtained using a PANalytical X'Pert Pro Diffractomer equipped with a Cu $K\alpha_1$ radiation source ($\lambda = 1.54 \times 10^{-10}$ M).

3.2.4. X-ray Photoelectron Spectroscopy (XPS)

Samples were prepared similarly as for AFM/EFM analysis (see section 3.2.2) in order to make direct correlation between the two sets of techniques (i.e. to determine the chemical identity of what is observed by AFM). XPS requires a higher density of DNA on the surface in order to obtain high photoelectron signal, therefore a solution of DNA (500 μg mL^{-1}, 60μL) was evaporated upon the SiO_2 surface. Silicon substrates used for XPS analysis were not modified with trimethylsilane in order to increase the wettability of the sample surface. In this way a thin film of DNA is adsorbed onto the surface. The sample was then placed in an oven at 60°C for 15 minutes to dry. Metallisation of the substrate was carried out as detailed before (section 3.2.2) except that the concentrations of the reagents were increased 5 fold in order to compensate for the higher density of DNA bound to the surface compared to AFM/EFM sample preparations.

XPS was carried out using a Thermo K-Alpha XPS system with a microfocused, monochromated Al Kα X-ray source at a take-off angle of 90°. The size of the X-ray spot was 400 μm x 700 μm. Linear backgrounds were used for singlet fitting and Shirley backgrounds in the case of doublets. Line shapes consisted of a mixture of Gaussian and Lorentzian models. Signal intensities are measured in counts (of photoelectrons) per second (CPS).

During data acquisitions, a low energy electron/ion gun was used for charge compensation of the sample. Fine binding energy adjustments were made by

referencing to the internal adventitious carbon peak at 284.8 eV ± 0.1 (C1s), which arises from carbon contamination from air. The presence of the adventitious carbon layer is a convenient charge reference for conducting samples on an insulating surface.[15, 16] For copper nanoparticles an adjustment of +0.7 eV was required for calibration of these spectral files. For Cu-DNA nanostructures a +2.3 eV correction was required.

3.2.5. Fourier-Transform Infra-Red (FTIR) Spectroscopy

Two samples were prepared for analysis by FTIR. Sample 'A' is prepared by adopting the usual two-step 'doping/reduction' approach on surface-immobilised DNA (as is used for all other studies in this chapter). Sample 'B' preparation follows the 'doping/withdrawal/reduction' approach (described below).

Sample A- *Formation of Copper Nanostructures via 'doping/reduction' approach on surface-immobilised DNA.*

The sample was prepared on a DNA-immobilised silicon substrate as for AFM analysis. DNA (CT-DNA, 1mg mL^{-1}, 60 μL) was deposited onto the surface by drop cast so as to produce a thick film for sufficient FTIR signal acquisition. An FTIR spectrum was recorded on the bare DNA film. Metallisation of the DNA film was then carried out, as described in section 3.2.2. An FTIR spectrum of metallised DNA was recorded.

Sample B- *Formation of Copper Nanostructures via 'doping/withdrawal/reduction' approach on surface-immobilised DNA*

The sample was prepared as follows, (i) the DNA film (prepared by drop cast technique) was treated with $Cu(CH_3CN)_4.PF_6$ (10 mM, 1 mL, dry CH_3CN) for 20 minutes under nitrogen and then (ii) removed from the solution, washed with dry acetonitrile and dried under a flow of nitrogen, and finally (iii) the Cu(I)-DNA film was treated with a solution of phenylsilane (20 mM, 1 mL, dry CH_3CN) under nitrogen, removed, washed with dry acetonitrile and finally dried. FTIR spectra of bare DNA, Cu(I)-DNA and metallised DNA were all recorded.

All FTIR spectra (in the range 600-4000 cm^{-1}) were recorded in transmission mode at room temperature with a Bio-Rad Excalibur FTS-40 spectrometer (Varian, Palo Alto,

CA) equipped with a liquid nitrogen cooled deutarated triglycine sulphate (DTGS) detector, and were collected at 512 scans with 2 cm^{-1} resolution.

3.2.6. AFM and EFM investigations

TappingMode AFM imaging of surface topography was performed in air on both a Multimode Nanoscope IIIa and Dimension Nanoscope V (Veeco Instruments Inc., Metrology Group, Santa Barbara, CA) using 'TAP300Al-G' or 'TESP7' probes (n-doped Si cantilevers, Veeco Instruments Inc., Metrology Group), with a resonant frequency of 234-287 kHz, and a spring constant of 20-80 Nm^{-1}. Data acquisition was carried out using Nanoscope version 5.12b36 (Multimode IIIA) and Nanoscope version 7.00b19 (Dimension Nanoscope V) software (Veeco Instruments Inc., Digital Instruments).

EFM measurements were carried out in air on a Dimension Nanoscope V system using MESP probes (n-doped Si cantilevers, with a metallic Co/Cr coating, Veeco Instruments Inc., Metrology Group), with a resonant frequency of ca. 70 kHz, a quality factor of 200-260, scan rate of 0.3 Hz and a spring constant of 1-5 N m^{-1}. Data acquisition was carried out using Nanoscope version 7.00b19 software.

For both SPM systems, vibrational noise was reduced with an isolation table/acoustic enclosure (Veeco Inc., Metrology Group).

EFM samples are prepared by aligning individual nanostructures on a thermally grown silicon oxide (200 nm) wafer. The backside of the wafer is chemically etched using HF to provide electrical contact to the AFM chuck. A conductive tip is used to probe the surface at a set lift height (typically 50-70 nm) above the surface. The tip is operated in "TappingMode^{TM}" AFM and makes two passes over the surface; the first past acquires a topography image of the sample and the second pass is performed at a set lift height and measure changes in the tip-substrate capacitance. We make the assumption that during the first pass the electrostatic forces are negligible compared to the short range atomic forces, whereas the electrostatic forces become dominant during the second pass. The lift height is chosen to be substantially larger than the amplitude of the tip so as to isolate any changes in the capacitance to the sample composition rather than changes in the tip-substrate distance. An independently controlled bias was used to create an

electric field between the tip and the sample (the tip was grounded, whilst the bias was applied at the sample).

3.2.7. Annealing of Cu-DNA nanostructures

These experiments were performed at the Department of Chemistry, Universidad Autónoma de Madrid (Spain), under the guidance and supervision of Dr Felix Zamora and his research team. The DNA-templated copper nanomaterial aligned on silicon substrates were placed in a 1 inch quartz tube filled with Ar to which an 800 sccm (standard cubic centimetre per minute) H_2 flow was added and the sample was heated to temperatures between 300°C and 500°C. Once the desired temperature was reached the sample was left to anneal for 1 hour and then the furnace was left to cool to room temperature before removing the sample.

3.2.8. Conductive-AFM (C-AFM)

These experiments were performed at the Department of Physics of Condensed Matter, Universidad Autónoma de Madrid (Spain), with the guidance and supervision of Dr Julio Gomez-Herrero and his research team. Samples of the annealed DNA-templated copper nanostructures were prepared and isolated on a TMS-modified Si/SiO_2 substrate as described in sections 3.2.1 and 3.2.2. A metal contact to the nanostructures was prepared by deposition of a thin layer of gold (~30 nm) onto the sample surface; firstly a mask, in the form of a Scanning Probe Microscopy (SPM) cantilever chip, was fixed onto the sample surface which was then placed in a vacuum chamber at a pressure of $\sim 5 \times 10^{-6}$ mbar. The sample was held face up using a bridge support with a gold filament (connected to a thermocouple and ammeter) positioned directly underneath the sample. A current was passed through the filament until a temperature of ~1000°C was recorded and the gold began to sublime at a rate of 0.6 $\text{Å}\ s^{-1}$. After which, the sample was flipped upside down until the correct thickness of gold was deposited onto the sample. The sample was then removed from the chamber and the mask was detached. A drop of silver ink was applied from the gold to the metallic chuck of the AFM to provide electrical connection. The circuit was completed via the contact of the metallic AFM tip to the Cu-DNA nanostructure.

Conductive-AFM (C-AFM) is usually carried out in contact mode for current imaging; however, "TappingMode™" was employed here to acquire topographical data before mechanical contact to the nanostructure was made to acquire current-voltage (i-V) data. The tips used were AFM cantilevers with a ~50 nm Au/Pd coating, which serves as the mobile electrode.

3.3. Results and Discussion

This section is divided into two parts: part (1) describes the characterisation of copper nanoparticles (CuNPs) produced from the reaction of Cu(I) with phenylsilane in the absence of DNA and part (2) describes the formation and characterisation of the DNA-templated form of this material.

(1) Non-templated Studies- Formation of Copper Nanoparticles

Investigations are made here into the compatibility of phenylsilane ($PhSiH_3$) for reduction of tetrakis(acetonitrile)copper(I) hexafluorophosphate ($Cu(CH_3CN)_4.PF_6$) in the preparation of copper nanoparticles (without presence of DNA to act as a template). This non-templated approach was investigated first in order to ensure the successful formation of metallic copper via the reaction scheme employed.

3.3.1. Synthesis & UV/Vis Spectroscopy

Initial studies, based upon spectroscopic evidence, were made to confirm that this approach provides a successful route to metallic copper. The first general indications of a chemical change in the reaction solution, following addition of phenylsilane to Cu(I), were conveyed by a colour change. The colourless Cu(I) acetonitrile solution immediately turns to dark golden brown upon injection of phenylsilane. After several hours of incubation a dark red/brown precipitate forms at the bottom of the container (see fig 3.3). This colour change was studied in more detail using UV-Vis Spectroscopy.

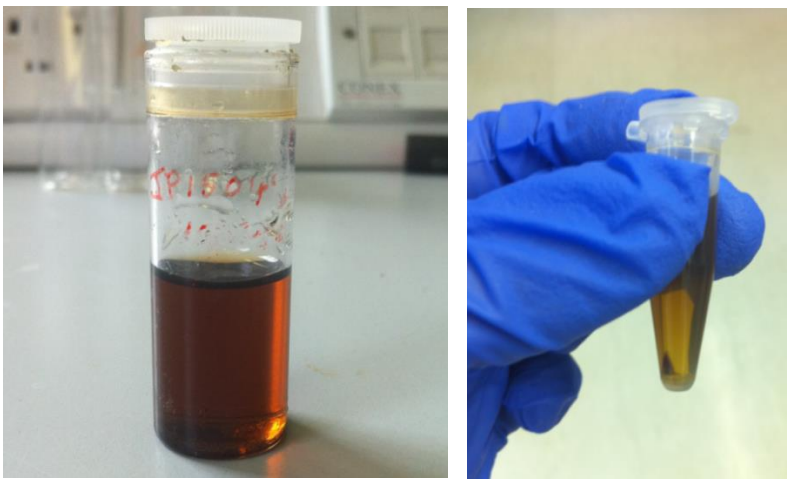

Figure 3.3: (left) Image of a solution containing a dispersion of copper nanoparticles in acetonitrile and (right) the same solution after centrifugation showing the formation of copper powder

The supernatant was decanted and centrifuged to remove residual solid, after which, the pure solution was diluted for analysis by UV/vis spectroscopy. The dried powder was kept behind for analysis by powder-XRD (discussed later in section 3.3.2.1).

Figure 3.4 shows the UV/Vis spectrum obtained for the CuNP solution. The broad absorption centred on ~530 nm is attributed to the surface-plasmon resonance of copper nanoparticles.[17] The resonance is due to oscillation of the free electron density on the surface of copper nanoparticles; whereby the plasmon is a quantisation of this phenomenon. The broadness of the absorption may be attributable to a large size distribution of the nanoparticles.

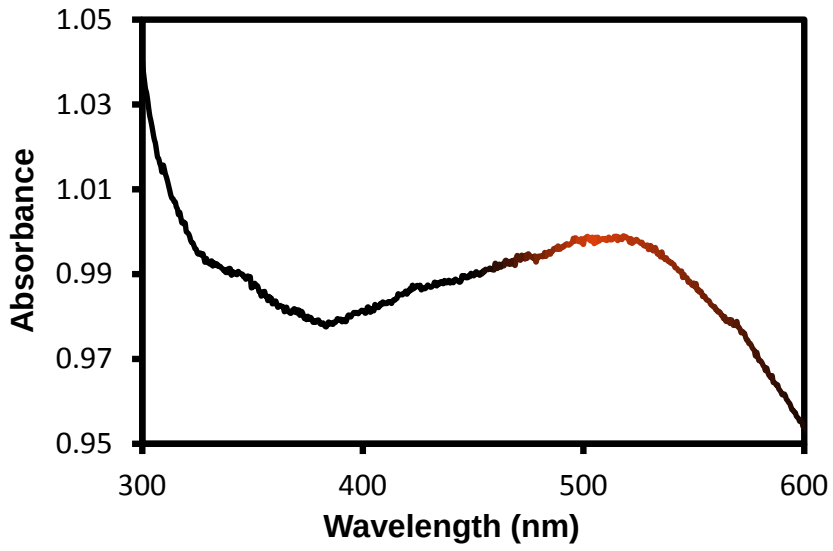

Figure 3.4: UV-Vis absorption spectrum copper nanoparticles dispersed in a solution of acetonitrile

The plasmon absorption at ~530 nm is blue shifted from the typical 560-580 nm bracket for plasmon absorption of copper nanoparticles found in the literature.[12, 18, 19] A blue shift could indicate a smaller mean size of copper nanoparticles; leading to an increase in the metal band gap. However, it is also known that, the position of the plasmon absorption is affected by other factors such as particle shape, solvent and reducing agent employed.[12]

As mentioned earlier for this reaction, according to Takahashi *et.al*., the solvent effect on particle size dispersity and purity was found to be small.[14] The same group also tested a range of reducing agents for a variety of Cu(I) salts (including $Cu(OCOCH_3)$, CuCl and CuBr) in different solvents.[14] They found $PhSiH_3$ to be the most effective at reducing Cu(I) salts into copper nanoparticles, which resulted in a fairly low degree of size dispersity (1-8 nm).

The solution of copper nanoparticles prepared here was diluted in acetonitrile and deposited onto a TMS-modified silicon substrate for structural analysis using AFM (figure 3.5, left). The nanoparticles were found to be spherical in shape and typically 4-10 nm in height; a value consistent with the nanoparticles formed in Takahashi's experiment.[14] Nanoparticles larger than this value (up to 20 nm) were also observed, but less frequently.

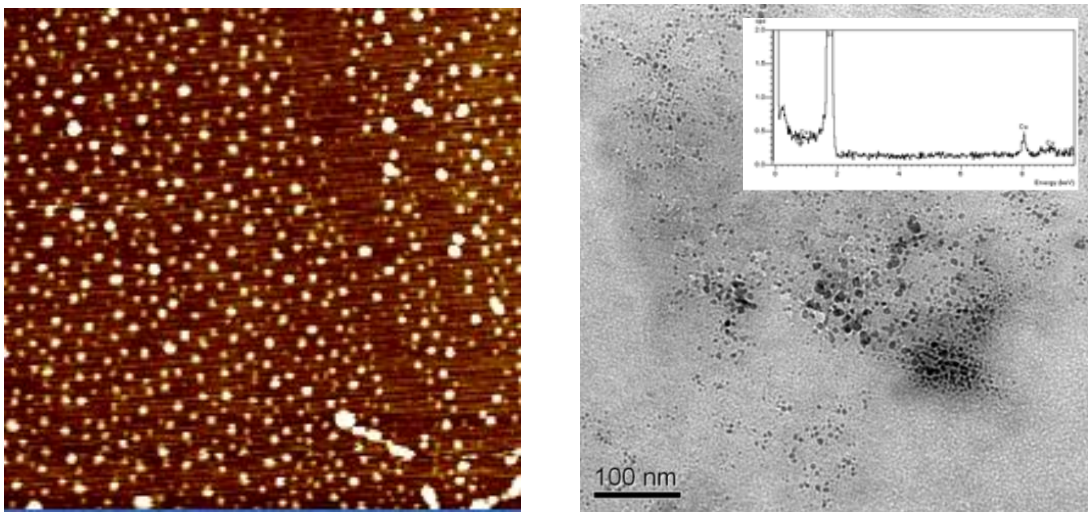

Figure 3.5: (left) AFM topography image of Cu Nanoparticles deposited on a silicon substrate from a dispersion of the reaction solution in acetonitrile. The heights of the particles observed were generally 4-5 nm. Data Scale= 10 nm. (right) TEM contrast image of Cu Nanoparticles dispersed on a Silicon Nitride grid. Inset: EDX spectrum of the same material indicating the presence of copper

The product was also analysed by Transmission Electron Microscopy (TEM) (figure 3.5, right) fitted with an Energy Dispersive X-ray (EDX) analyser to assess the elemental composition. EDX signals arise due to the emission of X-rays from the specimen under a focused electron beam. The electron beam may excite an inner-shell electron causing it to eject from the shell. This leaves a positive hole which is filled by an electron dropping down from an outer shell. The drop in energy is compensated by the release of an X-ray. The energy of the emitted X-ray is the difference between the inner-shell and outer-shell energies and is therefore characteristic of one particular element.

The EDX spectrum (inset figure 3.5, right) indicates the nanoparticles to consist of copper. Although EDX confirms the presence of copper, the technique is unable to determine oxidation state. Therefore EDX is unable to distinguish between copper as a metal or as an oxide, for example. The particles were found to be ~6-10 nm in diameter, corresponding quite well with nanoparticle heights measured from the AFM data (~4-10 nm). Measurement of the particle width using AFM is not very feasible, however. The large radius of the AFM tip (12 nm, maximum), restricts lateral resolution of surface features, rather substantially. The AFM height date on the other hand, as described, does correlate with the sizes obtained here.

The data obtained here has shown that copper nanoparticles can be prepared through reaction of Cu(I) with phenylsilane without the need for a stabilising agent in solution. We now sought to perform an in-depth chemical analysis of this product.

3.3.2. Chemical characterisation of nanoparticles

3.3.2.1. Powder X-ray Diffraction (XRD)

Powder XRD was employed for determining the chemical identity and crystallite phases of the nanoparticles. Figure 3.6 shows the XRD pattern obtained from the dried powder of the reaction. The main reflections seen at 2θ= 43.3°, 50.5°, 74.1°, 89.9°, 95.1° and 117.0° can be indexed to the crystallographic planes of Cu^0 in the order Cu (111), Cu (200), Cu (220), Cu (311), Cu (222) and Cu (400), respectively[12, 18] and a small peak at ~36° due to CuO.

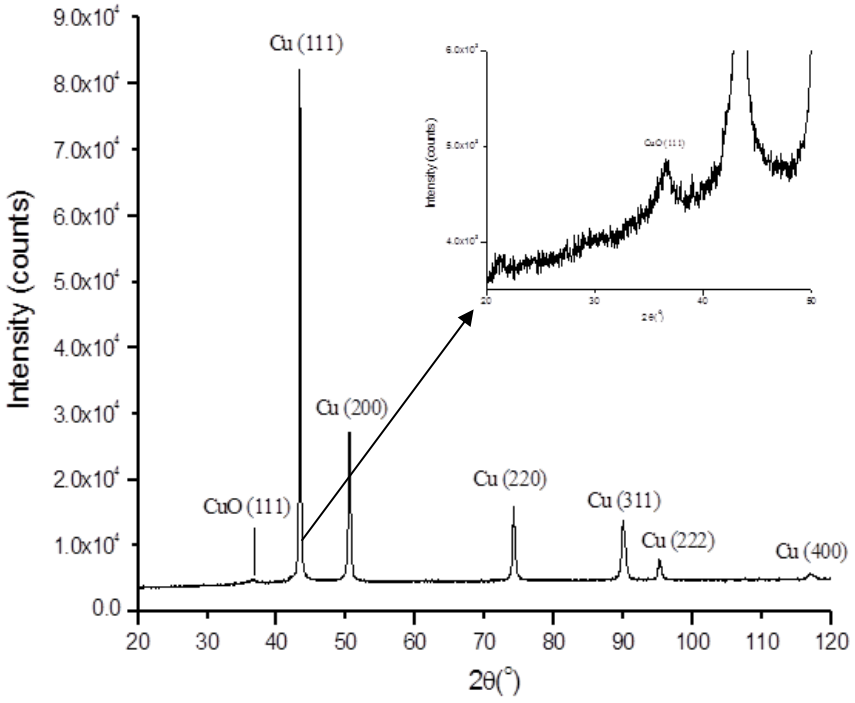

Figure 3.6: XRD pattern of Cu^0 powder prepared in solution by reaction of $Cu(CH_3CN)_4.PF_6$ with $PhSiH_3$. Inset: Expanded region 2θ= 20-50°, showing a minimal amount of oxidation has taken place. Analysis of the Cu(111) peak fitted to a Pseudo-Voigt profile using the Scherrer Equation indicates the average crystallite size to be ~40 nm. Repeat analysis on the CuO (111) peak gave an average crystallite size of the CuO ~ 4nm

Information from the diffraction pattern (FWHM of peaks) was also able to be used to assess the average crystallite diameter of the copper material produced, using Scherrer's Equation[†] (equation 3.1):

$$\tau = K.\lambda / \beta\cos(\theta) \quad \textbf{(equation 3.1)}$$

where τ= mean diameter of the crystallite, K= shape factor (constant), λ= X-ray wavelength β= *line broadening at full width half maximum (FWHM) and* θ= *Bragg angle*

The mean diameter of the metallic copper phase was 40 nm (based on analysis of the Cu (111) peak using X'Pert Data Viewer software). The inset of figure 4.6 shows an expanded region in the spectrum from 20-50°. This reveals a small peak at ~36° corresponding to the CuO (111) plane. Scherrers' equation was again employed, for

[†] It is noted that estimation of particle diameter using the Scherrer equation is limited to nanoscale objects and thus breaks down with crystallite dimensions >100 nm. The value also constitutes a lower bound to the estimate.

estimation of the mean diameter of the CuO phase; albeit to a low degree of accuracy due to the error associated with measuring the FWHM of this peak. The calculation gave a value of ~4 nm, which is considerably smaller than that obtained for Cu^0 and is unlikely to comprise much of the bulk material in the sample.

The copper surface however, is the most likely region for oxidation to occur and this will therefore be investigated by X-ray Photoelectron Spectroscopy (XPS), which is an ideal tool for surface composition analysis.

3.3.2.2. X-ray Photoelectron Spectroscopy (XPS)

XPS is quantitative technique for chemical analysis of solid samples and is highly surface sensitive. It is used here to elucidate the surface composition of copper nanoparticles, prepared in the absence of DNA to act as a template. Nanoparticles are drop cast from solution onto a silicon support for analysis. All peak values are quoted as binding energies; for 2p spectra these are in reference to the '$2p_{3/2}$' peaks only. The red line in the spectra represents the sum fit, the grey lines represent the individual peak fits and the hollow squares represent the actual data points.

The Cu2p spectrum (figure 3.7, top) shows a split band arising from the spin-orbit coupling of 2p electrons.[‡] The asymmetry in the main $Cu2p_{3/2}$ and $Cu2p_{1/2}$ envelope peaks, as indicated by the slight shouldering suggests the presence of multiple components in the spectrum. These can be assigned as comprising two sets of doublets.

Firstly, the peak at 932.7 eV (for $Cu2p_{3/2}$ with splitting= 19.8 eV) is known to originate from Cu^0 and is in good agreement with the literature values.[12, 20] However, there can be associated challenges/difficulties with the interpretation of the Cu2p spectra. The Cu2p binding energy values for Cu^0 and Cu^I species overlap considerably due to a small energy separation (~0.1 eV) of these spectral components and they cannot therefore be easily distinguished from one another. This incidence suggests that the peak at 932.7 eV could be due to two possible species, Cu^I or Cu^0. The interpretation is made especially difficult in view of the fact that neither species gives rise to characteristic satellite structure (as Cu^{II} does, explained later in this section) as a result of both species possessing a filled 3d sub-shell.[21] Evaluation of additional data such as XRD is

[‡] The +1/2 and -1/2 spins couple with the orbital angular momentum of the p orbital (which is 1) giving rise to a doublet in a 2:1 (*3/2 : 1/2*) ratio.

therefore necessary to make this distinction, in order for us to be confident that the species in question is indeed metallic copper. As discussed based on the XRD data in the previous section, the powder obtained from the reaction of Cu(I) with phenylsilane pointed to pure metallic copper rather than Cu^{I} species such as Cu_2O. This supports the assignment of metallic copper in the XPS data, here.

The other doublet at 934.5 eV (for $Cu2p_{3/2}$ with splitting= 20.1 eV) is attributable to $Cu(OH)_2$.[22] The integrated area of the Cu and $Cu(OH)_2$ doublets are ~38% and ~36%, respectively.

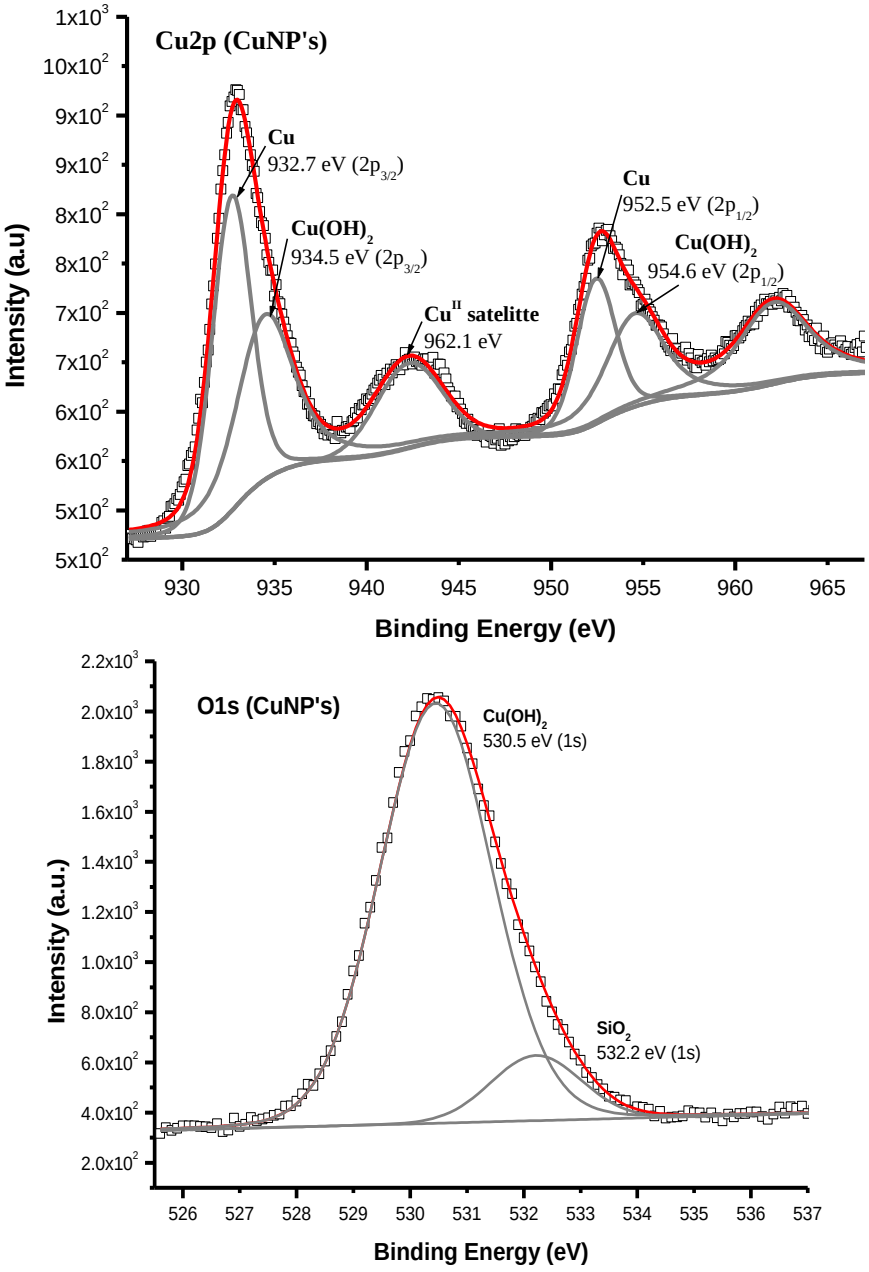

Figure 3.7: (top) Cu ($2p_{1/2}$ and $2p_{3/2}$) and (bottom) O (1s) XPS spectra of Cu powder NP's (as for XRD) deposited on a silicon support. The asymmetry of the Cu2p doublet peak suggests multiple lines arising from Cu^0 and $Cu(OH)_2$ at 932.7 eV and 934.5 eV, respectively, with splitting values of 19.8 eV and 20.1

eV, respectively. The existence of the satellite peak at ~942.3 eV is indicative of Cu(II) paramagnetic species, which confirms the presence of $Cu(OH)_2$

The presence of a Cu^{2+} "shake-up" satellite peak at 962.1 eV could also be identified and is fitted as a separate peak. The satellite peak originates from the poorly charge-screened state of Cu^{2+} ($2p^5 3d^9$) following a 2p electron ejection, whereas the main Cu^{2+} doublet peak corresponds to the well-screened state ($2p^5 3d^{10}$). The latter originates from charge-transfer of a ligand electron into a 3d orbital of copper.[23, 24] This serves to screen the core-hole charge following ejection of a core electron ($2p^5$). The satellite signal further verifies the existence of a Cu^{2+} species (i.e. $Cu(OH)_2$) on the sample surface.[22]

Analysis of the O1s spectrum (figure 3.7, bottom) of the CuNP's reveals an asymmetrical peak owing to the presence of two single components; $Cu(OH)_2$ at 530.5 eV, which is in good agreement with a previous report,[25] and SiO_2 at 532.2 eV.

In summary, XRD confirmed the nanoparticles to consist of metallic copper, but was unable to provide evidence of $Cu(OH)_2$ on copper in the sample. This is due to the technique's relativity low surface sensitivity compared to XPS. XRD is a bulk diffraction technique and can therefore provide positive identification of species in the bulk phase, only. Based on analysis of both sets of data, it is logical to assert that, the as formed nanoparticles are comprised of a metallic copper core (bulk) encapsulated by a $Cu(OH)_2$ shell layer. The presence of high oxidation species on the surface of copper is likely a consequence of the material being in contact with air. It has been noted in the literature that the formation of copper hydroxide, a metastable overlayer, is part of a mutually dependent process towards the full oxidation of metallic copper to the more stable CuO.[26]

(2) DNA-templated Studies- Formation of 1-D Copper Nanostructures

It has so far been demonstrated that copper nanoparticles can be successfully formed through the reduction of Cu(I) ions using phenylsilane as a reducing agent in low polarity solvent.

In the following section, reactions are performed at DNA-templates immobilised on TMS-modified silicon substrates. The role of DNA is to generate 1-dimensional nanostructures on the surface by guiding and controlling the formation of the previously described copper nanoparticles in a single uniform direction. In each experiment the 2-step ('doping/reduction') chemical templating approach (as described in section 3.2.2) on surface-immobilised DNA is adhered to. This involved (i) doping of DNA with Cu(I) ions and (ii) reduction of DNA-Cu(I) by addition of phenylsilane. Various techniques were employed to characterise the DNA-templated copper nanomaterial chemically (XRD, XPS), structurally (FTIR, AFM) and electrically (EFM, C-AFM).

Firstly, chemical characterisation of the product material was carried out using XRD and XPS.

3.3.3. Chemical characterisation of 1-D nanostructures

3.3.3.1. Powder X-ray Diffraction (XRD)

As well as preparing a surface-based sample by reduction of Cu(I) on surface-immobilised DNA, as described above, analysis of a copper "powder" was also obtained by carrying out a large-scale preparation in aqueous DNA solution (see section 3.2.3).

Surface-based sample. In order to obtain useful XRD data of surface based material, it is necessary to increase the density of both DNA and copper in the sample compared to usual AFM sample preparations; designed for single molecule analysis. It was found that typically flat silicon wafers do not support/hold a sufficient density of material on

the surface required to yield adequate 'signal to noise' ratio in the XRD spectra (even over long scan intervals). To overcome such limitations, one may increase the surface area of silicon.

Porous silicon has a large specific surface area capable of supporting a high density of material,[27, 28] such as DNA. It has been used extensively in the preparation of nanocomposite materials and doped/modified porous networks.[27, 29-31] Such materials have been shown to offer more efficient output properties, such as luminescence.[32] Electroless metallisation of porous silicon has also been used in the past to form metal contacts such as nickel.[29] Indeed thin copper films have been grown onto electrochemically prepared porous silicon and were characterised by XRD.[30] In this experiment the high surface area of the porous substrate, formed by electrochemical etching also, is exploited for pore filling by means of adsorption of DNA from solution. After which, the substrate is metallised by electroless deposition of copper, as described in section 3.2.2.

Electrochemical etching, using HF(aq.), of a clean silicon substrate resulted in a dense H-terminated porous silicon structure, as indicated by a simple FTIR transmission spectrum (figure 3.8). The spectrum reveals a split band owing to three separate Si-H stretches, at 2087.9 cm^{-1}, 2111.1 cm^{-1} and 2138.6 cm^{-1}, corresponding to SiH, SiH_2 and SiH_3, respectively.[33] Another strong absorption was found at 913.6 cm^{-1} which is assigned to the SiH_2 scissors mode.[34] The presence of these four distinct Si-H stretches in the FTIR spectrum confirmed the porous nature of the silicon substrate.

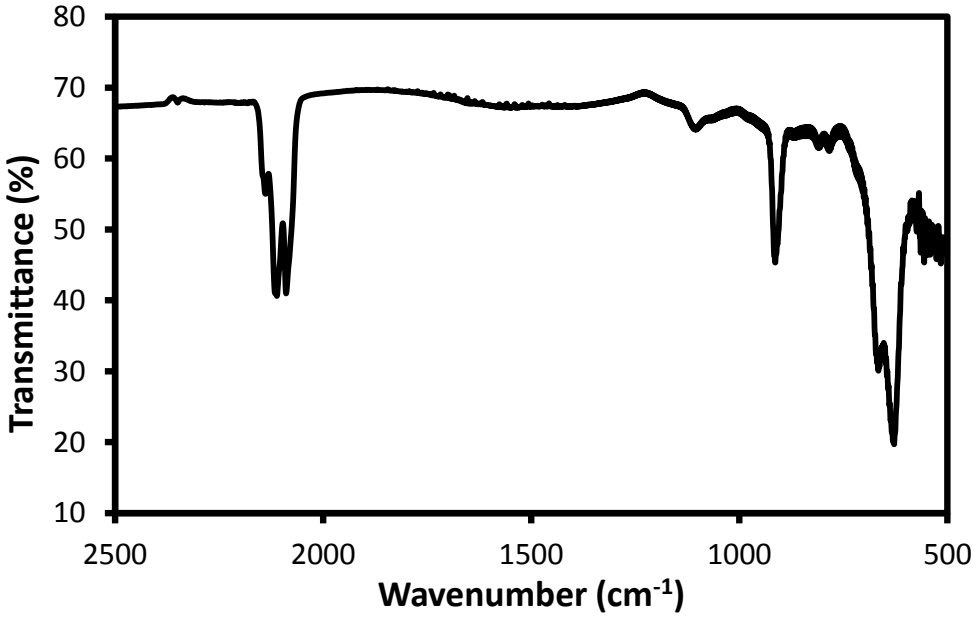

Figure 3.8: FTIR spectrum of porous silicon showing the distinct Si-H stretches synonymous with a porous silicon substrate

DNA was then deposited onto the porous silicon substrate and metallised with copper via the usual 2-step doping/reduction approach in dry acetonitrile. The XRD spectrum was recorded, as shown in figure 3.9, on this metallised DNA-porous silicon sample.

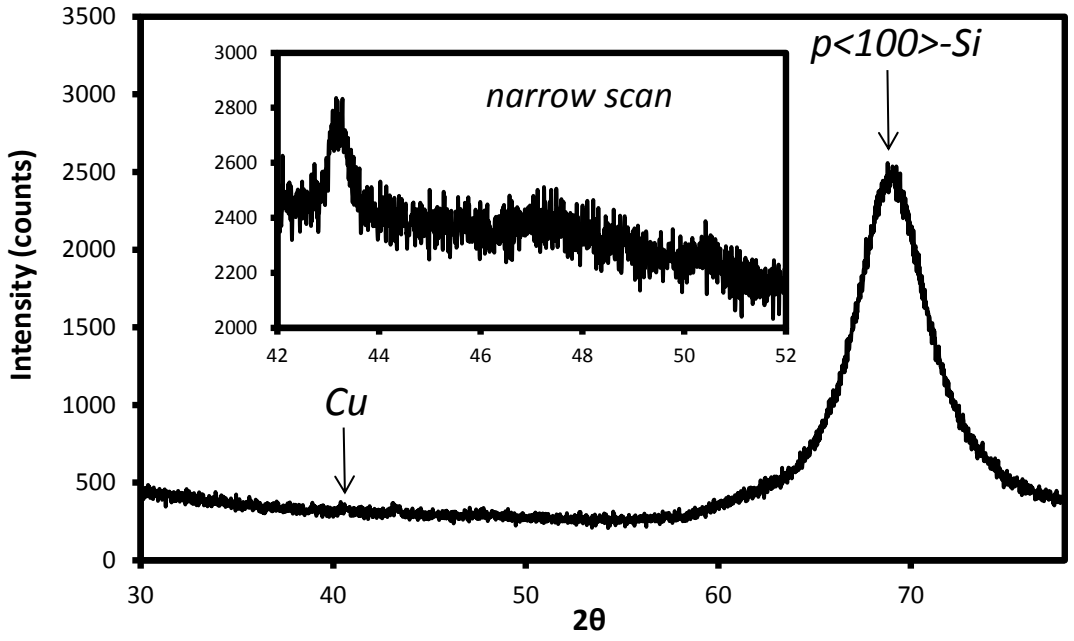

Figure 3.9: XRD spectrum in the region 30-80° of Cu-DNA nanomaterial formed on a porous silicon surface, with inset showing narrow scan containing the highest intensity reflection attributable to metallic copper

A weak copper signal is observed at ~43°; the expected position for the main reflection of metallic copper (111). The narrow scan at this region (figure 3.9, inset) shows this peak more clearly and provides evidence for metallic copper in this sample. In order to provide higher intensity XRD data, a sample is prepared in DNA solution in order to precipitate a 'powder' and a further spectrum is recorded.

Solution-based sample. This sample was prepared under different reaction conditions than for the surface-based sample. Namely, the sample was prepared in a solution of DNA. DNA is insoluble in acetonitrile, which is required for solubilising Cu(I) and phenylsilane, but is highly soluble in water. Therefore a mixed water/acetonitrile solvent system was used in this preparation. For the surface-based approach where DNA is fixed to the substrate, pure dry acetonitrile was used as solvent.

Figure 3.10 shows the powder-XRD spectrum obtained on the dried copper material obtained by precipitation from DNA solution. The set of reflections seen at 43.3° (FWHM= 0.64°), 50.5°, 74.1°, 90.0° and 95.2° can all be indexed to the crystallographic planes of metallic copper as quoted earlier in the chapter (section 3.3.2.1). The remaining two peaks at 36.5° (FWHM= 0.62°) and 61.5° are attributed to the two most intense reflections of cuprous oxide (Cu_2O), the (201) and (111) planes, respectively. Although, another intense reflection of Cu_2O is masked by the main Cu reflection at ~43°, where there is a clear shouldering of the peak present. The use of 'wet' solvent conditions (i.e. the presence of water) in this large-scale solution preparation may have led to the oxidation of copper to Cu_2O. Oxide species were not clearly present in the XRD for copper nanoparticles (see section 3.3.2.1), where almost pure metallic copper was formed, and this may be due to the use of entirely dry reaction conditions in their preparation.

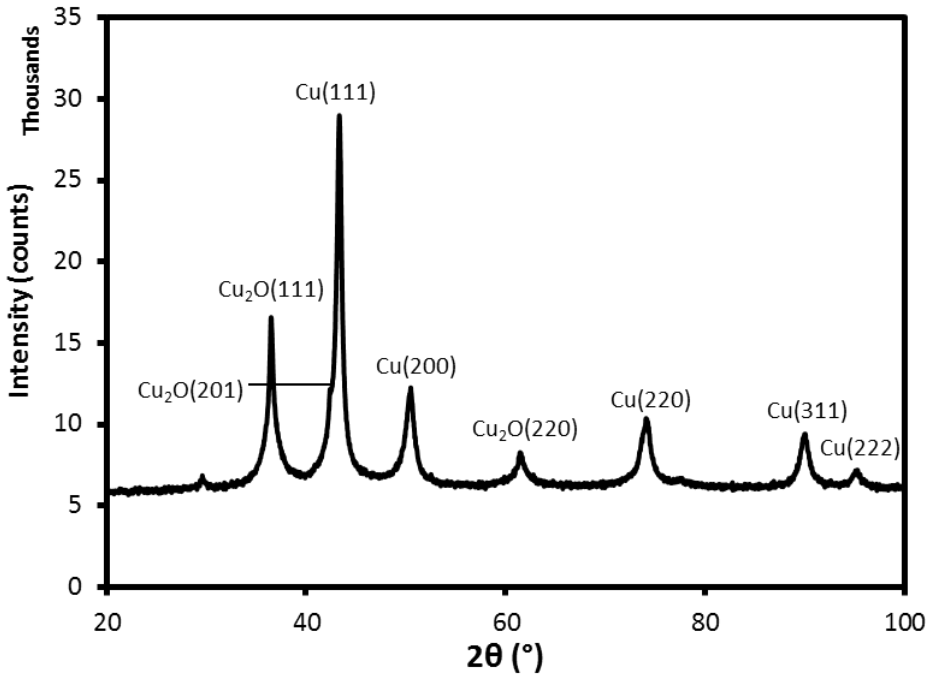

Figure 3.10: XRD spectrum of powder sample of Cu-DNA nanostructures formed in a solution of DNA

The mean crystallite size of Cu^0 based on the (111) reflection was calculated as 13.2 nm, based on the Scherrer equation (3.1). This value indicates that the material formed is nanoscale and may be in fact DNA-templated. Comparison of this value to that obtained for the non-templated copper nanoparticles at 40 nm mean diameter suggests that DNA is responsible for controlling the growth/aggregation of nanoparticles in solution. The role of DNA should, ideally, serve to produce efficient packing of copper material along the template axis for generation of smooth and continuous one-dimensional architectures. For Cu_2O the mean crystallite size was calculated as 13.3 nm, based on the (111) reflection also.

Powder-XRD studies conducted by Watson *et.al* on their DNA-templated copper powder samples revealed that the material formed was microcrystalline.[5] This is in contrast to the material obtained here which is nanoscale.

The data presented thus far has indicated that metallic copper has formed in the presence of DNA templates (and a small amount of oxidised species), in both solution and surface studies, and the resulting material is nanoscale.

3.3.3.2. X-ray Photoelectron Spectroscopy (XPS)

The aim of this experiment is to provide further evidence of metallic copper in the sample, as suggested by XRD, and assess the surface composition. XPS is a highly surface sensitive technique, which should provide conclusive evidence of (potential) surface oxidation species, such as CuO or $Cu(OH)_2$, residing on the nanostructures.

The C1s spectrum of the sample is shown in figure 3.11 (left) where the adventitious carbon peak is identified. The higher binding energy peaks fitted to the spectrum (four of them) are due to other carbon based functionality such as those that make up the DNA nucleobases and sugar groups.

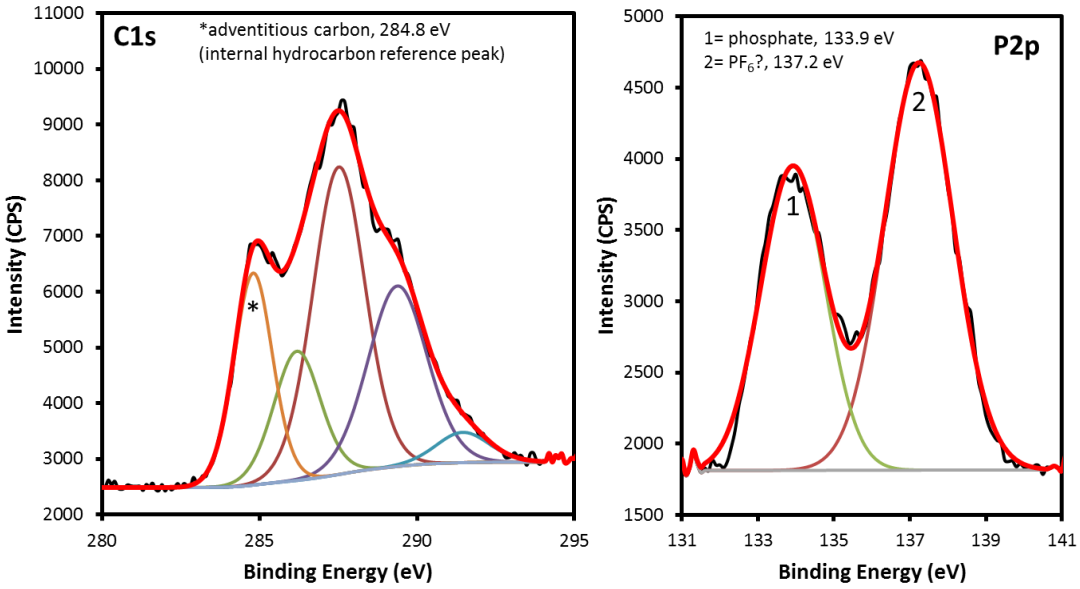

Figure 3.11: (left) C1s and (right) P2p spectra of Cu-DNA nanomaterial formed on a silicon substrate. TheC1s spectrum is used to identify adventitious carbon (marked with an asterisk) and the P2p spectrum is used to characterise DNA

The presence of DNA on the surface is confirmed by analysis of the P2p spectrum (figure 3.11, right). There are two sources of phosphorus in this sample: (i) DNA phosphate and (ii) PF_6^- counter ion of the Cu(I) salt. Both species were resolved in the P2p fit. The phosphate peak was identified at 133.9 eV which is in good accordance with the literature,[35] and the peak at 137.2 eV is close to the reported binding energies for salts containing the PF_6^- counter anion.[36] The presence of the counterion within the sample may suggest that the Cu(I) salt was not fully solubilised and had precipitated onto the surface.

The Cu2p spectrum, shown in figure 3.12, displays an asymmetrical doublet which can be ascribed as comprising three individual doublets. These lines were fitted to 932.8 eV (splitting=19.8 eV), 934.4 eV (splitting= 20.0 eV) and 936.2 eV (splitting= 19.9 eV), which match the binding energies and splitting values generally reported for Cu^0, $Cu(OH)_2$ and CuF_2,[37] respectively. The area under each peak was calculated as a percentage of the total area of the fitted spectrum. These values give an estimated % composition of the various forms of copper in the sample. The resulting composition of Cu^0, $Cu(OH)_2$ and CuF_2 was 42.9%, 29.3% and 15.5%, respectively, indicating much of the material to consist of metallic copper. The presence of copper and copper hydroxide in the sample agrees with the identification of these species in the XPS data of the non-templated copper nanoparticles (see section 3.3.2.2). This could originate from the disproportionation of Cu^+ to Cu^0 and Cu^{2+} (i.e. $Cu(OH)_2$. Another explanation offered, for the origin of Cu^{2+}, is due to the oxidation of copper metal upon being formed, after being in contact with air. Following prolonged exposure to air $Cu(OH)_2$ may convert to the more stable CuO.

CuF_2 on the other hand, is an impurity likely to originate from the presence of F^- of the counter ion. The presence of Cu^{2+} species in the sample is further supported by the origin of the Cu^{2+} satellite peak at 934.5 eV.

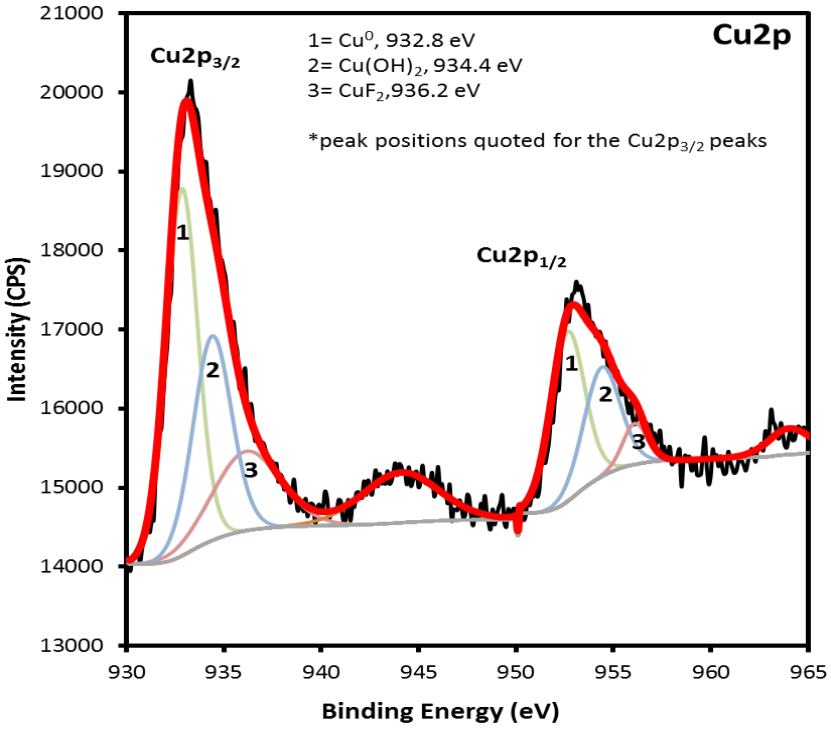

Figure 3.12: Cu2p ($p_{1/2}$ and $p_{3/2}$) spectrum of Cu-DNA nanomaterial showing doublet formation owing to the splitting of individual lines. The asymmetry of the main envelope peaks indicates the presence of multiple components in the sample. These are labelled 1-3

$Cu(OH)_2$ was identified as a singlet in the O1s spectrum (figure 3.13) at 531.3 eV, which is in good agreement with the literature.[38, 39] The remaining two peaks at 532.9 eV and 534.5 eV are due to the SiO_2 substrate and, to a lesser degree of confidence, ketone functionality.

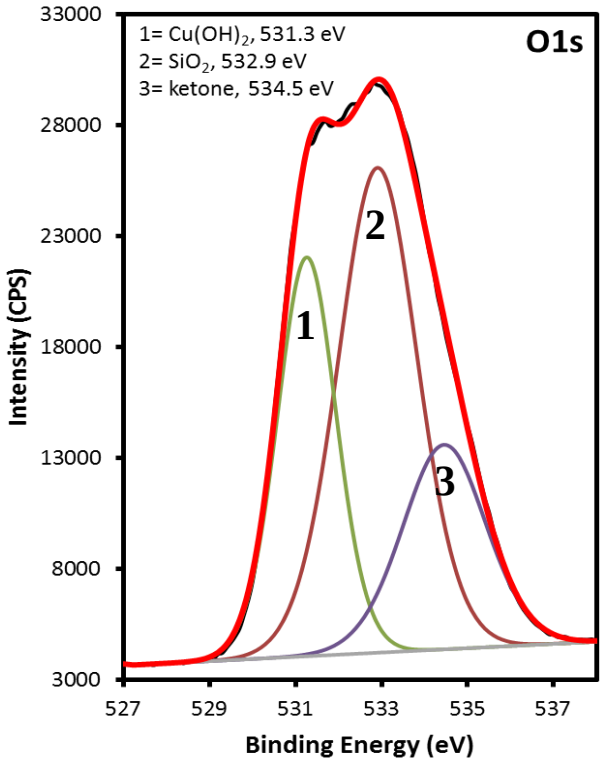

Figure 3.13: O1s spectrum of Cu-DNA nanomaterial formed the silicon surface. The peak was fitted to three different components as indicated by numbers 1-3

Copper hydroxide ($Cu(OH)_2$) is observed as a major component in the XPS spectra here, but was not identified in the XRD pattern. Based on this evidence it seems likely that the copper hydroxide resides primarily on the surface of the copper as a thin layer (as was hypothesised for copper nanoparticles). The low surface sensitivity of XRD could explain why $Cu(OH)_2$ was not observed in this case. Taking all of the XRD and XPS data into account, the Cu-DNA nanostructures produced from the surface-based reaction are likely to be comprised of a metallic copper core encapsulated with a copper hydroxide shell.

3.3.4 Structural characterisation of 1-D nanostructures

3.3.4.1. Fourier Transform Infra-Red (FTIR) Spectroscopy

FTIR spectroscopy is employed here as a technique to investigate and elucidate the interaction(s) of DNA with Cu(I) ions. The interaction of DNA with Cu(II) ions has been well reported,[10, 40-42] however to the best of our knowledge there are currently no spectroscopic data for the analogous interaction of DNA molecules with Cu(I). Investigations into the possibility of forming such DNA-complexes are limited to theoretical studies.[43, 44] Indeed, to the best of our knowledge there is no experimental evidence for Cu^{+} binding to nucleobase sites of DNA or at the phosphate groups. A search of the Cambridge Structural Database (CSD) did not return any results for Cu^{+} complexes binding to any of the nucleobases sites (unmodified or modified nucleobases).

The potential to use weakly coordinating solvents to solubilise the reaction components was a motivating factor for opting to use a Cu(I) precursor in preference to the standard Cu(II). The use of less polar solvents may lead to enhanced interaction of Cu(I) with DNA binding sites, as a result of the ions being 'free' of strongly coordinating molecules. These sets of experiments comprise the first FTIR studies, indeed the first experimental studies, reported for Cu(I) ion-DNA interaction. Furthermore the binding properties of copper metal on DNA are investigated by chemical reduction of the DNA/Cu(I) nanomaterial.

Two approaches to Cu-DNA nanostructures will be investigated by FTIR in this section. The first method is the 'doping/reduction' procedure (**Method A**), which involves combining the Cu(I) and phenylsilane solution (both in acetonitrile solvent) during reaction at surface-bound DNA to afford the *in situ* metallised DNA sample. This experiment allows for FTIR comparison of DNA before and after metallisation. The second method (**Method B**) is the 'doping/withdrawal/reduction' procedure, whereby surface bound DNA is doped with Cu(I) and examined by FTIR. After which, the Cu(I)-DNA sample will be placed into a pure reducing solution of phenylsilane, removed, and then another spectrum will be recorded (full details given in section 3.2.5). This experiment allows for FTIR comparison of DNA before and after complexation with Cu(I) ions and then reduction to the zero-valent metal.

Indications of Cu(I) and Cu(0) interaction with DNA are conveyed by significant changes in the DNA peak positions/intensities following treatment with Cu(I) and phenylsilane. All peak shifts reported are relative to the peak positions of bare DNA.

Method A- *Formation of Copper Nanostructures via 'doping/reduction' approach on surface-immobilised DNA*

The spectrum of bare DNA (figure 3.14, black line) displays a range of backbone and nucleobase vibrations/stretches of adenine (A), thymine (T), cytosine (C) and guanine (G). The split band centred at 1670 cm^{-1} (peaks 1 and 2) originates from C2=O stretches of guanine and cytosine, as well as the overlapping adenine, thymine and guanine stretches. Other intense peaks are attributable to the phosphodiester backbone stretches in the region 1050-1300 cm^{-1}. (peaks 10, 11 and 12). The remainder of the spectrum, 1300-1600 cm^{-1}, consist of less well defined peaks owing to the various C-C and C-N stretches of the nucleobases in the double helix, as well as the C-C and C-O stretches in the sugar moieties <1050 cm^{-1}. Full peak assignments are given in table 3.1 below and are supported by references.[5, 45-48]

A number of small peak shifts in the FTIR spectrum (figure 3.14) of DNA are observed, subsequent to the metallisation of DNA by treatment with combined Cu(I)/phenylsilane solution (orange line). The numbers highlighted in red are the peaks which are affected most strongly (>2 cm^{-1}).

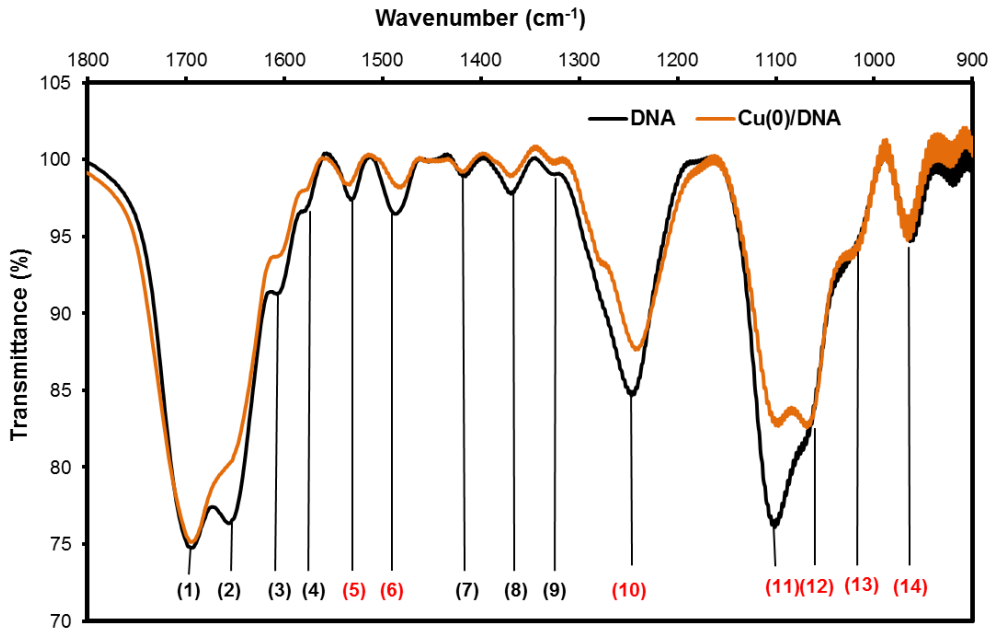

Figure 3.14: FTIR spectra overlay of DNA film before (black line) and after (orange line) treatment with $Cu(CH_3CN)_4.PF_6$ and phenylsilane. The numbers below the graph point to individual vibrations/stretches of the DNA backbone and nucleobases. The numbers highlighted in red refer to absorptions which have shifted by ≥ 2 cm^{-1} (the resolution of the spectrometer) due to DNA-Cu^+ complexation, and they correspond to the red numbers in the table below

Peak number	Assignment	Wavenumbers (cm^{-1})		
		DNA	DNA/Cu(0)	Shift
1	N-H thymine; Adenine vibration; C6=O stretch of guanine	1692.8	1693.3	0.5
2	In-plane vibrations of adenine, thymine and guanine; C2=O stretch of cytosine	1655.4	1657.2	1.8
3	C=N cytosine; N-H adenine; C=7 adenine	1606.7	1606.7	0
4	C=N guanine and adenine stretch	1578.9	1577.2	-1.7
5	In-plane vibration of guanine and cytosine	1529.8	1533.5	3.7
6	C8-N coupled with a ring vibration of guanine	1486.6	1481.4	-5.2
7	C-N stretch of thymine, guanine and cytosine	1415.7	1417.8	2.1
8	C-N stretch of guanine and cytosine	1369.4	1367.7	-1.7
9	C-N stretch of adenine	1324.8	1324.2	-0.6
10	PO2- asymmetric stretch	1246	1240.2	-5.8
11	PO2- symmetric stretch	1101.1	1097.4	-3.7
12	P-O or C-O backbone stretch	1075.1	1068.3	-6.8
13	C-O deoxyribose stretch	1024	1020.4	-3.6
14	C-C deoxyribose stretch	960.8	966.2	5.4

Table 3.1: Assignment of FTIR absorptions of DNA before and after metallisation with $Cu(CH_3CN)_4.PF_6$/phenylsilane. The corresponding wavenumber shifts of each stretch due to metal binding are shown in the table; the larger the shift the stronger the interaction. Each shift is in reference to the bare DNA peak position

Peaks 10-14 are all shifted by several wavenumbers. Each of these peaks is attributed to the phosphodiester backbone of DNA. In addition to a change in peak position, the phosphate band around 1050-1175 cm^{-1} (comprising peaks 11 and 12) is significantly reduced in intensity, indicating metal coordination at the DNA phosphate groups. The negative charge of oxygen within the phosphate groups facilitates the interaction with positive metal ions, providing partial charge neutralisation of the DNA duplex.[49] Binding of metal ions frequently occur at these sites, particularly hard metal ions.[41, 50]

Coordination to the nucleobases via the N and/or O donor sites may also be a possibility for Cu^{+} and is known for Cu^{2+}.[51-53] A combination of both nucleobase and phosphate binding has also been reported for Cu^{2+}.[50, 54] However there is no literature precedent for Cu^{+} binding to un-modified nucleobase sites of DNA.

In these current studies, interaction at the nucleobase sites of G and C is implied by peak shifts of the G and C ring vibrations (5 and 6) and a reduction in intensity at these positions, following metallisation of DNA. The in-plane vibration of G and C increased in wavenumber by 3.7 cm^{-1}, whereas the C8-N of adenine (A) decreases by 5.2 cm^{-1}. The N7 site of G and A is a major binding site and is particularly common for metal ions, irrespective of the nature of the metal ion.[50] Other common binding modes are at the O6 of G and N3 of A and C.[54]

It has been demonstrated in the literature that a GC rich DNA environment is more affected by addition of Cu^{2+} than for AT rich DNA, indicating interaction at G and C sites primarily.[9, 55] This result agrees with our FTIR data which indicated some interaction of copper with C and G. Basu *et.al* compared the interactions of the four nucleobases with individual Ag nanoparticles and determined the strength of interaction of Ag to nucleobase in the order C >G > A > T.[56] The exocyclic nitrogen of cytosine was thought bind Ag more strongly.

Interestingly in figure 3.14 the intensity of the C6=O stretch of guanine (peak 1) within the split band centred at around 1680 cm^{-1} remains unchanged after metallisation, whereas the C2=O stretch of cytosine (peak 2) is reduced in intensity following metallisation. This could indicate preferential binding to the cytosine nucleobases over guanine.

Method B- *Formation of Copper Nanostructures via the 'doping/withdrawal/reduction' approach on surface-immobilised DNA*

FTIR spectra (figure 3.15) were recorded for comparison of (a) bare DNA, (b) Cu(I) doped DNA and (c) Cu metallised DNA, via the 'doping/withdrawal/reduction' procedure described in section 3.2.5. The spectra are overlaid for direct comparison. Table 3.2 gives the position of each peak and corresponding peak shift for comparison.

The recorded FTIR spectrum of DNA after Cu(I) doping treatment (b) does not result in significant change to the spectrum relative to bare DNA (a). Additionally, there was little change to the FTIR spectrum following reduction of the DNA-Cu(I) sample to DNA-Cu(0) (c).

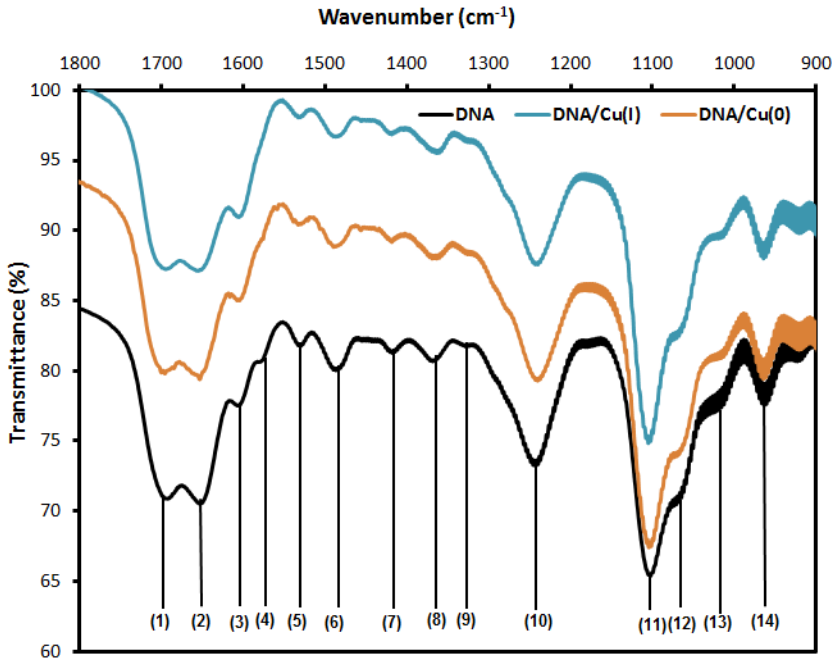

Figure 3.15: FTIR spectra comparison of DNA before (black line), after treatment with $Cu(CH_3CN)_4.PF_6$ (blue line) and then following subsequent treatment with phenylsilane (orange line). The numbers below the graph point to individual vibrations/stretches of the DNA backbone and nucleobases. There were no significant changes to report in peak positions or intensities

Peak number	Assignment	Wavenumbers (cm^{-1})				
		DNA	DNA/Cu(I)	Shift	DNA/Cu(0)	Shift
1	N-H thymine; Adenine vibration; C2=O stretch of guanine	1692.5	1694.7	2.2	1693.7	1.2
2	In-plane vibrations of adenine, thymine and guanine; C2=O stretch of cytosine	1653	1654.9	1.9	1653.3	0.3
3	C=N cytosine; N-H adenine; C=7 adenine	1606.9	1605.5	-1.4	1604.9	-2
4	C=N guanine and adenine stretch	1581.2				
5	In-plane vibration of guanine and cytosine	1530.3	1530.5	0.2	1529.8	-0.5
6	C8-N coupled with a ring vibration of guanine	1487	1486.1	-0.9	1489	2
7	C-N stretch of thymine, guanine and cytosine	1417.7	1418.6	0.9	1418.6	0.9
8	C-N stretch of guanine and cytosine	1368.7	1363.8	-4.9	1367	-1.7
9	C-N stretch of adenine	1326.2	1325	-1.2	1327	0.8
10	PO2- asymmetric stretch	1242.9	1240.4	-2.5	1240.3	-2.6
11	PO2- symmetric stretch	1102.5	1104.2	1.7	1101.9	-0.6
12	P-O or C-O backbone stretch	1068.7	1068.7	0	1068.1	-0.6
13	C-O deoxyribose stretch		1017.1		1016.3	
14	C-C deoxyribose stretch	963.5	964.4	0.9	964.2	0.7

Table 3.2: Assignment of FTIR absorptions of DNA before and after complexation with $Cu(CH_3CN)_4.PF_6$ and reduction with phenylsilane. The corresponding wavenumber shifts of each stretch due to Cu(I) binding Cu metal formation are shown in the table. Each shift is in reference to the bare DNA peak position

As noted, there were no significant changes in the peak positions after DNA was treated with Cu(I) ions. However, the most noticeable shifts included the C2=O stretch of G (1) which shifted by +2.2 cm^{-1}, the C-N stretch of G and C (8) shifting by -4.9 cm^{-1} and the PO^{2-} asymmetric stretch (10) shifting by -2.5 cm^{-1}. After the same sample was treated with a solution of phenylsilane, the spectrum revealed the peak positions of 1 and 8 shifted back to a position matching more closely that of bare DNA. Only the asymmetric phosphate stretch remained shifted (relative to bare DNA) after treatment with phenylsilane.

The lack of significant changes in the FTIR spectra here may suggest that copper is less strongly coordinated to the DNA template and/or less copper is bound per DNA phosphate. These FTIR results are in contrast to those obtained from 'Method A,' whereby reduction of Cu(I) at DNA took place *in situ*. That approach led to more change in the FTIR spectrum of bare DNA, in terms of changes in peak positions and absorption intensities.

Indeed, the AFM data (figure 3.16) of Cu-DNA nanostructures prepared by each respective method supports these results. An AFM topography image of a Cu-DNA

strand produced by 'Method B' indicates an incomplete level of metallic coverage along the template. In this example bare DNA is left exposed between particles, affording a 'beads-on-a-string' assembly (refer to figure 3.16b). This is in plain contrast to the Cu-DNA nanostructure prepared by 'Method A' which appears relatively smooth and 'wire-like' (figure 3.16 a).

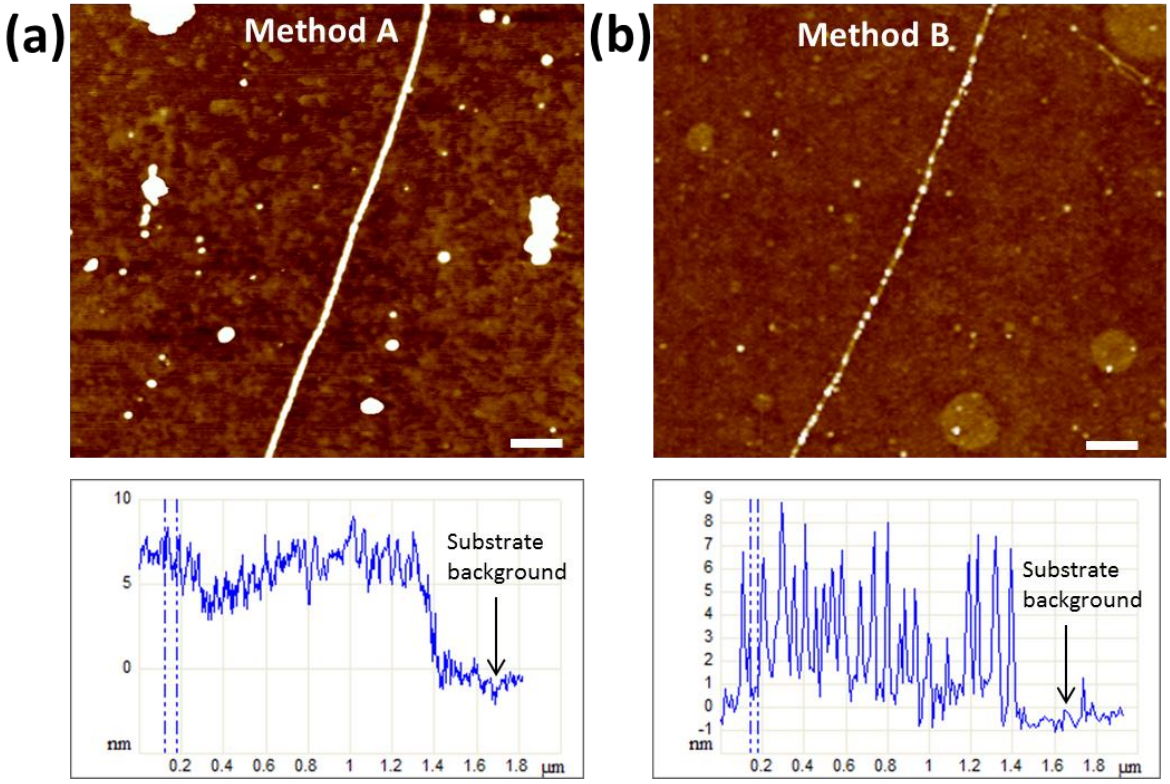

Figure 3.16: AFM topography images 'a' and 'b' of a Cu-DNA nanostructure prepared by 'Method A' and 'Method B,' respectively. Line traces are included underneath each image which shows the height profile along the length of each nanostructure. Height scales= 10 nm, scale bars= 200 nm

A line trace was recorded along the length of the nanostructure in each image (shown underneath) which displays the change in height as a function of distance along the 1-D structure. The series of sharp peaks observed in the line trace of nanostructure 'b' indicates the granular morphology arising from the structures being comprised of a series of nanoparticles, ~4-8 nm in height, distributed along the DNA template. The regions between the sharp peaks in the line trace are likely to be bare DNA, where the height is ~1-2 nm. The smoother line trace for nanostructure 'a' suggests the appearance of a 'wire-like' structure or at least a continuous assembly of nanoparticles where the height ranges from 5-8 nm.

These results give insight into the growth mechanism of copper on surface bound DNA. It has been previously reported that copper growth takes place via a 'nucleation and growth' pathway,[1, 5] whereby nucleation sites act as seed platforms for growth of metal to form 'wire-like' material. It is reasoned here that the 'doping/withdrawal/reduction' procedure ('Method B') does not provide nucleation sites in close enough proximity along the DNA template for continuous metal growth to occur. Furthermore, in 'Method B,' during chemical reduction of the Cu(I) bound DNA material, there is no further source of Cu(I) in the reaction solution (other than that already bound to DNA) to drive further metal growth. Conversely, for the 'doping/reduction,' procedure ('Method A') there is a further supply of Cu(I) in solution for extended metallisation of the DNA template to occur. However, it remains in doubt whether structure 'a' is consistent with nanoparticles densely packed together along the template or whether they are coalesced into a single coating.

Therefore, a more comprehensive study of the Cu-DNA nanostructure morphology prepared by 'Method A' is investigated by Atomic Force Microscopy (AFM). This is a useful imaging technique for obtaining topographical information regarding the nanoscale structures, and can be used to determine structure heights and morphology.

3.3.4.2. Atomic Force Microscopy (AFM)

AFM was carried out in "TappingMode^{TM}," which is useful in particular for imaging biological material, such as DNA. Structure sizes are determined by their heights using step profile analysis in the AFM software. This is drawn as a line intersecting the nanostructure at the point of interest.

As mentioned, this section is dedicated to the morphological analysis of the Cu-DNA nanostructures obtained via 'method A,' described in the previous section (3.3.4.1). An AFM image of a single nanostructure produced by this method was shown in figure 3.16a. However, before more of this data is discussed in detail, we first set out to establish how a suitable set of reaction conditions for obtaining these smooth and isolated Cu-DNA nanostructures (based on 'method A'), were originally determined. This was achieved by experimenting with the concentration of the reaction precursors, Cu(I) and phenylsilane, for metallisation of DNA. Initially, samples were prepared based on concentrations of 25 mM and 50 mM for Cu(I) and phenylsilane, respectively, on DNA-immobilised silicon substrates.

Figure 3.17 shows an AFM height image of a sample prepared in this manner. Inspection of the image reveals a single strand covered by a dense layer(s) of nanoparticles. Clearly the nanoparticles are non-selective for the DNA template under these conditions. Nanoparticles seemingly deposit randomly over the entire substrate. Thus, these concentrations lead to an excessive amount of non-specific deposition.

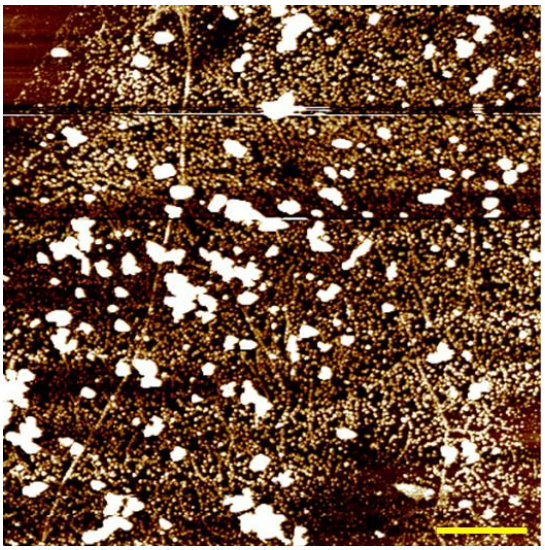

Figure 3.17: AFM "TappingMode™" height image of a Cu-DNA nanostructure formed using high concentrations of Cu(I) and phenylsilane. The high level of background material masks the 1-d nanostructure. Data scale= 50 nm. Scale bar= 2 μM

The concentration of Cu(I) and phenylsilane were reduced accordingly to 10 mM and 20 mM, respectively. At reduced concentrations less non-specific deposition was observed and copper nanoparticles become more selective for binding to the DNA template.

Figure 3.18 shows a selection of AFM topography images obtained of bare DNA (a) and Cu-DNA nanostructures (b,c,d) prepared at these concentrations. Height analysis of images 'a' and 'b' determined an increase in the structure height of bare DNA (~ 1 nm, typical height of bare DNA is 1–2 nm) compared to metallised DNA (~6 nm). The heights of the Cu-DNA nanostructures are uniform along the entire length of the structure, indicating that copper nanoparticles are deposited evenly along the template; thus affording smooth structure morphology.

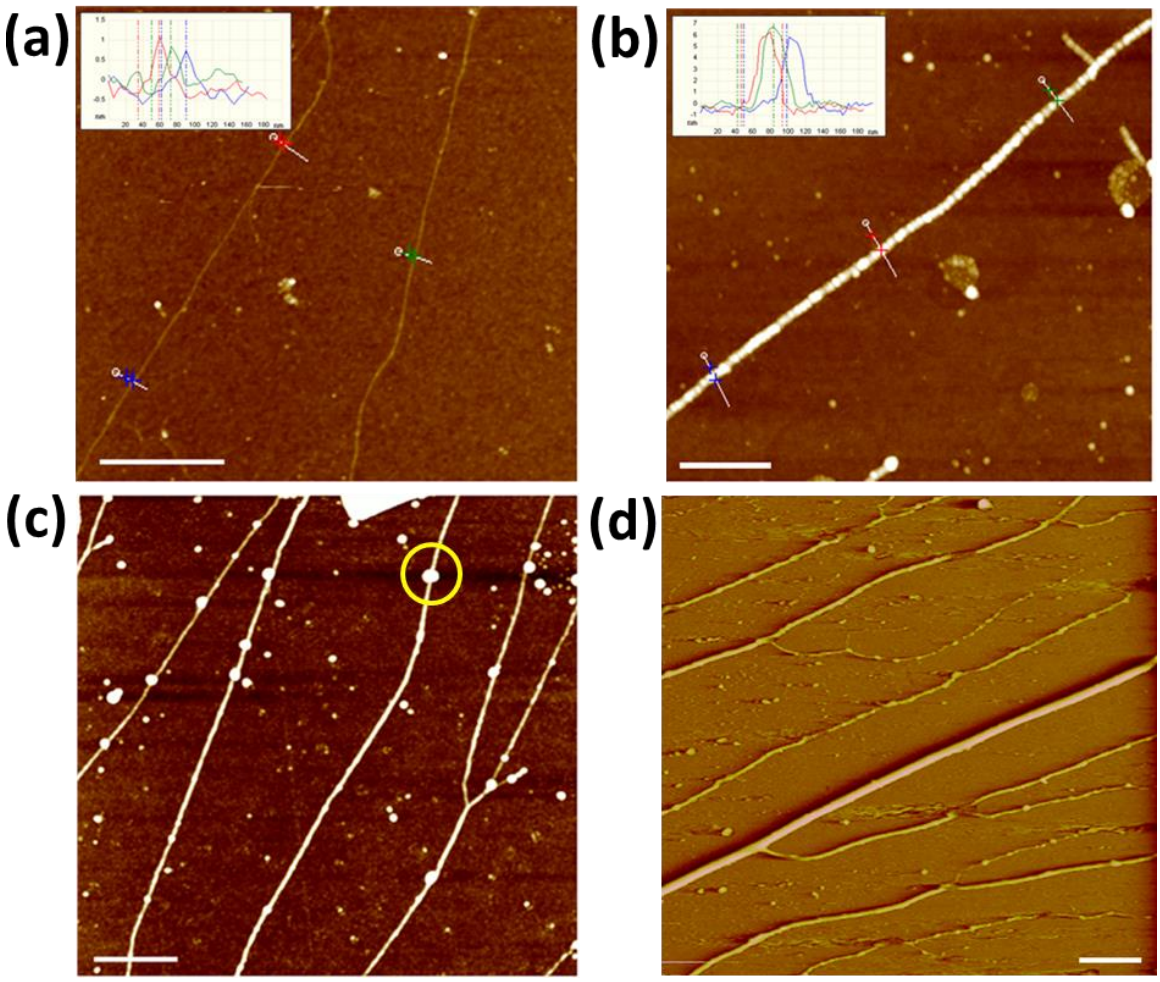

Figure 3.18: AFM "TappingMode™" height images of (a) bare DNA strands immobilised on a silicon wafer, (b) a Cu-DNA molecule showing the packing of individual nanoparticles along the template, (c) well aligned Cu-DNA nanostructures (yellow circle highlighting a large artefact residing on the nanostructure) and (d) AFM deflection error image of Cu-DNA nanostructures obtained in contact mode. Insets show height profiles of the nanostructures in reference to coloured markers in the image. Data scales= 10 nm. Scale bars= (a,c,d) 1000 nm and (b) 500 nm

Figures 3.18c is an AFM height image revealing 1-dimensional DNA-templated structures aligned on the surface. These structures appear to be smooth and continuous in morphology. Contamination on the substrate background resulting from the non-specific deposition of copper is relatively low, indicating good selectivity for DNA, compared to the poor selectivity observed in figure 3.17 where the concentration of precursors was higher. However, there are some artefacts on the surface which indicates that a small amount of copper is deposited non-specifically on to the surface. Occasionally aggregates of material are formed along DNA where large globular particles are located along the structure length (figure 3.18c, yellow circle highlights an example of this).

The alignment of the nanostructures is a direct result of the molecular combing technique used to comb DNA molecules onto the substrate prior to metallisation. This technique serves to stretch out individual molecules onto the surface, as is discussed in the techniques section (Chapter 2). The aligned molecules are approximately 16 μM in length, the typical length for lambda DNA which contains 48,502 base pairs. The long length and small width of the resulting Cu-DNA nanostructures offer excellent aspect ratio for potential use as interconnect lines in future microprocessors.

Further analysis of the structure morphology was made using contact mode AFM. Figure 3.18d is a deflection error image acquired at a different area on the sample surface. The deflection error is the measured tip deflection relative to the set point. This image again shows 1-dimensional structures aligned on the substrate, which appear to be smooth and continuous in morphology.

At a smaller AFM scan size, as in figure 3.18b (height image), one can observe an individual Cu-DNA nanostructure in which close interparticle packing of nanoclusters (~6 nm) along the template axis can be clearly identified. This closely packed assembly of nanoclusters appears to contain multiple particle-particle boundaries. This would suggest that the copper material deposited on DNA is polycrystalline, as opposed to a single-crystalline metal coating which would be absent of such boundaries. It is known that the intrinsic properties of nanoscale structures depend on cystallinity[57] (amongst other factors) where the focus has been made at producing single crystal nanowires.[58-61] It has been demonstrated elsewhere that the presence of grain boundaries can lead to increased electron scattering along the wire and therefore increase its electrical resistivity.[61, 62]

Despite the observation that nanoclusters are tightly packed along the template, these 1-dimensional strands are almost completely continuous in morphology. They resemble wires rather than a ‘beads on a string’ motif where nanoclusters are sparsely distributed along the template and bare DNA is exposed between these clusters. In that respect, the morphologies of the structures prepared in this route are notably different to Cu-DNA nanostructures prepared by other routes,[1, 5] as well as other metal-DNA nanostructures where the coatings are highly irregular and non-continuous (the ‘beads-on-a-string’ assembly).[63-65] The structural data provided in these current studies shows that the particles templated on DNA are more extensive in coverage. Despite observations of interparticle boundaries along the DNA template, it was observed that bare DNA is left

unexposed by copper. Therefore, these Cu-DNA nanostructures are described as consisting of a continuous metal coating, but of a polycrystalline nature.

However, further inspection of the AFM data revealed that, occasionally, gaps are formed in the copper coating. Figure 3.19 illustrates one example of where a 'gap' or break is observed in the nanostructure. A magnified region of the AFM image, shown to the right, illustrates this feature more clearly. Such defects may inhibit the flow of electrical current along the entirety of these nanostructures.

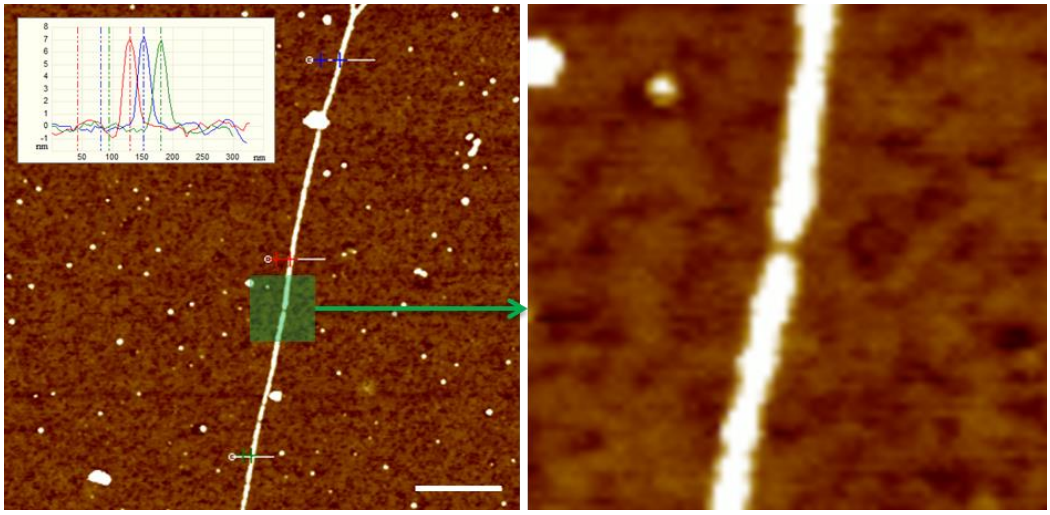

Figure 3.19: AFM topography images of DNA-templated copper nanostructures formed after solution treatment of surface immobilized λ-DNA with $Cu(CH_3CN)_4.PF_6$ and phenylsilane. Scale bar= 500nm (left). Data Scales= 10 nm

Statistical analysis of DNA and Cu-DNA strands were carried out in order to obtain a histogram of structure heights before and after metallisation. The results are shown in figure 3.20. The data was compiled by measuring the average height of 100 bare DNA strands and 100 metallised DNA strands over four identically prepared samples. In each measurement the average structure height was taken as the mean of three individual height measurements along each strand. In total 600 height measurements were made.

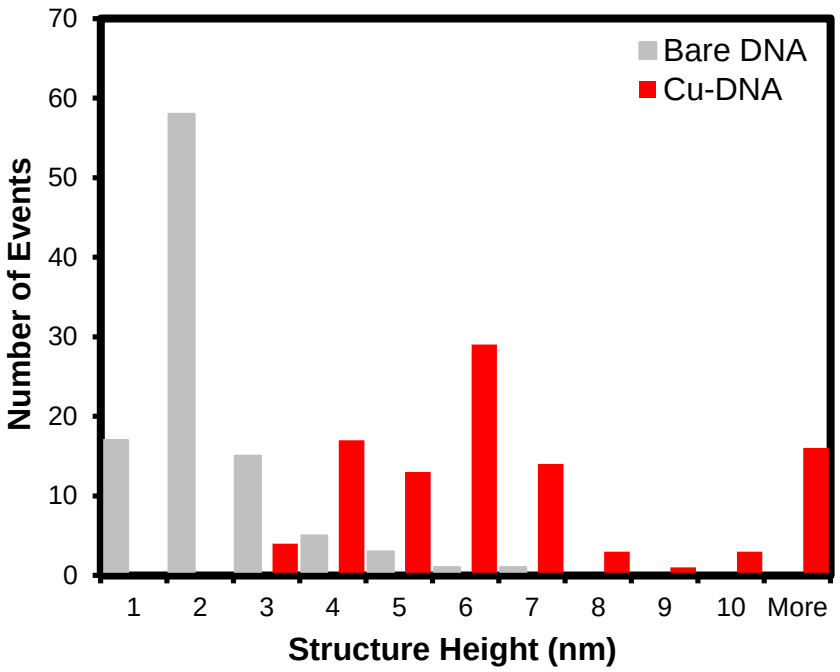

Figure 3.20: Height distributions of 100 bare DNA molecules aligned on silicon before and after treatment with Cu(I) and phenylsilane

For bare DNA, a positively skewed distribution is apparent with a peak modal value of 1-2 nm. Larger structure heights for bare DNA are the result of DNA 'bundling' in solution, which leads to the formation of 'DNA ropes.' This phenomenon has been documented in the formation of DNA-polypyrrole nanostructures.[66] DNA bundles have been shown to act as more efficient templates, than for single DNA duplexes, for growth of densely populated nanoparticle chains.[67]

Analysis of these Cu-DNA nanostructures reveals an almost symmetrical distribution of structure heights around a modal value of 5-6 nm and with a small spread of heights, typically 4–7 nm. The mean structure height was calculated as ~6 nm (s.d. ± 3.04 nm).

In an effort to metallise between the gaps in the coatings of these prepared Cu-DNA nanostructures a repeat metallisation treatment was performed on the sample. This repeat treatment would also be expected to increase the size of the resulting nanostructures. These so-called 'developing' steps have been implemented by numerous research groups including those of Braun *et al*[64] in their fabrication of Ag-DNA nanowires and Richter *et al*[68] in their Pd metallised DNA nanowires. In Braun's study the use of a developing step transformed the morphology of individual Ag nanoclusters on DNA to a continuous metal nanowire. In Richter's study the use of additional growth treatments demonstrated the ability to control the diameter of the nanowires. In such

treatments the nanoclusters attached to DNA act as a self-seeding platform to encourage further metal growth along the template axis. As stated, the aim in this experiment is to 'seal' any voids in the nanostructure coating, as well as potentially demonstrating control over the materials' size.

Figure 3.21 shows examples of copper metallised DNA strands following two successive growth treatments using Cu(I) and phenylsilane. The insets show height profiles of three points across the structures, with measured heights of 10-40 nm; a significant increase in height from the average 6 nm, estimated following a single metallisation treatment. However the metal coating has become less uniform in both size and shape, with large clusters of material forming at seemingly random points along the structure.

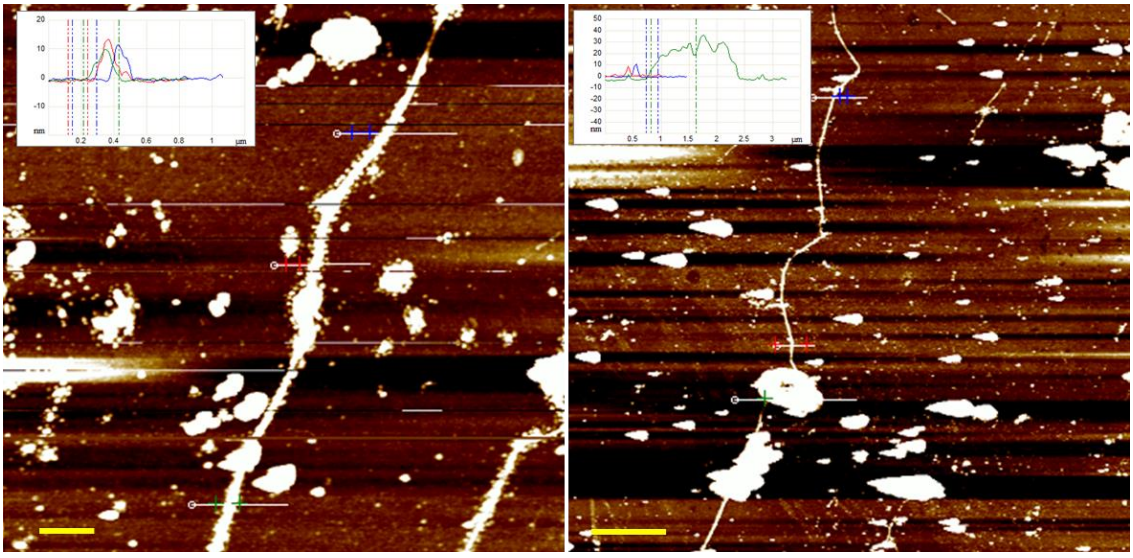

Figure 3.21: "TappingMode™" AFM height images of Cu-DNA nanostructures after two successive metallisation treatments with Cu(I) and phenylsilane. Insets show height profiles of at various locations across the nanostructures. Data scales = 10 nm. Scale bars= (left) 500 nm and (right) 2000 nm

The increased height of the metal nanostructures occurs at the expense of extensive non-specific deposition on the surrounding substrate surface. It may be the case that, material residing in the background from the initial treatment serves as catalytic seeds to encourage further aggregation. This would explain the observation of even larger artefacts in the background following the second treatment. Non-specific deposition of material across the substrate is undesirable and therefore the use of developing steps in this study cannot be exploited for the fabrication of larger nanostructures which are free of gaps in the metal coating. An alternative approach implemented by Richter *et al*[63] for

demonstrating control over the size of the material was to increase the incubation time used for metallisation. This led to the formation of ‘quasi-continuous’ Pd nanowires and exhibited good ohmic behaviour. Such an experiment could be attempted here as part of a future study.

In the next section of this chapter, Electrostatic Force Microscopy (EFM) will be used to assess the electrical properties of a single Cu-DNA nanostructure prepared using a single metallisation treatment.

3.3.5. Electrostatic Force Microscopy

Electrostatic Force Microscopy (EFM) is a form of Scanned Conductance Microscopy (SCM) and offers a convenient contactless method for measuring the conductance of single nanowires isolated on a dielectric Si/SiO_2 substrate. This technique is used for initial and rapid assessment of the wires' electrical performance, prior to utilisation of contact electrical techniques such as Conductive AFM for quantitative data. The EFM technique does not require dense deposits of wires on the surface or the need for metal electrodes to contact the structures.

EFM is a highly sensitive technique for measuring electrical conductance. Even at very low levels of detected current the technique would indicate conductance but not quantitatively. If the material is indeed *highly* resistive then the technique can provide a definitive answer to this question. EFM essentially provides a yes or no answer to the materials conductivity and is useful for initial verification.

The EFM set-up is comprised of a metal AFM tip held high above a silicon oxide dielectric surface, thus behaving essentially like two metal plates separated by an insulating gap, much like a capacitor. When a voltage (V) is applied a capacitance (C) is stored in the insulating gap. The presence of a nanowire perturbs the electric field, resulting in a phase shift relatable to the conductive nature of the 'wire.' For further details on EFM theory refer to Chapter 2.

An EFM image of a single Cu-DNA strand is shown in figure 3.22 (aligned onto a TMS-modified substrate by molecular combing). The left image shows AFM topography (height) and to the right is the phase map generated at a fixed bias of 10V. The nanostructure is of typical height of ~6.5 nm (see height profile, left inset). The height will affect the magnitude of the phase shift but will not affect the sign. As can be seen in the phase image, the 1-D nanostructure displays continuous positive (bright) contrast with respect to the background. Positive contrast was observed at all applied potentials, indicating that these nanostructures are highly insulating.

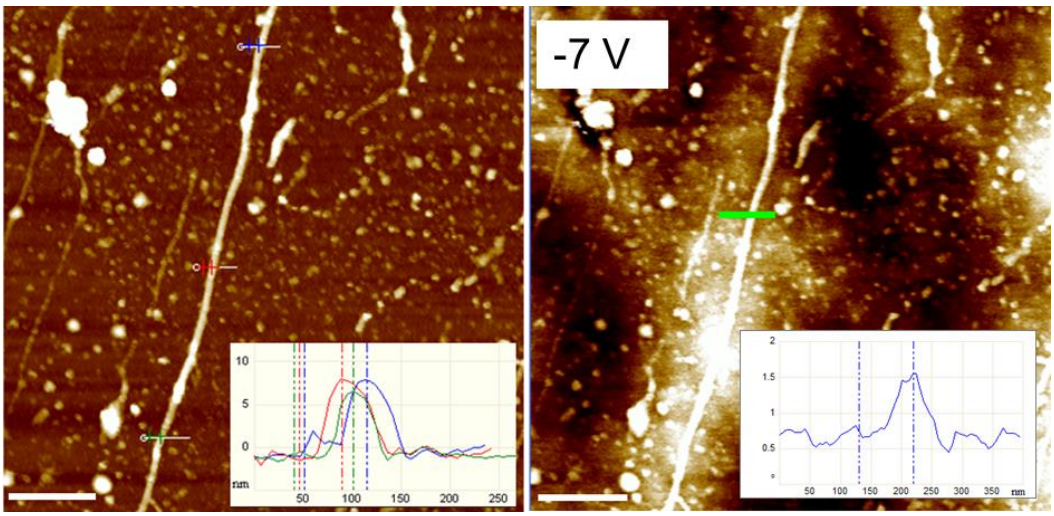

Figure 3.22: (left) AFM Topography image of a λ-DNA molecule subjected to treatment with $Cu(CH_3CN)_4.PF_6$ and phenylsilane as described in section 3.2.2 (inset: height profiles of copper nanostructure taken at various points along the structure) and (right) the corresponding EFM phase image map at an applied bias of 10V. Scale bars= 500 nm. Data scale scales are 20 nm and 2° respectively

The size of the phase shift decreases with decreasing voltage. When the voltage passes through zero to negative bias a positive phase shift is again obtained. A plot of tan(*Φ)* against voltage, shown in figure 3.23, produces a positive parabolic curve, as expected. This positive feature indicates that capacitance effects dominate tip-sample interactions, as opposed to the effects of conductance which are absent in this sample.

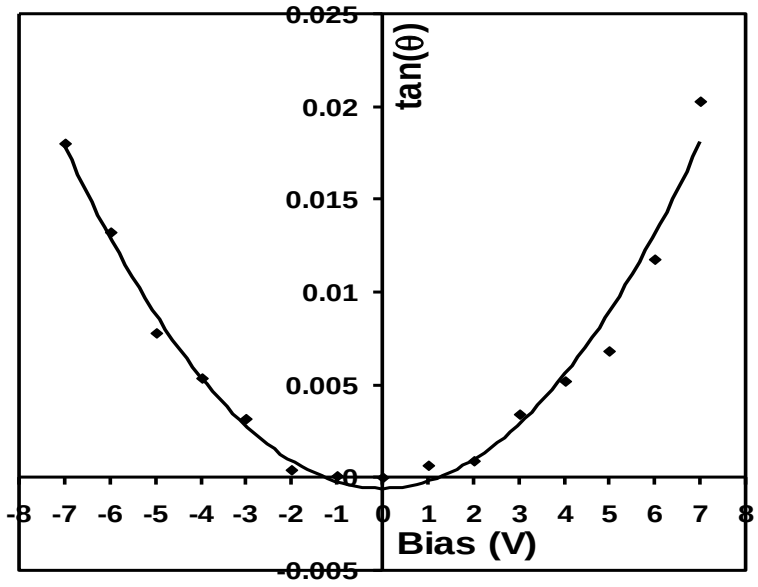

Figure 3.23: Plot of measured phase shift, corresponding to green cross section on phase image, versus a function of bias. The positive parabola obtained is indicative of a highly resistive structure

The positive EFM phase shifts obtained here are attributable to highly resistive structures. Lack of negative phase shift signals, indicate the lack of a viable conductive pathway along the nanostructure.

Based upon all of the results described in this chapter so far, there may be two contributing factors to the materials' high resistivity; (i) chemical impurity/oxidation of copper, i.e. $Cu(OH)_2$ overlayer on surface (as evidenced by XPS) and (ii) structural defects, such as inter-particle boundaries (as evidenced by AFM). The latter effect in particular, may lead to substantial electron scattering at the particle interfaces.

In an effort to transform Cu-DNA into nanowires (i.e. conductive) a thermal anneal process was applied in an attempt to sinter the particle-particle boundaries that are present in the copper nanostructures. The annealing was performed under an atmosphere of hydrogen, which will act to reduce any surface oxide to metallic copper.[69]

3.3.6. Annealing of 1-D nanostructures

Annealing involves a heat treatment whereby a materials' properties such as hardness and ductility is altered by the supply of energy and a structural transformation occurs. Annealing of nanostructured materials, copper interconnect lines for example, has been used for transforming the surface from rough or heterogeneous morphology to smooth homogenous morphology.[70-72] Thereby we aim to produce continuous (or single crystalline) Cu-DNA nanowires by eliminating grain boundaries. Previous reports have described the sintering of printed Cu interconnects and films in N_2/H_2 reducing atmosphere for reduction of surface oxide species (e.g. Cu_2O).[69, 73] The transformation occurs at temperatures between 250°C-500°C. Such structural reformations have led to improved electrical properties of the resulting material.

Initially we set out to establish the optimum annealing temperature. The first set of experiments involved annealing of Cu-DNA nanostructures aligned on Si/SiO_2 at 300°C for 1 hour. Structural analysis of the annealed structures was again carried out by AFM.

As can be seen in the AFM image shown in figure 3.24, the Cu-DNA nanostructure following annealing does not appear to be significantly transformed and shows a high degree of structural retention when compared to the non-annealed Cu-DNA nanostructures shown earlier in fig 3.18b. The resulting nanostructure still displays a smooth morphology with densely packed nanoparticles along the template, but the

particle-particle boundaries are still present. A height trace was measured along the length of the structure (see inset) and resulting profile is shown to the right of the image. The profile shows a regular height of ~6 nm, consistent with that observed prior to annealing. Occasionally large aggregates are formed along the structure (indicated by the two large peaks in the height profile). However this was not unusual even for the non-annealed nanostructures.

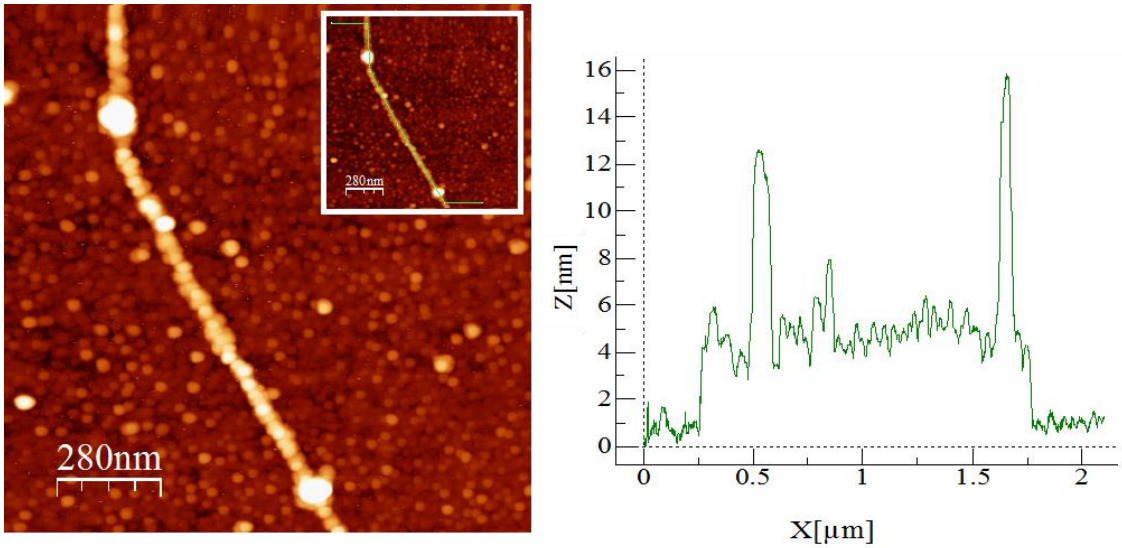

Figure 3.24: (top, a) AFM topography image of DNA-templated copper nanostructure (prepared as described in section 3.2.2) annealed at 300°C and (bottom, b) small scan size AFM image of structure. High levels of structural retention are observed after annealing. Data Scales= 10 nm. Insets: Topology height profile images with corresponding data scales shown to the right

Structural analysis of a freshly prepared sample annealed at a temperature of 400 °C for one hour was obtained. At this elevated temperature the Cu-DNA nanostructures undergo a significant structural transformation.

As shown in figure 3.25, with the corresponding height profile to the right, large clusters are located periodically along the entire length of the nanostructure. These particles are considerably larger in height than the portions of the structure which lie between the clusters (which we will call the 'base structure'). The height profile illustrates this more clearly where these two features can be easily distinguished. The base structure is ~3 nm in height (c.f. to ~ 6 nm observed in the nanostructure following annealing at 300 °C) and the large clusters are up to ~ 16 nm in height, indicated by the sharp peaks. These results suggest that formation of the larger particles along the template come at the expense of a reduction in size of the base structure; providing evidence for diffusion of copper within the structure. This could be explained by the

lowering of the melting temperature (T_m) phenomenon of nanoscale materials (T_m of Cu (bulk) ~1084 °C).[74]

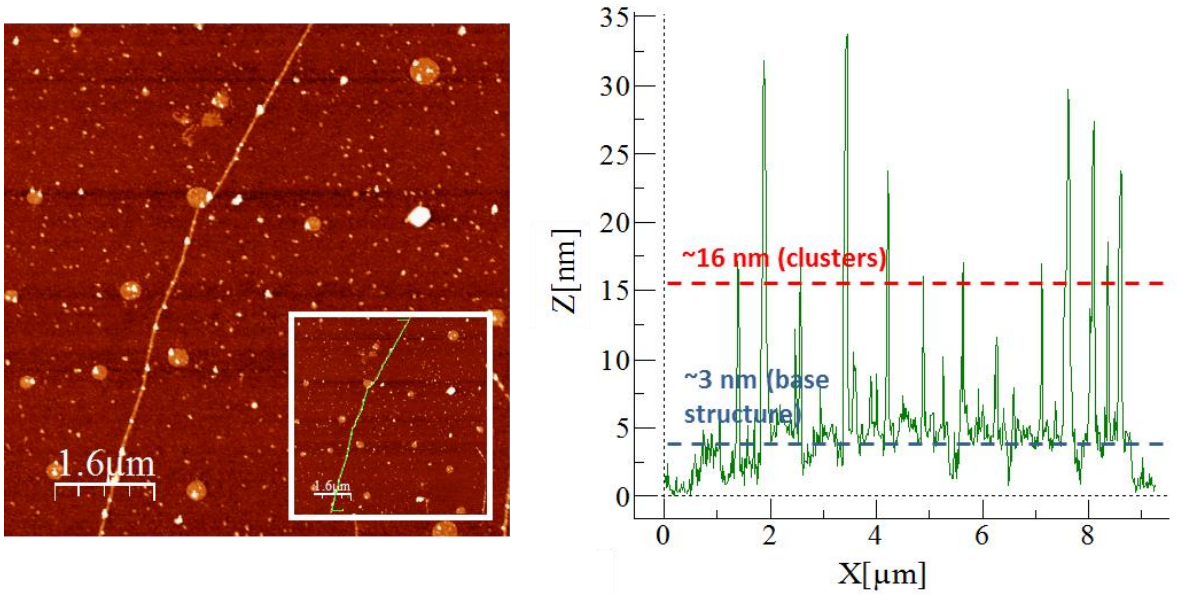

Figure 3.25: Cu-DNA nanostructures annealed at 400°C under an atmosphere of hydrogen for 1 hour. Data Scale= 10 nm. Inset: Topology height trace image with corresponding height profile shown to the right. A morphological change to the structure is apparent from this image (c.f. to the non-annealed samples). This is indicated by the formation of larger clusters (6-35 nm) at more regular points along the template at the expense of a decrease in height of the base structure (~3 nm)

Figure 3.26 shows a comparison between a non-annealed Cu-DNA strand (a) and an annealed Cu-DNA strand at 400°C (b). The height profiles are markedly different: a regular height in the non-annealed nanostructure indicates a smooth morphology and an irregular height profile in the annealed nanostructure (b) again indicates formation of nano clusters along the structure, which are indicated with arrows in figure 3.26b.

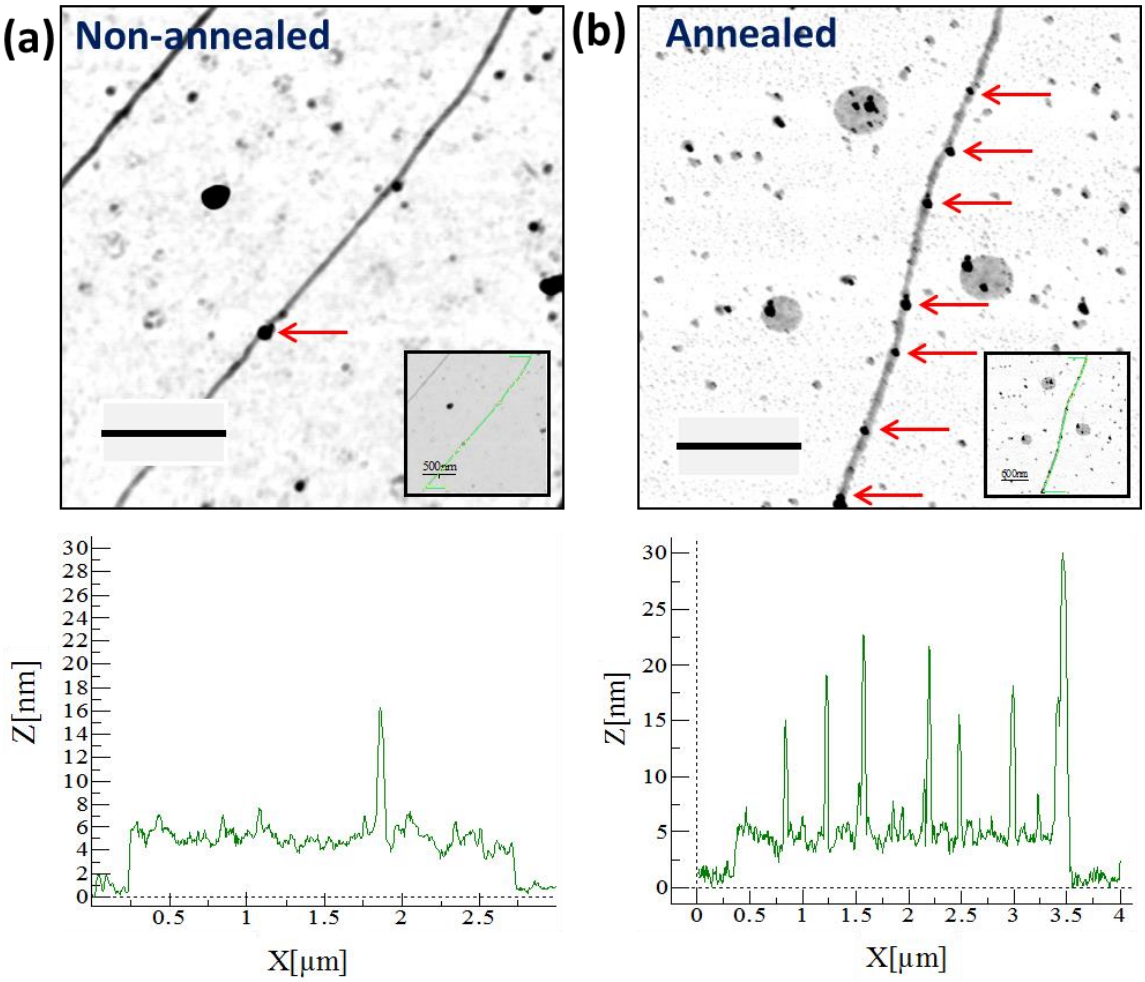

Figure 3.26: "TappingMode™" AFM height images of Cu-DNA before (a) and after annealing (b) at 400°C for 1 hour. A transformation of the nanostructure surface morphology is observed, as indicated by the height profiles (below). Red arrows point to locations of clusters along the structure. Insets show the path of the line trace along the nanostructure. Scale bars= 500 nm, height scales= 10 nm

The annealing process did not lead to the formation of smooth Cu-DNA nanostructures. The results were unexpected owing to the periodic formation of large clusters along the nanostructure. Nonetheless, despite the presence of these large clusters, the particle-particle boundaries along the 'base structure' may have been eliminated by the annealing. Consequently, the annealed copper nanostructures may present improved electrical properties over the non-annealed nanostructures. The final section of this chapter aims to examine these electrical properties using a 2-point probe technique, Conductive-AFM (C-AFM) where surface topography was imaged in "TappingMode™" and conductive measurements were made by bringing the tip into contact with the structure.

3.3.7. C-AFM of annealed 1-D nanostructures

The C-AFM technique, similarly as for EFM, delivers simultaneous mapping of both topography and conductance via two separate feedback loops. C-AFM is set apart from EFM as it is a contact technique consisting of two electrodes; a *stationary* electrode such as gold or conductive paste and a *mobile* electrode which is the metal coated AFM tip used to contact the nanostructure at the point of interest (or indeed anywhere on the sample). This feature is facilitated by the closed loop system of the AFM allowing movement of the cantilever to predefined positions on the sample surface. During mechanical contact between the tip and sample, a current-voltage (i-V) plot can be recorded. Figure 3.27 is a photograph of a typical C-AFM set up.

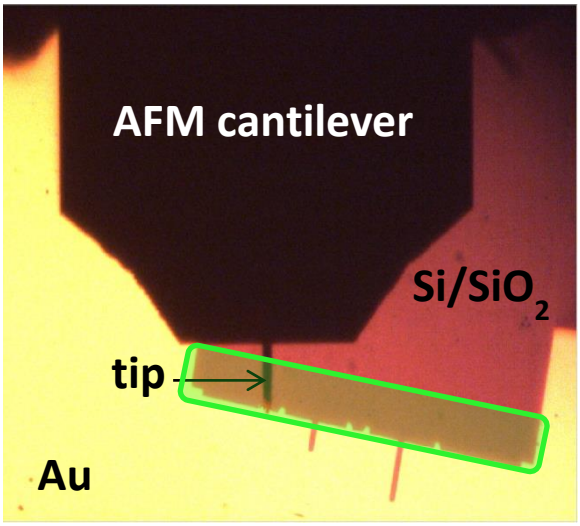

Figure 3.27: Photograph showing C-AFM set-up using a metallised tip and gold electrode connect to Cu-DNA nanostructures stretched across the surface. The green rectangle highlights the most likely area to find nanostructures touching the gold edge. Two lines can be seen protruding into the gold layer resulting from tips of the cantilever mask

In this experiment individual Cu-DNA nanostructures are formed on the surface using the previously established method described in sections 3.2.1 and 3.2.2. Then, with the aid of a suitable mask, gold is evaporated onto the sample to leave isolated copper nanostructures physically connected to the gold surface (see figure 3.28). The metal coated AFM tip is brought into mechanical contact with the nanostructure and the i-V properties were measured between set potentials (typically +3 to -3V).

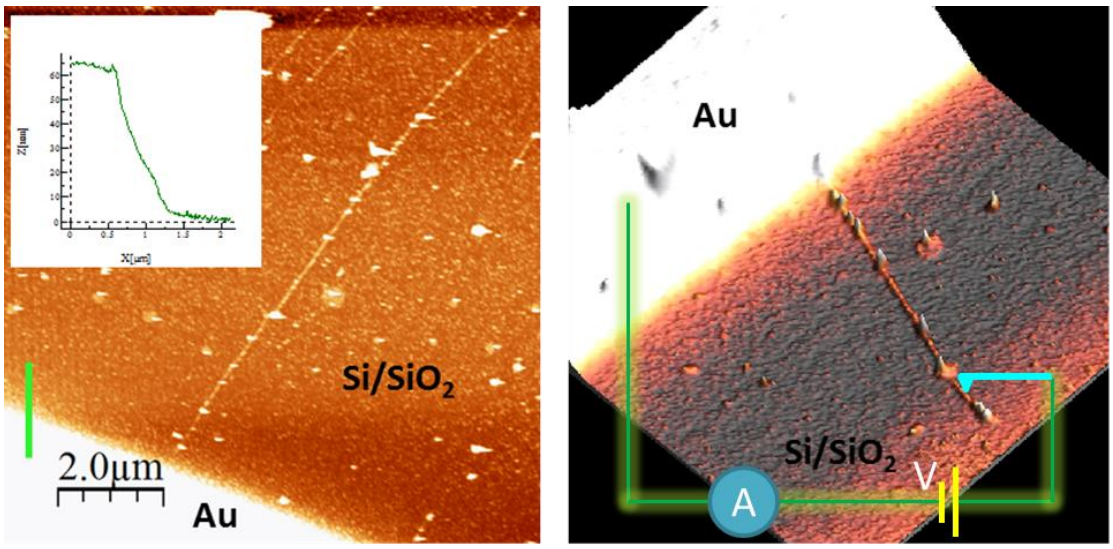

Figure 3.28: (a) AFM "TappingMode™" height image of a Cu-DNA nanostructure connected to the gold edge with inset showing height profile of gold edge (green line) and (b) 3d representation of same image with incorporated C-AFM schematic showing the connection from gold to the AFM tip contacting the nanostructure

Nanostructures could be located protruding from the gold edge (figure 3.28) at a maximum distance of 15 µM, the approximate length of lambda DNA. The height of gold was ~60 nm and shows a relatively sharp step edge as indicated by the height profile (inset figure 3.28, left) corresponding to the green line in the image. A 3-D C-AFM schematic of a Cu-DNA nanostructure connected to the gold is shown in figure 3.28 (right). The structure morphology is consistent to what was described in the previous section (3.3.6), where large clusters are observed at points along the structure.

Several contact attempts were made at the nanostructures in figure 3.28 and i-V plots were recorded at various distances from the gold. However, in each case there were no observations of ohmic behaviour or significant levels of current in the nanostructure, indicating that these nanostructures are not conductive. This may be because the anneal treatment did not result in nanoparticles coalescing along the DNA template and the metal coating is still of a polycrystalline structure. As discussed previously in section 3.3.4.2, this may lead to electron scattering at the grain boundaries, accounting for the high resistivity.

Figure 3.29 illustrates what happens to the topography of the nanostructures when a bias is applied to the sample during imaging of the topography. Three AFM images are recorded: (i) a nanostructure connected to the gold under zero bias, (ii) during application of a positive bias (2V) and (iii) during application of a negative bias (-2V).

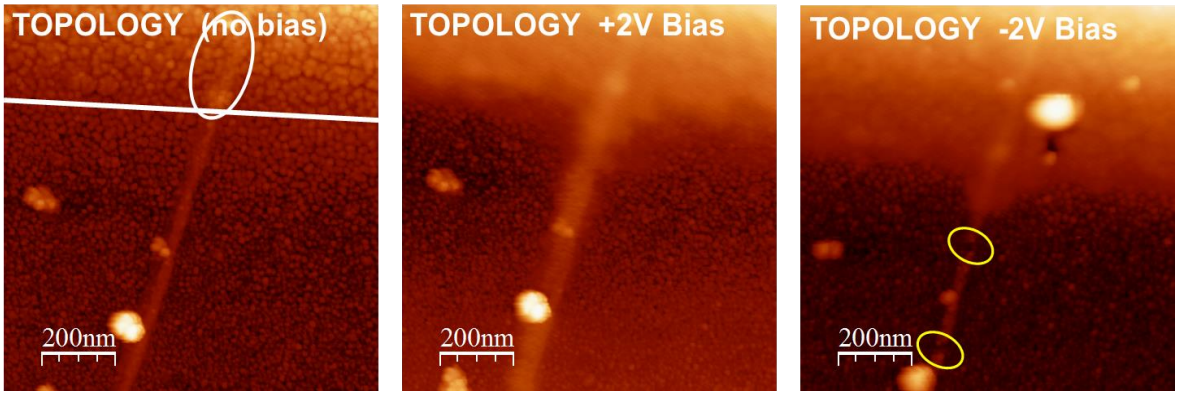

Figure 3.29: AFM height image of annealed DNA/Cu nanostructure contacting gold edge (left), with bias applied (center) and bias applied after contact attempts (right)

The nanostructure contrast appears thicker and more diffuse when under bias (middle and right image in figure 3.29) than compared to when no bias is applied (left). The contrast of the nanostructure is comparable to that of the gold surface when under bias. This is a clear indication of an attractive electrostatic interaction between the tip and nanostructure, which may suggest that the structure can carry some current. A similar effect has been observed in the Scanned Conductance Microscopy (SCM) studies of both single wall carbon nanotubes (SWNTs) and DNA attached to a gold-silicon substrate.[75, 76] In these experiments a bias is applied to the surface and a change in contrast is observed for SWNT's connected to the gold. For those that are not connected to the gold, no measurable interaction with the tip was recorded. For DNA, there was no change in contrast at all, indicating a lack of conductance (as expected).

Further attempts at measuring i-V properties were made, this time by increasing the vertical contact force to 'press' the tip harder onto the nanostructure in order to penetrate the surface oxide around the copper. However, this did not lead to improved i-V characteristics due to severe damage to the nanostructure, as seen in fig 3.29 (right) where clear breaks can be seen where the tip was in contact with the structure (marked by yellow circles). Interestingly from this image, the thick contrast of the nanostructure ends at the first break point, indicating that the attractive interaction with the tip is now lost.

3.4. Conclusions

The data contained in this chapter are the first reported for the templating of Cu(I) ions on DNA. Phenylsilane has been used as a reductant for Cu(I) to form nanoparticles with and without DNA to act as a template. The DNA-templated nanostructures, ~5-6 nm in height, are continuous by AFM but contain particle-particle boundaries and occasional gaps or breaks are observed in the structures. Reduction of Cu(I) at DNA with phenylsilane is most effective when carried out *in situ* as indicated by FTIR and AFM, which indicate more substantial metallisation of DNA. FTIR DNA peak shifts indicated that copper is mostly bound to the phosphodiester backbone as well as some coordination to the cytosine and guanine bases.

Chemical characterisation by XRD indicated the material to consist primarily of Cu^0. XPS analysis indicated a significant amount of Cu^{2+} in the form of $Cu(OH)_2$ and to a lesser extent CuF_2. These compounds are likely to reside on the surface of the nanostructures forming a shell layer which encapsulates the copper-DNA core.

Initial electrical characterisation by EFM indicated these nanostructures to be of high resistivity, which may be due to a combination of structural reasons, such as granularity of the copper coating, and oxidation of copper.

The structural morphology of the Cu-DNA nanostructures was transformed by thermal annealing. This led to diffusion of copper along the structure into large clusters. These were found to reside along the whole length of the template in a periodic fashion. C-AFM analysis of the annealed Cu-DNA nanostructures indicated that they were non-conductive. Future work may involve refining the annealing conditions in order to obtain smoother nanowires with improved electrical properties.

After considerable attempts to make conductive Cu-DNA nanostructures via surface based routes we now focus our attention to other possible methods. The next chapter describes the preparation and characterisation of Cu-DNA nanomaterial formed in solution.

3.5. References

1. C. F. Monson and A. T. Woolley, DNA-templated construction of copper nanowires. *Nano Letters*, 2003, **3**, 359-363.
2. R. M. Stoltenberg and A. T. Woolley, DNA-templated nanowire fabrication. *Biomedical Microdevices*, 2004, **6**, 105-111.
3. H. A. Becerril, R. M. Stoltenberg, D. R. Wheeler, R. C. Davis, J. N. Harb and A. T. Woolley, DNA-templated three-branched nanostructures for nanoelectronic devices. *Journal of the American Chemical Society*, 2005, **127**, 2828-2829.
4. A. Houlton and S. M. D. Watson, DNA-based nanowires. Towards bottom-up nanoscale electronics. *Annual Reports on the Progress of Chemistry - Section A*, 2011, **107**, 21-42.
5. S. M. D. Watson, N. G. Wright, B. R. Horrocks and A. Houlton, Preparation, Characterization and Scanned Conductance Microscopy Studies of DNA-Templated One-Dimensional Copper Nanostructures *Langmuir*, 2009.
6. H. A. Becerril, R. M. Stoltenberg, C. F. Monson and A. T. Woolley, Ionic surface masking for low background in single- and double-stranded DNA-templated silver and copper nanorods. *Journal of Materials Chemistry*, 2004, **14**, 611-616.
7. H. Kudo and M. Fujihira, DNA-templated copper nanowire fabrication by a two-step process involving electroless metallization. *IEEE Transactions on Nanotechnology*, 2006, **5**, 90-92.
8. B. H. Geierstanger, T. F. Kagawa, S. L. Chen, G. J. Quigley and P. S. Ho, Base-specific binding of copper(II) to Z-DNA. The 1.3-Å single crystal structure of d(m5CGUAm5CG) in the presence of CuCl2. *Journal of Biological Chemistry*, 1991, **266**, 20185-20191.
9. V. Andrushchenko, J. H. Van De Sande and H. Wieser, Vibrational circular dichroism and IR absorption of DNA complexes with Cu2+ ions. *Biopolymers - Biospectroscopy Section*, 2003, **72**, 374-390.
10. H. Fritzsche and C. Zimmer, Infrared studies of deoxyribonucleic acids, their constituents and analogues. 4. The binding sites of copper(II) in DNA. *European Journal of Biochemistry*, 1968, **5**, 42-44.
11. G. J. Kubas, B. Monzyk and A. L. Crumblis, *Inorganic Syntheses: Reagents for Transition Metal Complex and Organometallic Syntheses, Volume 28*, 1979.
12. M. Abdulla-Al-Mamun, Y. Kusumoto and M. Muruganandham, Simple new synthesis of copper nanoparticles in water/acetonitrile mixed solvent and their characterization. *Materials Letters*, 2009, **63**, 2007-2009.
13. V. A. S. Falcomer, S. S. Lemos, G. B. C. Martins, G. A. Casagrande, R. A. Burrow and E. S. Lang, Synthesis, structural characterization and reactivity of copper(I)-nitrile complexes: Crystal and molecular structure of [Cu(BzCN)₄][BF₄]. *Polyhedron*, 2007, **26**, 3871-3875.
14. M. Takahashi, J. Kamada, K. Iwata, K. Goto, H. Watanabe and S. Tamai, Hydrosilanes as reducing Reagents of copper salts into copper metal particles under remarkably mild conditions. *Bulletin of the Chemical Society of Japan*, 2008, **81**, 168-170.
15. D. J. Miller, M. C. Biesinger and N. S. McIntyre, Interactions of CO2 and CO at fractional atmosphere pressures with iron and iron oxide surfaces: One possible mechanism for surface contamination? *Surface and Interface Analysis*, 2002, **33**, 299-305.
16. T. L. Barr and S. Seal, Nature of the use of adventitious carbon as a binding energy standard. *Journal of Vacuum Science and Technology A: Vacuum, Surfaces and Films*, 1995, **13**, 1239-1246.
17. C. Vázquez-Vázquez, M. Bañobre-López, A. Mitra, M. A. López-Quintela and J. Rivas, Synthesis of small atomic copper clusters in microemulsions. *Langmuir*, 2009, **25**, 8208-8216.
18. S. H. Wu and D. H. Chen, Synthesis of high-concentration Cu nanoparticles in aqueous CTAB solutions. *Journal of Colloid and Interface Science*, 2004, **273**, 165-169.

19. N. A. Dhas, C. P. Raj and A. Gedanken, Synthesis, Characterization, and Properties of Metallic Copper Nanoparticles. *Chemistry of Materials*, 1998, **10**, 1446-1452.
20. Y. Wang, A. V. Biradar, G. Wang, K. K. Sharma, C. T. Duncan, S. Rangan and T. Asefa, Controlled synthesis of water-dispersible faceted crystalline copper nanoparticles and their catalytic properties. *Chemistry - A European Journal*, 2010, **16**, 10735-10743.
21. T. Ghodselahi, M. A. Vesaghi, A. Shafiekhani, A. Baghizadeh and M. Lameii, XPS study of the Cu@Cu2O core-shell nanoparticles. *Applied Surface Science*, 2008, **255**, 2730-2734.
22. X. Wen, Y. Xie, C. L. Choi, K. C. Wan, X. Y. Li and S. Yang, Copper-based nanowire materials: Templated syntheses, characterizations, and applications. *Langmuir*, 2005, **21**, 4729-4737.
23. G. Van Der Laan, C. Westra, C. Haas and G. A. Sawatzky, Satellite structure in photoelectron and Auger spectra of copper dihalides. *Physical Review B*, 1981, **23**, 4369-4380.
24. K. Okada, J. Kawai and A. Kotani, Triple-peak feature of Cu 2p x-ray-photoemission spectrum in copper acetylacetonate. *Physical Review B*, 1993, **48**, 10733-10738.
25. J. Hernandez, P. Wrschka and G. S. Oehrlein, Surface Chemistry Studies of Copper Chemical Mechanical Planarization. *Journal of the Electrochemical Society*, 2001, **148**, G389-G397.
26. V. Di Castro, M. Beccari, F. Bruni, F. Caprioli and F. Decker, Comparison of the protective effect of aromatic thiols adsorbed on copper. *Surface and Interface Analysis*, 2010, **42**, 601-604.
27. R. Hérino, Nanocomposite materials from porous silicon. *Materials Science and Engineering B: Solid-State Materials for Advanced Technology*, 2000, **69**, 70-76.
28. A. G. Cullis, L. T. Canham and P. D. J. Calcott, The structural and luminescence properties of porous silicon. *Journal of Applied Physics*, 1997, **82**, 909-965.
29. H. A. Andersson, G. Thungström and H. E. Nilsson, Electroless deposition and silicidation of Ni contacts into p-type Porous Silicon. *Journal of Porous Materials*, 2008, **15**, 335-341.
30. S. Ghosh, K. Hong and C. Lee, Structural and physical properties of thin copper films deposited on porous silicon. *Materials Science and Engineering B: Solid-State Materials for Advanced Technology*, 2002, **96**, 53-59.
31. Y. Piao and H. Kim, Fabrication of nanostructured materials using porous alumina template and their applications for sensing and electrocatalysis. *Journal of Nanoscience and Nanotechnology*, 2009, **9**, 2215-2233.
32. P. Zhang, P. S. Kim and T. K. Sham, Nanostructured CdS prepared on porous silicon substrate: Structure, electronic, and optical properties. *Journal of Applied Physics*, 2002, **91**, 6038-6043.
33. T. I. Gorbanyuk, A. A. Evtukh, V. G. Litovchenko, V. S. Solnsev and E. M. Pakhlov, Porous silicon microstructure and composition characterization depending on the formation conditions. *Thin Solid Films*, 2006, **495**, 134-138.
34. P. Rivolo, F. Geobaldo, M. Rocchia, G. Amato, A. M. Rossi and E. Garrone, Joint FTIR and TPD study of hydrogen desorption from p+-type porous silicon. *Physica Status Solidi (A) Applied Research*, 2003, **197**, 217-221.
35. D. Y. Petrovykh, H. Kimura-Suda, M. J. Tarlov and L. J. Whitman, Quantitative Characterization of DNA Films by X-ray Photoelectron Spectroscopy. *Langmuir*, 2004, **20**, 429-440.
36. R. Franke, T. Chassé, P. Streubel and A. Meisel, Auger parameters and relaxation energies of phosphorus in solid compounds. *Journal of Electron Spectroscopy and Related Phenomena*, 1991, **56**, 381-388.
37. S. W. Gaarenstroom and N. Winograd, Initial and final state effects in the ESCA spectra of cadmium and silver oxides. *The Journal of Chemical Physics*, 1977, **67**, 3500-3506.

38. N. S. McIntyre, S. Sunder, D. W. Shoesmith and F. W. Stanchell, CHEMICAL INFORMATION FROM XPS - APPLICATIONS TO THE ANALYSIS OF ELECTRODE SURFACES. *Journal of vacuum science & technology*, 1980, **18**, 714-721.
39. N. S. McIntyre and M. G. Cook, X-RAY PHOTOELECTRON STUDIES ON SOME OXIDES AND HYDROXIDES OF COBALT, NICKEL, AND COPPER. *Analytical Chemistry*, 1975, **47**, 2208-2213.
40. H. A. Tajmir-Riahi, M. Naoui and R. Ahmad, The effects of Cu 2+ and Pb 2+ on the solution structure of calf thymus DNA: DNA condensation and denaturation studied by Fourier Transform ir difference spectroscopy. *Biopolymers*, 1993, **33**, 1819-1827.
41. G. L. Eichhorn and Y. A. Shin, Interaction of metal ions with polynucleotides and related compounds. XII. The relative effect of various metal ions on DNA helicity. *Journal of the American Chemical Society*, 1968, **90**, 7323-7328.
42. J. Duguid, V. A. Bloomfield, J. Benevides and G. J. Thomas Jr, Raman spectroscopy of DNA-metal complexes. I. Interactions and conformational effects of the divalent cations: Mg, Ca, Sr, Ba, Mn, Co, Ni, Cu, Pd, and Cd. *Biophysical Journal*, 1993, **65**, 1916-1928.
43. N. Russo, M. Toscano and A. Grand, Gas-phase theoretical prediction of the metal affinity of copper(I) ion for DNA and RNA bases. *Journal of Mass Spectrometry*, 2003, **38**, 265-270.
44. M. Shakorian Fard Jahromi and A. Fattahi, DFT study of the interaction of thymine with Cu+ and Zn 2+. *Scientia Iranica*, 2009, **16**, 75-80.
45. S. Alex and P. Dupuis, FT-IR and Raman investigation of cadmium binding by DNA. *Inorganica Chimica Acta*, 1989, **157**, 271-281.
46. A. A. Ouameur and H. A. Tajmir-Riahi, Structural analysis of DNA interactions with biogenic polyamines and cobalt(III)hexamine studied by fourier transform infrared and capillary electrophoresis. *Journal of Biological Chemistry*, 2004, **279**, 42041-42054.
47. H. Arakawa, R. Ahmad, M. Naoui and H. A. Tajmir-Riahi, A comparative study of calf thymus DNA binding to Cr(III) and Cr(VI) ions. Evidence for the guanine N-7-chromium-phosphate chelate formation. *Journal of Biological Chemistry*, 2000, **275**, 10150-10153.
48. G. I. Dovbeshko, N. Y. Gridina, E. B. Kruglova and O. P. Pashchuk, FTIR spectroscopy studies of nucleic acid damage. *Talanta*, 2000, **53**, 233-246.
49. V. A. Bloomfield, Condensation of DNA by multivalent cations: Considerations on mechanism. *Biopolymers*, 1991, **31**, 1471-1481.
50. B. Lippert, Multiplicity of metal ion binding patterns to nucleobases. *Coordination Chemistry Reviews*, 2000, **200–202**, 487-516.
51. M. A. Galindo, D. Amantia, A. M. Martinez, W. Clegg, R. W. Harrington, V. M. Martinez and A. Houlton, Probing metal-ion purine interactions at DNA minor-groove sites. *Inorganic Chemistry*, 2009, **48**, 10295-10303.
52. C. Price, M. R. J. Elsegood, W. Clegg and A. Houlton, Directed metallation of adenine-N3 via nucleobase-ligand conjugation. *Journal of the Chemical Society - Series Chemical Communications*, 1995, 2285-2286.
53. J. A. Carrabine and M. Sundaralingam, The crystal structure of a copper-cytoside complex. *Chemical Communications (London)*, 1968.
54. L. G. Marzilli and T. J. Kistenmacher, Stereoselectivity in the binding of transition-metal chelate complexes to nucleic acid constituents: Bonding and nonbonding effects. *Accounts of Chemical Research*, 1977, **10**, 146-152.
55. C. Zimmer and H. Venner, Influence of copper 2+ ions on the denaturation and spectral properties of DNA and methylated DNA. *European Journal of Biochemistry*, 1970, **15**, 40-47.
56. S. Basu, S. Jana, S. Pande and T. Pal, Interaction of DNA bases with silver nanoparticles: Assembly quantified through SPRS and SERS. *Journal of Colloid and Interface Science*, 2008, **321**, 288-293.

57. H. A. Becerril and A. T. Woolley, DNA-templated nanofabrication. *Chemical Society Reviews*, 2009, **38**, 329-337.
58. B. Gates, B. Mayers, B. Cattle and Y. Xia, Synthesis and characterization of uniform nanowires of trigonal selenium. *Advanced Functional Materials*, 2002, **12**, 219-227.
59. T. Gao, G. W. Meng, J. Zhang, Y. W. Wang, C. H. Liang, J. C. Fan and L. D. Zhang, Template synthesis of single-crystal Cu nanowire arrays by electrodeposition. *Applied Physics A: Materials Science and Processing*, 2001, **73**, 251-254.
60. T. R. Kline, M. Tian, J. Wang, A. Sen, M. W. H. Chan and T. E. Mallouk, Template-grown metal nanowires. *Inorganic Chemistry*, 2006, **45**, 7555-7565.
61. A. Bid, A. Bora and A. K. Raychaudhuri, Temperature dependence of the resistance of metallic nanowires of diameter $\geqslant$15nm: Applicability of Bloch-Grüneisen theorem. *Physical Review B*, 2006, **74**, 035426.
62. T. H. Kim, X. G. Zhang, D. M. Nicholson, B. M. Evans, N. S. Kulkarni, B. Radhakrishnan, E. A. Kenik and A. P. Li, Large discrete resistance jump at grain boundary in copper nanowire. *Nano Letters*, 2010, **10**, 3096-3100.
63. J. Richter, R. Seidel, R. Kirsch, M. Mertig, W. Pompe, J. Plaschke and H. K. Schackert, Nanoscale palladium metallization of DNA. *Advanced Materials*, 2000, **12**, 507-510.
64. E. Braun, Y. Eichen, U. Sivan and G. Ben-Yoseph, DNA-templated assembly and electrode attachment of a conducting silver wire. *Nature*, 1998, **391**, 775-778.
65. Z. Deng and C. Mao, DNA-Templated Fabrication of 1D Parallel and 2D Crossed Metallic Nanowire Arrays. *Nano Letters*, 2003, **3**, 1545-1548.
66. S. Pruneanu, S. A. F. Al-Said, L. Dong, T. A. Hollis, M. A. Galindo, N. G. Wright, A. Houlton and B. R. Horrocks, Self-assembly of DNA-templated polypyrrole nanowires: Spontaneous formation of conductive nanoropes. *Advanced Functional Materials*, 2008, **18**, 2444-2454.
67. W. U. Dittmer and F. C. Simmel, Chains of semiconductor nanoparticles templated on DNA. *Applied Physics Letters*, 2004, **85**, 633-635.
68. J. Richter, M. Mertig, W. Pompe, I. MÃ¶nch and H. K. Schackert, Construction of highly conductive nanowires on a DNA template. *Applied Physics Letters*, 2001, **78**, 536-538.
69. H. K. Kim, J. A. Jeong, I. K. Yoo, J. B. Koo, H. H. Lee, K. H. Hur, D. H. Kim, S. E. Kim and B. H. Jun, Rapid thermal reduction of inkjet printed Cu interconnects on glass substrate. *Electrochemical and Solid-State Letters*, 2011, **14**, J65-J68.
70. W. Zhang, S. H. Brongersma, N. Heylen, G. Beyer, W. Vandervorst and K. Maex, Geometry effect on impurity incorporation and grain growth in narrow copper lines. *Journal of the Electrochemical Society*, 2005, **152**, C832-C837.
71. H. Lee, S. S. Wong and S. D. Lopatin, Correlation of stress and texture evolution during self- and thermal annealing of electroplated Cu films. *Journal of Applied Physics*, 2003, **93**, 3796-3804.
72. S. Tsukimoto, T. Kabe, K. Ito and M. Murakami, Effect of annealing ambient on the self-formation mechanism of diffusion barrier layers used in Cu(Ti) interconnects. *Journal of Electronic Materials*, 2007, **36**, 258-265.
73. S. Jang, Y. Seo, J. Choi, T. Kim, J. Cho, S. Kim and D. Kim, Sintering of inkjet printed copper nanoparticles for flexible electronics. *Scripta Materialia*, 2010, **62**, 258-261.
74. G. L. Allen, R. A. Bayles, W. W. Gile and W. A. Jesser, Small particle melting of pure metals. *Thin Solid Films*, 1986, **144**, 297-308.
75. C. Gómez-Navarro, F. Moreno-Herrero, P. J. De Pablo, J. Colchero, J. Gómez-Herrero and A. M. Baró, Contactless experiments on individual DNA molecules show no evidence for molecular wire behavior. *Proceedings of the National Academy of Sciences of the United States of America*, 2002, **99**, 8484-8487.
76. A. Gil, P. J. De Pablo, J. Colchero, J. Gómez-Herrero and A. M. Baró, Electrostatic scanning force microscopy images of long molecules: Single-walled carbon nanotubes and DNA. *Nanotechnology*, 2002, **13**, 309-313.

Chapter 4: Solution-based Preparation of Continuous DNA-templated Copper Nanowires

4.1. Introduction

4.1.1. Re-cap

Chapter 3 described a surface-based chemical approach for attempts to prepare conductive DNA-templated copper nanostructures from reduction of a Cu(I) salt at DNA. However the structures formed were of a polycrystalline nature and exhibited high resistivity. Additionally as outlined in section 1.5 of the introduction describing early work on surface metallisation of DNA with copper, it was found that Cu(II) coordination to surface-immobilised DNA, and the subsequent reduction by ascorbic acid, leads to granular structures.[1] Their high electrical resistivity was attributable to this granular nature. Moreover, the poor packing of copper nanoparticles on the template resulted in a non-continuous metallic pathway for electron transport along individual strands. Consideration of Cu(II) chemistry on surface-immobilised DNA led to the conclusion that polar solvent molecules (e.g. H_2O, DMSO) used in the delivery of Cu^{2+} ions would compete with the donor sites of template DNA for the metal, which would be expected to lead to less effective 'doping' of the DNA structure. As a result this would hinder the subsequent growth of metal along the template.

Therefore, the use of Cu(I) ions as a metal precursor was adopted (chapter 3) as Cu(I) salts are often more soluble in weakly, or even, non-coordinating (organic) solvents. Also, in choosing an organosoluble reducing agent, the entire metallisation process can be performed in a single weakly coordinating solvent. The idea of using a Cu(I) coordination compound was also appealing because there have been no previous reports of Cu(I)-based routes for the growth of copper nanostructures on DNA. The nanostructures resulting from this method were more continuous than those previously described in section 1.5, as copper deposited more homogenously along the template. However, upon closer inspection the structures were found to contain densely packed nanoparticles, and occasionally, significant gaps in the copper coating were observed. Similarly as for previous methods, the material was shown to be non-conductive.

Various attempts were made to improve the electrical properties of nanostructures and, despite attempts to transform the polycrystalline morphology of these nanostructures by

thermal annealing and repeat metallisation treatments, the electrical properties of the metallic nanostructures were not improved. Ultimately the lack of ohmic behaviour in the i-V curves encouraged other possibilities to be explored. Namely, the solution based approach to DNA-templated copper nanostructures, discussed here.

4.1.2. From surface to solution

Hitherto, all of the work in the literature describing the fabrication and characterisation of DNA-templated copper nanostructures have been performed on surface bound DNA,[1-5] whereby the preparative route is carried out in two consecutive treatment steps: (i) doping of surface-immobilised DNA with copper cations and (ii) chemical reduction of DNA/Cu^{n+} to produce the final DNA/Cu^{0} nanostructures.

A recurring issue amongst these surface based routes is the irregular morphology of the copper coating on DNA. An improved continuity in the structural morphology of such DNA-templated copper nanostructures was obtained by Kudo et al., who proceeded to develop more extensive copper deposition on the template by introducing a Pd 'primer' layer on DNA prior to the deposition of metallic copper in an electroless plating bath.[6] However, no chemical or electrical characterisation was carried out on the resulting product.

An interesting study utilised a 2-step treatment of surface-immobilised DNA for preparation of a compound semiconductor CdS on DNA templates.[7] In this experiment the surface-immobilised DNA strands were doped with Cd cations before addition of S^{2-} anions (substituting for the reduction step). It was revealed that a monodisperse array of CdS particles formed along the template, but lacked continuity (i.e. bare DNA was present between individual particles). In this same study, a remarkable difference in the structural morphology was observed when the entire reaction was performed in aqueous solution. Here smooth wire-like nanostructures of CdS templated on DNA were formed, which exhibited good electrical conductivity. Based on further observations in this study, the growth mechanism was likened to that of Ostwald's ripening of colloids.

A similar distinction between the surface and solution based approaches for DNA-templated nanostructures were observed in DNA-polypyrrole nanowires where it was found that surface-immobilised DNA inhibits the polymerisation process whereas the solution-based approach leads to smooth polymeric nanowires.[8] This striking

comparison between the surface-based route and a solution phase method gives an indication that the templated growth of copper nanostructures on DNA may be better performed in solution.

Additionally, other workers have found that the initial binding of Cu^{2+} to DNA inhibits rather than facilitates the subsequent reduction to Cu^{0}.[9] This may suggest that it is important to have the metal ion source and chemical reductant together in solution during the course of metal growth on DNA (as part of a one-pot procedure), as opposed to the 'doping/reduction' treatment on DNA-bound surfaces, which initially involves extensive doping of DNA followed by reduction to metallic copper. This was corroborated in the work done on Cu(I)-DNA interaction in chapter 3, where it was shown by FTIR and AFM that more extensive interaction/metallisation of copper takes place on the DNA template if reduction takes place *in-situ*.

There are few reports in the literature where double stranded DNA in solution has been used as a template for the formation of CuNPs.[9-11] However, these studies are focused on the use of DNA as a template to form small metallic clusters to act as fluorescent probes rather than Cu-DNA strands for purposes of electrical conduction. Furthermore they make no attempt to characterise the material structurally.

In this chapter, a simple solution reaction of aqueous $Cu(NO_3)_2$ and ascorbic acid in the presence of DNA is reported under mild conditions (room temperature, water as solvent, neutral pH). The aim is to produce continuous copper nanostructures using DNA as a template (< 10 nm height) which exhibit better structural properties (i.e. smoother metallic coatings) and improved electrical characteristics than those surface prepared Cu-DNA nanostructures described in previous reports.

A comprehensive study of Cu-DNA nanowires prepared in solution phase is presented. Firstly, the synthesis of the Cu-DNA product is described, before proceeding to characterise the material chemically using XRD and XPS. Structural information was acquired using FTIR, to elucidate the nature of the Cu-DNA interaction, and AFM to investigate structure morphology and sizes. Electrical characterisation of the final Cu-DNA nanowires was investigated by various techniques including EFM, C-AFM and 2-terminal device measurements.

4.2. Experimental

4.2.1. Cleaning and preparation of silicon wafers

Silicon <p-100> wafers were cut into 8 x 10 mm pieces with a diamond tip pen. The wafers were then serial washed in high purity acetone, propanol and Nanopure water before heating the wafers in a solution of surfactant (sodium dodecyl sulphate, 0.01g per 100 mL water) for 20 minutes followed by washing with copious amounts of Nanopure water. The wafers were then chemically oxidised in hot "piranha" solution (4:1 H_2SO_4:H_2O_2) for 45 minutes at ~50°C in order to oxidise the surface and remove organic residue. The wafers are then washed with Nanopure water and dried in an oven for 30 minutes. The surface was chemically modified by vapour deposition, which involved exposure of the bare silicon surface to chlorotrimethylsilane vapour (Me_3SiCl) for 8 minutes leading to formation of the trimethylsilane (TMS) self-assembled monolayer (Me_3SiCl). Static contact angle measurements were carried out on the TMS-modified Si substrates using a CAM100 system (KSV Instruments LTD., Helsinki, Finland), with Nanopure water as the probe liquid. Contact angles generally fall between 60°-70° (for a 6-10 min silination time).

Wafers used for EFM/C-AFM analysis had a 200 nm thick oxide layer on both sides to form an insulating barrier on the surface. Prior to the previously described cleaning method the backside of these wafers were treated with a solution of HF (10% aq.) to remove the native oxide layer and provide electrical contact for subsequent electrical measurements.

4.2.2. Preparation of Cu-DNA nanostructures

λ-DNA solution (500 μg mL^{-1}, in 10 mM tris-HCl, pH 8, 1 mM EDTA) was diluted down to 300 μg mL^{-1} with Nanopure water. Typically, to 10 μL of this solution in a small Eppendorf tube was added $Cu(NO_3)_2.3H_2O$ (aq. 50 μM, 10 μL) followed by the drop wise addition of ascorbic acid (aq. 2 mM, 10 μL). This gives a Cu^{2+} to phosphate ratio (n) of 0.05. The reaction mixture was left to incubate for 3 hours whilst gentle stirring on a mechanical roller. To purify the suspension of nanowires from nanoparticles, as well as unreacted starting material, the mixture was centrifuged at 8000 rpm for 2 minutes. The top fraction was discarded and the bottom fraction was collected for analysis.

4.2.3. Alignment of Cu-DNA nanostructures upon substrates

DNA-templated copper nanostructures were aligned on TMS-modified silicon surfaces, for purposes of SPM and C-AFM analysis, using a combination of combing and drop cast techniques: A 5 μL droplet of the DNA/Cu nanowires suspension was removed from the bottom of the Eppendorf tube containing the product and pipetted onto the substrate. The nanowires were then "combed" onto the substrate by slowly withdrawing a portion of the droplet using a micro pipette and then redepositing onto the surface. This routine was performed several times before finally allowing the droplet to evaporate in a ventilated laminar flow cabinet. This left a residual drying 'stain' on the surface from which nanostructures suitable for AFM analysis were seen to protrude from perpendicular to the edge of the drying mark.

4.2.4. UV/Vis Spectroscopy

Copper nitrate solution (aq. 500 μM, 120 μL) was added drop wise to calf-thymus DNA (300 μgmL^{-1}) and allowed to mix for 1 minute in a quartz cuvette. A UV/vis spectrum was recorded in the range 400-900 nm at 0.5 nm data intervals. Ascorbic acid (0.12 M, 10 μL) was then added to the cell and the spectrum was re-recorded. Concentrations were kept as low as possible to prevent precipitation whilst maintaining a Cu^{2+} to phosphate ratio (n) of ~0.05, which is consistent with the established preparation in this chapter for formation of smooth Cu-DNA nanowires.

Attempts to increase the amount of Cu-DNA material in the cell (in order to increase the UV absorption intensity) whilst maintaining a Cu ion to phosphate ratio (n) of 0.05 was prohibited due to saturation of the DNA solution at high concentration (> 1.2 $mgmL^{-1}$). Increasing the Cu^{2+}/ascorbic acid concentration leads to precipitation, thus restricting further measurements. At the concentration used in this study where n= 0.05, a miniscule particle forms in the reaction mixture after several days of incubation.

All spectra were subtracted from the background of Nanopure water. Spectra were recorded using a Varian Cary-100 Bio UV/vis Spectrometer.

4.2.5. Fourier-Transform Infra-Red (FTIR) Spectroscopy

Samples for FTIR analysis were prepared by mixing aqueous solutions of calf-thymus DNA (300 μg mL^{-1}, 250 μL) and $Cu(NO_3)_2.3H_2O$ (50 μM, 250 μL), before the drop wise addition of ascorbic acid (aq. 2 mM, 250 μL). The reaction mixture was left to incubate at room temperature whilst stirring on a mechanical roller for 3 hours. The reaction mixture was transferred to an Eppendorf tube and centrifuged at 8000 rpm for 2 minutes to separate the suspension of nanowires from nanoparticles. 60 μL of the solution was pipetted from the bottom of the tube onto a "piranha" cleaned n<100>-silicon wafer and left to evaporate overnight in a ventilated laminar flow cabinet to leave a thin film of copper coated DNA material on the surface. The film thickness was increased by repeating the above procedure twice.

FTIR spectra (in the range 600-4000 cm^{-1}) were recorded in transmission mode on a Bio-Rad Excalibur FTS-40 spectrometer (Varian., Palo Alto, CA) equipped with a liquid nitrogen cooled deutarated triglycine sulphate (DTGS) detector, and were collected at 512 scans with 2 cm^{-1} resolution.

4.2.6. X-ray Powder Diffraction (XRD)

Samples for X-ray powder diffraction were prepared by mixing aqueous solutions of calf-thymus DNA (1 mg mL^{-1}, 10 mL) and $Cu(NO_3)_2.3H_2O$ (0.5M, 10mL), before the dropwise addition of ascorbic acid (1.0M, 20 mL) affording a [Cu]:[DNA(P)] ratio (n) of ~ 150. An immediate colour change in the solution from bright blue to bright green was observed. The reaction mixture was left to stir overnight at room temperature after which a small amount of red precipitate was seen to have formed on the walls of the container. The mixture was then placed in a refrigerator for a further 24 hours during which time more red precipitate had formed and settled to the bottom of the flask. To obtain the product, the mixture was centrifuged at 8000 rpm for 30 minutes, after which the supernatant was decanted and the red solid was collected on a Buchner funnel, washed with Nanopure water, HPLC grade ethanol and dried under vacuum. Powder X-ray diffraction data was obtained using a PANalytical X'Pert Pro Diffractomer equipped with a Cu $K\alpha_1$ radiation source ($\lambda = 1.54 \times 10^{-10}$ M).

4.2.7. X-ray Photoelectron Spectroscopy (XPS)

Samples for X-ray Photoelectron Spectroscopy were prepared similarly as for XRD analysis. However the concentration ratio of [Cu]:[DNA(P)] was lowered to ~10. The product was deposited on "piranha" cleaned silicon substrates (silanisation of the substrate was omitted in order to increase the wettability of the substrate surface). A small particle was formed in the reaction solution which was then separated from the liquid, washed with ethanol and finally dispersed in Nanopure water. The solution was drop casted (60 μL) onto a clean silicon wafer and dried *in vacuo*. XPS analysis was obtained on the dried material. The density of Cu-DNA material deposited on the surface is higher than that for AFM samples but is necessary to obtain sufficient signal in the XPS spectra.

The supernatant from the product solution was kept behind and purified by centrifugation and then deposited onto a clean silicon wafer for AFM analysis.

XPS was carried out using a Thermo K-Alpha XPS system with a microfocused, monochromated Al Kα X-ray source at a take-off angle of 90°. An electron/ion gun was used to neutralise any charge build-up during analysis. The size of the X-ray spot was 400 μm x 700 μm. Calibration of binding energies was achieved by referencing to the internal hydrocarbon peak at 284.8 eV. Peak fitting was carried out using the CasaXPS software and a mixture of Guassian-Lorentzian peak shapes was used. Within the XPS spectra the black line shows the real data, the grey lines represent peak fits and the red line represents the sum fit. In all instances, the minimum number of peaks was fitted in order to obtain a good fit. This is to ensure that the number of components in the spectra is not overestimated; especially since it is not possible to resolve all of the components in the spectra in many cases. FWHM's were allowed to vary flexibly within the region of 1-2 eV and remain consistent for peaks within the same series. Linear backgrounds were used for all 1s spectra and Shirley backgrounds for 2p spectra. Two Shirley backgrounds were used for 2p fitting (for $2p_{3/2}$ and for the $2p_{1/2}$). The data was collected at grazing emission in order to enhance the surface sensitivity.

4.2.8. AFM/EFM studies

TappingMode AFM imaging of surface topography was performed in air on either a Multimode Nanoscope IIIa or a Dimension Nanoscope V instrument (Veeco

Instruments Inc., Metrology Group, Santa Barbara, CA). TESP7 probes (n-doped Si cantilevers, Veeco Instruments Inc., Metrology Group), with a resonant frequency of 234-287 kHz, and a spring constant of 20-80 Nm^{-1} were used as tips. Data acquisition was carried out using Nanoscope software version 5.12b36 (Multimode IIIA) and Nanoscope software version 7.00b19 (Dimension Nanoscope V) (Veeco Instruments Inc., Digital Instruments).

EFM measurements were carried out in air on a Dimension Nanoscope V system using MESP probes (n-doped Si cantilevers, with a metallic Co/Cr coating, Veeco Instruments Inc., Metrology Group), with a resonant frequency of ca. 70 kHz, a quality factor of 200-260, and a spring constant of 1-5 Nm^{-1}. Data acquisition was carried out using Nanoscope version 7.00b19 software. For both AFM systems, vibrational noise was reduced with an isolation table/acoustic enclosure (Veeco Inc., Metrology Group).

The reported EFM phase images show the phase of the tip oscillation at a set lift height above the sample surface (typically 40-100 nm). Samples used in EFM studies were deposited upon Si <n-100> substrates with a thermally grown 200 nm (± 10%) thick oxide layer on top, prepared as described earlier. Processing of data acquired from AFM and EFM experiments was carried out using both Nanoscope version 7.00b19 (Veeco Inc., Digital Instruments) and WSxM4.0 Develop 12.6 (Nanotech Electronica S. L., Madrid, Spain) software.

4.2.9. Conductive-AFM (C-AFM) studies

Conductive-AFM (C-AFM) was carried out in contact mode on samples of Cu-DNA nanostructures fixed to TMS-modified Si/SiO_2 supports, using the Dimension Nanoscope V instrument. Samples were prepared by drop casting 5-40 μL of the copper nanowire suspension onto the SiO_2 surface and leaving the droplet to evaporate at room temperature. The surface tension created by the receding meniscus is enough to align the wires on the substrate parallel to the direction of solvent withdrawal. This results in a small circular ‘stain’ on the surface, which contains a dense deposit of nanomaterial at its centre and aligned wires extending from the periphery of the main body. A drop of In/Ga eutectic was applied to the edge of the nanomaterial deposit and the metallic chuck of the AFM to provide electrical contact. The circuit is completed via the metallic AFM tip as it contacts the Cu-DNA nanostructure during imaging. The tip is positioned

on a nanowire of interest approximately 1mm from the eutectic contact. Typically, a bias of between 1-10 V was applied in order to obtain sufficient current signals for analysis. All measurements were made at room temperature.

4.2.10. 2-probe nanowire device fabrication and measurements

Two-terminal conductivity measurements were performed using gold electrodes deposited on clean silicon oxide substrates. Electrodes were fabricated in the School of Electrical Engineering, Newcastle University, by Prof. Nick Wright and his research team. First, an appropriate mask was prepared with four pairs of large pads and small fingers and patterned using a reverse photolithography process on the clean substrate. Next, reactive ion etching was used to make a 100 nm deep trench in a 220 nm thick SiO_2 dielectric; this reduces the step height at the boundary between the gold electrodes and the oxide gap in the final device and facilities alignment of nanowires across the gap. The trench was filled with e-beam-evaporated metals (10 nm Cr adhesion layer followed by 90 nm Au). Next, a lift-off process was used to remove unwanted Cr and Au. The gap between each pair of fingers was 3, 7, 9 and 14 μM and the two larger pads in each pair are separated by 80 μM. The two small gold fingers provide contact points to the DNA-templated copper nanostructures, with the two large gold pads serving as electrical contacts for macroscopic probes to the external circuit. Lastly the whole substrate was treated with Me_3SiCl vapour for 10 minutes to make the surface hydrophobic. This facilitates the combing motion used to deposit the nanowires and controls the density of material on the surface.

Cu-DNA nanostructures were aligned across the electrode gaps by placing two 2 μL droplets of an aqueous solution of Cu-DNA nanowire suspension on the electrodes and physically moving the drops across the gap using a 'soft' nitrogen flow.

Electrical measurements were performed on a probe station (Cascade Microtech) and a B1500A semiconductor analyser (Agilent). For each of the current-voltage (i-V) sweeps, the current was measured for applied voltages from -3 to 3 V in 30 mV steps. A further sweep was performed between -1 and 1 V for higher resolution data around 0V bias. All of the electrical measurements were carried out under a steady flow of nitrogen in the dark. i-V curves were acquired at a constant temperature of 20.0°C maintained in

the probing chamber using a thermal chuck system (Model ETC- 200 L, ESPEC, Japan). The probes used were tungsten, 9 μM radius.

4.3. Results and Discussion

4.3.1 Synthesis

Cu-DNA nanowires were prepared in solution phase by the addition of aqueous $Cu(NO_3)_2$ to a DNA containing solution prior to the addition of ascorbic acid, which serves as the chemical reductant. The reaction mixture was allowed to incubate for 3 hours on a mechanical roller. Figure 4.1 shows a graphical representation of the general reaction procedure: (i) DNA solution is measured out, (ii) copper nitrate is added to 'dope' DNA, (iii) ascorbic acid is added for reduction of copper ions on the DNA template, providing nucleation sites, (iv) the solution is incubated for 3 hours, during which time, further metal growth takes place at the boundaries of copper grains formed on DNA and (v) the final Cu-DNA product is obtained as a suspension of nanostructures in solution.

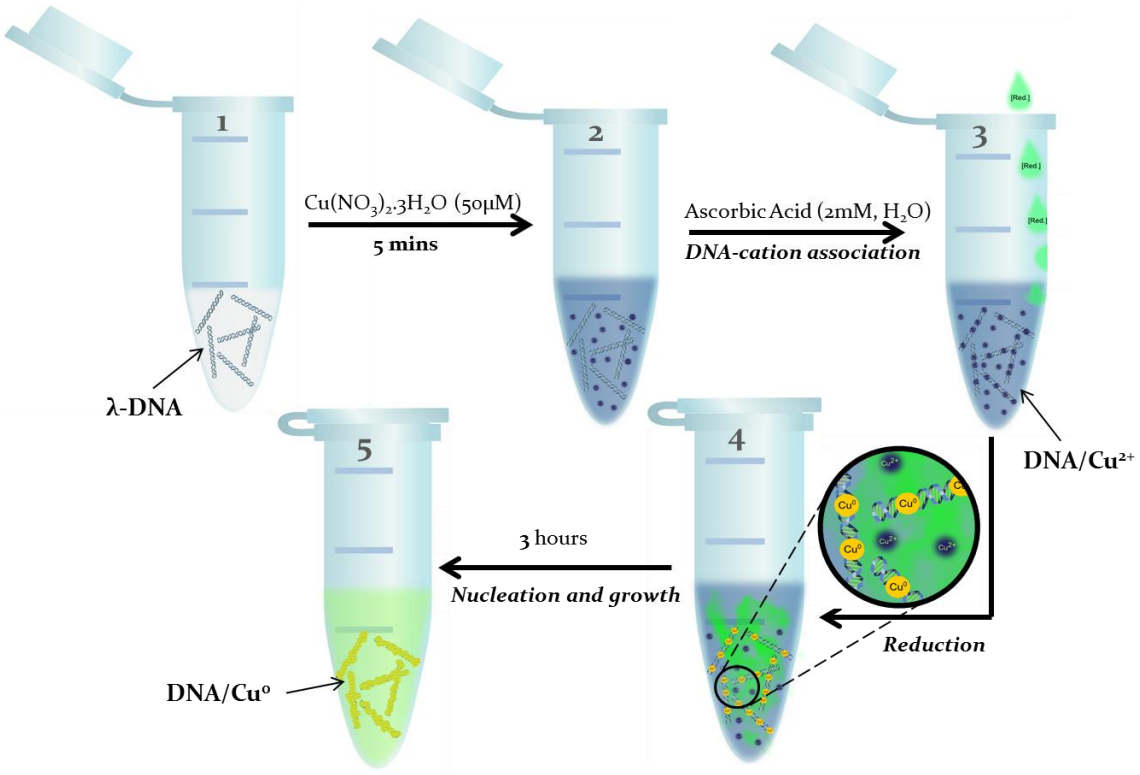

Figure 4.1: Image showing the general reaction procedure for the preparation of DNA-templated copper nanostructures in solution

Initial studies designed to establish suitable reaction conditions for the preparation of the target Cu-DNA nanowires relied on characterisation by Atomic Force Microscopy (AFM). These experiments sought to identify continuous coating of the DNA molecular

template which was smooth and regular in height. A variety of experimental conditions were explored in which the concentration ratio of Cu^{2+}: DNA (phosphate) is varied. These preliminary studies aimed to analyse copper metallised DNA structures isolated from the various different preparations. In all cases the concentration of λ-DNA used was 300 μgmL^{-1} (diluted from 500 μgmL^{-1} stock solution) and the concentration of Cu^{2+} was varied (excess ascorbic acid) to give varied [Cu]/[DNA(P)] ratios (n). Four ratios were investigated altogether; where n= 500, 25, 1 and 0.01.

Figure 4.2 shows a typical AFM height image (with corresponding height profile inset) for each ratio ('n') investigated.

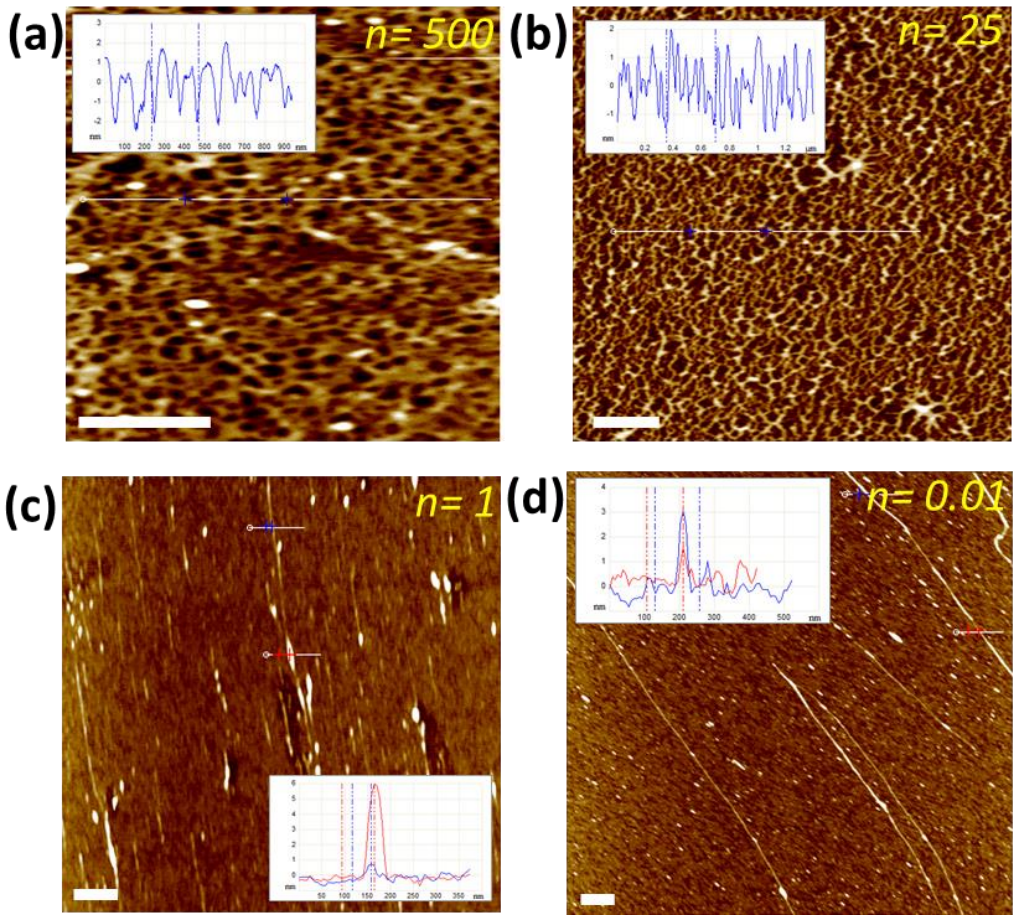

Figure 4.2: AFM height images of Cu-DNA nanomaterial prepared at various different ratios of Cu:DNA (Phosphate) (n): (a) n=500 (b) n=25, both images shows Cu-DNA in a highly packaged form, (c) n=1, Cu-DNA strands appear significantly shorter than expected and (d) n=0.01, long Cu-DNA strands with low levels of metallisation. Insets show heights profiles corresponding to the line traces in the image. Scale bars= 300 nm, height scales= 5 nm

It was found that at a high concentration of Cu^{2+} (500 mM) and ascorbic acid (1000 mM), relative to DNA (300 μgmL^{-1}) where n= 500 (figure 4.2a), the reaction did not

afford high aspect ratio copper "nanowires" as desired. Instead the AFM data revealed the product to consist of a dense aggregation of nanostructured material.

As can be seen in the AFM height image (figure 4.2b, n= 25) the product formed was also densely packed DNA nanomaterial with no evidence of extended, isolated 'wires.' Dilution of the mixtures in water as well as varying the incubation time did not lead to formulation of the desired morphology, nor did changing the method of deposition. Both images 'a' and 'b' show the height profiles (inset) corresponding to the line trace across the material in each AFM height image. These two profiles display a similar trend with sharp variations in the height between 1-2 nm reflecting the nature of the densely packed material.

Such features may result from the condensation of DNA brought about by the incorporation of positive metal ions to the DNA structure in aqueous solution.[12] The positive charge of the metal ion leads to charge neutralisation of the negative DNA (phosphodiester) backbone, thus minimising repulsive electrostatic forces between DNA strands in solution and allowing the formation of condensates which consist of tightly bound DNA aggregates. Although it is generally considered that cations of charge +3 or greater is required to induce DNA condensation, such as that brought about by incorporation of hexaammine cobalt(III) ($[Co(NH_3)_6]^{3+}$) to DNA,[13] *divalent* transition metal ions can result in DNA aggregation at high enough metal ion concentrations.[14, 15] It has even been suggested that the concentration of metallizing agents strongly influences the conformational behaviour of DNA in solution, and at high concentration, DNA condensates form.[16, 17]

DNA duplexes are also known to undergo cross-linking when incubated with divalent metal ions.[15] It is well established that metal ions can bind through the N7 atom of guanine and adenine of duplex DNA.[18] Cu(II) ions boast better DNA base binding ability compared to other metal ions such as Mg(II), Co(II) and Ni(II), which instead have higher affinity for phosphate.[19] This higher affinity for the bases (although interaction with the phosphate groups is still likely to be the major interaction) means copper(II) has a large destabilising effect on the DNA structure, at high concentrations, and lowers the melting temperature (T_m) of DNA.[20, 21] This is likely caused by disruption to Watson-Crick base pairing in the double helix. It has been demonstrated by Bloomfield *et.al*. that partially melted regions of DNA resulting from metal ion-base binding can cause cross-linking between individual metallo-DNA molecules.[15] This

could account for the highly aggregated appearance of Cu-DNA in these current studies. Aggregation may become more pronounced at higher concentrations of Cu^{2+} resulting from more available sites for cross-linking.

Indeed, early studies by Eichorn and Shin have indicated that above [Cu]/[DNA(P)] ratios of ~0.1, for divalent copper ions, the T_m (DNA) of calf-thymus DNA falls dramatically.[19] Thus Cu^{2+} can destabilise the DNA structure at high enough concentration of the metal ion. Figure 4.3 shows a graph of T_m against $[M^{2+}]$/[DNA(P)] for various divalent metal ions studied in the work done by Eichorn and Shin.[19] An abrupt drop in melting temperature of DNA upon increasing copper ion concentration is observed at > 0.1. This is contrary to what is seen for the various other metals investigated in the study, which don't exhibit such a significant destabilising effect on the DNA structure as much as Cu^{2+} does. FTIR studies in the literature have, likewise, indicated that denaturation of DNA begins at n= 0.1 and continues up to 0.5.[22]

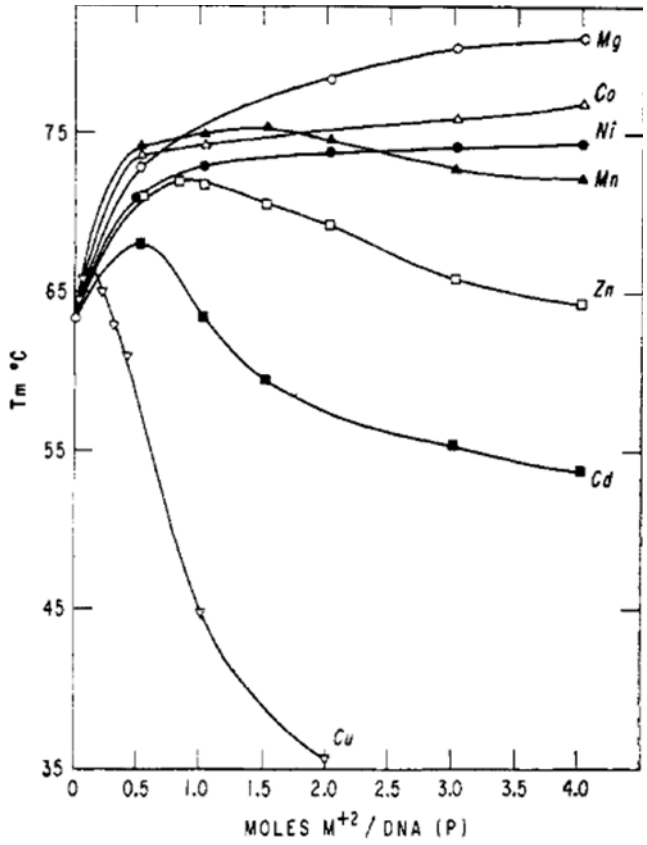

Figure 4.3: "Variations of T_m of solutions of DNA as a function of divalent metal ion concentration."[19]

Figure 4.2c shows an AFM image of the Cu-DNA product formed at n= 1. Networks are not observed at this ratio and instead individual strands are observed. However, these appear to have been cut, giving substantially shorter segments than the typical length expected for lambda DNA (16 μM). It is known that Cu^{2+}/ascorbic acid mixtures can generate hydroxyl radicals (HO·) *in situ* which are toxic towards DNA in solution and can lead to DNA cleavage.[9, 23-26]

According to the literature,[7] CdS templating on DNA in solution at n= 0.7 led to precipitation of material and no evidence of one-dimensional strands were observed. When the concentration of cadmium was lowered significantly evidence of nanowire formation was observed. The concentration dependence of cadmium and sulphide on the conformation of DNA has been investigated in the literature elsewhere.[17] Similarly in these current studies, when the concentration of Cu(II) in reaction mixture is low, ≤ 100 μM (n= <0.1), we begin to observe material with the desired feature of continuous, even, coverage (i.e. nanowires).

Figure 4.2d shows AFM data of Cu-DNA product formed at [Cu]/[DNA(P)] ratios of n= 0.01. Here, long one-dimensional strands of DNA (on the order of microns) were observed which appeared to be *partially* coated with copper in some regions due to low levels of metallisation. The red and blue cross sections of a single nanostructure (see figure 4.2d, inset) show contrasting heights along the same structure where the measured height of ~1 nm indicates bare DNA and a height of ~3 nm indicates a small amount of metallic coverage. These results suggest that a suitable regime for forming well-ordered copper metallised DNA is above n= 0.01 and below n= 1. Within this range (0.01- 1) one should expect to see increased metallisation of DNA without incurring any damage and/or change of shape to the DNA double helix.

Finally a ratio of n= 0.05- 0.1 was selected as giving the most suitable reaction conditions based on analysis of the products (discussed in detail in section 4.3.4.1). A suitable concentration of $Cu(NO_3)_2$ and ascorbic acid for a 3 hour incubation time was found to be 50 μM–100 μM and 2 mM, respectively. The concentration of DNA was diluted down to ~300 μg mL^{-1} to afford a $[Cu^{2+}]$/[phosphate] ratio ('n') within the range 0.05 to 0.1. Full AFM characterisation of these Cu-DNA nanostructures is presented in section 4.3.4.1.

So far, these studies have indicated that the use of high concentrations of Cu^{2+} (> 100 μM) and excess ascorbic acid, with respect to DNA concentration, do not facilitate the

formation of individual Cu-DNA nanostructures. A ratio of n=0.05 was found to be suitable for Cu-DNA wire formation. The remainder of this chapter is concerned with Cu-DNA nanowires prepared using the value of 'n.'

Purification

Processing of the Cu-DNA containing solution was required in order to separate unreduced starting material (salt residue) as well as non-templated material (CuNP's) from the desired DNA-templated copper nanostructures. This was achieved by centrifugation of the incubated product mixture at 8000 rpm for 2 minutes in an Eppendorf tube (see schematic in figure 4.4). AFM data of the top fraction (figure 4.4a) of the centrifuged solution shows an abundance of non-templated material in contrast to what is observed from the bottom fraction, which contained pure individual 1-D nanostructures (figure 4.4b). This procedure allows the large wire-like structures to be extracted from the lowest part of the Eppendorf tube, whereas the non-templated material can be discarded using a micropipette.

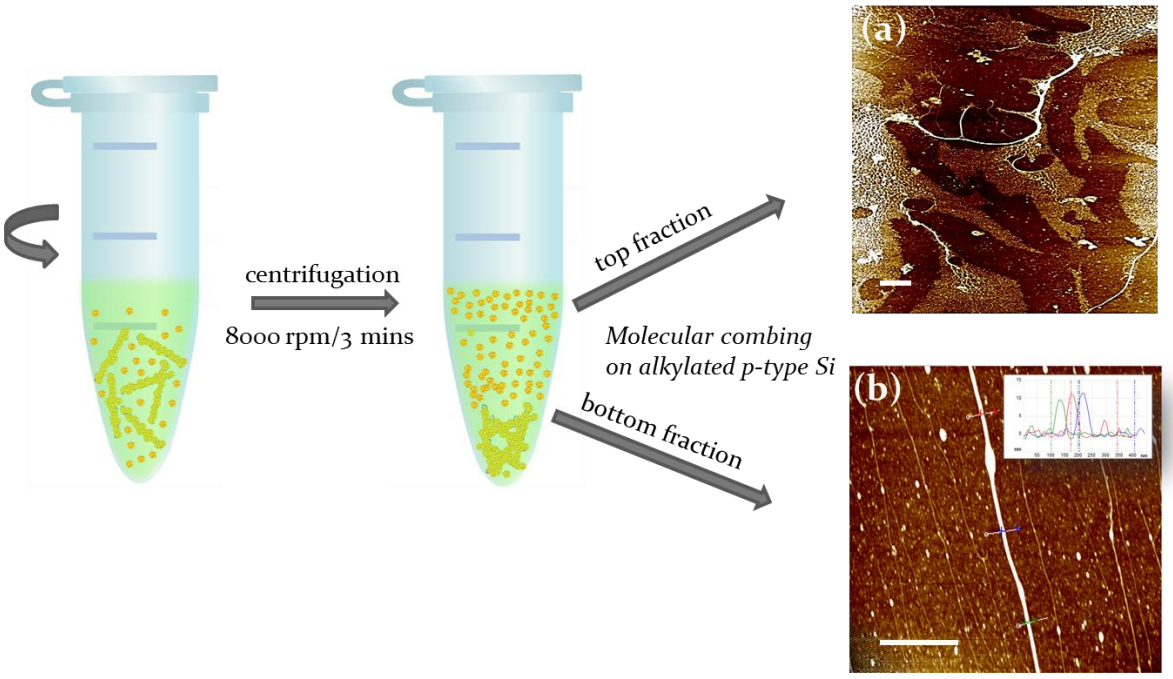

Figure 4.4: Schematic showing the purification procedure of Cu-DNA nanostructures by centrifugation. The top and bottom fractions are separated and combed onto two separate silicon wafers for analysis by AFM; (a) AFM height image of top fraction and (b) AFM height image of bottom fraction. Scale bars= 10 µm, height scales= 10 nm

Alignment of the Cu-DNA nanostructures was performed on a trimethylsilane (TMS)-modified silicon substrate using the well-established molecular combing method.[27, 28] Typically, a small droplet of the solution (5 μL) containing the 1-D nanostructures is combed across the TMS-silicon substrate several times using a micropipette tip and is then removed.

The TMS surface modification is achieved via time controlled surface exposure to the organosilane vapour which forms a self-assembled monolayer of TMS on the silicon surface. This makes the surface hydrophobic in order to facilitate the combing process. By controlling the surface exposure to silane vapour one can tailor the surface wetting properties. The ability to control the hydrophobicity/hydrophilicity in this manner allows one to control the density of material deposited on the surface. Thus, the surface tension was optimised in order to obtain well aligned and isolated 1-D nanostructures for the purposes of Scanning Probe Microscopy (SPM) analysis and electrical characterisation of isolated nanostructures. However, for FTIR and XPS studies it is favourable to have a *hydrophilic* surface in order to have a higher density of bound material on the silicon surface. The degree of surface wetting was analysed by contact angle measurements where the ideal contact angle of the surface/solution interface (for AFM studies) fell between 60–70°.

There are other benefits to using an organosilane monolayer on the silicon surface for alignment of copper nanostructures. As well as preventing diffusion of Cu into the SiO_2 layer at high temperatures, organo-silane monolayers also act as good coupling agents and adhesion enhancers at the Cu/dielectric (Si/SiO_2) interface.[29] These aspects will become important for all future Ultra Large Scale Integration (ULSI) methods.

4.3.2. Investigation into Cu binding to DNA

4.3.2.1. UV/vis studies

UV/vis Spectroscopy was used to study the reaction between Cu^{2+} ions and DNA (n= 0.05) and the subsequent treatment with ascorbic acid. Figure 4.5 shows the resulting data for measurements performed on a pure solution of DNA (blue line) and DNA incubated with Cu^{2+} before (red line) and after reduction with ascorbic acid (green line). The concentrations of reagents were chosen to afford n= 0.05, as used for the preparation of DNA-templated Cu nanostructures for AFM analysis. The main feature to point out from the UV data is the disappearance of the copper nitrate absorption at ~790 nm (red line) due to Cu^{2+} d-d transitions, upon treatment with ascorbic acid; indicating reduction. The reduction of Cu^{2+} is further indicated by the formation of a characteristic broad plasmon absorption between 540 to 630 nm due to copper metal (green line).[30]

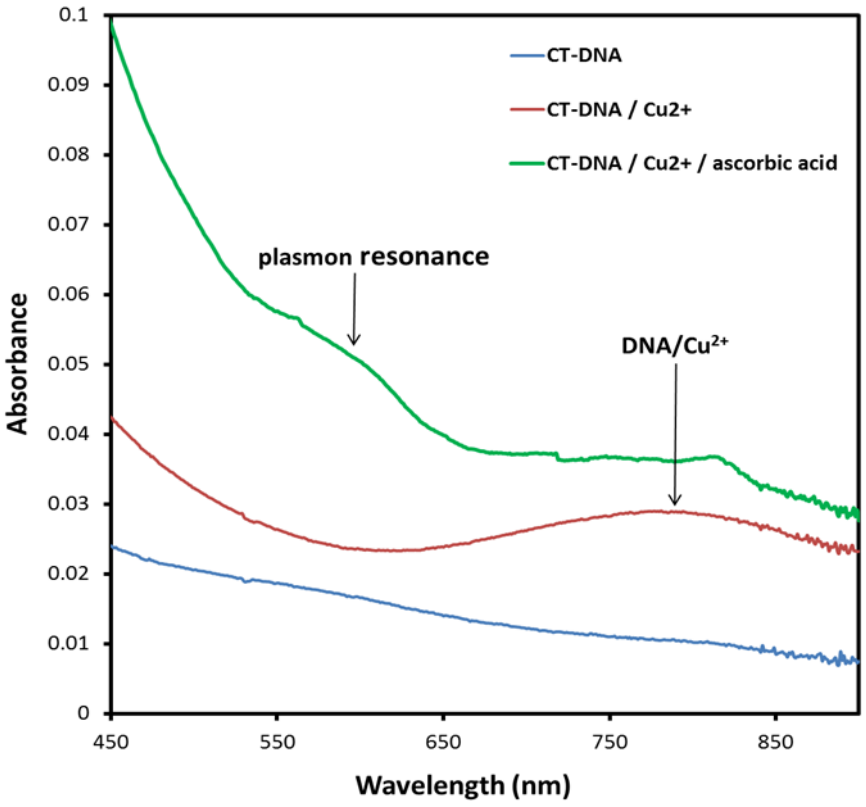

Figure 4.5: UV/Vis spectra of DNA (blue line), DNA after incubation with Cu^{2+} (red line) and DNA/Cu^{2+} after addition of ascorbic acid (green line). Solvent used was Nanopure water. An increase in absorption after reduction of Cu^{2+} is indicated by the shouldering of the green line at ~600 nm

At high values of 'n' (~25) an obvious colour change in the solution from bright blue to green is observed, which transforms to a golden brown colour following further incubation, indicating a change in oxidation state of Cu^{2+} (most likely to the zero valent metal).

The UV/vis results have indicated the formation of metallic copper. However, little information can be garnered regarding the interaction of copper with DNA, as the DNA absorption band (~260 nm) is not significantly affected upon addition of metal ions. In order to establish details of the interaction, including which of the possible DNA binding sites are targeted by copper ions, FTIR was employed.

4.3.2.2. FTIR studies

Fourier-Transform Infra-Red (FTIR) Spectroscopy is useful for functional group determination and obtaining information of chemical bonding and has been used quite extensively to probe the interaction of metal ions with DNA.[22, 31-33] The technique is used here to elucidate the interaction of copper atoms with DNA following reduction of Cu^{2+} with ascorbic acid, and hence ultimately determine which sites on DNA are predominantly influenced by templated copper. An investigation into the effects of metallisation of DNA was carried out rather than the effects of Cu^{2+}-DNA coordination as this has been previously reported in detail elsewhere,[1, 22, 31] whereas, FTIR characterisation of copper *metal* templated on DNA has not yet been reported. There is likely to be a significant increase in copper deposition on DNA when Cu^{2+} is reacted in the presence of reductant; mainly because metallic nanoclusters act as seed platforms to encourage further growth of metal along the template via a 'nucleation and growth' mechanism.[1, 2, 34]

FTIR spectra (figure 4.6) were recorded on films of both DNA and DNA/Cu^0 on silicon wafer and compared and analysed for changes in DNA vibrational peak positions/intensities. Full peak assignments are given in table 4.1 below and are supported by references.[1, 32, 35-37] Each peak is numbered in the assignment table (table 5.1) and these are referred to in the text.

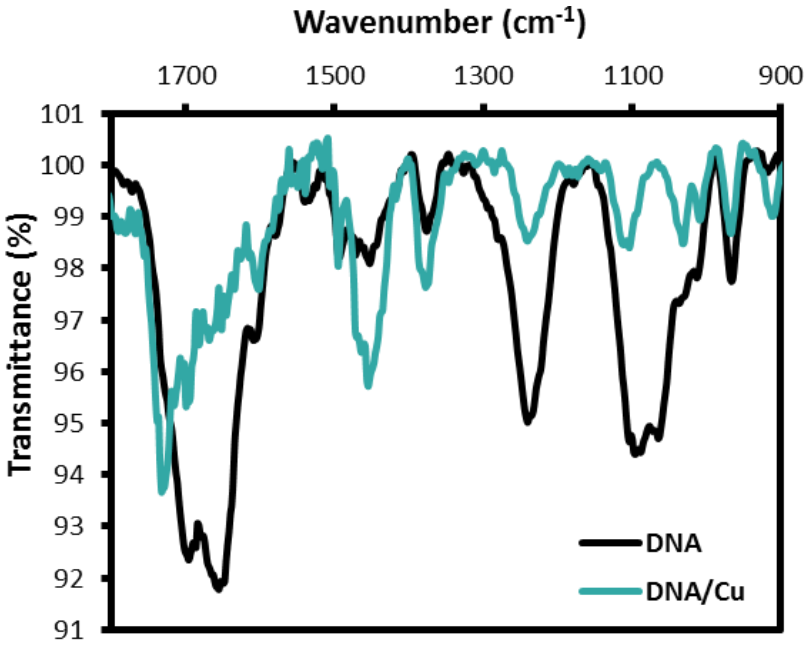

Figure 4.6: FTIR transmission spectra of DNA (black line) and copper metallised DNA (turquoise line) prepared in solution and deposited onto a solid silicon support. Data collected at 2 cm^{-1} resolution, 512 scans

Peak number	Assignment		Wavenumber (cm^{-1})	
		DNA	DNA/Cu	Shift
1	C6=O stretch of guanine	1696	1728	32
2	C2=O stretch of cytosine	1655	1695	40
3	C=N cytosine; N-H adenine; C7=N adenine	1607	1602	-5
4	C=N guanine and adenine stretch	1578	-	-
5	In-plane vibration of guanine and cytosine	1534	1539	5
6	C8-N coupled with a ring vibration of guanine	1491	1493	2
7	C-N stretch of thymine, guanine and cytosine	1452	1452	0
8	C-N stretch of guanine and cytosine	1376	1377	-1
9	C-N stretch of adenine	1326	-	-
10	PO^{2-} asymmetric stretch	1238	1238	0
11	PO^{2-} symmetric stretch	1097	1104	7
12	P-O or C-O backbone stretch	1064	1031	-33
13	C-O deoxyribose stretch	1013	1009	-4
14	C-C deoxyribose stretch	966	967	1

Table 4.1: Peak assignment table for selected FTIR stretching frequencies of DNA, before and after metallisation, with corresponding peak shift values. Data highlighted in red indicate the most prominent shifts in frequency for particular sites at DNA

As shown in figure 4.6 the FTIR spectrum for bare DNA (black line) shows the various stretches of the phosphodiester backbone and nucleobases. The bands in the region 900-1300 cm^{-1} come from the PO_2^- group and the ribose moiety. DNA base stretches are seen in the region 1300-1800 cm^{-1}. A split band containing two well defined peaks attributable to the C6=O stretch of guanine (1) and C2=O stretch of cytosine (2) is seen

at 1696 cm^{-1} and 1655 cm^{-1}, respectively. As for thymine, the C2=O and C4=O stretches are considered to overlap with the C2=O stretch of guanine and cytosine, respectively.[35, 36] The N-H of thymine is also expected to arise at ~1690-1700 cm^{-1}.[1]

Following metallisation (turquoise line) a rather dramatic shift in C=O bands are observed, whereby both are shifted to higher wavenumbers: 1728 cm^{-1} (1) and 1695 cm^{-1} (2). Additionally both peaks show a reduction in intensity. The large shifts observed for C2=O and C6=O of cytosine/thymine and guanine, respectively, indicate binding of copper metal at these locations. The C2=O site of cytosine is located in the minor of groove of DNA, whereas the C6=O site of guanine is located in the major groove of DNA. Therefore, shifts in FTIR absorption bands at these sites suggest that copper metal has templated around the entirety of the DNA double helix; affording the desired smooth wire-like metal DNA structure. The data presented here suggests that copper coordinates with both the phosphates and nucleobases of DNA.

The peaks observed at 1376 and 1452 cm^{-1} belonging to the coupled C-N stretches of guanine/cytosine and thymine/guanine/cytosine, respectively, remain unshifted but display an increase in intensity after complexation. According to the work carried out by Tajmir *et.al* in their studies of Cu^{2+} binding on the solution structure of DNA, this change in intensity is an indication of direct metal-base binding.[22] Coordination to the phosphodiester backbone is also evidenced by the dramatic shift in the P-O/C-O stretch of bare DNA (3) (1064 cm^{-1}) to lower wavenumbers in the DNA/Cu spectrum (1031 cm^{-1}). The relative intensity of this band displays a shoulder which becomes more pronounced after metallisation, but a significant reduction in intensity of the whole band is also apparent. A slight shift in the in-plane vibration of guanine and cytosine (4) is also notable in the two spectra.

As has been well documented in the literature, there are multiple sites available for metal ions to coordinate to the DNA structure.[18, 38, 39] Binding to the DNA backbone via the electrostatic attraction of positive metal ions to the negatively charged phosphates is a likely possibility. This results in full or partial charge neutralisation of the backbone and minimises repulsive forces between individual strands of the duplex. The most common nucleobase binding sites are at the purine bases at N-7 and O-6 of guanine and N-3 and O-2 of cytosine.[31, 38] Coordination of Cu^{2+} ions may also occur between two adjacent guanine bases on the same strand or inter strand complexation between a guanine and cytosine base pair. A combination of both nucleobase and phosphate

binding to form a mixed chelate is also possible, as shown in the scheme below (figure 4.7) for a single set of base paired nucleotides.[31]

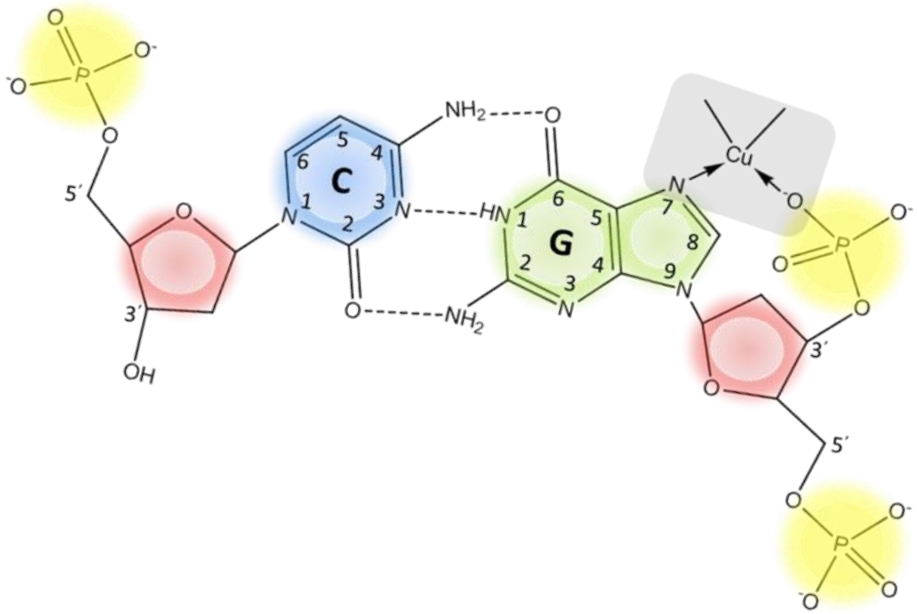

Figure 4.7: Proposed coordination complex of a guanine-cytosine base pair nucleotide with Cu(II) complex. Cu(II) coordinates with the N7 of guanine and a neighbouring oxygen from the phosphate on the same strand.

It has been demonstrated by Andruschenko *et.al* that the binding of Cu^{2+} ions to DNA is dependent upon the concentration of Cu^{2+} in solution.[31] Coordination to the nucleobases is promoted at high metal ion concentration, whereas binding to the backbone is the primary mode of interaction at lower metal ion concentration. The concentration dependence of Cu^{2+}-DNA binding in solution was the focal point in the work carried out by Tajmir *et.al* who showed that at a [Cu]/DNA[P] ratio of 0.025 the binding occurs primarily to the PO_2^- groups. At concentrations >0.05, as is used here, direct binding to the nucleobases and/or nucleobase/phosphate groups (i.e. N7 atom of guanine and a phosphate Oxygen) can occur.[22]

Previously reported solution FTIR studies of Cu^{2+} doped DNA revealed that a [Cu]/[phosphate] ratio (n) close to 0.1 (close to the ratio used in this study) results in primary interaction with the DNA backbone, neutralising the negative charge of the phosphates and increasing the stability of DNA.[31] Another study reveals that a [Cu]/[phosphate] ratio of above 0.1 can lead to denaturation of the DNA solution

structure,[22] possibly due to extensive coordination at nucleobase sites which may cause disruption of Watson-Crick base-paring. The ratio used in our Cu-DNA preparations is kept well below this value, at 0.05.

FTIR studies of Cu^{2+}/DNA coordination in the work conducted by Watson et al., found shifts in the phosphodiester backbone and a significant reduction of intensity in the P-O/C-O stretch of the DNA structure,[1] as was observed here. A shift in absorption from 1074 cm^{-1} to 1063 cm^{-1} was quoted for the P-O/C-O backbone stretch. However in our study, the reduced copper-DNA material afforded a more significant shift in frequency from 1064 cm^{-1} to 1031 cm^{-1}. This may suggest more extensive interaction of copper with the phosphodiester backbone of DNA when copper is reduced from Cu^{2+} to Cu^{0}. The results here are also notably different concerning the carbonyl stretches of guanine and cytosine, which are shifted quite dramatically- indicating interaction at these nucleobase sites. Whereas these same stretches remain largely unaffected for Cu^{2+} doped DNA, in the Watson *et.al* FTIR studies.[1]

4.3.3. Chemical characterisations

Samples for chemical characterisation are prepared slightly differently than those prepared for FTIR and AFM structural characterisations. The two techniques utilised below (XRD and XPS) require higher quantities of sample in order to obtain meaningful spectroscopic data. The following studies utilise large scale preparations in order to precipitate a "powder."

To achieve this, the concentration of Cu^{2+}/ascorbic acid mixture was increased with respect to the concentration of DNA. This affords a Cu:[DNA(P)] ratios (n) above what is used (i.e. > 0.1) for preparation of high aspect ratio Cu-DNA nanostructures studied by AFM in section 4.3.4.1. Comparison between the XRD and XPS data is made easier based on both samples being prepared as "powders" from the large scale preparations. The concentration of DNA is kept as high as possible (though below saturation) in order to keep the [Cu]:[DNA(P)] ratio (n) as close to that used for AFM studies (n= 0.05), but high enough to produce enough material for good signal acquisition in XRD (n= 150) and XPS (n= 10).

4.3.3.1. X-ray Diffraction (XRD) studies

X-ray powder diffraction was used to assess the chemical form and purity of nanomaterial obtained from these preparations by matching the reflections to a crystallographic database. This technique allows us to understand the chemical nature of the nanomaterial, determination of the crystallite size by Scherrers' analysis and possible signs of oxidation.

Figure 4.8 shows the XRD pattern for DNA-templated copper material precipitated from aqueous solution (black line). The reflections seen at 43.3°, 50.4°, 74.1°, 89.9° and 95.1° can be indexed to the (111), (200), (220), (311) and (222) crystallographic planes, respectively, of metallic copper (Cu^0). There is no evidence of oxidation of the copper as evident by the lack of signal at $2\theta = 36.4°(111)$, which is attributable to the most intense reflection of Cu_2O. Nor is there any evidence of higher oxidation species such as the more stable CuO phase ($2\theta = 35.5°(002)$). Even after 24 hours exposure to air, the sample remained free of signs of oxidation as indicated by the overlaid XRD pattern below (refer to figure 4.8, red line), which shows formation of pure elemental copper and no apparent oxidation species.

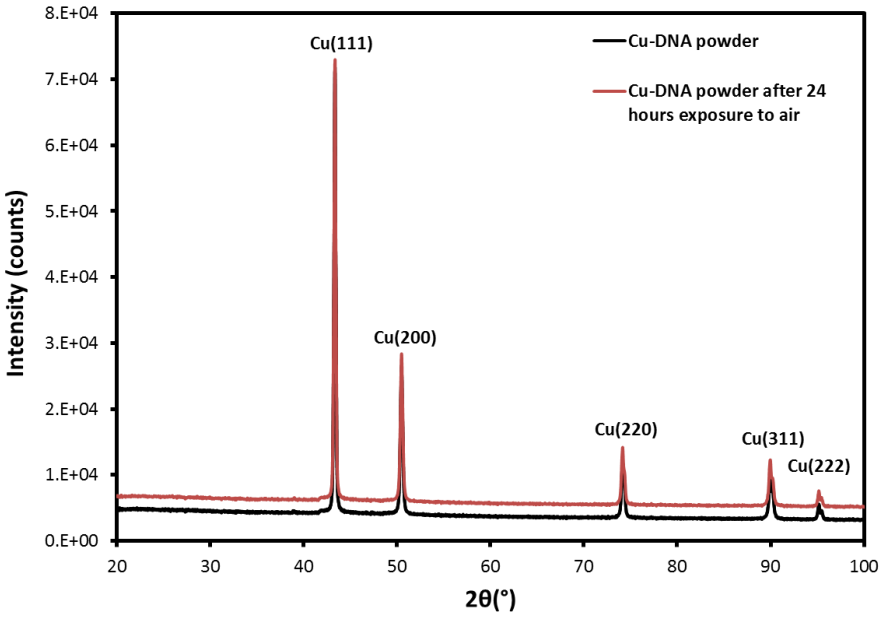

Figure 4.8: XRD pattern of Cu-DNA powder prepared in solution (black) and same sample after 24 hours exposure to air (red). The reflections are consistent with metallic copper

Using the Scherrer equation the average crystallite size (τ) was calculated to be ~35 nm, based on a pseudo-Voigt fit of the Cu(111) peak with FWHM 0.24°. This value is in accordance with the precipitated material being nanoscale. However, this value does not correlate with the heights of the Cu-DNA nanostructures obtained via AFM analysis, which are considerably lower (avg. ~7 nm) (see section 4.3.4.1). The crystallite sizes may be significantly increased as a result of using higher Cu^{2+}/ascorbic acid concentrations for XRD sample preparation.

As a control, a sample of copper was prepared in the absence of DNA to act as a template and the sample was analysed by powder-XRD. In this case it was found that the average crystallite size from the Cu(111) peak, to be ~42 nm (FWHM = 0.2°); slightly larger than that obtained when DNA is present. This result indicates that the DNA plays a role in affecting the growth of copper in solution.

The XRD results indicate that the "powder" material obtained from the large scale preparation is copper metal and shows no or little oxide formed, at least over short time periods. However, XRD cannot provide information on surface composition of the nanomaterial and this is where oxidation is most likely occurring. It is therefore important to make assessment of this using X-ray Photoelectron Spectroscopy (XPS). Therefore, XPS was employed as a tool to further investigate the chemical composition of the Cu-DNA nanomaterial.

4.3.3.2 X-ray Photoelectron Spectroscopy (XPS) studies

The higher surface sensitivity of the XPS technique (c.f. to XRD) will allow evaluation of the chemical state of the nanostructure surface. It is expected that these nanostructures consist of metallic copper, but as copper oxidises readily in air it is also expected that the surface contains oxide species.[40] The corrosion of copper has been well studied using XPS as an analytical tool.[41, 42] Table 4.2 below shows typical binding energies of the $Cu2p_{3/2}$ and O1s regions for various copper containing compounds.

	Binding Energy (eV)		
Compound	***Cu2p$_{3/2}$***	***O1s***	**Refs**
Cu	932.5-932.8		30
	932.6		42
	932.67		43
	932.4		44
	932.6		45
Cu_2O	932.5	530.5	42
	932.6	530.3 ± 0.1	45, 46
	932.67	530.8	43, 45
CuO	933.1		30
	933.7	529.5 ± 0.1	42, 46
	933.8	530.3	43, 45
	934.1		45
$Cu(OH)_2$	935.1	531.7	42
	934.75	531.1 ± 0.15	43, 46

Table 4. 2: Binding energies of $Cu2p_{3/2}$ and O1s XPS peaks for various copper containing compounds

Figure 4.9 shows Cu2p XPS data of the Cu-DNA sample prepared as discussed in the experimental (5.2.7). The asymmetry of the $Cu2p_{3/2}$ and $Cu2p_{1/2}$ spectral envelope suggest the presence of multiple components, which can be fitted to two separate doublets. The two doublets appear at binding energies expected for metallic copper (Cu^0)- peak 1, and cupric hydroxide $Cu(OH)_2$- peak 2. The Cu^0 line in the $Cu2p_{3/2}$ region is observed at binding energy 932.8 eV and is split by 19.8 eV, consistent with the literature.[30] The $Cu2p_{3/2}$ line at binding energy 934.9 eV (splitting = 19.9 eV) falls in the range expected for $Cu(OH)_2$.[43, 47] This is further supported by the origin of the satellite structure where two peaks arise within the region 938 - 947 eV. These are attributable to the presence of Cu^{2+} species in the sample.[48] These peaks are commonly referred to as the Cu^{2+} "shake up" satellite peak and arise due to a charge screening

effect of the unfilled 3d state, where the main copper doublets represent the screened state and the satellite peaks represent the un-screened state.[49] Integration of peaks 1 and 2 reveal the % composition of Cu^0 and $Cu(OH)_2$ to be in a 1:1 ratio, approximately.

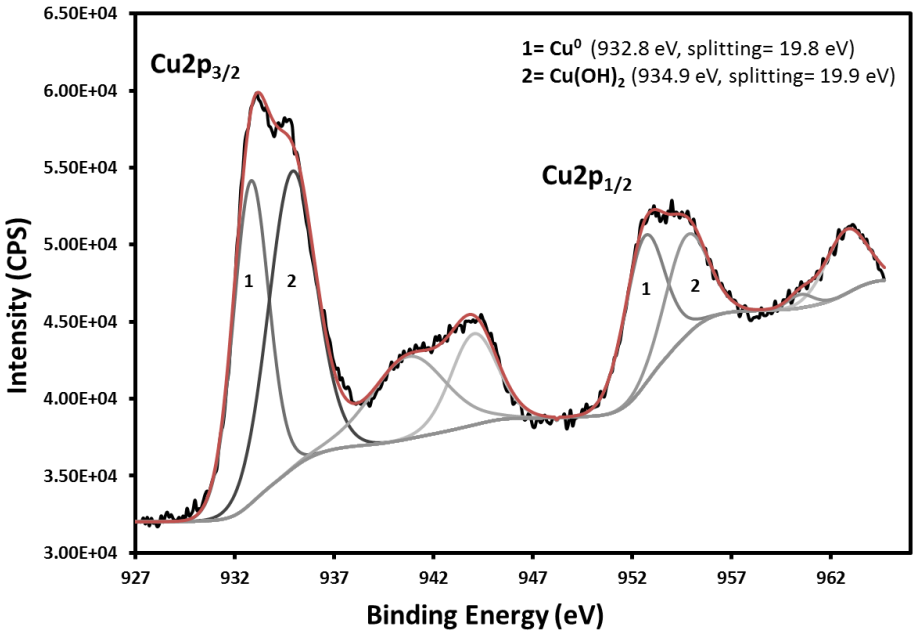

Figure 4.9: Cu2p ($p_{1/2}$ and $p_{3/2}$) XPS spectrum of Cu-DNA nanomaterial from large-scale preparation fitted to two individual chemical species. The black line shows the real data, the grey lines show the individual peak fits (treated as doublets) and the red line shows the sum fit

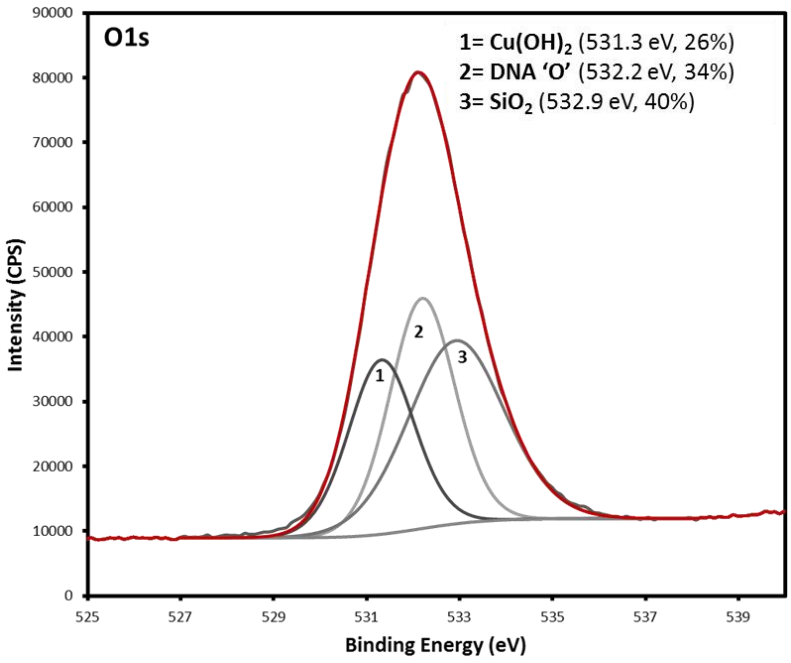

Figure 4.10: O1s XPS spectrum of Cu-DNA nanomaterial from large-scale preparation. The asymmetry of the singlet peak suggests the presence of multiple components

Figure 4.10 shows the O1s data for the sample which can be deconvoluted into three peaks. The peak at binding energy 531.3 eV in the spectrum corresponds to that of cupric hydroxide ($Cu(OH)_2$), which is of a typical value for this compound and supports the assignment of copper hydroxide based on the Cu2p data.[46, 47] The peak at 532.9 eV arises from the SiO_2 background.[50] The remaining peak resolved in the O1s spectrum at 532.2 eV is assigned as the oxygen in the phosphate group of the DNA backbone.[51] Considering that this peak shows higher intensity relative to copper hydroxide suggests that there is bare DNA present in the sample and/or the coating around individual DNA duplexes is quite thin. In order to understand this from a theoretical standpoint one may consider that the mean free path of the escaping electron is on the order of tens of *Angstroms* from the top of the sample surface, compared to the depth at which ionisation takes place (several *micrometres*).[52] Confirmation of DNA in the sample was judged from the presence of the P(2p) signal in the survey spectrum. A value at peak maxima of 134.4 eV was obtained.[51] The existence of the phosphorus signal is good evidence for DNA as this is the only source of phosphorus in the sample.

Since Cu^0 and $Cu(OH)_2$ were detected in the XPS spectra but only pure elemental Cu^0 was identified in the XRD pattern it gives reason to suggest that the $Cu(OH)_2$ species forms an overlayer around Cu^0.

The complementary data allows us to postulate about the compositional nature of the nanomaterial. Two possible structure models are proposed (figure 4.11): (i) nanostructures consist of a metallic copper core encapsulated by a copper hydroxide shell, as stated above, or (ii) nanostructures are less structurally ordered, consisting of a mixture of copper and copper hydroxide crystallites arranged randomly along the template. In both cases the DNA molecule remains as the inner thread running through the centre of the metal-containing sheath.

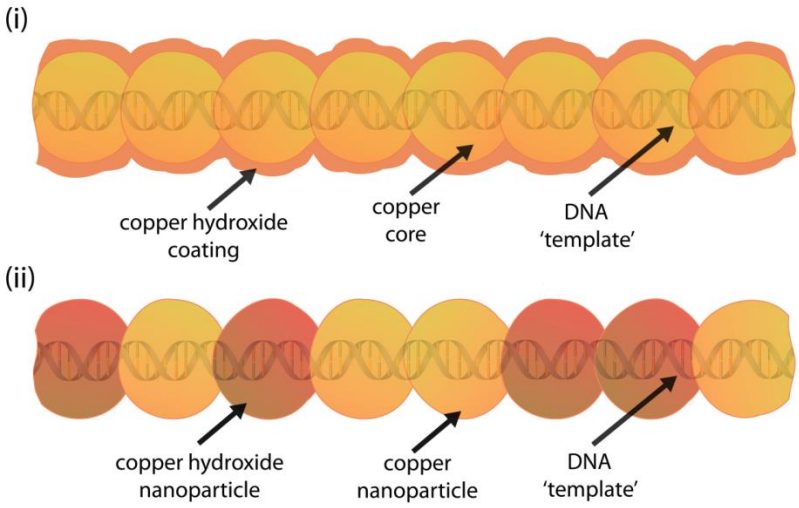

Figure 4.11: Scheme showing the two proposed structures of (i) copper hydroxide shell encasing tightly clustered metallic copper-DNA core and (ii) formation of random distribution of copper hydroxide and copper nanoclusters on DNA template

It is a reasonable assumption that explanation (ii) is more unlikely than (i) as this would require evidence for copper hydroxide in the XRD, which is not the case. In view of the fact that XPS provides the only evidence for $Cu(OH)_2$ formation it is suggested that the hydroxide resides on the surface, making scenario (i) most probable. This is the same conclusion drawn from the XPS data for Cu-DNA nanostructures prepared from the organosoluble route in chapter 3.

Atomic Force Microscopy (AFM) data for the Cu-DNA nanostructures is now presented to provide more structural evidence and to investigate the size and morphology of the prepared nanomaterial.

4.3.4. Structural characterisations by Atomic Force Microscopy (AFM)

4.3.4.1. Cu-DNA nanowires

It has been demonstrated in section 4.3.1 that high values of 'n' (>0.1) leads to undesirable structural morphologies. In order to avoid these effects, the ratio of Cu^{2+} to phosphate ('n') is kept relatively low, at ~0.05 resulting in thinly coated DNA nanostructures (~5 nm in height) as is desired. In this regime, copper metallisation of DNA appears to take place in a well-ordered fashion along the whole length of the structure. The following AFM images are of Cu-DNA structures prepared at this value of 'n.'

Figure 4.12 shows a typical Cu-DNA nanostructure formed at n=0.05, aligned on a TMS-modified silicon substrate by combing. The image illustrates the continuous nature of the wire which is evenly coated along the entire length of template. XPS and XRD studies have previously identified this coating to consist of metallic copper, with some residual copper hydroxide on the surface. Three separate height profiles were recorded along the length of the structure and the heights obtained (~5 nm) were similar (see inset in fig 4.12) indicating a smooth wire. The height is significantly larger than what would be expected for the dimensions of a single DNA duplex (<2 nm). A 3-D representation of the nanostructure is shown to the right in figure 4.12 which shows the continuity of coverage and smooth morphology more clearly. The homogenous morphology of the nanostructure is typical of what is observed in several other samples which were analysed by AFM. It is clear from the image that there appear to be no gaps in the copper coating that could potentially hinder the flow of electrical current. Furthermore the AFM data does not appear to show boundaries between individual particles along the DNA template; indicating formation of a densely packed succession of nanoparticles or a single-crystalline entity.

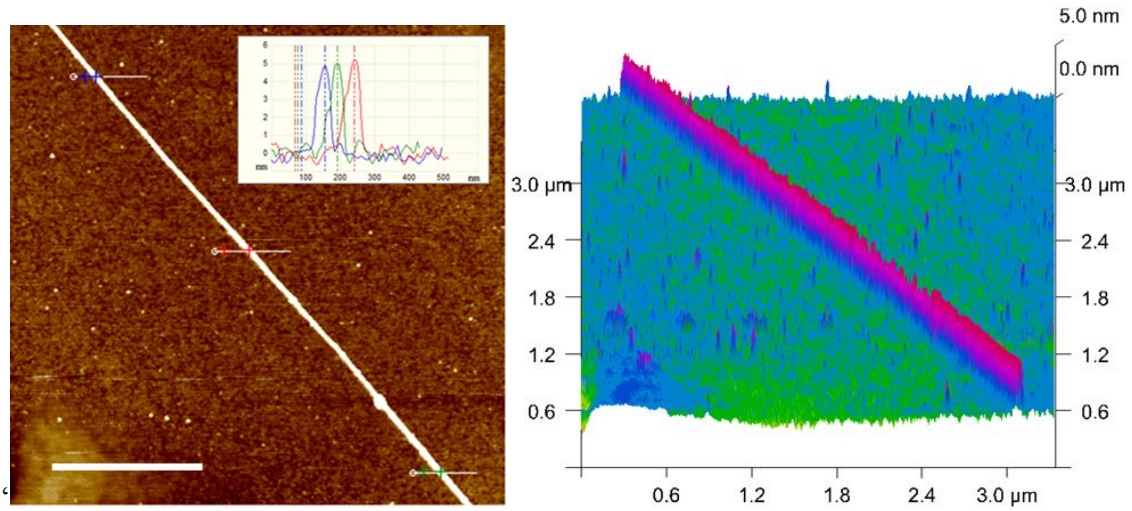

Figure 4.12: (left) AFM height image of a single Cu-DNA nanostructure prepared at n= 0.05, aligned on a clean TMS-modified silicon substrate and (right) 3-D image of the same structure. Inset shows the height profiles of 3 intersections of the structure. The consistent height values indicate the smoothness of the nanostructure. Scale bar= 1000 nm, height scale= 10 nm

Figure 4.13 shows further AFM height images of Cu-DNA nanowires aligned on TMS-modified silicon substrates prepared at n= 0.05. Four identical syntheses were carried out and the material was combed onto four separate TMS-modified silicon wafers for analysis. The images are obtained in order to illustrate the reproducibility of this method across the four samples. The resulting nanostructures are highly continuous in coverage and display smooth morphologies. In each image a-d, there was no observation of 'beads-on-a-string' structure morphology as has often been observed in the past for metal coated DNA nanostructures. Additionally at this concentration ratio (n= 0.05), DNA is rarely exposed.

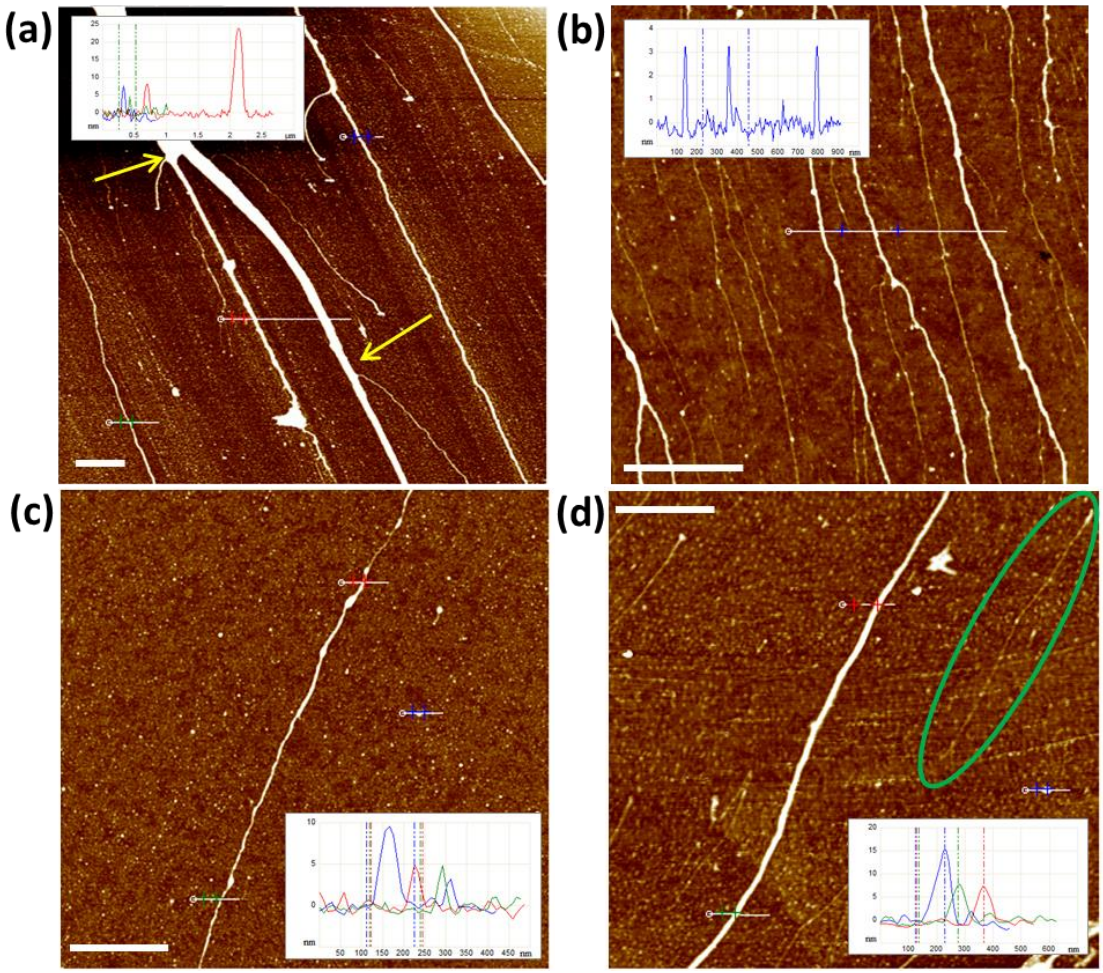

Figure 4.13: Four AFM height images a-d of Cu-DNA nanostructures prepared at n=0.05 obtained from 4 separate identically prepared samples. The similarity in structure morphology and generally particulate free background across these images illustrate the reproducibility of the method. Insets show the various height profiles relating to the cross sections in the image (colour coded). Yellow arrows in image (a) point to DNA branching points. Green circle in image (d) identifies a bare DNA strand. Scale bars (a), (c), (d)= 1000 nm and (b)= 500 nm, height scales= (a), (c), (d)= 10 nm and (b)= 6 nm

The heights of the Cu-DNA nanostructures in figure 4.13a are ~6-7 nm as indicated by the red and blue step profiles (inset). Occasionally smaller sub-3 nm high nanostructures are obtained (see green profile, fig 4.13a), which are approaching typical measured heights for bare DNA. For comparison figure 4.13d shows both a well-formed smooth Cu-DNA nanowire of typical height (~ 6nm) next to a much smaller strand of essentially a single molecule of bare DNA (circled in green).

Less commonly observed were nanostructures of a disproportionately large height, >20 nm (see red profile in figure 4.13a). Such structures are expected to be a result of DNA bundling in solution, which has been described in the past to explain the formation of so-called "nanoropes," [53] rather than a consequence of excessive copper metallisation on

a single molecule of DNA. Furthermore, evidence of DNA bundling is shown in figure 4.13a where branching locations of the DNA nanostructure can be seen (marked by yellow arrows).

Parallel alignment of single nanowires on the surface, as opposed to nanowire aggregates or 'networks,' can be encouraged by tailoring the surface properties of the substrate surface. This is achieved by increasing the hydrophobicity of silicon which reduces the adherence of DNA molecules to the surface and thus the density of attached material. This enables isolated strands to be aligned as seen in the AFM images. Figure 4.13b is an example of where these Cu-DNA nanowires are aligned very neatly on the substrate surface, resulting from the combing action used for depositing the wires. The heights of the wires in this example are consistent to one another, falling in the range 3-4 nm, as indicated by the step profiles.

Also, in each of these images the substrate backgrounds are largely free of contamination which may result from deposition of non-templated material. One of the key requirements for integration of copper nanostructures into an integrated transistor layout is a clean substrate background, free from impurities. Earlier surface-based methods for metal-DNA nanowire synthesis have generally led to relatively high levels of non-specific deposition on the substrate surface.[2, 3, 54] However it seems the solution based method can circumvent such issues by introduction of a centrifugation step to discard of impurities from the solution, such as non-templated material. These samples display remarkably clean backgrounds, which will be beneficial for future device fabrication within integrated technology.[55]

4.3.4.2. Statistical analysis

A detailed statistical analysis of the Cu-DNA structure heights was carried out over the four previously discussed samples to give a more thorough insight into the size distribution of Cu-DNA nanostructures in the sample. For each observed wire three separate height measurements were recorded and an average height taken. This process was repeated on 100 individual Cu-DNA nanowires split over the four samples and the data was compiled into a histogram (figure 4.14). The numbers on the x-axis represent the maximum structure height value for a given discrete interval. For instance, the bar at '2 nm' denotes the number of structures measured whereby the height falls in the range 0-2 nm and the bar at 4 nm contains the range between 2 and 4nm, and so on.

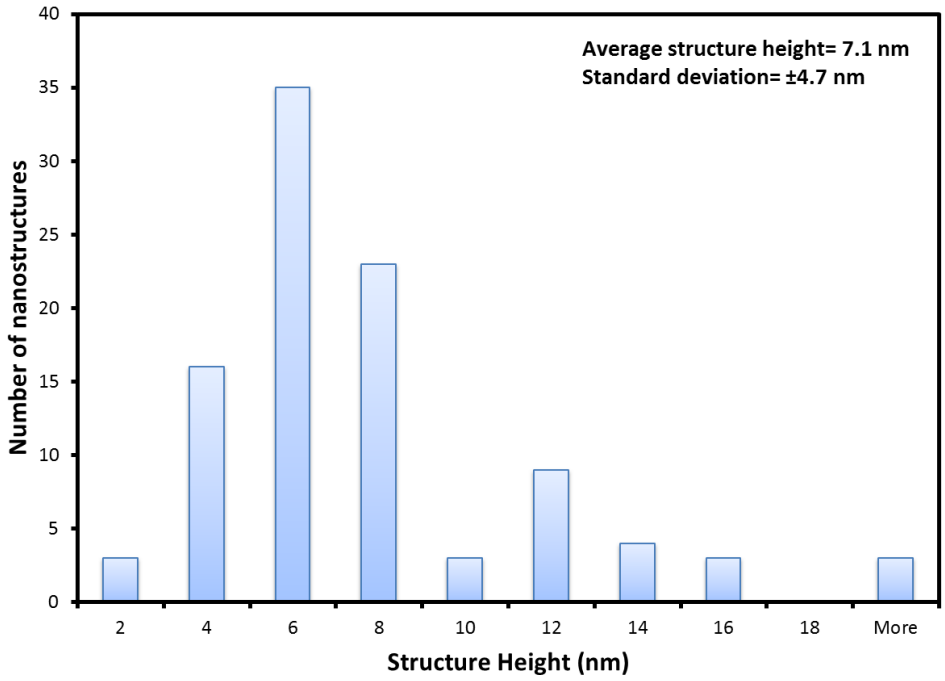

Figure 4.14: Histogram showing height distribution of 100 metallised DNA strands (average of 3 measurements per strand) after treatment with $Cu(NO_3)_2.3H_2O$ and ascorbic acid. Data collected over 4 identically prepared samples

The chart displays the distribution of the nanostructure heights, which gives a monomodal distribution. A positive skewness in the data is also reflected where the peak modal range falls between 4-6 nm. A series of less frequent observations fall within the intervals at the tail end of the chart up to 14-16 nm. The mean structure height was calculated as 7.1 nm with a standard deviation (σ) of 4.7 nm. This value confirms the successful templating on DNA (i.e. significantly > 2nm in height). These height values also proffer a size small enough for significant downscaling in interconnect dimensions for future consideration.

4.3.4.3. Insights into the growth mechanism

In a few images some strands were observed which had a variety of different structured regions. Inspection of these gave some indication of the possible mechanism of growth of copper along the template. Further AFM analyses of these Cu-DNA nanostructures were carried out.

Figure 4.15 shows an AFM height image containing two individual Cu-DNA nanostructures aligned in parallel. The nanostructure on the left is smooth and uniform compared to the nanostructure to the right where the extent of metallisation, as indicated

by height, varies quite considerably. While much of the length of the structure is quite regular, the indicated region shows individual nanoparticles to be tightly packed along the template axis with regions of low structure height in between the particles. A smaller scan size image of this non-uniform metallised region of DNA is also shown. One could interpret this observation as an intermediate growth phase of copper on DNA. Two cross sections are measured across the nanostructure to the right (blue and green markers) in order to record the heights at these positions for comparison. The height at the green cross section is ~6 nm whereas the height at the blue cross section is ~3 nm which indicates a lower degree of metallisation at this region. This result provides further evidence that copper growth is occurring on DNA and that the increased heights associated with these nanostructures compared to bare DNA (~1 nm) are not an artefact of DNA bundling which could conceivably lead to formation of larger strands.

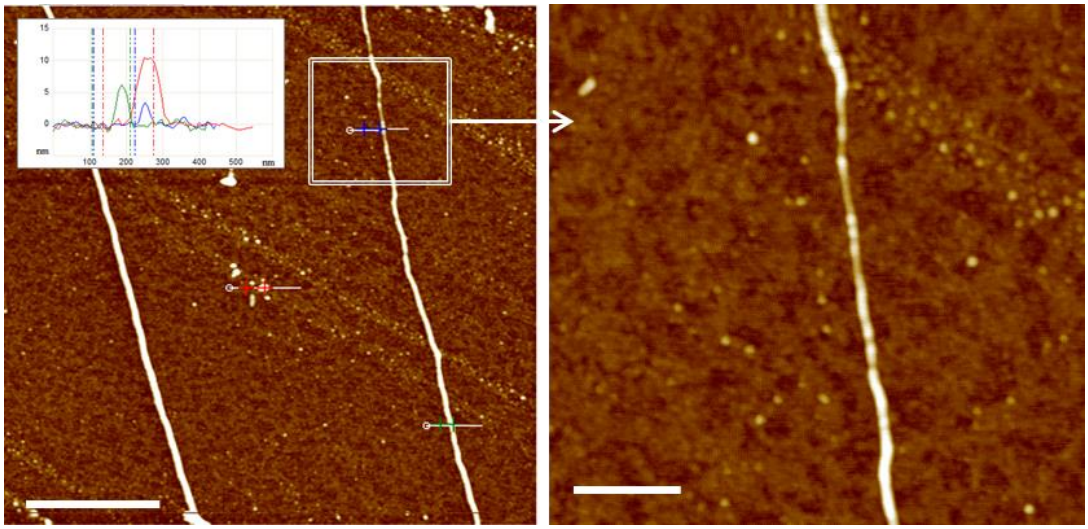

Figure 4.15: AFM height images of (left) two well aligned Cu-DNA nanostructures prepared at n=0.05 and (right) a magnified area of the nanostructure to the right (shown by white box) to show the formation of individual nanoparticles along the template. The nanostructure to the right shows different morphology than the one to the left, which appears very smooth. Inset shows height profiles (colour coded). Scale bars (left)= 1000nm and (right)= 300 nm. Height scales= 10 nm

Figure 4.16 shows another example of where nanostructures are observed to be at seemingly various stages of metal growth along DNA. In this example multiple Cu-DNA nanostructures are aligned on the surface, within the same scan area. These display large differences in their structural morphologies indicating these structures to be at varying stages of metal growth, despite being prepared in the same reaction and deposited onto the surface simultaneously (see AFM image, figure 4.16).

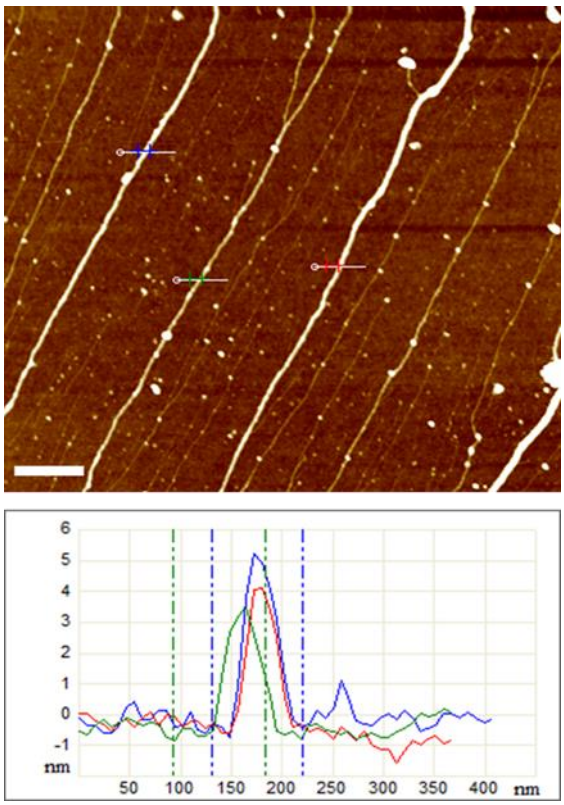

Figure 4.16: AFM height image of several Cu-DNA nanostructures at varying stages of metal growth along the template. Some strands can be seen to show thicker metal coverage than others, indicating that those are metallised to a higher extent. The colour coded height profiles show the difference in heights for three separate strands; ~3 nm (green profile), ~4 nm (red) and ~5 nm (blue). Height scale= 10 nm. Scale bar= 500 nm

Figure 4.17a shows three identical AFM height images of the one shown above (figure 4.16). In each respective image a line section is recorded along the entire length of one of nanostructure 1, 2 and 3 (from left to right), as indicated by the green line in the AFM image. The height profiles shown underneath (figure 4.17b) illustrate the variation in structural morphologies of the respective nanostructures. Structure 1 shows a strand of DNA with low levels of metallisation (~2 nm high) and a seemingly random distribution of bound particles along the template, as illustrated by the sharp peaks in the height profile (4- 6 nm), thus resembling a dilute 'beads-on-a-string' motif, as has been described in the past for metal nanowires.[8, 56] Structure 2 shows a more heavily metallised strand of DNA where the average height of the structure is ~4 nm, and a more continuous structure with less frequent attachment of particles. The height profile of structure 3 indicates an altogether smoother morphology where individual particles are not obvious in the image and the height of the structure has increased again to ~4-7 nm. In almost all cases the observed structural morphology of the isolated material fall

into the latter category (structure 3), demonstrating the suitability of this method for forming copper nanowires.

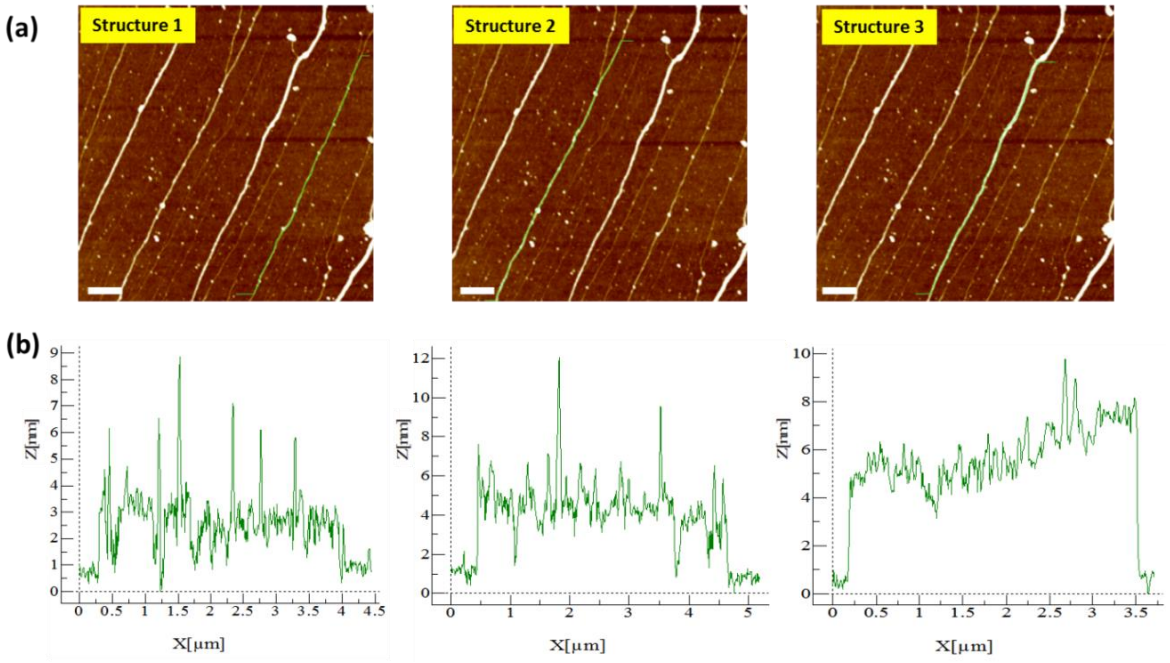

Figure 4.17: (a) AFM height images of Cu-DNA nanostructures aligned on silicon by combing; including a line trace along the length of three separate structures 1, 2 and 3 (green lines) for structure height analysis and (b) height profiles of each structure shown above corresponding to the line trace in the image. The differences in structure morphologies between structure 1 (granular) and structure 3 (smooth) gives an insight into the growth mechanism. Scale bars= 500 nm, height scales= 10 nm

Taking these results into account, it is suggested that the growth of copper on DNA occurs in a competitive manner to form the 'beads-on-a-string' morphology or smooth wires. The thermodynamics of templating material on DNA can be defined by two competing energy terms; (i) the line energy, which represents the adhesion of material to the template and (ii) the surface tension of copper.[57] The line energy (negative) is responsible for the adhesion of nuclei along the length of the template, whereas the surface tension of the material (positive) is what drives individual particle formation. The resulting morphology between 'beads-on-a-string' or smooth wire formation is determined by the reaction stoichiometry. If the volume of copper remains under a certain limit with respect to the length of template then smooth wire formation is favoured. Use of high concentration metal precursors has previously led to the formation of 'beads-on-a-string' type assemblies when the reaction is performed on surface immobilised DNA.[2, 4, 56] A possible explanation for this behaviour may relate to the increased surface tension of the copper surface as a result of the high copper loading

on DNA and the favoured formation of individual nanoparticles along the axis of the template (giving the so-called 'beads-on-a-string' motif).

This process is similar in effect to the Ostwalds' ripening of colloids, which has been used as a model in the past to describe the formation of CdS nanowires in solution.[7] It may also be suggested, that, for the formation of smooth nanowires, it is important if not critical that the reaction is performed in DNA solution rather than on surface-immobilised DNA. It has also been demonstrated in polymer DNA-based nanowires that the polymerisation process is inhibited on surface DNA, whereas in solution they form highly continuous nanowires.[8]

4.3.5. Electrical characterisation of Cu-DNA nanostructures

The electrical characteristics of the DNA-templated copper nanostructures were surveyed using several techniques in order to establish if they were genuine nanowires, i.e. electrically conducting. The first technique employed was EFM, a non-contact method of conductance imaging that is a rapid and convenient means to gauge the 'wire-like' properties.

4.3.5.1. Electrostatic Force Microscopy (EFM)

Figure 4.18 shows the AFM height image (left) of Cu-DNA nanomaterial combed on to a TMS-modified Si/SiO_2 (200 nm) substrate; the height profile is shown beneath. The tip oscillation phase images at -10V (middle) and +10V (right) bias are also shown. The phase profiles are shown underneath the respective images, relating to the cross section over the left most 1-D strand in the image.

As was observed from previous AFM images, the height of the measured 1-D nanostructure was ~5 nm (shown by the red, blue and green cross sections intersecting the nanostructure). By comparison, the central strand was ~2 nm and the strand to the right was ~3 nm in height. The material observed at the edges of the image is a consequence of non-DNA-templated material (nanoparticles) and was not removed during the purification step. The blue cross section across the nanowire is taken as the point of measurement for phase shift analysis.

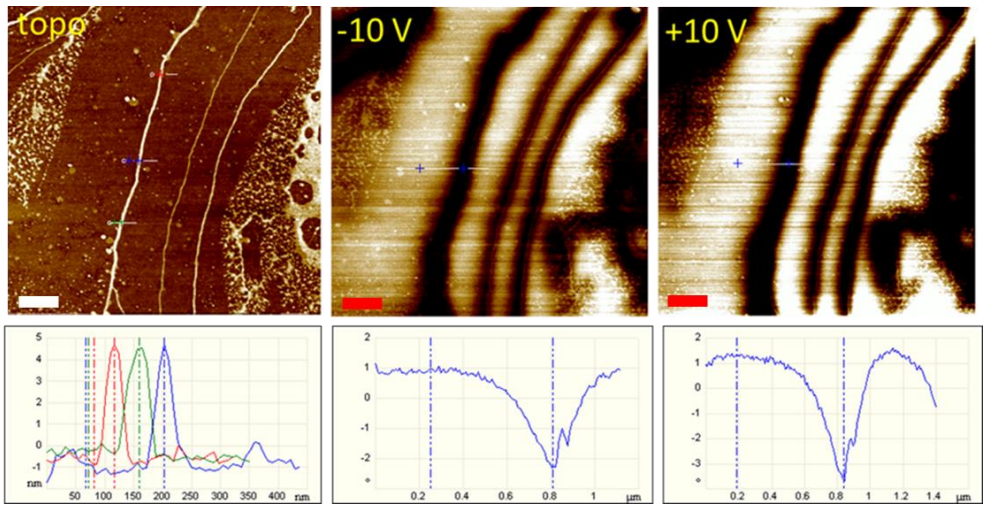

Figure 4.18: (top, left) AFM height image of 3aligned Cu-DNA nanowires, (top, middle) EFM phase image at -10V bias, (top, right) EFM phase image at +10V bias. Height and phase profiles corresponding to each image are shown below. Each nanowire displays negative phase shifts along the entire length of the structure. EFM data collected for analysis from left most wire in the image, at the intersection colour coded in blue. Data scales= 10 nm (left) and 3.0° (middle, right). Scale bars= 500 nm

The phase images (middle and right in figure 4.18) show negative phase shifts (Δθ) (black contrast), at both positive and negative potentials, associated along the length of the Cu-DNA nanostructures with respect to the surface background, which is positive (white). Negative phase shifts were observed at biases ranging from -10 to +10 V which become more intense at higher potentials. This indicates that a viable conductive pathway exists along the entire length of these nanostructures. However, the magnitude of the conductance cannot be determined from this type of experiment. A plot of tan(Δθ) versus 'V' (figure 4.19) gives the characteristic negative parabolic curve, as predicted from EFM theory, for conductive 1-D nanostructures.[58, 59]

Also observed are negative phase shifts (Δθ) in the two smaller Cu-DNA nanowires to the right of the one measured, despite the reduced thickness (2-3 nm in height). This demonstrates the sensitivity of the EFM technique but also illustrates that even DNA-templated copper structures with much lower levels of metallisation can still provide conduction pathways over several microns. The non-templated nanomaterial on the other hand shows positive phase shifts (Δθ), which indicates they are insulating.

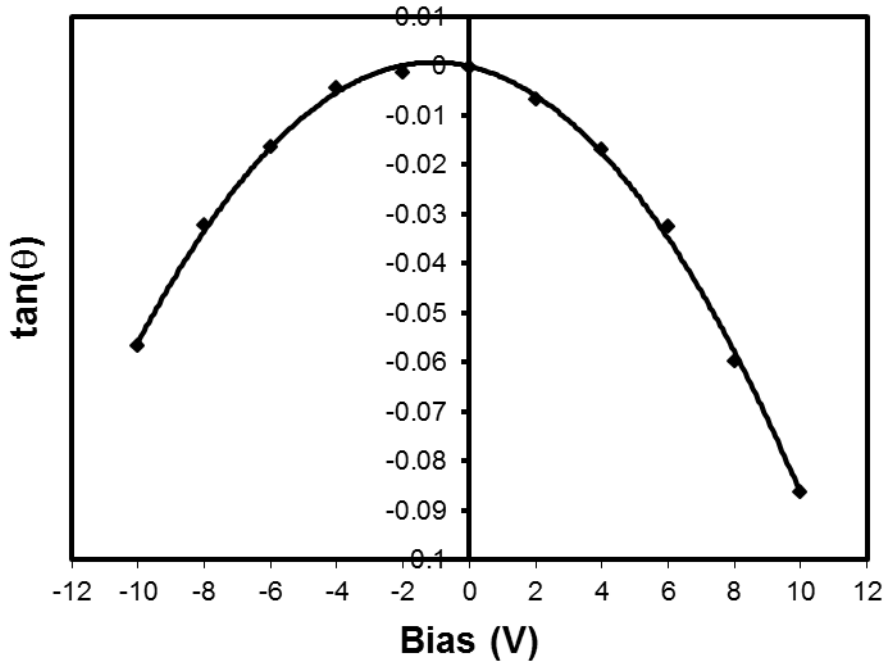

Figure 4.19: EFM phase shift data showing plot of tan(Δθ) in radians against bias (V). The trend shows negative parabolic dependence (as indicated by the second order polynomial line of best fit, solid line)

Negative phase shift (Δθ) behaviour is a good indication that the electrons are mobile along the length of the Cu-DNA nanowire and are not confined to regions directly beneath the tip which would be the case for a polarisable insulator, where a positive shift (Δθ) would be expected. However it is not feasible to quantitatively determine the conductivity from this technique and it is therefore necessary to use alternative methods, such as conductive-AFM.

4.3.5.2. Determination of conductivity using Conductive-AFM (C-AFM)

C-AFM was employed as an additional electrical characterisation technique in order to establish a more comprehensive understanding of the electrical properties of the nanowires. C-AFM is a 2-point contact technique which can be used to acquire surface topography using AFM as well as simultaneously measuring the current along the wire. The technique can also provide direct 'point and shoot' analysis to record current-voltage (i-V) curves at any point along the nanowire/surface allowing the collection of distance-dependent i-V curves. The 'point and shoot' function is enabled by the system's closed loop positioning mechanism. In a C-AFM experiment, images are obtained in contact mode.

Figure 4.20 illustrates the C-AFM set-up specifically developed in our laboratory for this type of analysis. Details of the experimental method are provided in the experimental section 4.2.9. Figure 4.20a is a photograph obtained via the AFM microscope showing the Ga/In eutectic paste contacting the macrodeposit of nanomaterial and the AFM tip positioned directly over the edge of the material that has receded during the drying process. Figure 4.20b is a zoomed in image of this particular area showing the protrusion of very thick nanowires from the edge of the macrodeposit, from which, smaller nanowires can be located using contact AFM as shown in figure 4.20c. Figure 4.20d is a current map of the previous image at an applied bias of 5V. The inset shows the current line trace for a single intersection (blue cross section) across the nanowire of interest (denoted by the black arrows).

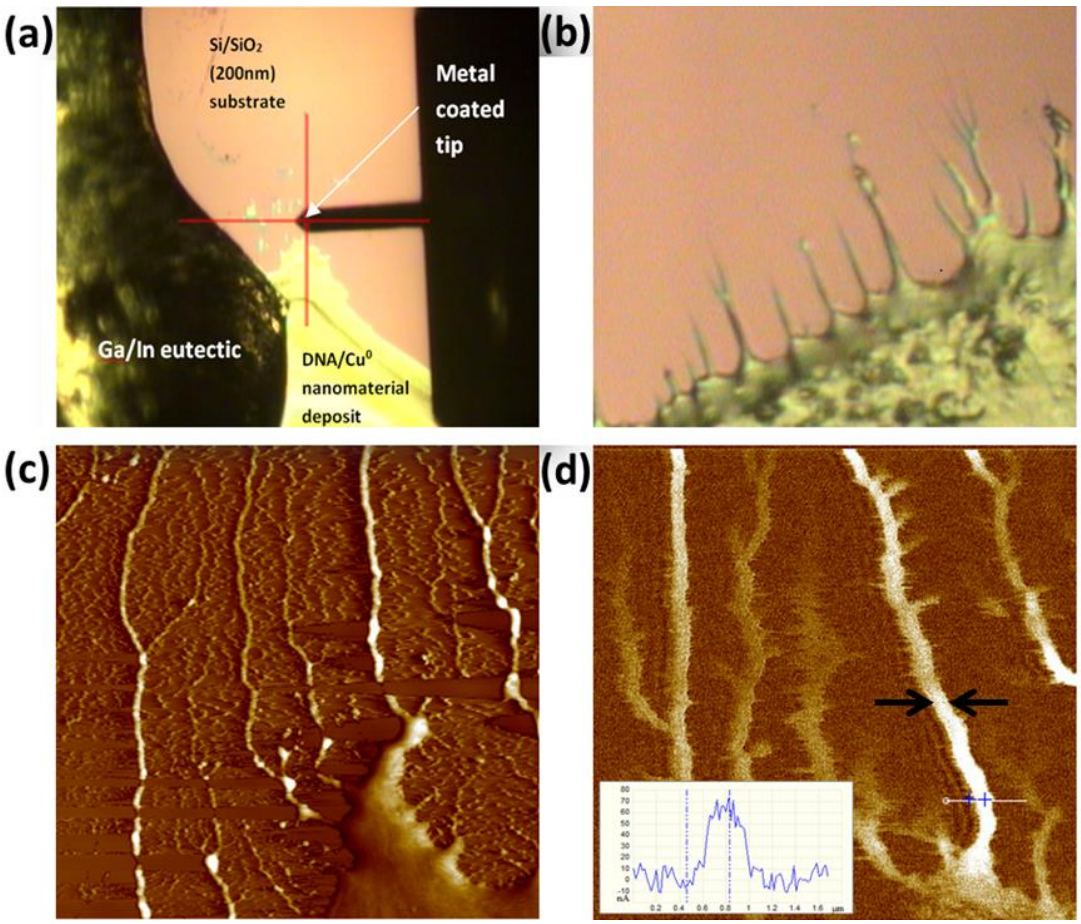

Figure 4.20: Images demonstrate the C-AFM set-up for measuring conductance in our Cu-DNA nanowires deposited on a Si/SiO_2 substrate; (a) photograph of area of analysis showing eutectic paste contacting the macrodeposit and cantilever positioned over the edge of the receded solution, (b) magnified image of the same area showing extension of wire-like material from the macrodeposit, (c) C-AFM deflection error image of several Cu-DNA nanowires protruding from the edge of the droplet and (d) C-AFM current map of the nanowires showing current in the region of tens of nanoamps (as shown by current profile, inset). Black arrows indicate the nanowire that was analysed and cross section (white line with blue markers) indicate the point of current measurements

As shown in figure 4.20d, current signals can pass along the nanowire, as indicated by the white contrast with respect to dark background. Current was measured by taking a step profile over a single point across the nanowire (see blue line trace (inset) in figure 4.20d). Current of the order of tens of nAs were detected at applied biases ranging between 1–10 V. These values are substantially lower than would be required for use as copper-based interconnect. They do however represent the first example of measured conductance in DNA-templated copper nanostructures.

Figure 4.21 is a current-voltage (i-V) plot obtained by varying the voltage between 0 and 10V (2V increments) and measuring the current at each stage at the same point on the wire. This plot displays a near ideal linear trend as expected for a conductor as indicated by the straight line of best fit (solid line).

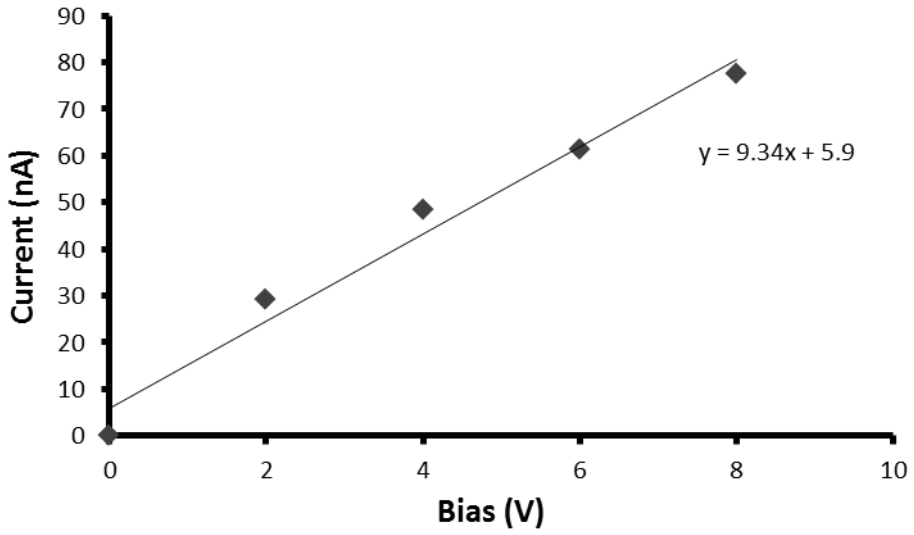

Figure 4.21: i-V plot of a Cu-DNA nanowire. Current measurements were obtained by measuring the current over a single intersection of the wire at different biases. The linear plot indicates ohmic behaviour

Direct measurement of the i-V nanowire properties was achieved by increasing the vertical contact force of the tip, which results in mechanical contact with the AFM tip and nanowire surface, and then recording the current over a range of voltages (-3 to +3V). Figure 4.22 shows an i-V plot obtained after pressing the tip onto the nanowire. The graph, again, displays linear current-voltage dependence, which is indicative of conductive behaviour. However, the sign of the current is dependent on the scan direction which suggests an additional contribution to the circuit resistance from capacitive effects (e.g. stray capacitance). The scatter in the data is due to external 'noise' which is not filtered out by the systems vibrational isolation system. In addition, the data points do not intersect the origin as expected for an ideal conductor. The non-zero intercept is significant due to the small standard of error on the intercept (70.0 ± 0.4). This may be explained by stray capacitance in the circuit, as mentioned.

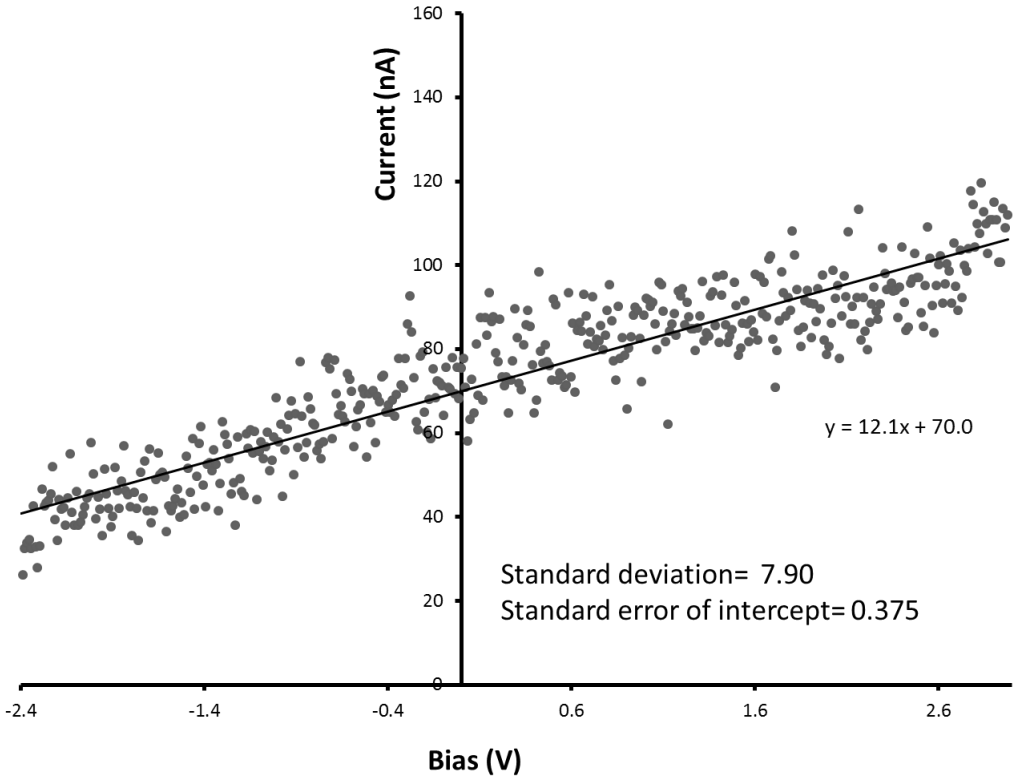

Figure 4.22: C-AFM i-V Plot of a Cu-nanowire prepared in a solution of DNA. A bias was applied to the wire ranging from -3 to +3V and the current monitored as a function of bias. The length of the connection comprised by the wire, in this example, was ~560 nm

For this experiment it is important to consider all of the various resistances which are inherent to the circuit, as each resistance will contribute to the overall current levels detected. Treating the set-up as a simple series circuit there are three contributions to the overall resistance which include, R_{tip}, R_{ext} and R_{wire}(d) where R_{tip} is the tip to wire contact resistance, R_{ext} is the resistance of the wire to the external circuit and R_{wire}(d) is the resistance of the wire between the tip contact point and the end of the wire ('d' represents the relative distance along the nanowire). R_{ext} cannot be adequately determined as this may vary significantly depending on the quantity of bulk material and the distance between the macrodeposit and the AFM chuck (typically ~1 mm). Clearly, however, R_{wire} is the resistance one needs to measure in order to determine nanowire conductivity.

The Cu-DNA nanowire resistivity can be estimated using an alternative approach known as the 'transmission line method.' In this method, the wire resistance is calculated by recording a series of i-V sweeps as a function of distance along the wire.[60] This method allows wire resistance to be extracted from other contributions to the circuit resistance (such as contact resistance, R_{tip}). For this experiment, a suitable wire

was located protruding from the macro deposit using standard contact mode AFM (as shown earlier in figures 4.20c and 4.20d). The average height of the wire was measured as ~15 nm as determined from the mean of 15 different height measurements along the structure length. Current signals were detected along the whole length of the nanowire (as shown in figure 5.19d). i-V curves over the range -3V to +3V were collected at 9 points periodically along a 4.5 μm length of the nanowire (~560 nm spacing). Electrical resistivity (ρ) can be calculated from this simple equation:

$$\rho = R(A/L) \qquad \textbf{(equation 4.1)}$$

'R' is resistance, 'A' is cross-sectional area of wire and 'L' is the wire length. Conductivity (σ) is obtained from the inverse of the above equation.

Figure 4.23 shows the graph of resistance against relative distance along the nanowire. The effect of distance against resistance was monitored by recording several i-V plots (an example of which is shown in figure 4.23) as stated in the previous paragraph. The resistance around zero bias for each of these measurements was calculated from the inverse gradient of the i-V graph and then plotted against the relative distance (relative tip position to the point of wire protrusion from the macrodeposit). The gradient of the resulting graph gives units of resistance per unit length ($\Omega.cm^{-1}$). The resistivity is determined from this gradient (without needing to know R_{tip} and R_{ext}) by multiplying through the cross-sectional area of the nanowire, which was calculated as 1.77×10^{-12} cm^2 based on the assumption that the nanowire adopts an ideal cylindrical shape with a measured height of 15 nm. Finally, the resistivity was calculated to be 1.06 Ω.cm, or in terms of conductivity, 0.94 Scm^{-1}. While this number comprises the lower boundary estimate to the conductivity, it is still many orders of magnitude lower than bulk copper (5.96×10^5 Scm^{-1}).

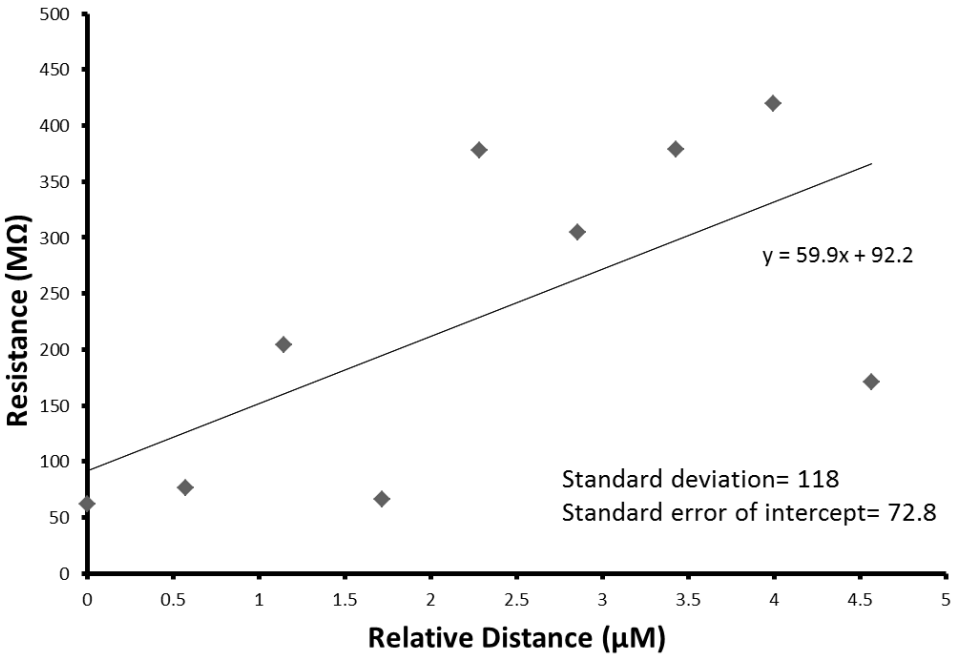

Figure 4.23: Graph showing distance dependence for resistance in a single Cu-DNA nanowire. Resistance values were obtained from single i-V plots over various points along the wire. Solid line shows a linear line of best fit

The graph in figure 4.23 displays a linear trend but not ideal as expected for a metallic conductor. An ideal linear trend is expected only if the resistance of the wire (R_{wire}) is the dominant factor in the experiment. If the dominant contribution to the overall resistance is due to contact resistance, then the trend may become more sporadic. Indeed, the line of best fit (solid line) displays a significant non-zero intercept (92 MΩ ± 73). The standard error is large but is insufficient to account for all of the resistance. The remaining contribution is due to the contact resistance (~20-150 MΩ). This makes it difficult to accurately determine the nanowire conductivity.

Modified C-AFM set-up

In an attempt to make a more conclusive estimate of Cu-DNA conductivity we modified the C-AFM set-up by using a thin gold layer deposited onto Si/SiO_2 as the macro electrode, instead of a dense nanomaterial deposit used previously. This was prepared using a cantilever chip as a mask and evaporation of gold over the sample; resulting in a portion of the substrate surface untouched by gold (fabrication of this type of device is discussed in chapter 3, section 3.2.8). The metal AFM tip was used as the secondary mobile electrode as usual. Cu-DNA nanowires are then combed across the gold edge(s)

resulting in physical contact between the gold edge and the wire, stretched out onto the bare silicon oxide surface. In this manner the length (L) of the nanowire can be precisely measured using SPM software analysis, negating the need to perform several i-V measurements along the nanowire.

Figure 4.24a shows a deflection error AFM image obtained in contact mode of several Cu-DNA nanowires overhanging from the straight gold edge. Figure 4.24b is the current image of these nanowires contacted to the gold. However, when attempting to perform measurements, the current signal is lost midway during the scan due to the extreme force exerted on the sample at the gold-nanowire interface, as indicated by the 'noise' in the image. This results in the nanowires being cleaved from the surface and no current flows.

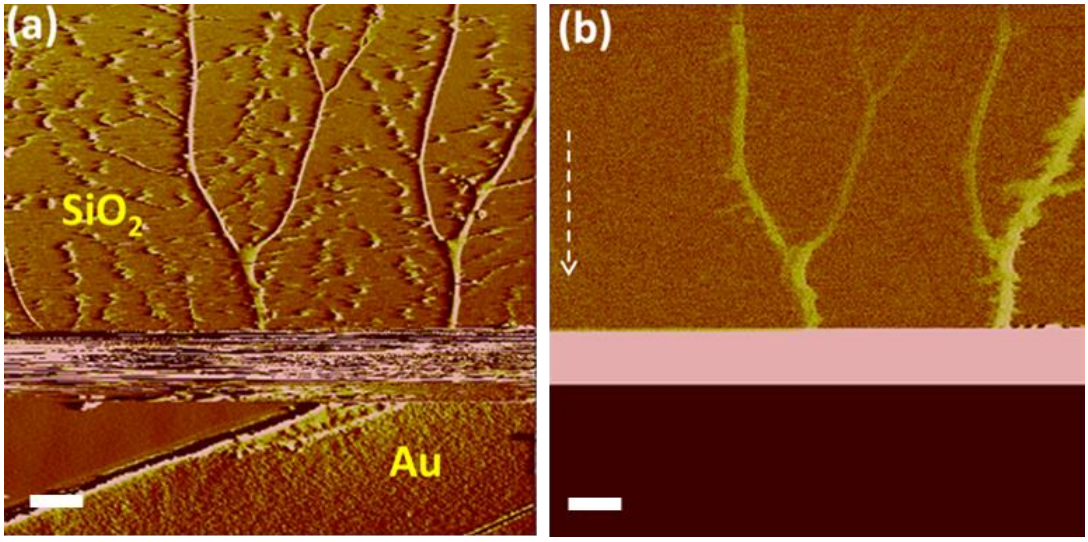

Figure 4.24: (a) C-AFM deflection error image of Cu-DNA nanowires connected to a layer of gold deposited on to Si/SiO_2 wafer and (b) C-AFM current map of the same image showing the ability of the nanowires to carry current until the signal is lost due to a broken connection. Dotted white line shows the slow axis scan direction. Scale bars= 1 µm, data scales= 5 nm (a) and 100 nA (b)

In contact mode, the AFM tip exerts substantial force on the nanowires which can cause mass movement of the material on the substrate surface. In some instances, when the set point is exceptionally low, the nanostructures can be damaged or even cut by the force experienced from the tip. An example of this behaviour is shown in figure 4.25 where the nanowire is cut and displaced from its original position. The yellow arrows in the deflection error image (a) denote the points of nanowire cleavage. In the corresponding current image (b) the current signal (white contrast with respect to background) along the nanowire is lost between these two broken points. It is likely that both points were

cleaved simultaneously, dislodging a portion of the wire. Thus the current can no longer traverse this part of the wire until the tip reaches the next in-tact portion of the wire connected to the circuit via the macrodeposit (point 2). One of the challenges in operating C-AFM is to optimise the parameters to produce suitable current levels whilst maintaining good image quality. The technique becomes increasingly challenging when dealing with small nanostructures as these can become more displaced or damaged, as is the situation with the Cu-DNA nanowires produced by this method.

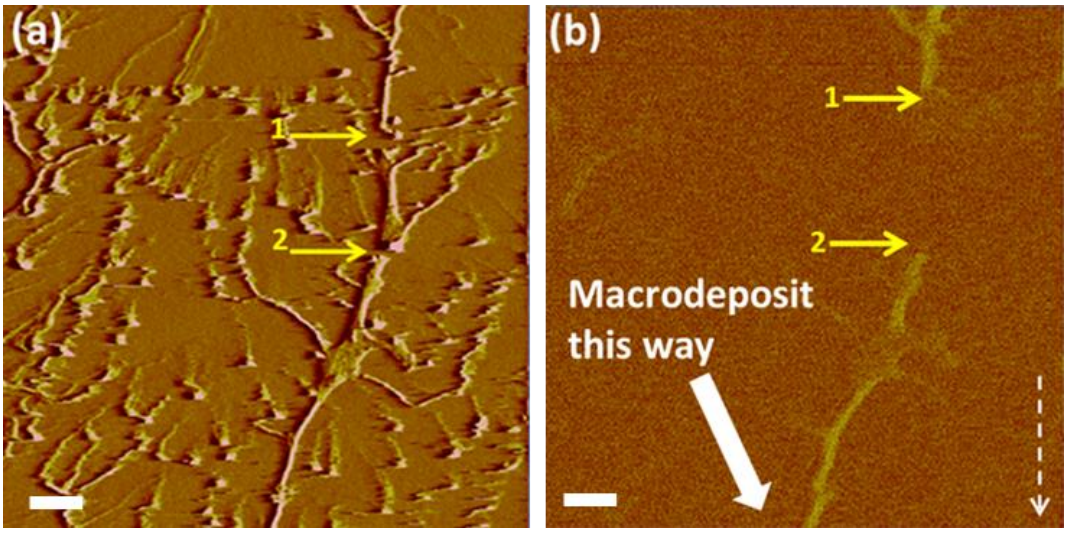

Figure 4.25: (a) C-AFM deflection error image of a single Cu-DNA nanowire after being cut by the tip in two locations (shown by yellow arrows) and (b) C-AFM current map of same image showing loss of current within these two regions. Dotted white line denotes slow axis scan direction. Scale bars= 1 µm, data scales= 5 nm (a) and 100 nA (b)

4.3.5.3. Determination of conductivity by fabrication of a 2-terminal nanowire device

Now, an alternative two-terminal technique is utilised, in order to overcome the limitations of C-AFM, using a variable-temperature semiconductor device analyser and probe station.

In this set of experiments the i-V properties of a single Cu-DNA nanowire were measured, aligned between two gold 'fingers.' The fingers are connected to gold macro electrodes which can be probed using two tungsten tips. The electrodes are fabricated so as to lie flush with the surface to facilitate the subsequent alignment of wires across the inter-electrode gap, as well as minimising contact resistance with the nanowire-gold interface. A single Cu-DNA nanowire was aligned between the electrodes and was located using "TappingMode^{TM}" AFM. Full details of the device fabrication can be found in the experimental section (4.2.10).

Figure 4.26a shows an AFM height image of a Cu-DNA nanowire bridging the electrode gap. It is ~13-18 nm in height (see line sections, inset) and spans the gap of ~3 μM (the nanowire is slightly longer in length due to its curvature). An EFM phase image was recorded of the device (figure 4.26b) and shows a continuous negative phase contrast extending from the gold finger along the wire to the second gold finger; thus indicating a continuous conduction pathway for the device. The nanowires which lie horizontally across the image give positive phase shifts indicating they are non-conductive. These are likely to be bare DNA strands or so thinly coated with metal that they appear highly-resistive by EFM.

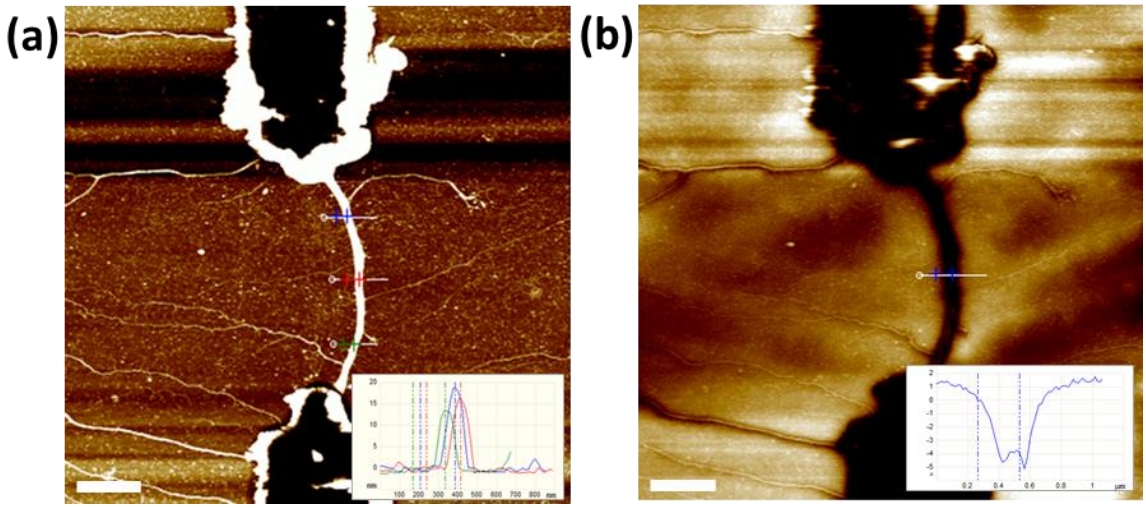

Figure 4.26: (a) AFM height image of a Cu-DNA nanowire spanning across two gold electrodes and (b) corresponding EFM phase image showing negative contrast along the nanowire. Scale bars= 1000 nm, height scale= 10 nm, phase scale= 10°

The performance of the device was electrically tested by carrying out a series of i-V sweeps in the range +3 to -3 V at a constant temperature of 20°C. Figure 4.27 shows the i-V curve of the device (turquoise line) obtained from one of these sweeps. The graph is non-linear and affords negligible current (< picoamps) around zero bias indicating high resistivity. To check the instrument for comparison, measurements were made on a single gold electrode which was shown to exhibit excellent ohmic behaviour in the mA regime at close to zero bias (see inset, figure 4.27).

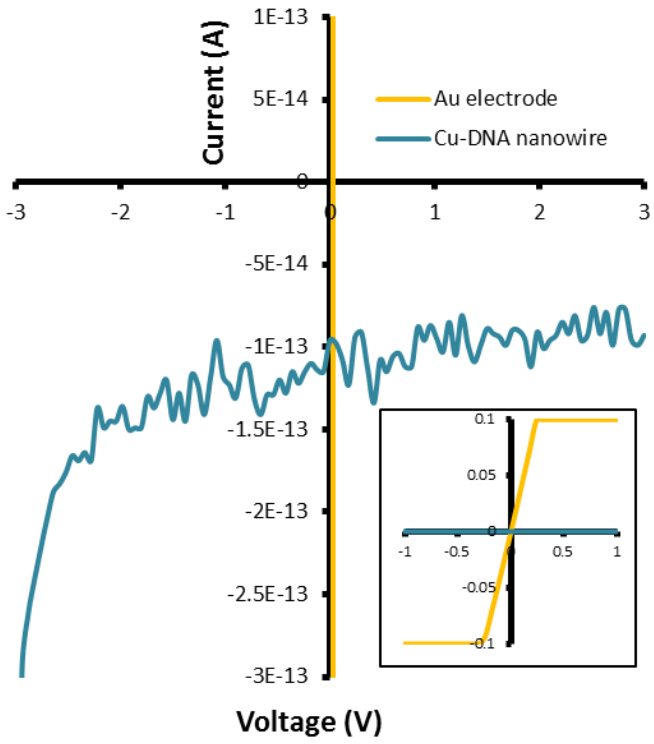

Figure 4.27: i-V plot of Cu-DNA nanowire device (blue line) and gold electrode (yellow line). Inset shows the same graph on a different 'y-scale.' The device shows very low levels of current, whereas the electrode is highly conductive and ohmic

It has been demonstrated in the literature by Braun *et.al* in their electrical studies of a DNA-templated Ag nanowire fixed across two gold electrodes that an initial non-linearity of i-V behaviour can be transformed to more ohmic characteristics by application of high voltages.[61] This is expected to remove surface oxide residing on the copper surface which could potentially constitute a substantial tunnelling barrier to electron transport between particles. We performed repeated i-V sweeps through a large voltage range (-20 to +20 V) and then fixed the potential at 20 V for 1 minute. However this did not lead to a transformation in the i-V curves or enhancement in the level of detected current, as hoped.

This data contrasts with the previously described electrical data obtained using EFM and C-AFM for Cu-DNA nanowires. It was observed from the EFM data that a viable conductive pathway exists between the electrodes (along the wire itself). However it must be noted that the EFM technique has far greater sensitivity than the 2-probe i-V analyser. C-AFM on the other hand is *less* sensitive (µA – nA's) than the probe station (approaching femtoamps), but yet indicated a substantially higher level of current (tens of nA's), which is well within the detection limits of the 2-probe device analyser.

Therefore it would be expected that i-V curves from this device exhibit current in the nanoamp range at least. It is especially surprising that such low levels of current are observed given the continuous nature of these nanowires. The lack of current measurable in the device is suggested as being due to a contact issue between the gold electrode and the copper nanowire, rather than the electrical capabilities of the nanowire itself. Evidence to support this was found in further AFM studies.

A 3-d AFM topography image (figure 4.28) of the two-terminal nanowire device reveals a 'break' at the nanowire-gold junction (indicated by the white circle). A 'break' or 'gap' of this nature would lead to substantial hindrance to the flow of current from wire to electrode, assuming the gap is too long for electron tunnelling. Hence this could explain the poor electrical properties exhibited in the i-V curve.

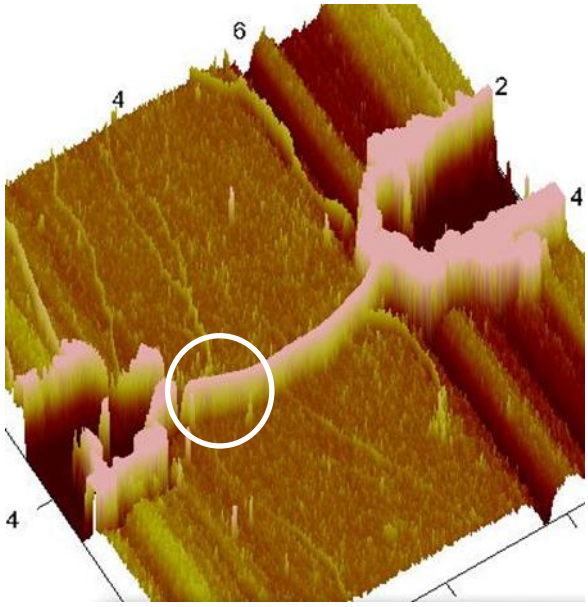

Figure 4.28: AFM 3-D representation of the Cu-DNA nanowire device showing a clear break at the nanowire-gold junction (circled in white)

Attempts were made to improve the wire to gold contact using heat (200°C) whilst under vacuum for a period of 24 hours. Thermal annealing of Cu lines and surfaces is a process often used for the sintering of individual copper grains to form uniform structures/films.[62-65] It was hoped that annealing would fuse the copper-gold interface. However, despite this further attempt to transform the structural/electrical properties of the device, the i-V curves did not change in figure 4.27.

AFM images recorded after the thermal anneal treatment revealed a considerable structural transformation in the Cu-DNA nanowire (figure 4.29). The nanowire break remained, but the templated material was found to diffuse along the DNA strand, aggregating to form one large particle (>100 nm in height) shown circled in yellow in figure 4.29c. The formation of this particle comes at the expense of a reduction in height of the nanowire itself from ~15 nm to ~6 nm, suggesting that copper metal diffuses along the length of the template driving further aggregation. The height of the structure also becomes non-uniform with regions of low height in some places and large height in others affording the granular appearance. Similar structural observations were made on the annealed Cu-DNA nanostructures in chapter 3, where larger particles formed along the template rather than one continuous structure.

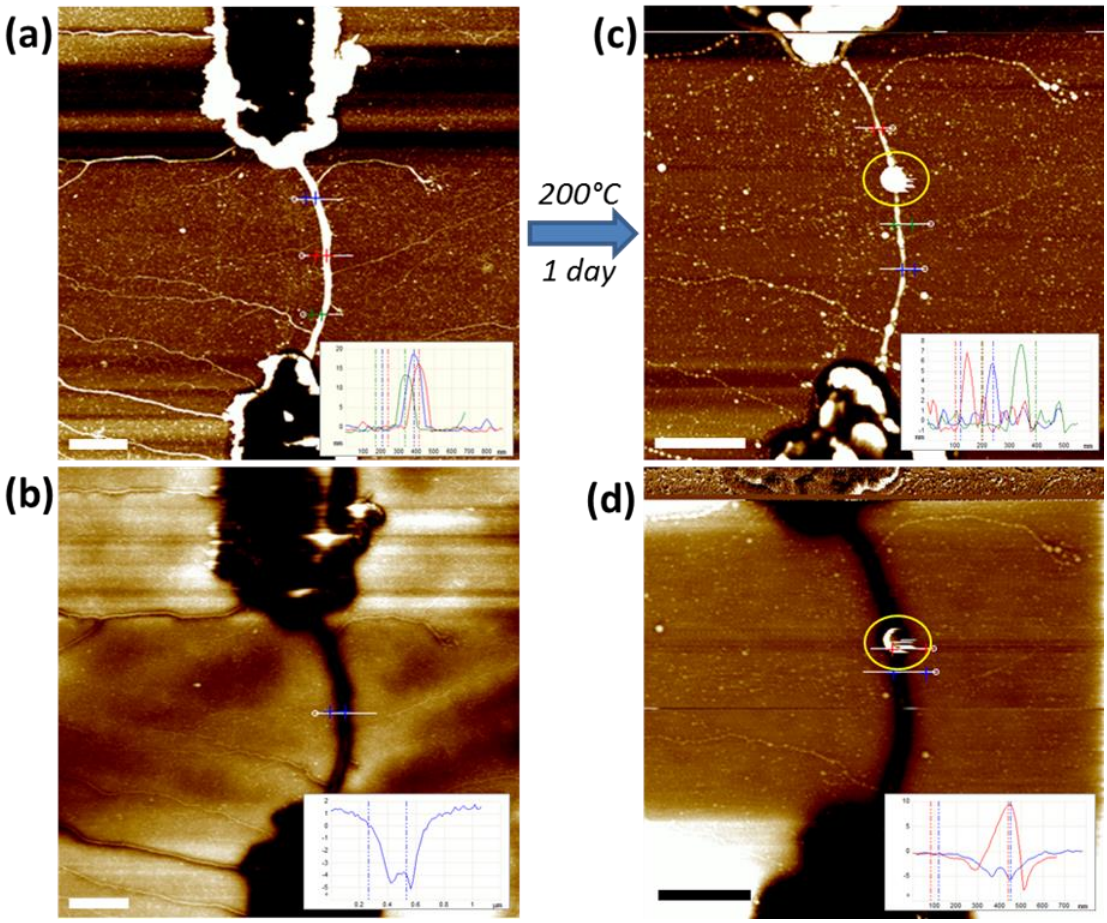

Figure 4.29: Thermal annealing of Cu-DNA nanowire device: (a) AFM height image of the device, (b) EFM phase image of the device, (c) AFM height image of the device after anneal and (d) EFM phase image of the device after anneal. Formation of a large particle in the middle of the nanowire (circled in yellow) is a result of the heat treatment. Scale bars= 1000 nm, height scales= 10 nm, phase scales= 10°

The evidence provided in this experiment and figure 4.29 seems to concur with a recently published theory relating to the thermodynamics of DNA-templating.[57] It states

that if too much material is supplied to the template and the system is allowed to reach equilibrium then a single particle on a chain is the desired morphology. This is due to increased surface tension with respect to the line energy. In order to minimise the surface energy it is favourable to form a single spherical particle. The so called 'beads-on-a-string' assembly may also form if the right templating conditions are met. Based on the evidence, there is justification to assert that, at elevated temperatures the barrier to formation of such structures is lowered. In almost all studies where DNA metal nanostructures have exhibited a granular morphology of this nature, they have either been shown to exhibit low conductivity or electrical measurements have simply not been performed.[1, 2, 7, 66]

The EFM phase image of the Cu-DNA nanowire device after annealing (figure 4.29d) indicates that the nanowire exhibits negative phase shifts when under bias. However, a large positive phase shift is encountered at the location of the large particle. This feature of the EFM image indicates that the large particle is electrically insulating and may therefore disrupt passage of current through the structure.

When assessing the electrical capabilities of a metal nanowire it is worth considering the effect size has on conductivity. There are two main effects which cause resistance in a metal: (i) electron scattering off lattice vibrations, particularly at grain boundaries (due to mismatch in metal lattice) and (ii) surface scattering; where a higher proportion of the materials' electrons reside near the surface, becoming more significant as the materials' dimensions shrink.[67-69]

The continuous morphology of the nanowires prepared in this work ensures that lattice/grain boundary scattering is kept as low as possible, whereas surface scattering may become more significant due to the small width of the nanowires. However, it must be noted that this explanation alone is insufficient to account for the number of magnitudes drop in conductivity of copper. While the nanowires prepared in this work appear highly continuous by AFM, it may be that the wires are still granular or are of a polycrystalline nature, which may indicate that the contribution of scattering at particle-particle interfaces along the structure is highly significant. This effect, along with the combination of increased surface scattering (due to small size) and contact resistance, may account for severe drops in conductivity relative to the bulk material. The presence of copper hydroxide in the Cu-DNA nanowire may also cause a conductivity drop in the nanowire. An insulating layer around copper particles may constitute a tunnelling

barrier to electron transport along the wire. However this is perhaps unlikely to be the major factor causing resistance in the wire, as DNA-templated conductive Cu_2O nanowires (12-23 nm in height) have been prepared elsewhere,[70] which are in fact more conductive (2.2-3.3 Scm^{-1}) than the copper nanowires prepared here (0.94 Scm^{-1}).

4.4. Conclusions

DNA-templated copper nanowires were successfully formed in DNA solution at a low Cu^{2+}:DNA(phosphate) ratio (0.05). The concentration of copper relative to DNA was found to be critical in controlling the formation of Cu-DNA aggregates or nanowires. AFM studies revealed that the resulting nanowires were highly continuous and reproducible, and the growth mechanism was likened to the Ostwalds' Ripening of Colloids. Product solutions were purified by centrifugation. Copper was found to bind to the DNA structure through primary interaction with the phosphate groups as well as interaction with the guanine and cytosine bases, as indicated by the appropriate FTIR peak shifts. A combination of XPS and XRD techniques confirmed that metallic copper had grown on the DNA template and an overlayer of copper hydroxide ($Cu(OH)_2$) had formed on the surface.

EFM and C-AFM confirmed the conductive nature of the nanomaterial; the first example of conductive DNA-templated copper nanowires. However, the low current values obtained by the latter technique were accounted for by the high contact resistance of the tip-nanowire interface. Fabrication of a two-terminal Cu-DNA device was successful but electrical characterisation was thwarted by the poor electrode-wire contact. Attempts to improve the contact issue by thermal annealing resulted in a substantial change in the nanowire morphology and suggested that transformation to 'beads-on-a-string' morphology was promoted at elevated temperature. Ultimately the low conductivity of these nanowires may be due to a combination of contact resistance and the possibility for electron and surface scattering taking place along the wire, as well as the insulating barrier presented by the presence of copper hydroxide.

4.5. References

1. S. M. D. Watson, N. G. Wright, B. R. Horrocks and A. Houlton, Preparation, Characterization and Scanned Conductance Microscopy Studies of DNA-Templated One-Dimensional Copper Nanostructures *Langmuir*, 2009.
2. C. F. Monson and A. T. Woolley, DNA-templated construction of copper nanowires. *Nano Letters*, 2003, **3**, 359-363.
3. H. A. Becerril, R. M. Stoltenberg, C. F. Monson and A. T. Woolley, Ionic surface masking for low background in single- and double-stranded DNA-templated silver and copper nanorods. *Journal of Materials Chemistry*, 2004, **14**, 611-616.
4. R. M. Stoltenberg and A. T. Woolley, DNA-templated nanowire fabrication. *Biomedical Microdevices*, 2004, **6**, 105-111.
5. H. A. Becerril, R. M. Stoltenberg, D. R. Wheeler, R. C. Davis, J. N. Harb and A. T. Woolley, DNA-templated three-branched nanostructures for nanoelectronic devices. *Journal of the American Chemical Society*, 2005, **127**, 2828-2829.
6. H. Kudo and M. Fujihira, DNA-templated copper nanowire fabrication by a two-step process involving electroless metallization. *IEEE Transactions on Nanotechnology*, 2006, **5**, 90-92.
7. L. Dong, T. Hollis, B. A. Connolly, N. G. Wright, B. R. Horrocks and A. Houlton, DNA-templated semiconductor nanoparticle chains and wires. *Advanced Materials*, 2007, **19**, 1748-1751.
8. D. Liqin, T. Hollis, S. Fishwick, B. A. Connolly, N. G. Wright, B. R. Horrocks and A. Houlton, Synthesis, manipulation and conductivity of supramolecular polymer nanowires. *Chemistry - A European Journal*, 2007, **13**, 822-828.
9. A. Rotaru, S. Dutta, E. Jentzsch, K. Gothelf and A. Mokhir, Selective dsDNA-templated formation of copper nanoparticles in solution. *Angewandte Chemie - International Edition*, 2010, **49**, 5665-5667.
10. J. Chen, J. Liu, Z. Fang and L. Zeng, Random dsDNA-templated formation of copper nanoparticles as novel fluorescence probes for label-free lead ions detection. *Chemical Communications*, 2012, **48**, 1057-1059.
11. Z. Zhou, Y. Du and S. Dong, Double-strand DNA-templated formation of copper nanoparticles as fluorescent probe for label-free aptamer sensor. *Analytical Chemistry*, 2011, **83**, 5122-5127.
12. V. A. Bloomfield, DNA condensation. *Current Opinion in Structural Biology*, 1996, **6**, 334-341.
13. J. Widom and R. L. Baldwin, Cation-induced toroidal condensation of DNA: Studies with Co3+(NH3)6. *Journal of Molecular Biology*, 1980, **144**, 431-453.
14. J. G. Duguid, V. A. Bloomfield, J. M. Benevides and G. J. Thomas Jr, Raman spectroscopy of DNA-metal complexes. II. The thermal denaturation of DNA in the presence of Sr2+, Ba2+, Mg2+, Ca2+, Mn2+, Co2+, Ni2+, and Cd2+. *Biophysical Journal*, 1995, **69**, 2623-2641.
15. J. G. Duguid and V. A. Bloomfield, Aggregation of melted DNA by divalent metal ion-mediated cross-linking. *Biophysical Journal*, 1995, **69**, 2642-2648.
16. A. A. Zinchenko, Templating of inorganic nanomaterials by biomacromolecules and their assemblies. *Polymer Science - Series C*, 2012, **54**, 80-87.
17. S. Pu, A. Zinchenko and S. Murata, Conformational behavior of DNA-templated CdS inorganic nanowire. *Nanotechnology*, 2011, **22**.
18. B. Lippert, Multiplicity of metal ion binding patterns to nucleobases. *Coordination Chemistry Reviews*, 2000, **200–202**, 487-516.
19. G. L. Eichhorn and Y. A. Shin, Interaction of metal ions with polynucleotides and related compounds. XII. The relative effect of various metal ions on DNA helicity. *Journal of the American Chemical Society*, 1968, **90**, 7323-7328.

20. L. Zhao, Z. Liu, Y. Zu, Z. Zhou and T. Sun, Influence of Mg 2+, Ni 2+, and Cu 2+ on DNA assembly on HOPG surfaces: Atomic force microscopy study. *Scanning*, 2012, **34**, 68-75.
21. G. L. Eichhorn, Metal ions as stabilizers or destabilizers of the deoxyribonucleic acid structure. *Nature*, 1962, **194**, 474-475.
22. H. A. Tajmir-Riahi, M. Naoui and R. Ahmad, The effects of Cu 2+ and Pb 2+ on the solution structure of calf thymus DNA: DNA condensation and denaturation studied by Fourier Transform ir difference spectroscopy. *Biopolymers*, 1993, **33**, 1819-1827.
23. M. H. Zareie, G. Erdem, C. Öner, R. Oner, A. Öğüş and E. Pişkin, Investigation of ascorbate-Cu (II) induced cleavage of DNA by scanning tunneling microscopy. *International Journal of Biological Macromolecules*, 1996, **19**, 69-73.
24. G. Erdem, C. Oner, A. M. Onal, D. Kisakurek and A. Ogus, Free radical mediated interaction of ascorbic acid and ascorbate/Cu(II) with viral and plasmid DNAs. *Journal of Biosciences*, 1994, **19**, 9-17.
25. A. Samuni, J. Aronovitch and D. Godinger, On the cytotoxicity of vitamin C and metal ions. A site-specific Fenton mechanism. *European Journal of Biochemistry*, 1983, **137**, 119-124.
26. S. H. Chiou, DNA- and protein-scission activities of ascorbate in the presence of copper ion and a copper-peptide complex. *Journal of Biochemistry*, 1983, **94**, 1259-1267.
27. A. Bensimon, A. Simon, A. Chiffaudel, V. Croquette, F. Heslot and D. Bensimon, Alignment and sensitive detection of DNA by a moving interface. *Science*, 1994, **265**, 2096-2098.
28. J. Zhang, Y. Ma, S. Stachura and H. He, Assembly of highly aligned DNA strands onto Si chips. *Langmuir*, 2005, **21**, 4180-4184.
29. A. Inberg, E. Glickman, T. Asher, N. Fishelson and Y. Shacham-Diamand, Electrical properties of sub-100 nm Cu films deposited by electroless plating on amino-terminated silicon oxide activated with Au nano-particles. *Surface and Coatings Technology*, 2009, **204**, 520-524.
30. Y. Wang, A. V. Biradar, G. Wang, K. K. Sharma, C. T. Duncan, S. Rangan and T. Asefa, Controlled synthesis of water-dispersible faceted crystalline copper nanoparticles and their catalytic properties. *Chemistry - A European Journal*, 2010, **16**, 10735-10743.
31. V. Andrushchenko, J. H. Van De Sande and H. Wieser, Vibrational circular dichroism and IR absorption of DNA complexes with Cu2+ ions. *Biopolymers - Biospectroscopy Section*, 2003, **72**, 374-390.
32. H. Arakawa, R. Ahmad, M. Naoui and H. A. Tajmir-Riahi, A comparative study of calf thymus DNA binding to Cr(III) and Cr(VI) ions. Evidence for the guanine N-7-chromium-phosphate chelate formation. *Journal of Biological Chemistry*, 2000, **275**, 10150-10153.
33. H. Fritzsche and C. Zimmer, Infrared studies of deoxyribonucleic acids, their constituents and analogues. 4. The binding sites of copper(II) in DNA. *European Journal of Biochemistry*, 1968, **5**, 42-44.
34. J. Richter, M. Mertig, W. Pompe, I. MÃ¶nch and H. K. Schackert, Construction of highly conductive nanowires on a DNA template. *Applied Physics Letters*, 2001, **78**, 536-538.
35. S. Alex and P. Dupuis, FT-IR and Raman investigation of cadmium binding by DNA. *Inorganica Chimica Acta*, 1989, **157**, 271-281.
36. A. A. Ouameur and H. A. Tajmir-Riahi, Structural analysis of DNA interactions with biogenic polyamines and cobalt(III)hexamine studied by fourier transform infrared and capillary electrophoresis. *Journal of Biological Chemistry*, 2004, **279**, 42041-42054.
37. G. I. Dovbeshko, N. Y. Gridina, E. B. Kruglova and O. P. Pashchuk, FTIR spectroscopy studies of nucleic acid damage. *Talanta*, 2000, **53**, 233-246.
38. L. G. Marzilli and T. J. Kistenmacher, Stereoselectivity in the binding of transition-metal chelate complexes to nucleic acid constituents: Bonding and nonbonding effects. *Accounts of Chemical Research*, 1977, **10**, 146-152.

39. M. Sundaralingam and J. A. Carrabine, Stereochemistry of nucleic acids and their constituents. XIX. Copper binding sites and mechanism of G·C selective denaturation of DNA. Crystal and molecular structures of guanine·copper(II) chloride and cytosine·copper(II) chloride complexes. *Journal of Molecular Biology*, 1971, **61**, 287-309.
40. M. E. Toimil Molares, E. M. Höhberger, C. Schaeflein, R. H. Blick, R. Neumann and C. Trautmann, Electrical characterization of electrochemically grown single copper nanowires. *Applied Physics Letters*, 2003, **82**, 2139-2141.
41. S. K. Chawla, B. I. Rickett, N. Sankarraman and J. H. Payer, An X-ray photo-electron spectroscopic investigation of the air-formed film on copper. *Corrosion Science*, 1992, **33**, 1617-1631.
42. I. Platzman, R. Brener, H. Haick and R. Tannenbaum, Oxidation of polycrystalline copper thin films at ambient conditions. *Journal of Physical Chemistry C*, 2008, **112**, 1101-1108.
43. J. Hernandez, P. Wrschka and G. S. Oehrlein, Surface Chemistry Studies of Copper Chemical Mechanical Planarization. *Journal of the Electrochemical Society*, 2001, **148**, G389-G397.
44. M. Abdulla-Al-Mamun, Y. Kusumoto and M. Muruganandham, Simple new synthesis of copper nanoparticles in water/acetonitrile mixed solvent and their characterization. *Materials Letters*, 2009, **63**, 2007-2009.
45. B. R. Strohmeier, D. E. Levden, R. S. Field and D. M. Hercules, Surface spectroscopic characterization of Cu Al2O3 catalysts. *Journal of Catalysis*, 1985, **94**, 514-530.
46. N. S. McIntyre, S. Sunder, D. W. Shoesmith and F. W. Stanchell, CHEMICAL INFORMATION FROM XPS - APPLICATIONS TO THE ANALYSIS OF ELECTRODE SURFACES. *Journal of vacuum science & technology*, 1980, **18**, 714-721.
47. N. S. McIntyre and M. G. Cook, X-RAY PHOTOELECTRON STUDIES ON SOME OXIDES AND HYDROXIDES OF COBALT, NICKEL, AND COPPER. *Analytical Chemistry*, 1975, **47**, 2208-2213.
48. K. Okada, J. Kawai and A. Kotani, Triple-peak feature of Cu 2p x-ray-photoemission spectrum in copper acetylacetonate. *Physical Review B*, 1993, **48**, 10733-10738.
49. G. Van Der Laan, C. Westra, C. Haas and G. A. Sawatzky, Satellite structure in photoelectron and Auger spectra of copper dihalides. *Physical Review B*, 1981, **23**, 4369-4380.
50. M. L. Miller and R. W. Linton, X-ray photoelectron spectroscopy of thermally treated SiO 2 surfaces. *Analytical Chemistry®*, 1985, **57**, 2314-2319.
51. S. Ptasińska, A. Stypczyńska, T. Nixon, N. J. Mason, D. V. Klyachko and L. Sanche, X-ray induced damage in DNA monitored by X-ray photoelectron spectroscopy. *Journal of Chemical Physics*, 2008, **129**.
52. C.D.Wagner, W.M.Rigg, L.E.Davis, J.F.Moulder and G.E.Mullenberg, Handbook of X-ray Photoelectron Spectroscopy. 1979.
53. S. Pruneanu, S. A. F. Al-Said, L. Dong, T. A. Hollis, M. A. Galindo, N. G. Wright, A. Houlton and B. R. Horrocks, Self-assembly of DNA-templated polypyrrole nanowires: Spontaneous formation of conductive nanoropes. *Advanced Functional Materials*, 2008, **18**, 2444-2454.
54. K. Keren, M. Krueger, R. Gilad, G. Ben-Yoseph, U. Sivan and E. Braun, Sequence-specific molecular lithography on single DNA molecules. *Science*, 2002, **297**, 72-75.
55. I. Kobayashi, T. Miyazawa, M. Fujimoto, H. Kawaguchi and T. Hara, Investigation of copper contamination into interlayer dielectrics by copper process. *Thin Solid Films*, 2004, **462-463**, 231-234.
56. S. M. D. Watson, N. G. Wright, B. R. Horrocks and A. Houlton, Preparation, characterization and scanned conductance microscopy studies of DNA-templated one-dimensional copper nanostructures. *Langmuir*, **26**, 2068-2075.

57. S. M. D. Watson, A. Houlton and B. R. Horrocks, Equilibrium and non-equilibrium thermodynamics of templating reactions for the formation of nanowires. *Nanotechnology*, 2012, **23**.
58. M. Bockrath, N. Markovic, A. Shepard, M. Tinkham, L. Gurevich, L. P. Kouwenhoven, M. W. Wu and L. L. Sohn, Scanned Conductance Microscopy of Carbon Nanotubes and Î»-DNA. *Nano Letters*, 2002, **2**, 187-190.
59. C. Staii, A. T. Johnson Jr and N. J. Pinto, Quantitative analysis of scanning conductance microscopy. *Nano Letters*, 2004, **4**, 859-862.
60. A. Houlton and S. M. D. Watson, DNA-based nanowires. Towards bottom-up nanoscale electronics. *Annual Reports on the Progress of Chemistry - Section A*, 2011, **107**, 21-42.
61. E. Braun, Y. Eichen, U. Sivan and G. Ben-Yoseph, DNA-templated assembly and electrode attachment of a conducting silver wire. *Nature*, 1998, **391**, 775-778.
62. H. K. Kim, J. A. Jeong, I. K. Yoo, J. B. Koo, H. H. Lee, K. H. Hur, D. H. Kim, S. E. Kim and B. H. Jun, Rapid thermal reduction of inkjet printed Cu interconnects on glass substrate. *Electrochemical and Solid-State Letters*, 2011, **14**, J65-J68.
63. S. P. Riege and C. V. Thompson, Modeling of texture evolution in copper interconnects annealed in trenches. *Scripta Materialia*, 1999, **41**, 403-408.
64. H. Lee and S. D. Lopatin, The influence of barrier types on the microstructure and electromigration characteristics of electroplated copper. *Thin Solid Films*, 2005, **492**, 279-284.
65. G. Herrmann, H. Gleiter and G. Bäro, Investigation of low energy grain boundaries in metals by a sintering technique. *Acta Metallurgica*, 1976, **24**, 353-359.
66. Z. Deng and C. Mao, DNA-Templated Fabrication of 1D Parallel and 2D Crossed Metallic Nanowire Arrays. *Nano Letters*, 2003, **3**, 1545-1548.
67. D. Josell, S. H. Brongersma and Z. Tokei, Editon edn., 2009, vol. 39, pp. 231-254.
68. R. L. Graham, G. B. Alers, T. Mountsier, N. Shamma, S. Dhuey, S. Cabrini, R. H. Geiss, D. T. Read and S. Peddeti, Resistivity dominated by surface scattering in sub-50 nm Cu wires. *Applied Physics Letters*, **96**.
69. A. Bid, A. Bora and A. K. Raychaudhuri, Temperature dependence of the resistance of metallic nanowires of diameter ⩾15nm: Applicability of Bloch-Grüneisen theorem. *Physical Review B*, 2006, **74**, 035426.
70. R. Hassanien, S. A. F. Al-Said, L. Šiller, R. Little, N. G. Wright, A. Houlton and B. R. Horrocks, Smooth and conductive DNA-templated Cu 2O nanowires: Growth morphology, spectroscopic and electrical characterization. *Nanotechnology*, 2012, **23**.

Chapter 5: Passivation of Cu-DNA Nanowires by thiol self-assembly

5.1. Introduction

In chapter 4, Cu-DNA nanowires formed in solution were confirmed to be conducting, but electrical analysis indicated a conductivity value many orders of magnitude less than for bulk copper. This was despite the wires appearing highly continuous by AFM. Chemical characterisation indicated that the nanowires are composed of a DNA-metallic core encapsulated by a shell of copper(II) hydroxide (see chapter 4, section 4.3.3).

According to some recent studies,[1-3] the formation of the hydroxide overlayer on copper comprises one part of a mutually-dependent process towards the full oxidation of copper to cupric oxide (CuO). Firstly, formation of Cu_2O via ionic transport of Cu towards the oxide-oxygen interface occurs, followed by growth of the metastable $Cu(OH)_2$ overlayer before finally converting to the more stable CuO upon lengthy exposure to the atmosphere.

The presence of the hydroxide layer on the surface of copper will diminish the conductive capability of the nanowires. Passivation of the copper surface may prevent this from occuring. A chemically assembled passivating adlayer on the surface will serve to block the initial formation of oxide/hydroxide and prevent further oxidation of copper in air. It is particularly important for the performance of copper-based interconnect that the surface remains free of oxide and is suitably protected from other corrosive species such as those present during wet etch processes (e.g. F^- and Cl^- based chemicals).[3, 4]

Thiols have proved to be a useful class of molecules for self-assembly onto metal surfaces such as gold,[5, 6] silver[7] and copper[3, 4, 8, 9] and can afford an array of different surface chemistries.[10] The thiol groups form strong bonds with these metals through the sulfur atom, particularly with gold,[11] affording a protective layer on the surface which is stable and easy to prepare. Unlike gold however, copper is easily oxidised in air,[12] making the ability to form protective layers on copper surfaces extremely important. When thiols react at copper they form a self-assembled thiolate adlayer. It is thought that the initial assembly step involves oxidation of thiol to disulfide, which concurrently reduces surface copper oxide to the zero-valent metal.[4] The resulting oxidised thiol species desorb from the surface and are replaced by new thiol molecules, which

assemble on the pure copper surface to form the ordered copper-thiolate interface. Thus, it is considered possible for thiols to form a self-assembled metal-organic interface which acts to reduce surface oxide and protect copper against corrosion.[8]

Evidence suggests the resulting thiolate (Cu-SR) may oxidise to sulfonates in air (Cu-SO_3^-R).[4, 13] The oxidised thiol species (e.g. sulfonate) desorb more easily from the surface than the thiolates do. Upon desorption the oxidised thiol species are subsequently replaced by new thiol molecules from solution. In such a way, the UV mediated oxidation of thiol-modified copper surfaces has been demonstrated in order to create patterned surfaces using a mask.[14] The unexposed areas of the surface are oxidised by irradiation to create the patterned substrate. The sample was then placed into a different thiol-derivative containing solution, which acts to selectively replace the oxidised thiols bound to the surface for this alternative thiol, thus affording a chemically patterned surface.

Alkanethiols have been shown to form densely packed monolayers on copper, which makes the surface strongly hydrophobic.[8, 9, 15, 16] The resulting thiolate layer is hydrophobic and forms a diffusion barrier between O_2 and other attacking species potentially capable of corroding the surface. These properties make alkanethiolate coatings extremely useful for retarding the atmospheric oxidation of copper. It has been demonstrated that the protection efficiency is good and increases with chain length as a result of the increased crystallinity of the monolayer.[9, 17, 18]

Self-assembled monolayers (SAMs) formed from aromatic thiols also afford densely packed arrangements on metal surfaces and form uniform molecular assemblies, thus providing good surface passivation.[1] However, these have been less extensively investigated than alkane thiols.[19-21] The packing ability of aromatic thiols is perhaps enhanced by the ability of individual thiol molecules to π-stack through benzene rings. This may afford a more efficient corrosion barrier than alkanethiols.

This work is aimed at the use of an aromatic thiol, *para*-mercaptobenzoic acid (figure 1a), for passivation of DNA-templated copper nanowires. The thiol can be solubilised in an ethanol/water mixture, which can also solubilise DNA and the metallising agents to be used ($Cu(NO_3)_2$ and ascorbic acid). Consequently, modification of the DNA-Copper surface with thiol can be performed as a one-pot reaction. The chemical structures of potential oxidation species of *para*-mercaptobenzoic acid are shown in figure 5.1. A

schematic showing the proposed structure of the thiolate SAM on a Cu-DNA nanowire is shown in figure 5.2.

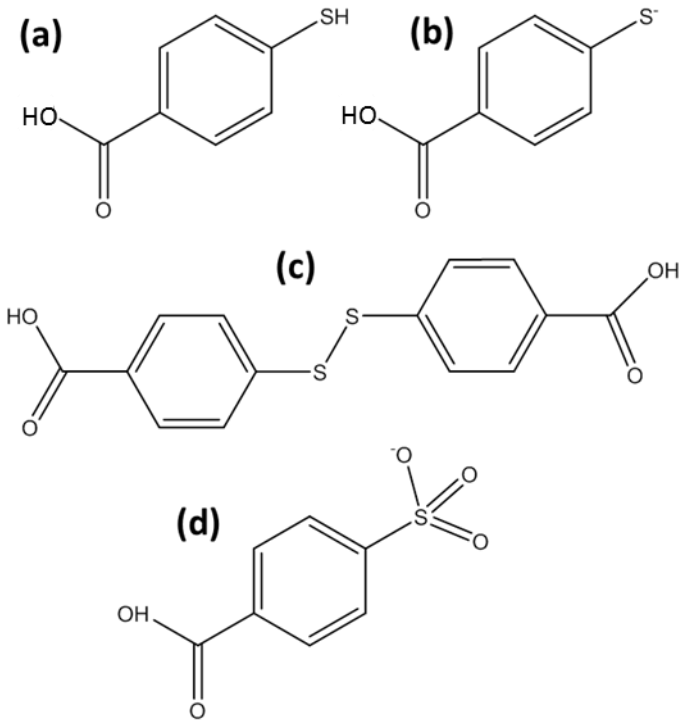

Figure 5.1: (a) *para*-mercaptobenzoic acid, (b) thiolate form, (c) disulfide and (d) sulfonate

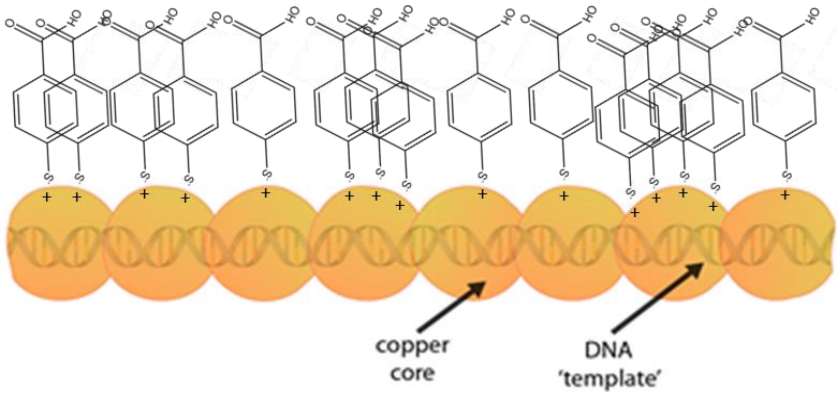

Figure 5.2: Schematic showing thiolate adlayer formed on oxide-free surface of DNA-templated copper nanowire by self-assembly of *para*-mercaptobenzoic acid in solution. The thiolate molecules are shown to overlap in some cases to illustrate the potential for high density stacking

Aside from acting as a corrosion barrier for copper, thiolate SAMs may stabilise nanoparticles, control the particle size dispersity and suppress the aggregation of clusters in solution.[22, 23] This was explained in the work by Dow *et.al* involving the formation of uniform thiolate SAMs on Cu films by adsorption of disulphide.[24] In these

studies it is noted that disulfides can react with metallic copper to generate Cu(I)-thiolate clusters. This can lead to progressive etching of the copper-modified surface due to the ability of the Cu(I)-thiolate clusters to precipitate and resolubilise in solution.[5] Such a process therefore helps to restrict the aggregation of nanoparticles. Hostetler *et.al*., demonstrated remarkable control over nanoparticle size by varying the reaction conditions such as thiol concentration and the rate of reduction.[22] Furthermore, the synthesis of less aggregated and stable nanoparticles may provide for better packing of individual grains along the DNA template. Figure 5.3 shows a schematic of a thiolate-capped CuNP. Such a structure should also be prevented from developing into larger clusters due to the hydrophobic thiolate layer surrounding the particle.

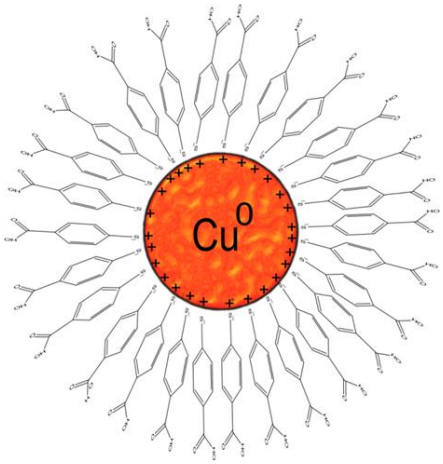

Figure 5.3: Schematic of a thiolate-protected copper nanoparticle

In this chapter Cu-DNA nanowires are modified by thiol SAM in effort to protect the copper surface from oxidation. The thiolate-capped Cu-DNA nanostructures formed in this chapter are characterised using XPS, AFM, EFM and C-AFM.

5.2. Experimental

All general chemical reagents were obtained from Sigma-Aldrich unless otherwise stated, and were Analar grade or equivalent. Lambda (λ) DNA was from New England Biolabs, cat no. N3011S (New England Biolabs (UK) Ltd. Hitchin, Herts, United Kingdom). Silicon <p-100> wafers, boron doped, 100 mm. diameter, 525 ± 50 μm thickness, 1-10 Ω cm resistance were purchased from Compart Technology LTD. (Peterborough, Cambridgeshire, United Kingdom). Silicon <n-100> wafers with 200 nm SiO_2 layer, Arsenic doped, 100mm. diameter, 500 ± 25 μm thickness, ≤ 0.005 Ω cm were purchased from Virginia Semiconductor (1501 Powhatan St., Fredericksburg VA 22401).

5.2.1. Preparation of thiol-modified Cu-DNA nanowires

λ-DNA solution (500 μg mL^{-1}, in 10 mM tris-HCl, pH 8, 1 mM EDTA) was diluted to 300 μg mL^{-1} with Nanopure water. Solution A was prepared by addition of $Cu(NO_3)_2.3H_2O$ (*aq*. 50 μM, 10 μL) to the λ-DNA solution (10 μL) and was left to incubate for 5 minutes. Solution B was prepared by mixing ascorbic acid (*aq*. 2 mM, 10 μL) and 4-mercaptobenzoic acid (68 μM, 10 μL) in a 1:1 H_2O:EtOH mixture. Equal parts of solution B were then added to solution A and the solution was left to incubate for 3 hours, with gentle stirring on a mechanical roller. To separate the suspension of nanowires from nanoparticles/aggregates, the mixture was centrifuged at 8000 rpm for 2 minutes. The top fraction was discarded and the bottom fraction was collected for analysis.

The concentration of the thiol was chosen to afford a copper:sulfur ratio of 0.74:1, as has previously been used in the preparation of thiol stabilised gold nanoparticles.[5, 23] Prior to use, 4-mercaptobenzoic acid (pKa~ 6) was pH adjusted from a reading of pH 4.3 to a reading of pH 8.0 by addition of 50 mM NaOH (*aq*.) aliquots. However in some experiments, the pH of the thiol was not adjusted.

5.2.2. Cleaning and preparation of silicon wafers

Silicon <p-100> wafers were cut into 8 x 12 mm pieces with a diamond tip pen. The wafers were serial washed in high purity acetone, propanol and Nanopure water, after

which the wafers were heated in a solution of surfactant (sodium dodecyl sulphate, 0.01g per 100 mL water) for 20 minutes followed by washing with copious amounts of Nanopure water. The wafers were then chemically oxidised in hot "piranha" solution (4:1 H_2SO_4:H_2O_2) for 45 minutes at ~50°C in order to oxidise the surface and remove organic residue. The wafers are then washed with Nanopure water and dried in an oven for 30 minutes. The surface was chemically modified by vapour deposition, which involved exposure of the bare silicon surface to chlorotrimethylsilane vapour (Me_3SiCl) for 8 minutes leading to formation of the trimethylsilane (TMS) self-assembled monolayer (Me_3SiCl). Static contact angle measurements were carried out on the TMS-modified Si substrates using a CAM100 system (KSV Instruments LTD., Helsinki, Finland), with Nanopure water as the probe liquid.

Wafers used for EFM/C-AFM analysis contained a 200 nm thick oxide layer on both sides to form an insulating barrier on the surface. Prior to the previously described cleaning method the backside of these wafers were treated with a solution of HF (10% aq.) to remove the native oxide layer and provide electrical contact for subsequent electrical measurements.

5.2.3. Alignment of thiol-protected Cu-DNA nanowires upon substrates

For purposes of SPM and C-AFM analysis, thiol-protected DNA-templated copper nanowires were aligned upon TMS-modified silicon substrates by a combination of combing and drop cast techniques: A 5 µL droplet of the nanowire suspension was obtained from the bottom fraction of the product containing Eppendorf tube and pipetted onto the substrate. The nanowires were then "combed" onto the substrate by slowly withdrawing a volume of the droplet using a micro pipette and then redepositing onto the surface. This routine was performed several times before finally allowing the droplet to evaporate in a ventilated laminar flow cabinet. This left a residual drying stain on the surface from which nanowires suitable for AFM analysis were seen to protrude from.

5.2.4. AFM/EFM studies

TappingMode AFM imaging of surface topography was performed in air on either a Multimode Nanoscope IIIa or a Dimension Nanoscope V (Veeco Instruments Inc.,

Metrology Group, Santa Barbara, CA) using TESP7 probes (n-doped Si cantilevers, Veeco Instruments Inc., Metrology Group), with a resonant frequency of 234-287 kHz, and a spring constant of 20-80 Nm-1. Data acquisition was carried out using Nanoscope software version 5.12b36 (Multimode IIIA) and Nanoscope software version 7.00b19 (Dimension Nanoscope V) (Veeco Instruments Inc., Digital Instruments).

EFM measurements were carried out in air on a Dimension Nanoscope V system using MESP probes (n-doped Si cantilevers, with a metallic Co/Cr coating, Veeco Instruments Inc., Metrology Group), with a resonant frequency of ca. 70 kHz, a quality factor of 200-260, and a spring constant of 1-5 Nm^{-1}. Data acquisition was carried out using Nanoscope version 7.00b19 software. For both AFM systems, vibrational noise was reduced with an isolation table/acoustic enclosure (Veeco Inc., Metrology Group).

The reported EFM phase images show the phase of the tip oscillation at a set lift height above the sample surface (typically 40-100 nm). Samples used in EFM studies were prepared upon Si <n-100> substrates with a thermally grown oxide layer, 200 nm (± 10%) thick on top, prepared as described earlier. Processing of data acquired from AFM and EFM experiments was carried out using both Nanoscope version 7.00b19 (Veeco Inc., Digital Instruments) and WSxM4.0 Develop 12.6 (Nanotec Electronica S. L., Madrid, Spain) software.

5.2.5. Dynamic Light Scattering (DLS)

Particle size and particle size distributions of the thiol-capped copper nanoparticles were determined by Dynamic Light Scattering (DLS) measurements using a HPPS (Malvern) instrument at 25 ± 0.1 °C and a scattering angle of 173° (backscatter detection). Nanoparticles were prepared and dispersed in Nanopure water as in section 5.2.1 in the absence of DNA. The sample solutions were then placed in low volume disposable PMMA cuvettes and measurements were repeated for accuracy.

5.2.5. X-ray Photoelectron Spectroscopy (XPS)

Samples for X-ray Photoelectron Spectroscopy were prepared and deposited on “piranha” cleaned silicon substrates by drop cast. Silanisation of the silicon substrate was omitted in order to increase the wettability of the sample surface.

Thiolated Cu-DNA nanomaterial was prepared by addition of 4-mercaptobenzoic acid (1:1 H_2O:EtOH, 6.8 mM, 20 µL, ~pH 8) to the ascorbic acid solution, before addition of this combined solution to the DNA/Cu^{2+} containing mixture for a 3 hour incubation, as in section 5.2.1. The concentration of copper nitrate used was calculated to give a final Cu^{2+}: S ratio of 0.74:1. The concentration ratio of [Cu]:[DNA(P)] was 10:1 (c.f. 0.05 for SPM analysis).

A small amount of solid formed in the eppendorf tube during incubation. The reaction mixture was purified by centrifugation to remove the solid, diluted in ethanol and then evaporated onto a clean silicon wafer for XPS analysis. The amount of material attached to the surface is denser than that for AFM samples but is necessary to acquire high photoelectron signal.

XPS was carried out using a Thermo K-Alpha XPS system with a microfocused, monochromated Al Kα X-ray source at a take-off angle of 90°. An electron/ion gun was used to neutralise any charge build-up during analysis. The size of the X-ray spot was 400 µm x 700 µm. Calibration of binding energies was achieved by referencing to the internal hydrocarbon peak at 284.8 eV. Peak fitting was carried out using the CasaXPS software. All peak shapes were defined from a convolution of standard Gaussian and Lorentzian except for the fitting of the metal where an asymmetric Lorentzian function with extended tail parameter (LF) was opted for. FWHM's varied between 1.2 and 2.0 and remain consistent for peaks within the same series. All fitted $2p_{3/2}$:$2p_{1/2}$ peaks were in a ~2:1 ratio. For the fitted XPS spectra the grey lines denote peak fits and the red line represents the sum fit, which matches as close as possible to the real data points (black line). In all instances the minimum numbers of peaks necessary were fitted to the spectrum which resulted in a good fit, simply because it is not always possible to resolve all of the components in the spectra. Linear backgrounds were used for all 1s spectra and Shirley backgrounds for 2p spectra. The data was collected at grazing emission in order to enhance the surface sensitivity.

5.2.6. Conductive-Atomic Force Microscopy (C-AFM) Studies

Conductive-AFM (C-AFM) was carried out in contact mode on samples of thiolated Cu-DNA nanowires fixed to TMS-modified Si/SiO_2 supports, using the Dimension Nanoscope V instrument. Samples were prepared by drop casting 5-40 µL of the copper

nanowire suspension onto the SiO_2 surface and leaving the droplet to evaporate at room temperature. The surface tension created by the receding meniscus is enough to align the wires on the substrate parallel to the direction of solvent withdrawal. This results in a small circular ‘stain’ on the surface, which contains a dense deposit of nanomaterial at its centre and aligned wires extending from the periphery of the main body. A drop of In/Ga eutectic was applied to the edge of the nanomaterial deposit and the metallic chuck of the AFM to provide electrical contact. The circuit is completed via the metallic AFM tip as it contacts the Cu-DNA nanostructure during imaging. The tip is positioned on a nanowire of interest approximately 1mm from the eutectic contact. Typically, a bias of between 1-10 V was applied in order to obtain sufficient current signals for analysis. All measurements were made at room temperature.

5.3. Results and Discussion

5.3.1. Morphological studies of thiol-protected Cu-DNA nanowires by AFM

Examination of the products formed from the reactions of *para*-mercaptobenzoic acid with copper in the presence of DNA, have indicated a structural dependence of the resulting material based on the reaction conditions. Two of the most prominent factors influencing the structure of the thiol-modified nanomaterial were found to be (i) pH of thiol and (ii) order of addition (of thiol) to the reaction mixture. Control over these factors can lead to the formulation of nanowires or nanoparticles. The method of preparation of nanowires was via the two-step 'doping/reduction' DNA-templating route, with the addition of thiol first into the reducing solution (ascorbic acid) or addition of thiol last, after formation of the nanowires.

(i) pH dependence

In these set of experiments, the thiol was added first into the solution of ascorbic acid. Figure 5.4 shows AFM analysis of the material formed from thiol assembly on Cu-DNA nanowires. Figure 5.4a shows 1-D nanostructures formed by addition of thiol at its regular pH in EtOH/H_2O (1:1) (pH 4.3). The as-prepared thiolated 1-D nanostructures display a highly aggregated and irregular appearance. The image revealed large aggregates of nanomaterial attached to DNA ~20-40 nm in height (these appears as large clusters in the image), as opposed to single continuous nanowires as expected. The aggregates are observed to (seemingly) form at random points along the DNA template. In view of the fact that these clusters are not randomly deposited onto the background substrate, indicates that DNA is indeed acting as a template for alignment of these clusters in one dimension. The shapes of the particles are spherical, but slightly elongated. The ability of thiol-modified nanoparticles to precipitate and resolubilise in solution may be a factor in causing anisotropic growth.[5, 16]

A similar aggregation effect was observed for the thiolate-protected CuNP's (i.e. no DNA present in the reaction mixture). Flocculation of nanoparticles was seen to occur to form 'island' like features (figure 5.4c) on the surface. It was reasoned that the thiolated copper species may aggregate via inter-molecular hydrogen bonds through the carboxyl terminated thiol group. A similar observation of the flocculation effect of

thiol-stabilised gold nanoparticles has been made previously.[5] In this report, the same thiol was used, *para*-mercaptobenzoic acid. The aggregation was ascribed to H-bonding between the carboxylic acid groups of the thiolate layers surrounding individual particles.

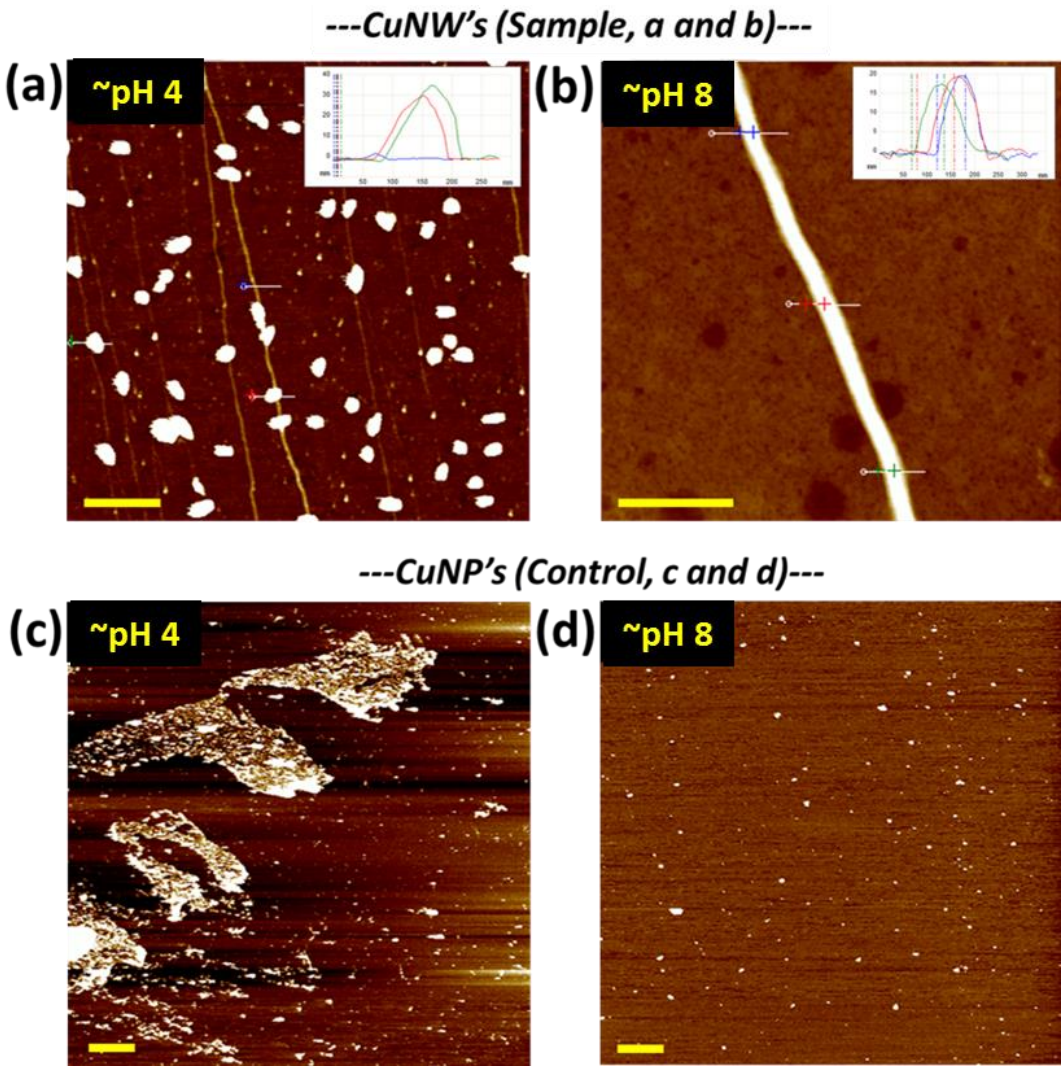

Figure 5.4: Evidence for pH sensitivity on the structure of thiolate-Cu-DNA nanowires. AFM height images of (a) thiolate-Cu-DNA nanowires formed using *para*-mercaptobenzoic acid (pH 4), (b) thiolate-Cu-DNA nanowires formed using *para*-mercaptobenzoic acid (pH 8), (c) thiolate-Cu nanoparticles formed using *para*-mercaptobenzoic acid (pH 4) and (d) thiolate-Cu nanoparticles formed using *para*-mercaptobenzoic acid (pH 8). Scale bars= 500 nm (a,b), 2000 nm (c,d). Height scales= 10 nm (a,c,d) and 30 nm (b)

In an effort to restrict or supress the aggregation of material through H-bonding, NaOH was added to the thiol-containing solution in an effort to generate the anionic carboxylate form. This form is no longer capable of self-complementary H-bonded dimers, or indeed any such H-bonding with itself. The introduced anionic charge would be expected to further reduce aggregation due to electrostatic repulsion effects between

the carboxylate moieties. In this experiment the pH of the thiol EtOH/H_2O mixture was increased to ~pH 8 (above the pKa of the acidic proton of the carboxylic acid (~6.0 in 60% EtOH)) by addition of NaOH. In both instances, for nanowires (5.4b) and nanoparticles (figure 5.4d), aggregation was restricted. AFM analysis of the resulting materials showed evidence of individual nanowire (figure 5.4b) and/or nanoparticle (figure 5.4d) formation on the surface.

In Evans *et.al*. work, involving the formation of a carboxylic acid (-COOH)-terminated thiol-SAM onto a gold surface, the subsequent binding of SiO_2 nanoparticles was demonstrated to be pH sensitive.[25] This was in regards to how well the nanoparticles adhere to the surface. The pH of the solution containing the SiO_2 nanoparticles for deposition onto the SAM surface was the determining factor. At low pH values (1 and 3) there was significant adhesion of nanoparticles onto the surface. Whereas, at high pH values (5 and 9), there was little adhesion to the surface. This was ascribed to repulsive forces acting between the resulting deprotonated COOH group and deprotonated Si-OH of the SiO_2 nanoparticles, at high pH. Our work is essentially a reversal of this process, whereby –COOH terminated thiol SAMs on copper nanoparticles interact with the SiO_2 surface. It is clear from image 5.4c that there is significant adhesion of nanoparticles onto the surface at pH 4. Contrarily, at pH 8, there is significantly less adhesion onto the surface. This may again be due to repulsive forces acting between the surface and the deprotonated COOH group of the thiol-modified copper nanoparticles.

(ii) Order of addition of thiol dependence

The order of addition of thiol into the reaction mixture was also found to have an influence on the isolated material. As copper thiolates can be resolubilised and precipitated in solution due to the ability of thiols to etch metal particles,[5, 11] it is thought that addition of the thiol, last, to the already formed copper nanowires will lead to etching of the copper surface and formation of nanoparticles. Conversely, if the thiol is added to the reaction solution concurrently with the reductant (ascorbic acid) the copper nanoparticles will be capped by thiol soon after reduction of Cu^{2+} at DNA templates, or at early stages of growth. Thus, it is suggested that wire-like structures will be the result as opposed to nanoparticles.

All experiments here are performed at pH 8, which was previously found to restrict aggregation of nanomaterial. The first set of experiments involved addition of the thiol

to the as-prepared Cu-DNA nanowires. For comparison of the resulting material, the Cu-DNA solution was divided into two halves; one half (a) was deposited onto a silicon wafer (non-thiolated Cu-DNA, see AFM figure 5.5a) and the other half (b) was subsequently reacted with the thiol for 30 minutes and deposited onto a separate silicon wafer (thiolated-Cu-DNA, figure 5.5b).

The AFM results (figure 5.5) of the two samples are quite different. For the non-thiolated Cu-DNA material (figure 5.5a), isolated nanowires are formed, with a relatively clean substrate background. This preparation is in fact identical to the one used in chapter 4 (see section 4.2.2) and the samples appear very similar. The thiolated Cu-DNA material (figure 5.5b) on the other hand, results in nanowires and an array of isolated nanoparticles on the surface. The nanoparticles in this image (b) vary in size somewhat between ~5 and 20 nm in height and appear to deposit randomly across the substrate background. The formation of individual nanoparticles subsequent to the addition of the thiol may suggest that the copper surface of the nanowire is etched by thiol. The nanowire in this image varies in height from top to bottom (~35 nm at the top and ~15 nm at the bottom); an effect of the wire protruding from an evaporated drying mark (where the wires become thinner the further they are from the edge of the deposit).

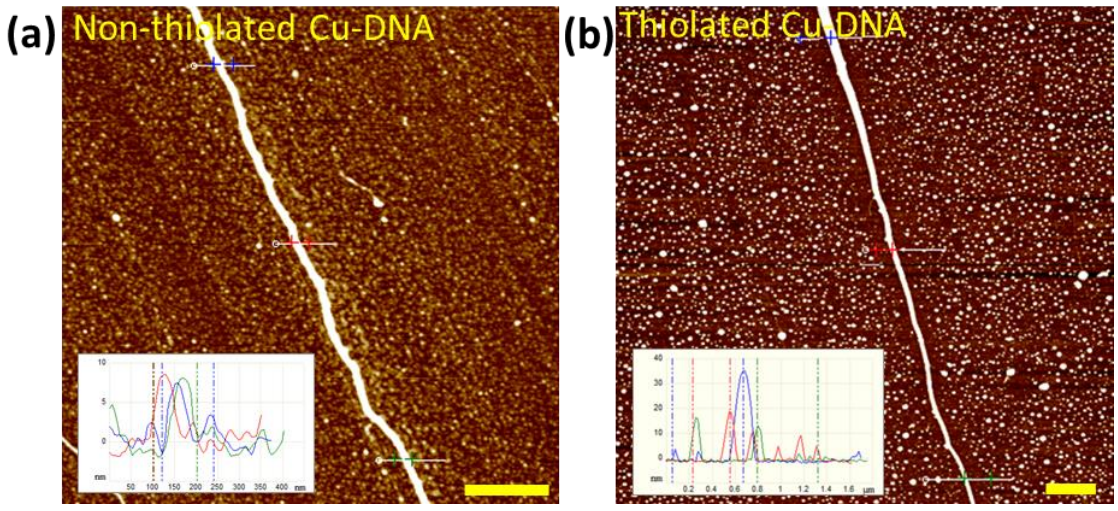

Figure 5.5: AFM height images of (a) Cu-DNA nanowire formed in the absence of thiol and (b) Cu-DNA nanowire formed in the presence of thiol (pH8). Height scales= 10 nm, scale bars = 500 nm (a) and 1000 nm (b). Insets show height profiles over nanowire

When the reaction is performed by addition of all the reagents at once (i.e. thiol is added to the Cu^{2+}/DNA mixture concurrently with ascorbic acid), individual nanowire formation is observed and, importantly, a negligible amount of non-templated material

(see figure 5.6 below) is generated. This suggests that most of the thiolate protected copper nanoparticles remain bound to the template. Under these conditions, the assembly of thiol molecules on the surface of copper occurs directly after the reduction of copper ions on DNA, thereby capping the seeds and suppressing the size of nanoparticles grown. The effect may be increased when the thiol concentration is in excess to the metal, as is used here, which will result in a smaller mean size of nanoparticles.[22]

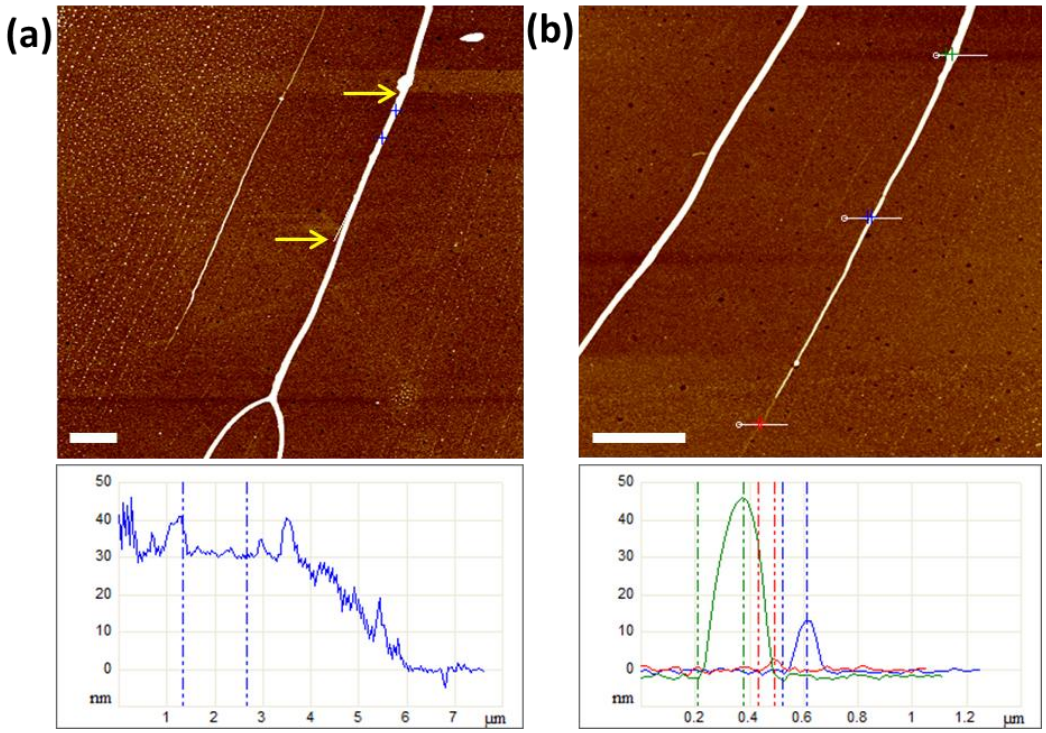

Figure 5.6: AFM height images (a and b) of thiolated-Cu-DNA nanowires aligned on the surface by combing. Aggregation of structures is limited due the increased pH and nanoparticle formation is limited by correct order of addition of thiol to the reaction. Height scales= 10 nm (a) and 20 nm (b). Scale bars= 2 µm.

Figure 5.6 shows AFM images of the thiolated-Cu-DNA nanowires, prepared under these conditions (as described in experimental section 5.2.1.), whereby the anionic form of the thiol is added concurrently with ascorbic acid to the reaction solution. The AFM data shows the resulting nanowires to be smooth and continuous in morphology. For the nanowire shown in figure 5.6a a height profile was recorded along a section of the structure. The height profile indicates uniform structure morphology in the range 30-40 nm, with respect to the substrate background at 0 nm. There are regions where the height changes abruptly as indicated by sharp peaks in the profile where substantial growth or aggregation has occurred at these regions.

The AFM image in figure 5.6b shows two aligned nanowires; the nanowire to the left is particularly smooth indicating well-ordered growth of the Cu-thiolate SAM on DNA, whereas the structure to the right shows a gradual decrease in structure height from top to bottom. The green, blue and red cross sections indicate decreasing heights of 48.1 nm, 13.9 nm and 3.4 nm, respectively. The latter measurement at 3.4 nm (marked by line with red crosshairs in figure 5.6 b) could indicate that DNA is uncoated at this region (or coated to a small degree). Further up the image however, the nanostructure is more heavily coated suggesting a thicker 'thiol-SAM' on copper. A varying height profile along the structure length, as observed here, was also observed in other Cu-DNA based samples, whereby the method of nanowire deposition was identical (dropcast). This phenomenon may be explained based on the idea that bare DNA provides an 'anchoring point' to the silicon surface, due to its high charge, as the meniscus edge of the solution droplet recedes during evaporation.

5.3.2. Determination of particle size by Dynamic Light Scattering (DLS)

Dynamic Light Scattering (DLS) is used here to determine the mean particle size of thiol-capped copper nanoparticles formed at thiol pH ~4.3 and adjusted pH ~8.0. DLS is a method commonly used to analyse the particle size distribution of particles suspended in a dilute solution. The technique is based on the idea that monochromatic light scatters off the particles in all directions (Rayleigh scattering) whilst the particles undergo random Brownian motion in solution. The signal intensity received is a time-dependent variable, which can be analysed by mathematical models to provide information on particle size and particle size distribution, which is related to the polydispersity index (PdI).

In this experiment, two dispersions in water were prepared at dilute concentrations: (a) containing thiolate-protected CuNP's (pH 4.3) and (b) containing deprotonated thiolate-protected CuNP's (pH ~8.0). The results are displayed by size distribution analysis of intensity (%) to particle size (nm) (see figure 5.7). The average particle radii of dispersion (a) was calculated to be 363 nm (PdI= 0.158) based on a monomodal distribution (shown in black). The value obtained, along with information provided by AFM in section 5.3.1, indicates a highly aggregated assembly of nanoparticles.

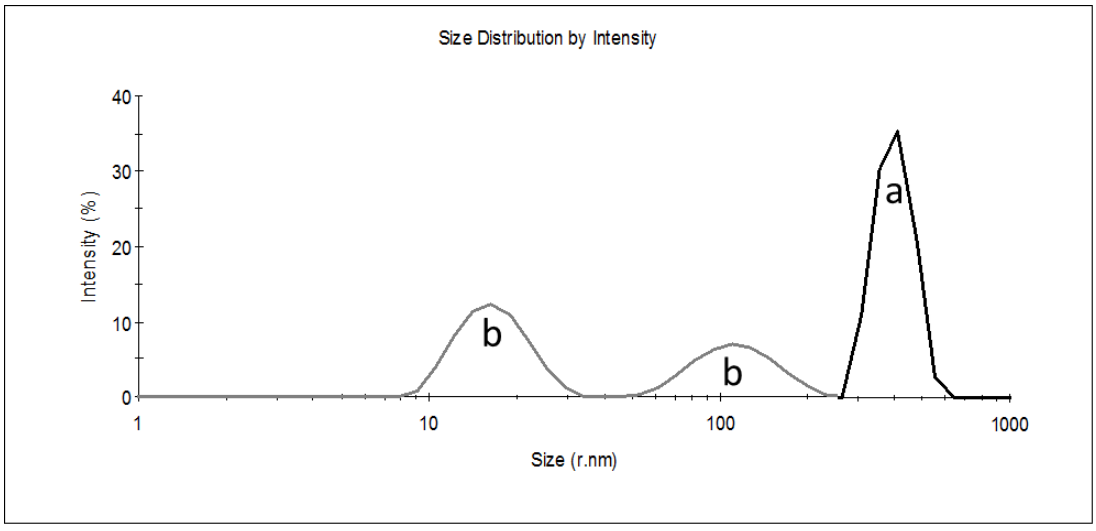

Figure 5.7: Size distribution by intensity of dispersion 'a' (black line) and dispersion 'b' (grey line)

For dispersion (b) a value of 30.9 nm (PdI= 0.383) was obtained. In this analysis a bimodal distribution (shown in grey) of particle sizes was obtained as shown by two distinct peaks centred on ~15 nm and ~100 nm. The smaller value may comprise single nanoparticles and the larger value may comprise a cluster of nanoparticles. The average

particle radius is based on analysis of both of these peaks. For a monodisperse sample a PdI value of 0.1 or lower is expected. However, both PdI values obtained here are higher than 0.1 and the peak widths are quite large, suggesting a high degree of polydispersity for each sample.

The results indicate a substantial reduction in the particle size when the pH of the solution is increased. The DLS data is in good agreement with the AFM data which showed that flocculation of nanoparticles occurred to give larger aggregations, the formation of which was subsequently restricted by increasing the pH. A high polydispersity in particle size was also observed in the AFM data.

5.3.3. X-ray Photoelectron Spectroscopy (XPS) studies

XPS is used as a tool here to elucidate the composition of *para*-mercaptobenzoic acid modified Cu-DNA nanowires. It is expected that the Cu(I)-thiolate interface is formed from assembly of thiol on copper. The corrosion resistance of the SAM is also examined by analysis of the Cu2p region to identify the presence of copper oxidation species, or lack thereof.

The following data presented is for the thiolated-Cu-DNA nanowires formed using pH adjusted thiol solutions (pH 8) as part of a one-pot reaction procedure (see section 5.2.1 for experimental details). The material was deposited onto a clean silicon wafer by drop cast to leave a thin coated film/network of nanowires on the surface.

The DNA template was identified by analysis of the P2p spectra. This showed the presence of a single species which could be fitted to a doublet at $P2p_{3/2}$ 134.0 eV (split by 0.87 eV) owing to the phosphate groups in DNA. This is consistent with examples in the literature.[6, 26]

As can be seen from the Cu2p spectrum shown below (figure 5.8) the near symmetrical Cu2p doublet is observed with a slight shouldering of the spectral envelope towards the higher binding energy side. The shape of the spectrum seems to indicate the presence of a single majority component and a minor secondary component. The $Cu2p_{3/2}$ lines are fitted to 932.8 eV and 934.9 eV which are attributable to the presence of metallic copper and copper(II) hydroxide, respectively.[2, 27] Both splitting values are consistent with metallic copper (19.8 eV) and oxidised copper; Cu^{2+} (20.0 eV). Copper hydroxide was

also identified in the O1s spectrum at 531.6 eV, which agrees with another report.[2] Several other metal hydroxides are found near to this value, including $Ni(OH)_2$.[28]

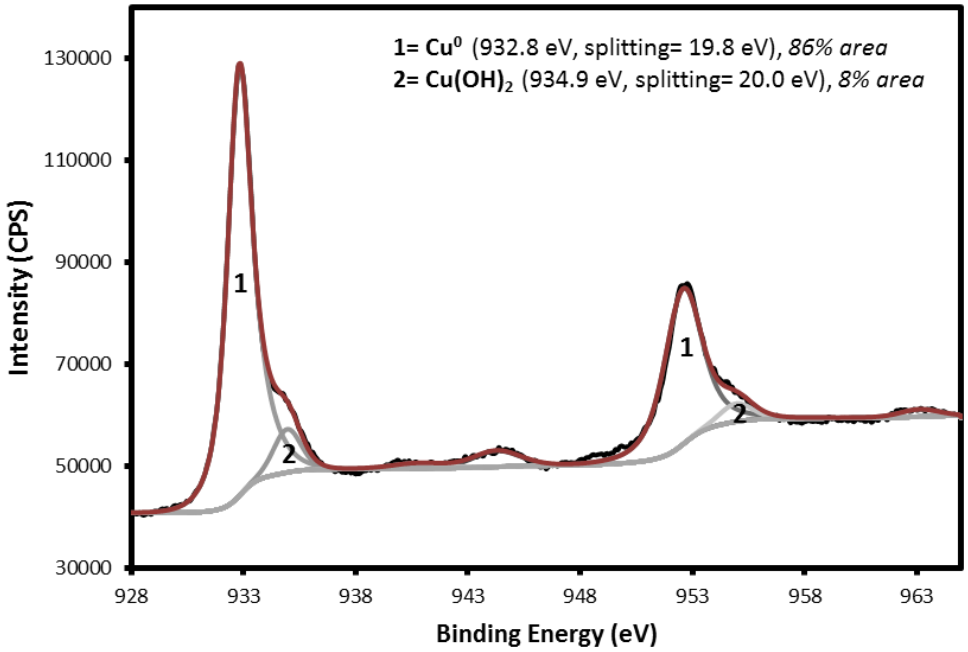

Figure 5.8: Cu2p XPS spectrum of thiolate-Cu-DNA on silicon. Doublet formation is observed primarily for copper metal and copper hydroxide to a small extent

The atomic composition for the whole Cu2p doublet region containing copper and copper hydroxide were determined from the 'CasaXPS' software at 86% and 8%, respectively, a ratio of ~11:1 Cu: $Cu(OH)_2$. Comparing this ratio to that obtained for the non-thiolated Cu-DNA nanomaterial in Chapter 4, which was ~1:1, indicates that the formation of copper hydroxide has reduced significantly in the presence of thiol and virtually pure copper has formed. There is also an almost complete loss of the Cu^{2+} "shake-up" peak centred on ~945 eV. This peak disappearance was reported in the literature for alkanethiol adsorption on oxidised copper surfaces, showing that thiols act to remove oxide residue.[13] These results reveal that the oxidation of copper on DNA is significantly reduced by the presence of thiol in solution.

The chemical nature of the thiol adlayer on copper was determined by analysis of the S2p region (figure 5.9).

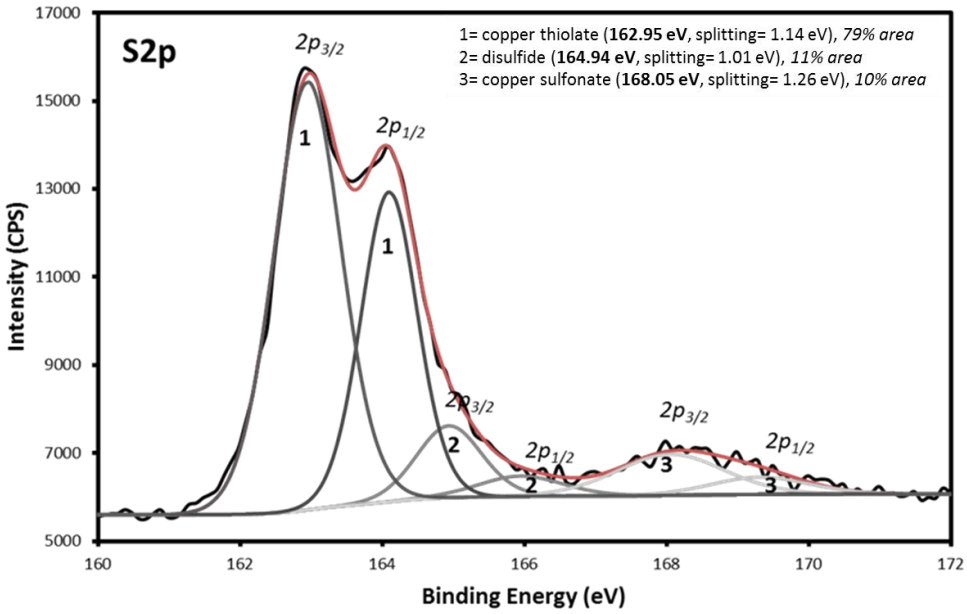

Figure 5.9: S2p XPS spectrum of thiolate-Cu-DNA on silicon. Three doublets are fitted to the spectrum for copper thiolate, copper sulfonate and disulfide. The thiolate adlayer is the main species present and oxidised sulfur species are minor components

All fitted peaks in this region ought to be due to the thiol as this is the only source of sulfur in the sample. Three sets of doublets were fitted to the spectrum. The major form of sulfur on copper was identified to be copper-thiolate ($Cu(I)SC_6H_4COO^-$) at binding energy 162.9 eV ($S2p_{3/2}$) and splitting value of 1.14 eV, which is consistent with other literature values.[1, 9, 19] Integration of the copper thiolate doublet area reveals a 79% composition of sulfur in this form.

There is a slight shouldering of the main doublet which indicates the presence of an additional component between 164-167 eV. This was fitted as a spin-orbit doublet at binding energy 164.9 eV ($2p_{3/2}$) and is attributed to disulphide ($HOOC\text{-}C_6H_4S)_2$ (see chemical structure in figure 5.1).[29] Despite being an unwanted side-product of the reaction, the disulfide constitutes only a small proportion of sulfur-containing product in the sample (~11%). A reduction in the degree of surface copper hydroxide formation (compared to nanowires formed in chapter 4) and the presence of oxidised sulfur may suggest that the two events are related.[16]

A third doublet is also observed, well separated from the remainder of the spectrum at $Cu2p_{3/2}$ 168.1 eV with a splitting value of ~1.26 eV. This is attributable to copper sulfonates,[4] indicating that a small amount of thiolate (~10%) is oxidised from oxidation state S(II) to the sulfonate (RSO_2^-) which has oxidation state S(VI). The co-existence of

copper sulfonate and copper thiolate has often been reported in the literature.[3, 4] We have shown that the presence of copper thiolate has coincided with an increase in the % composition of metallic copper and a decrease in the % composition of copper hydroxide in the sample. Indeed, it has been reported that the oxidation of sulfur occurs on the surface of copper/copper oxide and thus reduces higher oxidation state copper species to elemental copper at the same time.[9] These findings support the assessment made in the literature, which suggests that the reduction of copper, formation of Cu(I) thiolate and the oxidation to sulfonates are all related events.[4] In a sense, thiols can act to reduce copper. The effect in our studies is likely to be enhanced by the presence of ascorbic acid.

A similar idea was proposed by Laibinis and Whitesides in their work involving alkanethiol stabilised copper films.[9] It was shown that thiols play a role in the reduction of Cu(II). Indeed this explains the presence of disulfides in their sample, which are oxididation by-products of thiol following the reduction of Cu(II) by thiol. Sung *et.al*. proposed a mechanism for the reduction of CuO films by thiols and the subsequent oxidation of the thiol to disulphide.[13] Earlier work by Keller *et.al* proposed the same redox chemistry.[16] In this work it is claimed that thiols do not adsorb directly onto the oxidised surface, but reduce the surface oxide first forming disulphide in the process:

$$2HSR + CuO \rightarrow (SR)_2 + Cu + H_2O \quad \textbf{(1)}$$

Or for $Cu(OH)_2$ overlayer on copper we propose:

$$2HSR + Cu(OH)_2 \rightarrow (SR)_2 + Cu + 2H_2O \quad \textbf{(2)}$$

The thiolate monolayer can then form on the pure copper surface, likely by oxidative addition of the S-H bond and then reductive elimination of hydrogen, as in the formula:

$$HSR + Cu(0) \rightarrow RSCu + 1/2H_2 \quad \textbf{(3)}$$

The presence of sulfonate (as indicated by XPS) in these current studies are likely to form by oxidation of the thiolate in air. Another study reveals that the oxidised sulfur species (also identified as sulfonates) are easily displaced from the surface and are replaced by thiol molecules in the solution to re-form the copper thiolate adlayer.[8]

It is clear from the Cu2p and S2p data obtained here that thiol adsorption onto the copper surface (i) removes the copper hydroxide overlayer and/or (ii) prevents (to some extent) the oxidation from taking place in the first place. It is reasoned here that the

latter explanation is more likely since the thiol adsorption on copper nanoparticles occurs immediately after their formation, meaning that copper metal is passivated. The small amount of oxidised sulfur in the form of disulfides indicates that the thiol may indeed act to reduce copper hydroxide. As only a small amount of copper hydroxide was observed in the sample, compared to that previously observed for the non-thiolated Cu-DNA in chapter 4, it indicates the effectiveness of the thiol to passivate the copper surface.

In conclusion the thiol SAM is formed on the surface of the copper metal affording the Cu(I) thiolate self-assembled monolayer. This serves to reduce the oxidation of copper by forming a barrier layer between the copper and oxygen interface.

5.3.4. Electrostatic Force Microscopy (EFM) Studies

EFM is used to establish if the Cu-DNA nanowires remain conductive following the assembly of thiolate. EFM theory allows one to ascertain if the valence electrons are mobile and can spread along the whole portion of the nanostructure under investigation (i.e. a current can flow) or the electrons polarise directly beneath the tip, as in the case of an insulator. The sign of the phase shift ($\Delta\theta$) can distinguish between these two possibilities; for a conductor a negative $\Delta\theta$ is expected with respect to the sample background and positive $\Delta\theta$ for an insulator. The EFM experiment performed here is qualitative and will therefore not give information relating to the magnitude of conductance.

A sample of nanowires was prepared as described in section 5.2.1 and deposited upon a TMS-modified Si/SiO_2 (200 nm) substrate by combing. Thiol-protected Cu-DNA nanowires were found by standard "TappingMode^{TM}" AFM in topography mode (see AFM figure 5.10, left). The nanowires lie parallel to one another resulting from the uniform withdrawal direction of the droplet CuNW suspension. A phase image was recorded (see figure 5.10, right) by scanning the metal coated AFM tip across the surface at a set lift height (70 nm) whilst the sample was under bias in the range -10 to +10 V.

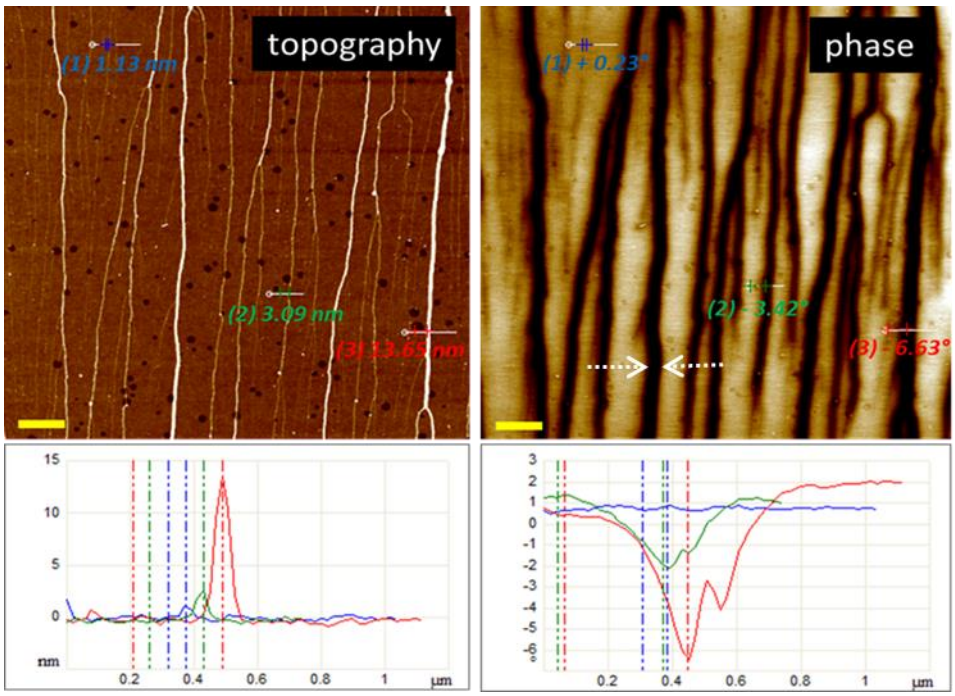

Figure 5.10: EFM topography image (left) and phase image (right) of aligned thiolate-Cu-DNA nanowires on a TMS-modified Si/SiO_2 substrate, with corresponding height and phase profiles shown underneath (colour coded). Phase map obtained at -10 V applied bias. Height scale= 10 nm, phase scale= 5°, scale bars= 1000 nm

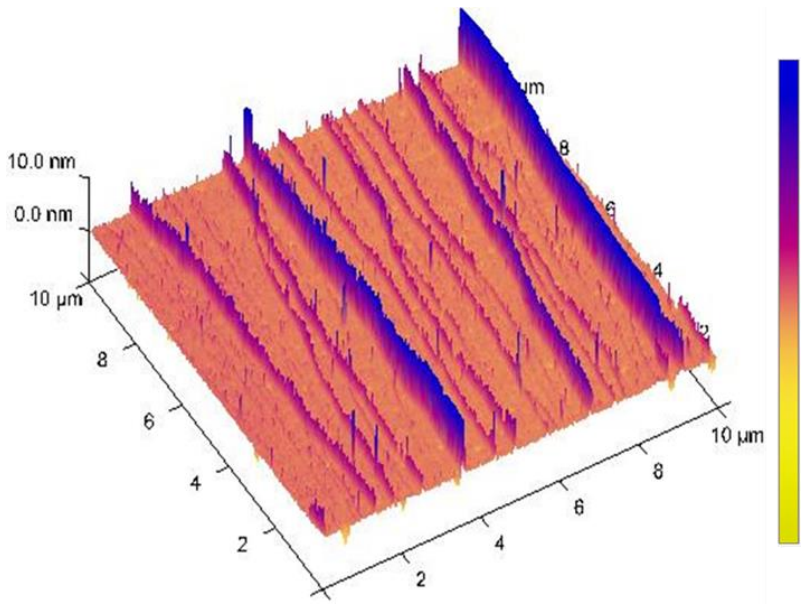

Figure 5.11: 3-D image of nanowires from figure 5.10

It is clear from the topography image (figure 5.10, left) that not all of the wires are the same size in height and there is a varied amount of coverage along the length of the DNA strands; the 3D representation of the topography image (see figure 5.11 above) is

able to show this more clearly. This is useful as it allows comparison of well-coated DNA strands (large height) with less well coated DNA strands (small height). One would expect to obtain positive phase shifts where regions of bare DNA are exposed (insulating) compared to negative phase shifts where DNA is coated with copper metal (conducting). Additionally, one would expect to see higher magnitude negative phase shifts for thicker metallised DNA nanowires, and indeed, both of these characteristics were observed.

A cross-section was taken across three nanostructures of varying heights. The blue, green and red cross-sections in figure 5.10 gave nanostructure heights of (1) 1.13 nm, (2) 3.09 nm and (3) 13.65 nm, respectively. The first of these measurements is in accordance with the height of bare DNA. The corresponding phase profile at this intersect gives a small positive phase shift of 0.23° (1) as expected for a structure of high resistivity such as DNA.[30] The second intersect in green giving a nanostructure height of 3.09 nm (2) is indicative of DNA with low metal coverage and expectedly gives a corresponding negative phase shift (– 3.42° (2)) as signified by the dark contrast. For the nanostructure of the largest height, 13.65 nm (3), the phase shift is also negative and predictably the largest at -6.63° indicating that the conductance and/or capacitance is higher for the thicker nanowire.

For further analysis, a range of direct current (dc) voltages from -10 V to +10 V was applied in 2V steps as the tip scanned across the surface. For determination of $\Delta\theta$ a single step profile was taken across a chosen nanowire at the same position for each voltage step (indicated by dotted arrows in the phase image, figure 6.10). The height of the nanowire at this position is ~8.8 nm. This is a suitable nanowire for EFM analysis due to its typical size and smooth morphology.

Figure 5.12 shows three phase images collected at 10 V, 0 V and -10 V. The phase shift data shows that we obtain zero $\Delta\theta$ across the nanowire at zero bias, as predicted by EFM theory.[31, 32] At positive and negative bias, negative phase shifts are observed across the nanowire with respect to the background. Negative $\Delta\theta$ is observed along the entire length of the nanowires, signifying a viable current pathway. The inset figures show the phase profile cross section (blue line) which provides a quantitative value of $\Delta\theta$ in degrees. Measuring $\Delta\theta$ of the nanowire for each voltage applied to the sample provides a series of data (see figure 5.13) with parabolic dependence, also predicted

from EFM theory. The graph of tan(Δθ) vs. voltage (figure 5.13) shows a negative parabolic shape which is attributable to a conductive nanowire.

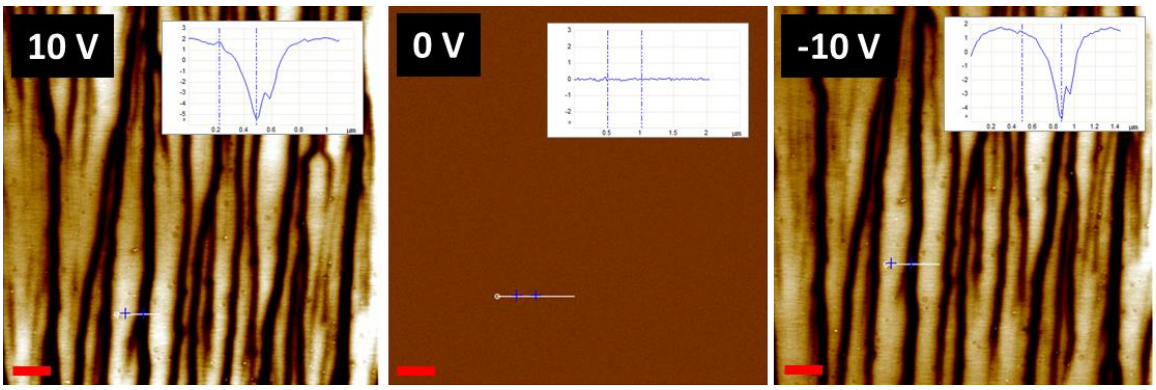

Figure 5.12: EFM phase maps of thiolate-Cu-DNA nanowires obtained at applied biases of 10V, 0V and -10V (from left to right). Cross sections (white line with blue cross hairs) denote the point of measurements. Insets show the corresponding phase profiles across the nanowire. Negative phase shift behaviour is observed at all non-zero bias. Phase scales= 5°, scale bars= 1000 nm

bias (V)	Δθ (deg)	Δθ (rad)	tan(Δθ)
-10	-6.270	-0.109	-0.110
-8	-3.873	-0.068	-0.068
-6	-1.769	-0.031	-0.031
-4	-0.890	-0.016	-0.016
-2	-0.187	-0.003	-0.003
0	0	0	0
2	-0.132	-0.002	-0.002
4	-0.679	-0.012	-0.012
6	-1.729	-0.030	-0.030
8	-3.627	-0.063	-0.063
10	-7.279	-0.127	-0.128

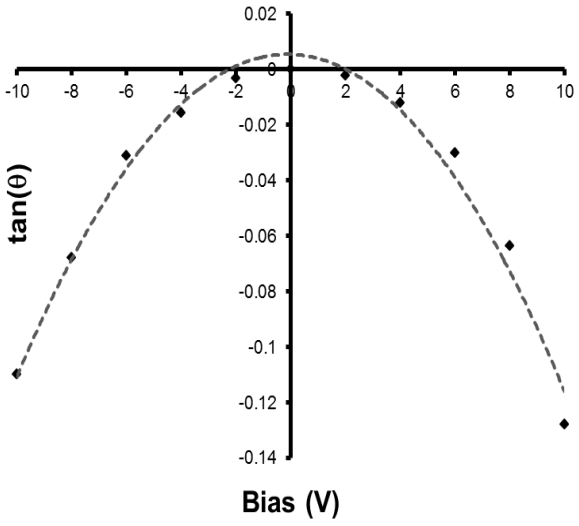

Figure 5.13: (left) Table of phase shift values at different applied biases and (right) plot of tan(Δθ) against bias. Solid points represent real data points and dotted line is a second-order polynomial best fit. Negative parabolic dependence confirms conductive nature of nanowire

The technique has confirmed that the thiol-protected Cu-DNA nanostructures are conductive. The dependence on structure height to the magnitude of the phase shift was also demonstrated. Bare DNA was confirmed as non-conductive but larger nanostructures (with presumably templated metal) are conductive. Quantification of conductance is not possible using this technique. We therefore seek to address this question by use of a quantitative method for mapping conductance in C-AFM.

5.3.5. Determination of conductivity using Conductive-AFM (C-AFM)

A sample of nanowires was deposited onto the silicon oxide surface using the drop cast technique. This left a drying stain on the surface following evaporation of the solution. Nanowires could be found to extend from the periphery of the macrodeposit using contact mode AFM. When a bias is applied to the sample, during contact between the AFM tip and the sample, current was observed to flow along the nanowires.

Figure 5.14 shows an optical image of the material on the surface. The macrodeposit is shown to the top left of the image where wires are seen to extend from. Smaller nanowires are often found to lie between the visible 1-D structures on the surface. Figure 5.15 shows two images of nanowires imaged using different feedback loops (deflection and current). The deflection error image in figure 5.15a reveals the smooth morphology of the nanowires. Towards the top of the image the wire appears thicker as it approaches the point of extension from the macrodeposit. The largest wire has an average measured height of 37.8 nm based on 10 individual measurements along the length. The wires branching off have heights of ~5-10 nm. These smaller nanowires were more easily displaced from the surface or cut by the shear stress applied to the nanowire by the movement of the AFM tip. Therefore the larger nanowire was chosen for electrical analysis due to its stability during imaging.

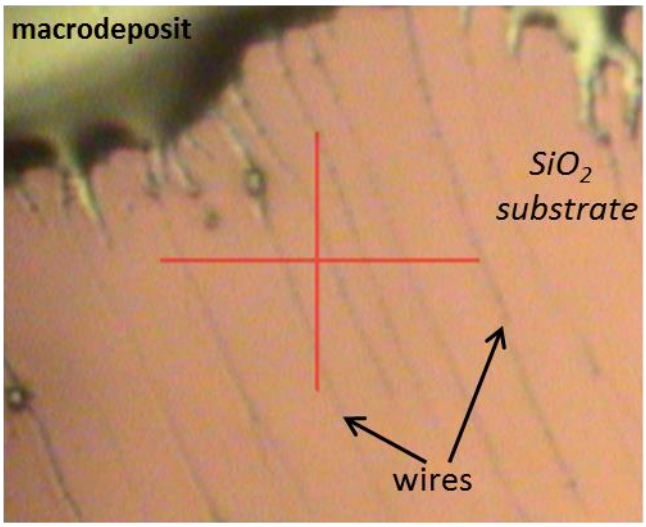

Figure 5.14: Image showing protrusion of wires from the main macrodeposit on a TMS-modified silicon oxide substrate. The material was deposited by the drop cast technique where a dispersion of nanowires was evaporated upon the surface. Image obtained using the in-built AFM camera lens.

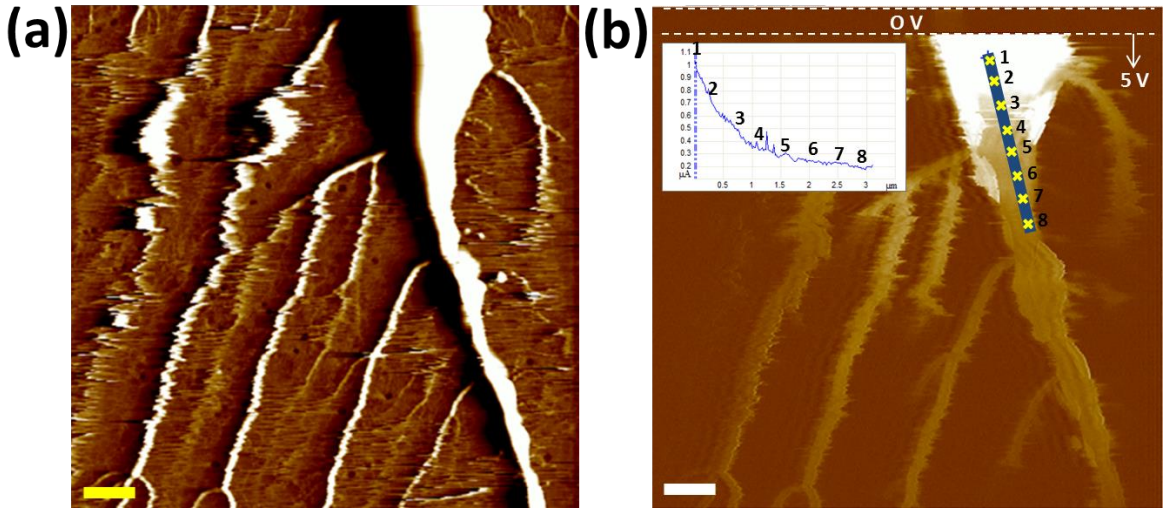

Figure 5.15: C-AFM analysis of thiol-protected copper nanowires aligned on a TMS-modified silicon oxide substrate. (a) Deflection error image of nanowires extending downwards from the macrodeposit, (b) current image of same scan area showing continuous current pathways along the wires. Line trace (blue) was recorded to show change in detected current as the wire extends from the macrodeposit and corresponding current profile is shown (inset). Points 1-8 indicate the contact position of the metallised AFM tip with the nanowire for acquisition of i-V curves and resistance measurements. Current was obtained at a 5V bias. A 0V bias was applied for the first few scan lines to show that no current is detected. Scale bars= 1 µM, data scales= (a) 10 nm (height) and (b) 1 µA (current)

The current image (figure 5.15b) demonstrates that when no bias is applied (0V) there is no current, as expected. Upon application of a bias (5V) to the sample, current signals (bright contrast) are detected along the length of the large wire as well as the smaller wires branching off it. The detected currents were in the range 100 nA – 1 µA+. The SiO_2 background appears dark as this is non-conducting. The leftmost wire in image (a) however does not appear to carry any current as this has been heavily damaged by the AFM tip.

A line trace was recorded along a 3 µm stretch of the thickest wire in the current image. As can be seen in the current profile (inset) the current decreases further down the nanowire and there is a particularly steep current drop-off between points 1 and 3. Visual inspection of the image shows a clear change from bright contrast (points 1 and 2) to a lighter contrast (points 3-8). Points 1 and 2 are approaching the edge of the macrodeposit where the resistance is assumed to be negligible due to the high density of conductive material.

By measuring the resistance at each point 1-8 and plotting these values against the relative distance along the wire (relative to point 1) the resistivity of the nanowire is determined due to the linear relationship between the total resistance and distance:

$$R_{(tot)} = R_{(contact)} + (\rho/A).x \qquad \textbf{(Equation 5.1)}$$

$R_{(tot)}$= total resistance in circuit (VA^{-1} or Ω), $R_{(contact)}$= tip/wire contact resistance (VA^{-1} or Ω), ρ= resistivity of wire (Ω.cm), A= cross-sectional area of wire (cm^2), x= relative distance along the wire from edge of macrodeposit (cm)

Based on the assumption that point 1, at the edge of the macrodeposit, carries zero resistance then the size of the intercept of the graph, resistance vs. distance, is equal to the contact resistance. Regardless of the assumption however, the gradient of the graph is equal to the resistivity over cross-sectional area (of nanowire). To measure the resistance of the wire at each point, a current-voltage (i-V) plot was recorded between -3 and +3 V.

Figure 5.16 shows the graph of resistance against relative distance. A linear relationship was observed indicating conducting behaviour in the nanowire.

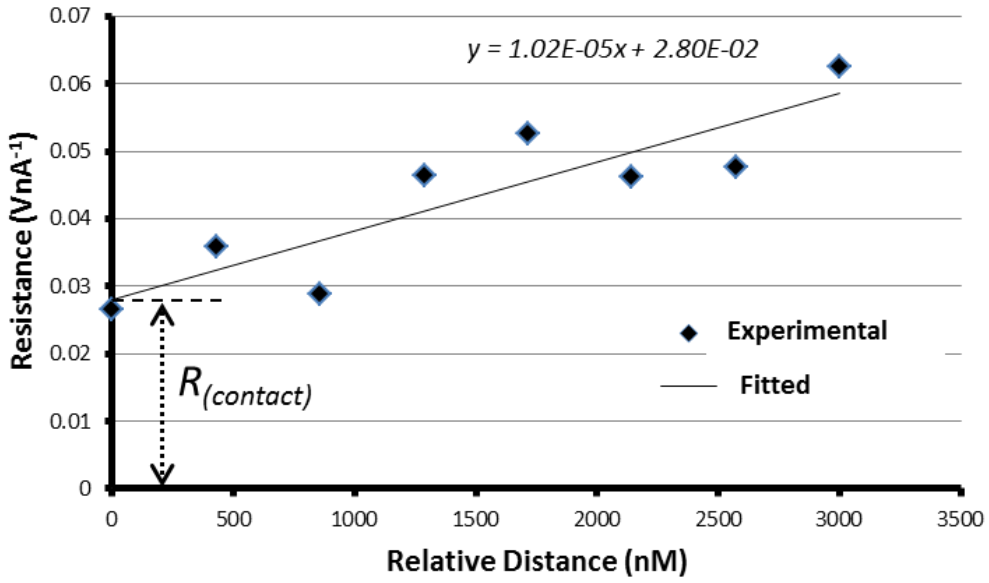

Figure 5.16: Graph of measured resistance against relative distance along the nanowire from the macrodeposit. Resistance was determined from a series of i-V measurements along the nanowire. Line of best-fit indicates a linear relationship for the data-set. Large intercept indicates a significant contribution of contact resistance

A line of best fit was fitted to the data. The gradient of the line was 1.02 $x10^4$ Ω nm^{-1} (with standard error on the slope equal to ±0.006), which is equal to the resistivity divided by the cross-sectional area of the nanowire. Based on the assumption that the wire adopts an ideal cylindrical shape, multiplying the gradient by the cross-sectional

area of the nanowire (9.74 x10^{-6} nm^2), gave a resistivity value of 0.93 Ω cm. In terms of conductivity, the value is equal to 1.01 S cm^{-1}. The intercept value is 28 MΩ ± 4 which indicates a significant contribution from the contact resistance ($R_{contact}$) between the metallised tip and nanowire.

The conductivity of the nanowire is only slightly higher than that measured for the non-thiolated copper nanowire in chapter 4 (0.94 S cm^{-1}). Yet the distance dependence graph obtained here has a significantly lower standard error on the slope indicating more ohmic behaviour. However due to the estimated error (10 %) on the calculated conductivity values, both values can be considered as close to 1 S cm^{-1} and are essentially the same. This would indicate that there was no improvement in the conductivity of the Cu-DNA nanowires prepared in chapters 3 and 4.

5.4. Conclusions

DNA-copper nanowire surfaces were successfully modified by self-assembly of the aromatic thiol, para-mercaptobenzoic acid, to form the Cu(I)-thiolate interface. These structures were suitably protected from oxidation of copper in aqueous solvent and to some extent the thiol was shown to act as a reducing agent for copper hydroxide to metallic copper. The resulting nanowires were found to be highly continuous by AFM and they remained conductive following thiolation. For preparation of thiol-protected copper nanowires it was found that the choice of pH and order of addition of thiol to the reaction mixture influenced the structural nature of product (i.e. nanoparticles or nanowires). For formulation of high purity thiolated-nanowires, the carboxylic acid group of the thiol must be deprotonated prior to use and should be present in the reaction solution during the reduction of copper nitrate on DNA.

5.5. References

1. V. Di Castro, M. Beccari, F. Bruni, F. Caprioli and F. Decker, Comparison of the protective effect of aromatic thiols adsorbed on copper. *Surface and Interface Analysis*, 2010, **42**, 601-604.
2. I. Platzman, R. Brener, H. Haick and R. Tannenbaum, Oxidation of polycrystalline copper thin films at ambient conditions. *Journal of Physical Chemistry C*, 2008, **112**, 1101-1108.
3. C. M. Whelan, M. Kinsella, H. M. Ho and K. Maex, Corrosion Inhibition by Thiol-Derived SAMs for Enhanced Wire Bonding on Cu Surfaces. *Journal of the Electrochemical Society*, 2004, **151**, B33-B38.
4. P. G. Ganesan, A. Kumar and G. Ramanath, Surface oxide reduction and bilayer molecular assembly of a thiol-terminated organosilane on Cu. *Applied Physics Letters*, 2005, **87**.
5. S. R. Johnson, S. D. Evans and R. Brydson, Influence of a terminal functionality on the physical properties of surfactant-stabilized gold nanoparticles. *Langmuir*, 1998, **14**, 6639-6647.
6. C. Y. Lee, P. Gong, G. M. Harbers, D. W. Grainger, D. G. Castner and L. J. Gamble, Surface coverage and structure of mixed DNA/Alkylthiol monolayers on gold: Characterization by XPS, NEXAFS, and fluorescence intensity measurements. *Analytical Chemistry*, 2006, **78**, 3316-3325.
7. S. Frey, V. Stadler, K. Heister, W. Eck, M. Zharnikov, M. Grunze, B. Zeysing and A. Terfort, Structure of thioaromatic self-assembled monolayers on gold and silver. *Langmuir*, 2001, **17**, 2408-2415.
8. M. Whitley, M. Newton, G. McHale and N. Shirtcliffe, The self assembly of superhydrophobic copper thiolate films on copper in thiol solutions. *Zeitschrift fur Physikalische Chemie*, 2012, **226**, 187-200.
9. P. E. Laibinis and G. M. Whitesides, Self-assembled monolayers of n-alkanethiolates on copper are barrier films that protect the metal against oxidation by air. *Journal of the American Chemical Society*, 1992, **114**, 9022-9028.
10. M. Brust and C. J. Kiely, Some recent advances in nanostructure preparation from gold and silver particles: A short topical review. *Colloids and Surfaces A: Physicochemical and Engineering Aspects*, 2002, **202**, 175-186.
11. J. C. Love, L. A. Estroff, J. K. Kriebel, R. G. Nuzzo and G. M. Whitesides, Self-assembled monolayers of thiolates on metals as a form of nanotechnology. *Chemical Reviews*, 2005, **105**, 1103-1169.
12. M. E. Toimil Molares, E. M. Höhberger, C. Schaeflein, R. H. Blick, R. Neumann and C. Trautmann, Electrical characterization of electrochemically grown single copper nanowires. *Applied Physics Letters*, 2003, **82**, 2139-2141.
13. M. M. Sung, K. Sung, C. G. Kim, S. S. Lee and Y. Kim, Self-Assembled Monolayers of Alkanethiols on Oxidized Copper Surfaces. *Journal of Physical Chemistry B*, 2000, **104**, 2273-2277.
14. M. J. Tarlov, D. R. F. Burgess Jr and G. Gillen, UV photopatterning of alkanethiolate monolayers self-assembled on gold and silver. *Journal of the American Chemical Society*, 1993, **115**, 5305.
15. V. S. Dilimon, J. Denayer, J. Delhalle and Z. Mekhalif, Electrochemical and spectroscopic study of the self-assembling mechanism of normal and chelating alkanethiols on copper. *Langmuir*, 2012, **28**, 6857-6865.
16. H. Keller, P. Simak, W. Schrepp and J. Dembowski, Surface chemistry of thiols on copper: An efficient way of producing multilayers. *Thin Solid Films*, 1994, **244**, 799-805.
17. G. K. Jennings, J. C. Munro, T. H. Yong and P. E. Laibinis, Effect of chain length on the protection of copper by n-alkanethiols. *Langmuir*, 1998, **14**, 6130-6139.

18. G. K. Jennings, T. H. Yong, J. C. Munro and P. E. Laibinis, Structural effects on the barrier properties of self-assembled monolayers formed from long-chain ω-alkoxy-n-alkanethiols on copper. *Journal of the American Chemical Society*, 2003, **125**, 2950-2957.
19. C. Schmidt, J. Götzen and G. Witte, Temporal evolution of benzenethiolate SAMs on Cu(100). *Langmuir*, 2011, **27**, 1025-1032.
20. Y. Tai, A. Shaporenko, H. T. Rong, M. Buck, W. Eck, M. Grunze and M. Zharnikov, Fabrication of thiol-terminated surfaces using aromatic self-assembled monolayers. *Journal of Physical Chemistry B*, 2004, **108**, 16806-16810.
21. S. Y. Heriot, H. L. Zhang, S. D. Evans and T. H. Richardson, Multilayers of 4-methylbenzenethiol functionalized gold nanoparticles fabricated by Langmuir-Blodgett and Langmuir-Schaefer deposition. *Colloids and Surfaces A: Physicochemical and Engineering Aspects*, 2006, **278**, 98-105.
22. M. J. Hostetler, J. E. Wingate, C. J. Zhong, J. E. Harris, R. W. Vachet, M. R. Clark, J. D. Londono, S. J. Green, J. J. Stokes, G. D. Wignall, G. L. Glish, M. D. Porter, N. D. Evans and R. W. Murray, Alkanethiolate gold cluster molecules with core diameters from 1.5 to 5.2 nm: Core and monolayer properties as a function of core size. *Langmuir*, 1998, **14**, 17-30.
23. M. Brust, J. Fink, D. Bethell, D. J. Schiffrin and C. Kiely, Synthesis and reactions of functionalised gold nanoparticles. *Journal of the Chemical Society, Chemical Communications*, 1995, 1655-1656.
24. W. P. Dow, G. L. Liao, S. E. Huang and S. W. Chen, Modification of Cu nanoparticles with a disulfide for polyimide metallization. *Journal of Materials Chemistry*, 2010, **20**, 3600-3609.
25. J. Bowen, M. Manickam, S. D. Evans, K. Critchley, K. Kendall and J. A. Preece, The pH-dependent adhesion of nanoparticles to self-assembled monolayers on gold. *Thin Solid Films*, 2008, **516**, 2987-2999.
26. D. Y. Petrovykh, H. Kimura-Suda, M. J. Tarlov and L. J. Whitman, Quantitative Characterization of DNA Films by X-ray Photoelectron Spectroscopy. *Langmuir*, 2004, **20**, 429-440.
27. J. Hernandez, P. Wrschka and G. S. Oehrlein, Surface Chemistry Studies of Copper Chemical Mechanical Planarization. *Journal of the Electrochemical Society*, 2001, **148**, G389-G397.
28. N. S. McIntyre and M. G. Cook, X-RAY PHOTOELECTRON STUDIES ON SOME OXIDES AND HYDROXIDES OF COBALT, NICKEL, AND COPPER. *Analytical Chemistry*, 1975, **47**, 2208-2213.
29. O. J. Furlong, B. P. Miller, Z. Li, J. Walker, L. Burkholder and W. T. Tysoe, The surface chemistry of dimethyl disulfide on copper. *Langmuir*, 2010, **26**, 16375-16380.
30. C. Gómez-Navarro, F. Moreno-Herrero, P. J. De Pablo, J. Colchero, J. Gómez-Herrero and A. M. Baró, Contactless experiments on individual DNA molecules show no evidence for molecular wire behavior. *Proceedings of the National Academy of Sciences of the United States of America*, 2002, **99**, 8484-8487.
31. C. Staii, A. T. Johnson Jr and N. J. Pinto, Quantitative analysis of scanning conductance microscopy. *Nano Letters*, 2004, **4**, 859-862.
32. M. Bockrath, N. Markovic, A. Shepard, M. Tinkham, L. Gurevich, L. P. Kouwenhoven, M. W. Wu and L. L. Sohn, Scanned Conductance Microscopy of Carbon Nanotubes and Î»-DNA. *Nano Letters*, 2002, **2**, 187-190.

Chapter 6: Physical Vapour Deposition of Copper on Suspended DNA Templates

6.1. Introduction

Physical Vapour Deposition (PVD) is a vacuum-based method commonly used to coat thin metal films onto a solid surface (e.g. semiconductors).[1, 2] The method principally involves evaporation of a solid (or liquid) phase material (*source*) into the gaseous phase and then condensation of the gas onto the solid substrate (*target*). PVD is a bottom-up technique for growth of nanomaterials whereby the film thickness and uniformity can be controlled by optimisation of the deposition process (e.g. deposition rate/exposure time, vacuum strength and temperature). The method differs from alternative coating techniques such as Chemical Vapour Deposition (CVD), which is based on a chemical reaction of the gaseous atoms/molecules at the solid surface. In the context of this thesis PVD offers an alternative approach to the electroless deposition of metal nanostructures, which generally relies on solution chemistry. Such chemical based approaches have been used extensively in our efforts to fabricate conductive nanowires.

PVD encompasses a range of techniques. Two of the most commonly used routes for physical deposition of metals are by direct thermal evaporation or via plasma-assisted sputtering in a sealed vacuum chamber. For evaporative deposition, the process is carried out under vacuum (< 1 mbar) in order to lower the temperature required to transform the material into the gaseous phase and allow transport of metal atoms, as well as preventing the deposition of impurities onto the target substrate (e.g. atmospheric particles). Sputtering involves the addition of an inert gas (e.g. Ar) into the vacuum-pumped chamber which is then ionised by application of an electric field to form energetic Ar^+ ions. These ions impact onto the source material (cathode) and dislodge metal atoms, or clusters of atoms, from the surface and into the plasma. The metal then deposits onto the target substrate to form thin metal films.

The physical method has a number of advantages over wet chemical routes; namely it does not involve the use of wet chemicals (which is environmentally-friendly) and is relatively simple and quick to perform. One of the disadvantages of using PVD for forming metal films is that the technique works less well for unevenly structured surfaces. For target surfaces which are uneven, the homogeneity of the deposited film

may be poor. The homogeneity and structure of the resulting film can be manipulated by controlling the pressure of the system. At low pressures there are a relatively low number of collisions between source atoms with the background gas. Thus, deposition of material at the target becomes highly directional. This may cause ‘shadow effects’ at steps and raised features on the surface. However this ‘shadowing’ effect can be useful in some cases, as will be illustrated later in this chapter. At high pressures, the impact of atoms with background gas molecules increases. Thus the directionality of the moving vapour atoms will be reduced and the shadow effects will be diminished, resulting in a more uniform film.

It has been shown that, in order to form 1-dimensional nanostructures using the PVD method, a template is required to guide the formation of the deposited material in an anisotropic fashion along one axis. There have been several papers published in the field of physical templating, whereby molecular templates consisting of carbon nanotubes[3-7] and DNA[6-9] have been utilised. Various different metals or metal alloys have been coated onto the templated substrate to form a working device. This approach involves suspending a molecular template above the target surface. The material of choice can then be deposited along the template using PVD in order to form a nanowire, as illustrated in figure 6.1. For preparation of nanowires it would be tremendously beneficial to have the template fixed between a pair of raised electrodes so as to study the electrical properties of the resulting nanowire.

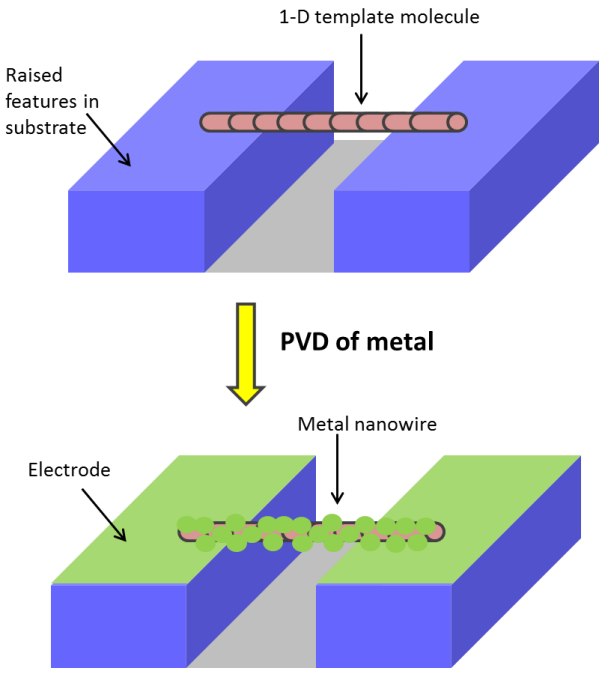

Figure 6.1: Schematic illustrating physical templating approach for fabrication of a metal nanowire device based upon a suspended molecular template. Physical vapour deposition of the metal is performed over the entire device

Figure 6.2 displays images of various metals grown on suspended templates. PVD allows the size of the resulting metal nanowires to be controlled via the time at which the target (template) is exposed to the vapour. Also, the length of the nanowire can be controlled by varying the inter-electrode distance. For good electrical conduction, the resulting nanowires should be homogenous in morphology and the metal coatings continuous.

The physical deposition approach on suspended template molecules was originally employed by Bezryadin *et.al*. for fabrication of superconducting Mo/Ge nanowires using carbon nanotubes (CNTs) as templates.[3] Other groups have since used CNTs as templates for deposition of various metals including Nb[5] and Os.[6] Other metals such as Au, Pd, Fe, Al and Pb have also been templated on suspended CNT molecules.[4] However, these form discontinuous metallic coatings on the template. This has been ascribed to the weak interaction of carbon with the metal and a high diffusion rate of metal atoms on the surface of the nanotube. Ti on the other hand forms homogenous coatings on CNTs due to titanium's low diffusion rate. Titanium was hence used as a primer layer (~ 1 nm) for deposition of a second metal to form continuous metallic nanowires.[4] The resulting nanowires are very thin (≤ 10 nm) and smooth, as evidenced

by Transmission Electron Microscopy (TEM) (figure 6.2, middle). However, the functional properties of these nanowires were not examined.

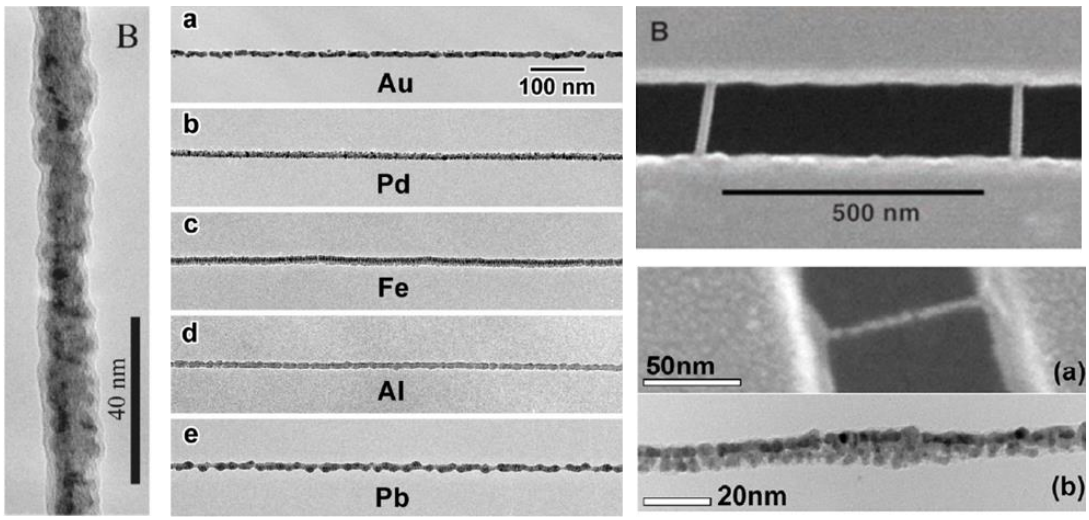

Figure 6.2: 1-D metal nanostructures formed by PVD over suspended template molecules. TEM image of Nb nanowire formed by sputter deposition on a freely suspended carbon nanotube template (left); to prevent oxidation the wire is further coated with Si. (Adapted from ref.[5]). TEM images of various metal nanowires (5 nm) containing a 1 nm Ti buffer layer grown on carbon nanotubes (middle). (Reprinted from ref.[4]). SEM image of a λ-DNA molecule stretched across a 100 nm trench with AuPd (1.5 nm) grown on top, and below TEM image of an equivalently prepared wire showing the granularity of the coating (bottom right). (Reprinted from ref.[6]). SEM image of a two-nanowire device consisting of DNA coated with Mo/Ge alloy for fabrication of a SQUID (top right). (Adapted from reference [9])

DNA has also been used as a template for PVD to form nanowires consisting of Os, Nb and AuPd alloy.[6] AuPd formed a granular coating on the template (figure 6.2, bottom right) and thus could not be considered useful for device purposes. Os and Nb on the other hand deposited onto the template in a more uniform fashion to generate smooth nanowires.

DNA has been used more extensively for the deposition of Mo/Ge alloy for the fabrication of a superconducting quantum interference device (SQUID) (see figure 6.2, top right).[7-9] Templating of the conductive material on the DNA-immobilised substrate was carried out by sputter deposition. The resulting thin nanowires (5-10 nm) (see figure 6.2, top right) make seamless contact to the electrodes, are homogenous in morphology and become superconducting at low temperatures (as low as 0.3 K).

A molecular template such as DNA is well suited for this process as it has the correct dimensionality to form nanowires; long and thin enough (~2 nm wide) for potential application in the next generation of electronic circuits. However, as described, the template must be suspended above the surface for isolation from the underlying

substrate, which will become conductive following deposition of metal. In principle, many different metals could be coated onto DNA by this method, making this an attractive approach to the fabrication of templated metal nanowires. In view of the fact that copper has not been used as a material for DNA-templating by PVD (or any other template) the aim of this work is to advance this method for the fabrication of highly conductive DNA-templated copper nanowires.

In this type of approach, DNA is used as a physical template/support to guide the deposition of metal in one uniform direction between the raised electrodes. In previously described *chemical* approaches to metallised DNA, DNA is exploited primarily for its expansive ability to bind metal ions through multivalent interactions with phosphate groups and specific nucleobase sites of DNA. These doped DNA nanostructures then act as seed platforms to grow more metal atoms in the presence of a chemical reductant. Such chemical routes have been relied upon throughout this thesis, and have not led to highly conductive Cu-DNA nanowires. This is despite the observed continuous coatings on DNA, in most cases. In this physical-based approach, copper metal is deposited onto the template, rather than copper ions, negating the requirement for an effective reducing agent.

In this chapter we have implemented a similar physical-based approach to those previously described for fabrication of a simple two-terminal metal nanowire device by DNA-templating. In this work, DNA molecules are suspended and isolated between pairs of raised electrodes over a trench etched into the SiO_2 substrate. The entire sample is then coated with metallic copper by evaporative vapour deposition, resulting in metallised DNA nanowires across the trench and a film of copper upon the SiO_2 surface. Images of the device are collected using Scanning Electron Microscopy (SEM). Chemical characterisation of the metallised device is performed using X-ray Photoelectron Spectroscopy (XPS). The conductance of the nanowire device is measured using a 2-probe i-V device analyser to contact the electrode pads. High definition images of the nanowires for morphological analysis are collected using Transmission Electron Microscopy (TEM), where wires are suspended across holes in a perforated silicon nitride (Si_3N_4) TEM grid.

Use of the word ‘device’ in this chapter refers to the two-terminal electrode set-up with a nanowire bridging between the two electrodes.

6.2. Experimental

6.2.1. Electrode fabrication

The electrode substrates were prepared in the School of Electrical Engineering, Newcastle University, by Prof. Nick Wright. The fabricated substrate afforded an array of two-terminal electrodes for i-V analysis of single nanowires (see figure 6.3). The electrodes are comprised of aluminium, raised ~3.5 μM above a SiO_2 (200 nm thick) layer on a Si support. HF (60%) was used as the etchant to create the channels and undercuts of the electrodes, whereby the substrate was held ~2 cm above a solution of the etchant within the vapour. The fumes of HF cause isotropic etching into the SiO_2 substrate. Over a long time period, horizontal etching into the aluminium electrodes occurred. The surface area of the electrodes was ~80 μM^2 and the distances between the electrodes were typically 2-5 μm. Figure 6.3 shows a typical SEM image of the trench formed between two aluminium electrodes on the SiO_2 substrate.

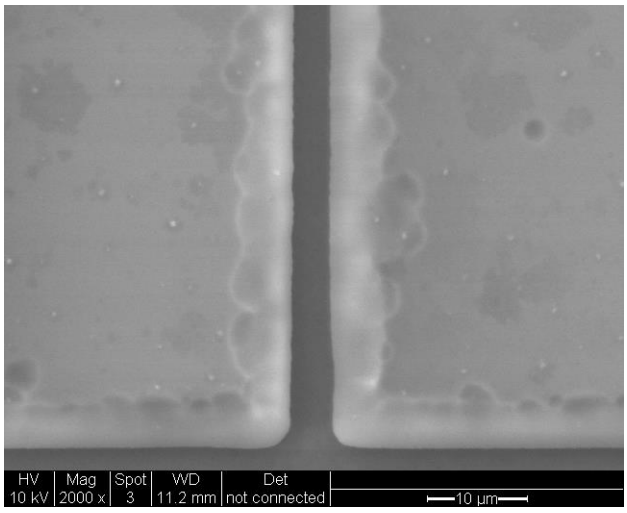

Figure 6.3: SEM image of a trench (~3 μm) formed between two raised electrodes

6.2.2. Deposition of DNA and Metallisation

A stock solution of λ-DNA with concentration 500 μgmL^{-1} was diluted to 5 μgmL^{-1} using Nanopure water. This concentration was found to be suitable for obtaining isolated nanowires across the trench for fabrication of a single nanowire device, or for obtaining single nanowires across holes in a TEM grid. The DNA was aligned between electrodes by placing a 10 μL droplet onto the surface (see photograph in figure 6.4) and allowing the solution to dry in a vacuum desiccator. The sample was then rinsed in Nanopure water to remove residual salt from the surface, originating from DNA buffer.

For evaporation of copper, the DNA-immobilised sample was placed in an evaporation chamber. The chamber was evacuated to a pressure of ~$1x10^{-6}$ Torr and copper metal was then deposited onto the sample by heating and evaporating the copper. A thickness monitor was used to define a 20 nm thick layer of deposited copper onto the surface, at a rate of ~0.5 nm per second. Figure 6.4 shows an SEM image of electrodes following deposition of DNA and copper. The 'layered' appearance of the electrodes as denoted by a change in contrast between the top and bottom layers could indicate the presence of copper on top of the aluminium.

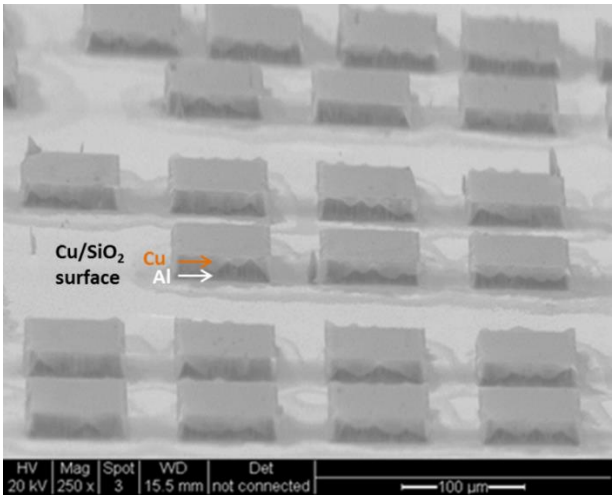

Figure 6.4: SEM image obtained at 85° tilt angle of the electrode device following deposition of DNA and copper. The raised electrodes consist of aluminium and the surface is SiO_2 on Si. Both electrodes and DNA have a 20 nm thick layer of copper deposited on top

Inspection of the sample by Scanning Electron Microscopy (SEM), discussed in section 6.3.4, reveals that nanowires are pulled taut across the trench and lie very straight.

A control sample consisting of a chip which has no DNA deposited was also prepared by evaporation of copper onto the surface.

6.2.3. X-ray Photoelectron Spectroscopy (XPS)

X-ray Photoelectron Spectroscopy (XPS) analysis was carried out upon the metallised nanowire device as prepared in section 6.2.2, using a Kratos AXIS Nova XPS system with a monochromated Al Kα X-ray source at a take-off angle of 90°. Charge neutralisation was used for analysis. The analysis area was 400x700 µm. Calibration of binding energies was achieved by referencing to the internal hydrocarbon peak at 284.8

eV. Peak fitting was carried out using the CasaXPS software. Peak shapes consisted of an asymmetric Lorentzian function with extended tail parameter (LF). Two Shirley backgrounds were used for fitting (for $2p_{3/2}$ and for the $2p_{1/2}$).

6.2.4. Transmission Electron Microscopy (TEM)

Substrates used for Transmission Electron Microscopy (TEM) analysis were 'holey' silicon nitride (Si_3N_4) grids, obtained from SPI Supplies (West Chester, PA, USA). These are perforated silicon nitride membrane window grids with a 200 µm frame thickness, 0.5 mm^2 membrane size, 50 nm membrane thickness and 2 µm diameter holes on 4 µm centres. There are 113 x 113 rows/columns of holes within the membrane, accounting for 12,545 holes per membrane. All holes are evenly sized and spaced and are almost entirely defect-free (refer to figure 6.5 for TEM image of the substrate).

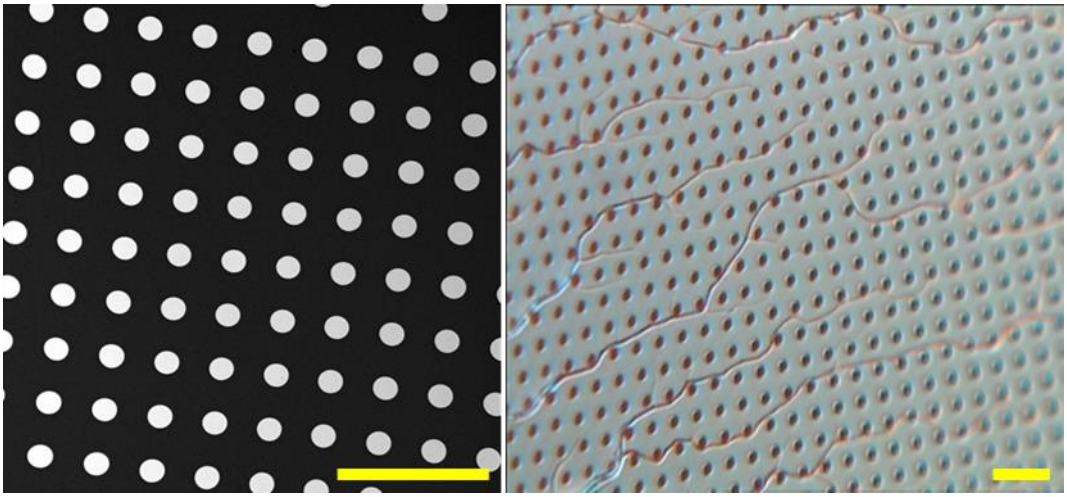

Figure 6.5: (left) TEM image of a bare holey grid and (right) light microscope image of TEM grid following deposition of DNA and copper. Thick bundles of nanowires are seen to extend across the surface. Scale bars= 10 µm

Samples were prepared, by first pipetting a solution of λ-DNA (5 μgmL^{-1}, 2 µL) onto the TEM grid. The solution was left to dry in a desiccator whilst under vacuum, for 30 minutes. Solution remaining on the surface was wicked off using filter paper. Copper was then evaporated onto the sample, as described in section 6.2.2. Inspection of the sample under an optical microscope revealed very thick strands (at least 500 nm thick) extending over the entirety of the holey substrate, from which smaller nano-sized wires

are believed to branch off of (see figure 6.5, right). These thick strands are interpreted as bundles of nanowires. Evidence to support this bundling of nanowires is provided by SEM and is discussed in section 6.3.4. These bundles seemingly 'avoid' the holes on the substrate (as they are not observable in the TEM), whereas individual nanowires (visible to the TEM) *do* extend across the holes.

TEM analysis was conducted on a Philips CM100 TEM with Compustage and high resolution digital image capture.

6.2.5. Scanning Electron Microscopy (SEM)

Scanning Electron Microscopy (SEM) was used to locate nanowires spanning across the electrode trenches, formed as in sections 6.2.1 and 6.2.2. Measurements were performed using a FEI XL30 ESEM-FEG (Environmental Scanning Electron Microscope-Field Emission Gun) in low vacuum mode (10 Torr chamber pressure) between 10 and 20 keV. Isolated nanowires were found to lie perpendicular to the trench and span across the raised electrodes. Nanowires were also observed to lie flat on the surface itself.

6.2.6. Electrical Studies

i-V measurements were carried out upon DNA-templated copper nanowires suspended between two raised electrodes over a trench etched into the SiO_2 layer supported on a Si substrate (prepared as in sections 6.2.1 and 6.2.2). Electrical measurements were made by using a Probe Station (Cascade Microtech, Inc., Oregon, USA) and B1500A Semiconductor analyser (Agilent Technologies UK Ltd., Edinburgh, UK), equipped with Agilent Easy EXPERT software. I–V measurements were conducted at 293 K under a N_2 atmosphere, without light illumination, and by using a voltage range of -3 to +3 V in steps of 0.03 V.

6.3. Results and Discussion

6.3.1. Device Design and Process

This section details the strategy involved in the fabrication of a DNA-templated nanowire device by copper evaporation. Arrays of electrodes were fabricated on the surface so as to make electrical measurements on individual pairs, where isolated nanowires are likely to reside (see figure 6.6).

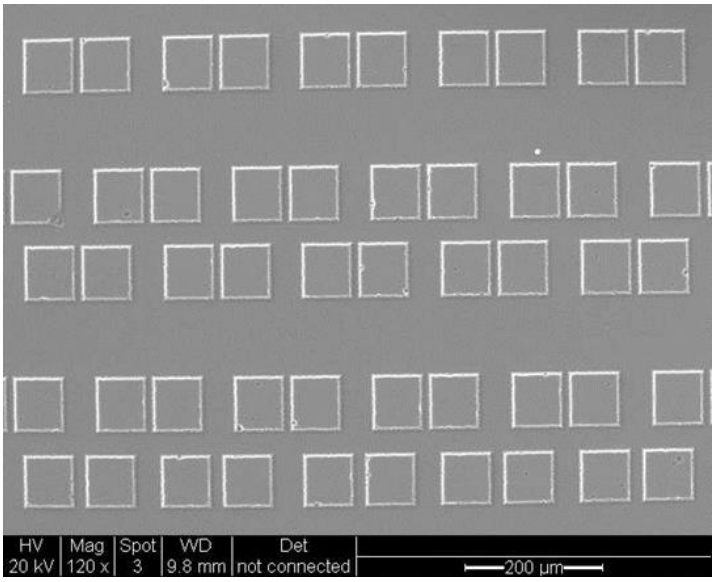

Figure 6.6: SEM image of the raised aluminium electrode array on a Si/SiO_2 substrate.

There are important considerations to make regarding the design of the electrodes for deposition of DNA and for metallisation. Figure 6.7 shows a Scanning Electron Microscopy (SEM) image of a typical fabricated electrode pair. The image was acquired at a high tilt angle (85°) for lateral inspection of the electrode construct. It can be seen from this SEM image that the electrodes are undercut at the base (see dotted yellow markers).

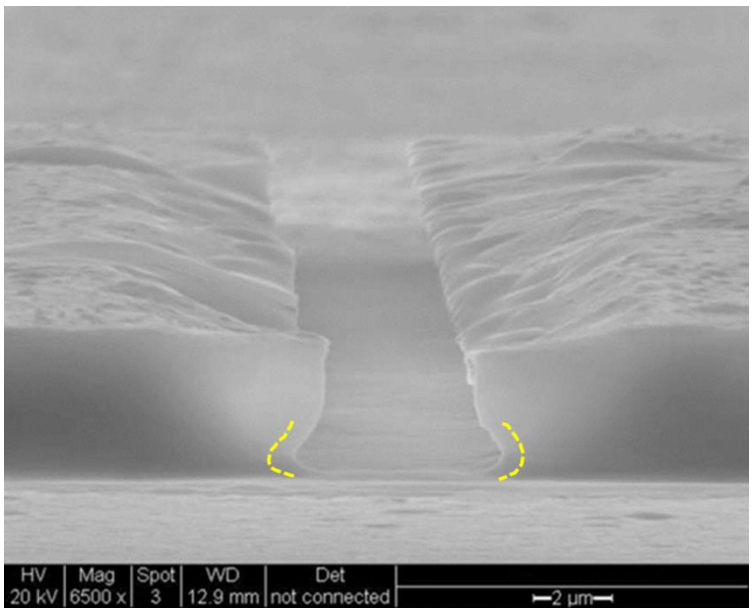

Figure 6.7: SEM image obtained at high tilt angle (85°) of a pair of raised aluminium electrodes. The importance of the image is to show the undercut at the base of each feature

The undercuts form due to an isotropic etch into the SiO_2 channel where the etch rate of SiO_2 is significantly faster than for aluminium. The channels are over-etched to generate more pronounced features. Although not clear from this image, the undercuts are present on all four sides of the electrode feature. The resulting shape of the electrode is best described as an inverted 3-dimensional trapezoid.

The undercut is very important for the operation of the resulting metallised device. The electrodes act to mask the deposition of copper which causes a shadow effect around the perimeter of the electrodes. This provides an insulating enclosure, leaving the electrodes isolated from the surrounding conductive surface. Thus the shadowing effect can prevent the formation of short-circuits by deposition of copper at the electrode-surface interface. A short-circuit can be defined as one which permits the flows of current down an un-intentional pathway. Therefore, such a design makes it relatively simple to measure the device conductance where the conductance is attributable exclusively to copper templated on DNA (i.e. nanowires), rather than non-templated copper (i.e. the copper film on the surface). Figure 6.8 shows a schematic illustration of the metallisation process used in this chapter.

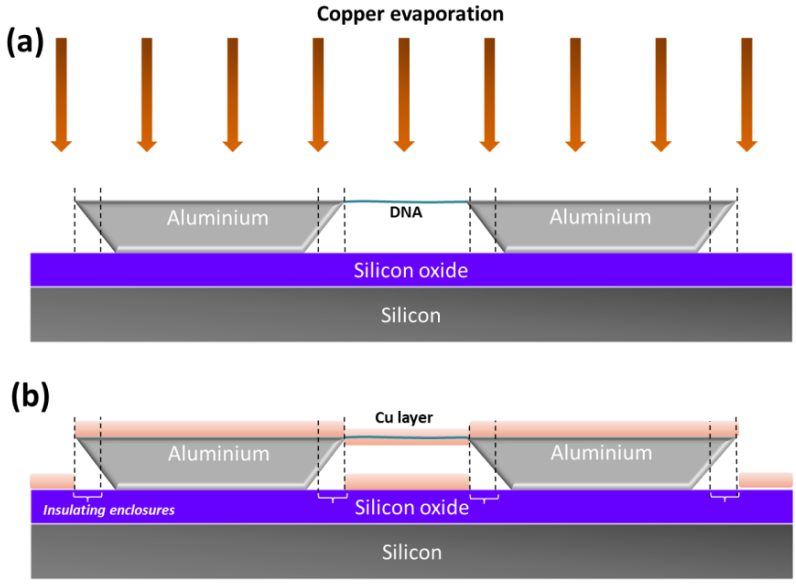

Figure 6.8: Schematic of the metallisation process on the device with DNA molecules bridging across the raised electrodes. The undercut electrodes act as a mask to prevent deposition of copper at the surface-electrode interface, resulting in an insulating enclosure around the electrodes

As can be seen from the illustration in figure 6.8 the metal is expected to deposit across the face of the electrodes and along the DNA-bridge. Copper is also deposited upon the substrate surface. As discussed, the shape of the electrodes helps to restrict the deposition of copper around the perimeter of the electrodes and prevent short-circuits. This affords an isolated and a potentially electrically conductive DNA-templated nanowire device. A set of electrodes which does not have DNA deposited is used as a control in order to establish that without DNA bridges the deposition of copper does not produce conductive devices. The electrical data from both sets of samples is presented later in this chapter in section 6.3.5.

For deposition of DNA the inter-electrode distances should be made short enough to facilitate the alignment of DNA molecules across the gap. The DNA used here is λ-DNA, which is ~16 µM long. The inter-electrode distances were typically 2-5 µM and the trench depth was ~3.5 µM. These dimensions permit the alignment of DNA across the electrodes, which are raised high enough from the surface for DNA to be freely suspended. Molecules were stretched across the trench by evaporation of a solution of DNA. It was found that a DNA concentration of 5 μgmL^{-1} (diluted from a stock solution of 300 μgmL^{-1}) was appropriate for this experiment to afford isolated bridges.

For deposition of copper, the pure metal was thermally evaporated onto the substrate, rather than by the alternative method involving plasma-assisted sputtering. The evaporation technique results in a more directional and uniform coverage of copper on the substrate and DNA bridges. This controlled deposition helps to further restrict the deposition of metal around the undercuts of the electrodes. The directionality of evaporated metal atoms can be enhanced at lower pressures, which results in less frequent collisions of metal atoms with the background gas. The random direction of sputter deposition on the other hand, may lead to deposition of copper at the undercuts of the electrodes causing the un-wanted short connection.

6.3.2. Chemical Characterisation

X-ray Photoelectron Spectroscopy (XPS) is used here to confirm that the device is composed of copper metal, as expected. XPS is also used here to establish if the copper surface is oxidised. The figure below (figure 6.9) is an optical microscope image of the metallised sample, which shows the approximate area under examination, for collection of XPS signals. The reddish-brown colour of the sample is a minor indication that copper metal is present on the surface.

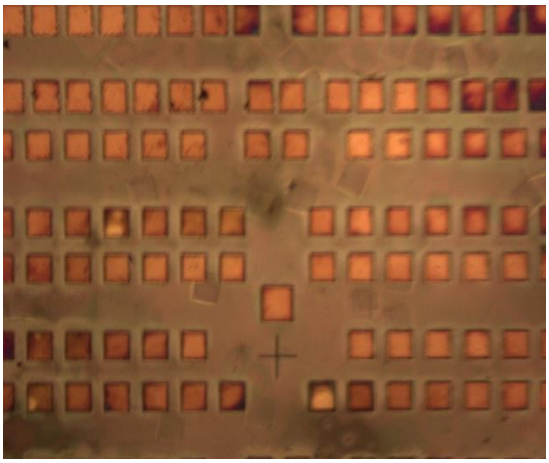

Figure 6.9: Optical microscope image of the metallised sample showing the approximate area under XPS examination

For pure copper metal, a symmetrical doublet would be expected to arise in the Cu2p spectrum. For copper metal that is marginally oxidised to Cu^{2+} (e.g. CuO), a slight shouldering of the copper doublet peak may be expected, accompanied by the growth of satellite peak(s).[10] For a significantly oxidised copper surface, the shouldering of the doublet becomes exceedingly pronounced that inclusion of an additional doublet is necessary to account for copper oxide as a separate component.

Figure 6.10 shows the Cu2p spectrum obtained for this sample. Analysis of the spectrum revealed an *almost* symmetrical doublet at the expected binding energy for pure metallic copper (932.6 eV for $2p_{3/2}$),[11] and with the correct splitting value (19.8 eV).

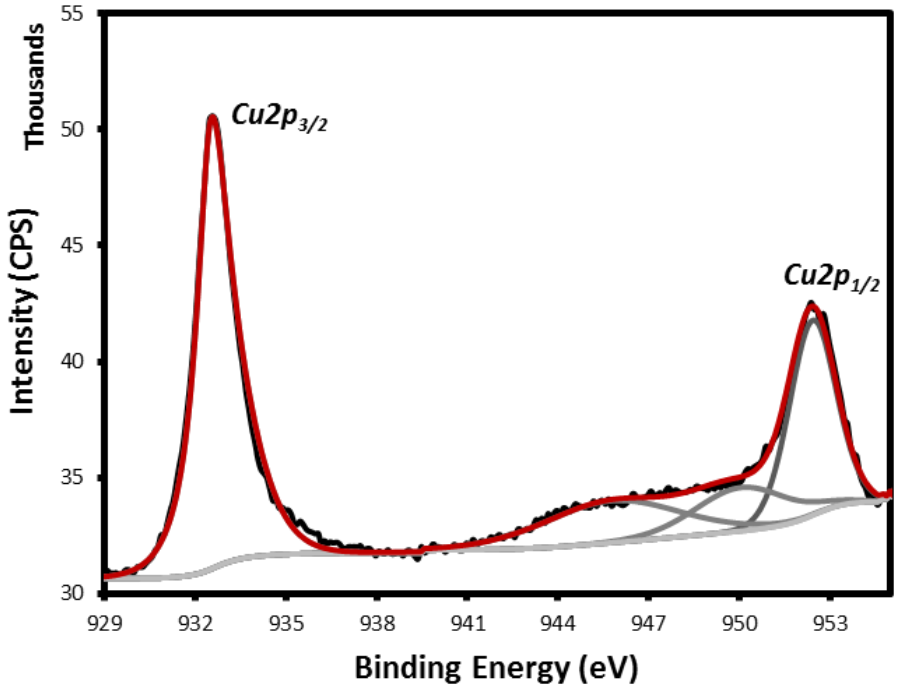

Figure 6.10: Cu2p XPS spectrum of the sample surface following deposition of DNA and evaporation of copper. The doublet is attributed to metallic copper. The low intensity satellite structure indicates a small amount of oxidation of copper

A further two peaks were fitted to the spectrum at binding energies 950.1 eV and 945.8 eV, whereby the latter corresponds characteristically to a Cu^{2+} "shake up" satellite peak; an indication that some copper is oxidised at the surface. The peak at 950.1 eV is incorporated into the overall fit in order to fit the sloped background profile of the spectrum, which rises in intensity towards the $Cu2p_{1/2}$ region. Copper satellite structure arises due to the presence of Cu^{2+} species in the sample.[12] Satellite peaks form as a consequence of charge transfer to a copper 3d orbital when in the Cu^{2+} state (with electron configuration $3d^9$). Charge transfer acts to screen the core hole charge, which is present following ejection of a copper 2p electron. Satellite structure is absent for samples containing Cu^0 and/or Cu^+ species as these have a full 3d sub-shell (d^{10}) and therefore charge screening via charge transfer does not occur.

The low intensity of the satellite structure with respect to the copper doublet, as well as the near perfect symmetry of the copper doublet peak shape, led us to determine that assigning Cu^{2+} species as a seprate doublet component was not the correct procedure. Instead, to account for the slight assymetry, the copper doublet peak shapes were allowed to tail off assymetrically.

6.3.3. Nanowire Characterisation

Transmission Electron Microscopy (TEM) was used to examine the morphology of the DNA-templated copper nanowires formed by evaporation of copper onto suspended DNA molecules. In order to prepare a sample for TEM, based on this approach, a specific type of substrate was required. These were perforated silicon nitride (Si_3N_4) TEM grids. The DNA was stretched across the holes in the substrate by evaporating a solution of DNA; in the same manner used to align DNA molecules across trenches in the electrode based device. Metallisation (by evaporation of copper) of the DNA-templated TEM substrate was achieved in the same way as for the DNA-templated electrode substrate. Identical sample preparations, albeit on different substrates, ensures that both the device and the TEM sample contain nanowires of a similar appearance.

Figure 6.11 shows a large scan size TEM image (~29 μm^2) of the substrate following absorption of DNA and metallisation with copper. It is apparent that there are large strands (at least 500 nm thick) extending across the surface which avoid crossing over the holes. These large strands are perhaps representative of those observed under the optical microscope, shown to the right of figure 6.11, and alluded to in section 6.2.4.

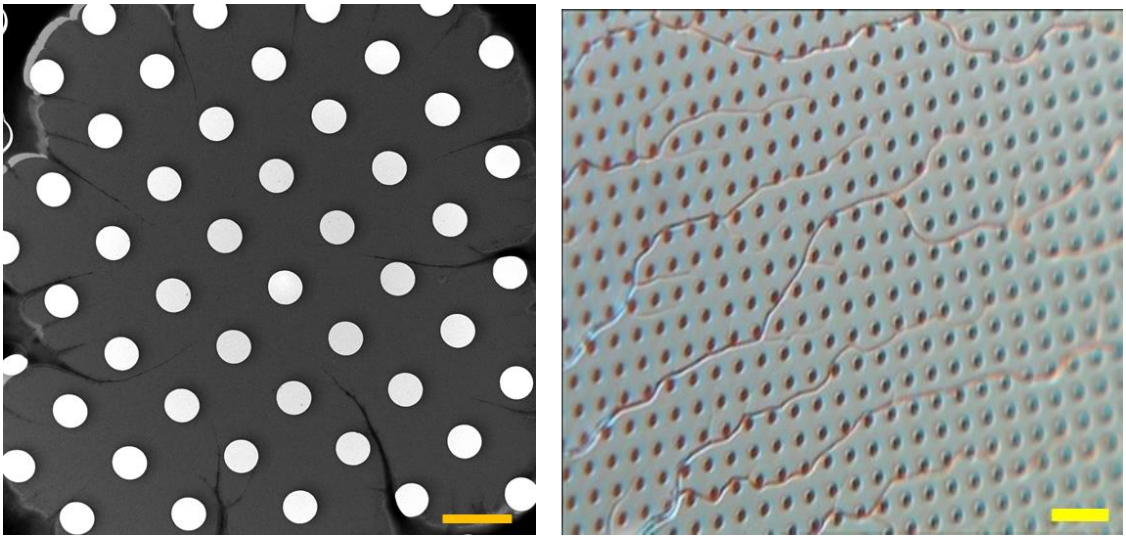

Figure 6.11: (left) TEM image of a perforated silicon nitride grid following deposition of DNA and copper, (right) optical microscope image of the same sample. Scale bars= (left) 4 µm and (right) 10 µm

Further inspection of the sample by TEM revealed smaller nano sized wires to bridge across the holes in the substrate. Figure 6.12 shows a selection of small scan size images of nanowires bridging across the holes. These images are used to assess the morphology of the nanowires prepared by this method.

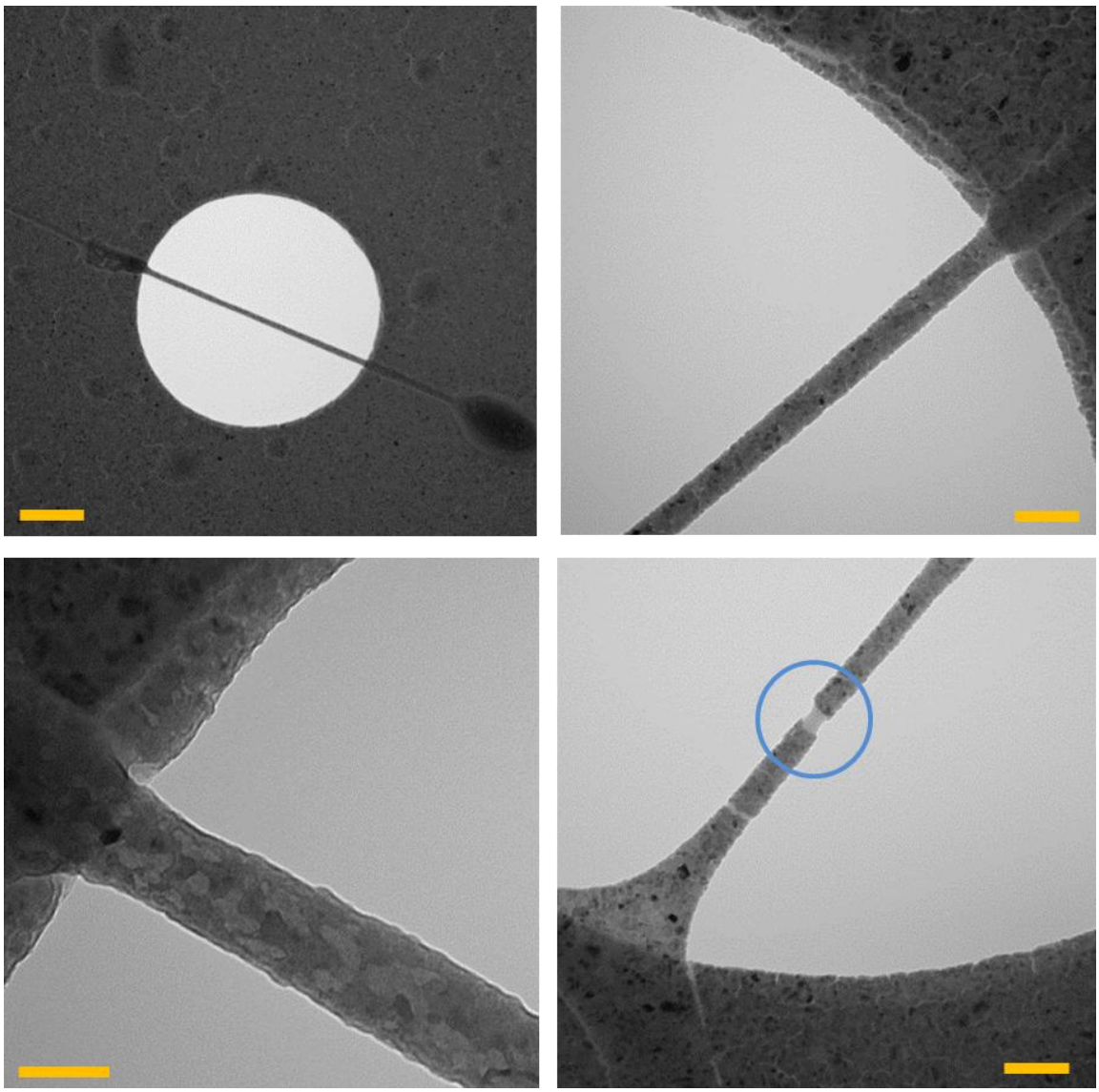

Figure 6.12: Small scan size TEM images of DNA-templated copper nanowires bridging across holes in a perforated silicon nitride TEM grid. Top left/right and bottom left are all images of the same nanowire. The widths of the nanowires are ~50 nm. Scale bars= (top left) 500 nm, (top right, bottom left) 100 nm and (bottom right) 50 nm

These images reveal the nanowires to be continuous and highly uniform in width (~50 nm). The image to the top left shows a nanowire pulled taut across one of the holes (2 µm in diameter). Magnified images of this nanowire are shown in figure 6.12 (top right and bottom left). These images show the nanowire to be highly continuous and uniform in copper coverage. These structures do not appear to exhibit granular defects in the copper coating and appear highly crystalline. It is also apparent that the DNA template is left completely unexposed by copper. DNA is not easily observed by TEM due to a lack of contrast and usually requires a stain to image the nanostructure or other, innovative, techniques.[13] As we observe good continuous contrast along the whole

length of these wires under TEM it seems likely that the copper coating is also continuous. The image to the bottom right is an example of a nanowire where the uniformity of the coating appears to change along the length of the structure and reveals an underlying coating on the template (shown circled in blue). The high tension of the nanowire as a result of it being pulled taut may cause the copper to diffuse slightly. This result may demonstrate that copper is mobile along the length of the nanowire.

A control sample (see TEM images in figure 6.13) was prepared by evaporation of copper onto a TEM substrate which does not have DNA deposited. As can be concluded from these images, the deposition of copper does not result in wire-like material, without the presence of DNA to act as a template/bridge. Even so, the morphology of the copper coating on the substrate, shown clearly in the image to the right of figure 6.13, is similar to that observed in figure 6.12 (where DNA was present), affording a highly uniform copper film.

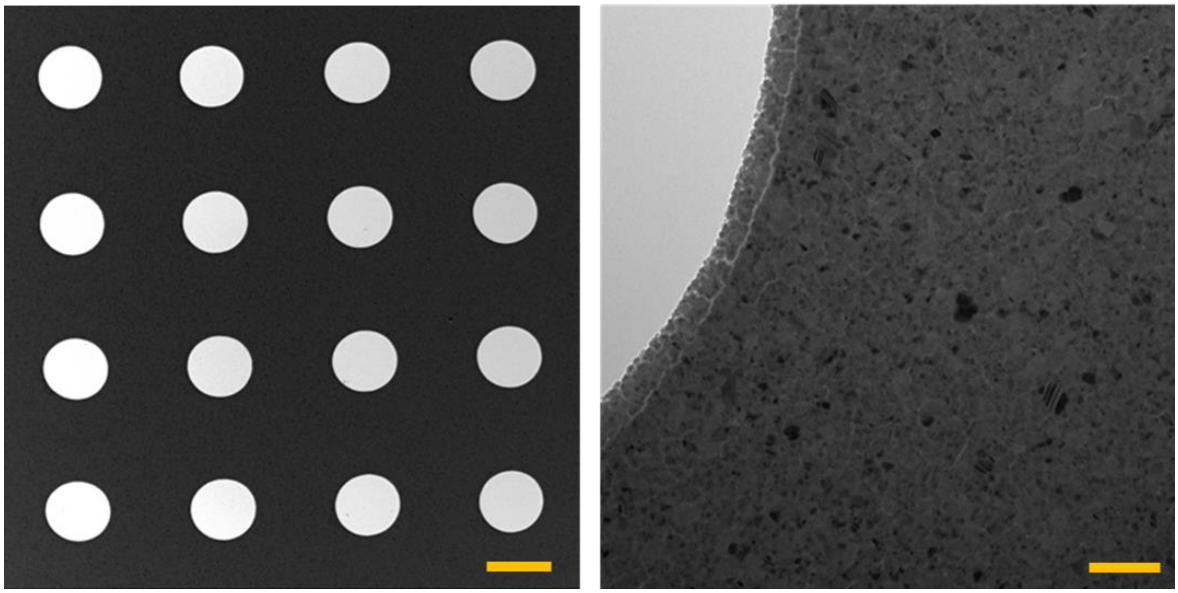

Figure 6.13: TEM images of the control sample; copper metallised TEM grid without DNA templates. The figure to the left indicates that no wires are formed on the substrate and the figure to the right shows the morphology of the metallised surface. Scale bars= (left) 2 µm and (right) 100 nm

6.3.4. Device Characterisation

Scanning Electron Microscopy (SEM) was used to characterise the metallised electrode device and locate nanowires bridging across the trench. SEM is an electron microscopy method used to acquire topography information of conductive samples, usually by scanning across the surface in a raster pattern with an electron beam. The electrons interact with atoms at the surface whereby a variety of signals can be measured in response to this interaction. Typically, the measured signal is due to secondary electrons (SE) which are ionization products of the specimen under scrutiny. The energy and intensity of these SE signals can be used to determine the topography of the sample with resolution of features below 1 nm. The detected signal varies as the beam scans across the sample due to changes in the surface topography. The image contrast is used to convey surface topography which varies in response to the detected signal.

Figure 6.14 shows an SEM image of a pair of raised electrodes with a trench formed in between, following deposition of DNA and copper onto the chip. The image to the right shows a smaller scan size image between these two electrodes where the trench is located. A nanowire (~ 100 nm in width) is seen to bridge across the electrodes (~ 4 µm gap) and is freely suspended above the trench. The nanowire makes seamless contact at the electrode interface and appears to homogenise with the electrode surface. Namely, there is no observable anchoring point for the ends of the strand onto the electrode surface. The wire also appears to be uniform in width and is highly continuous in coverage.

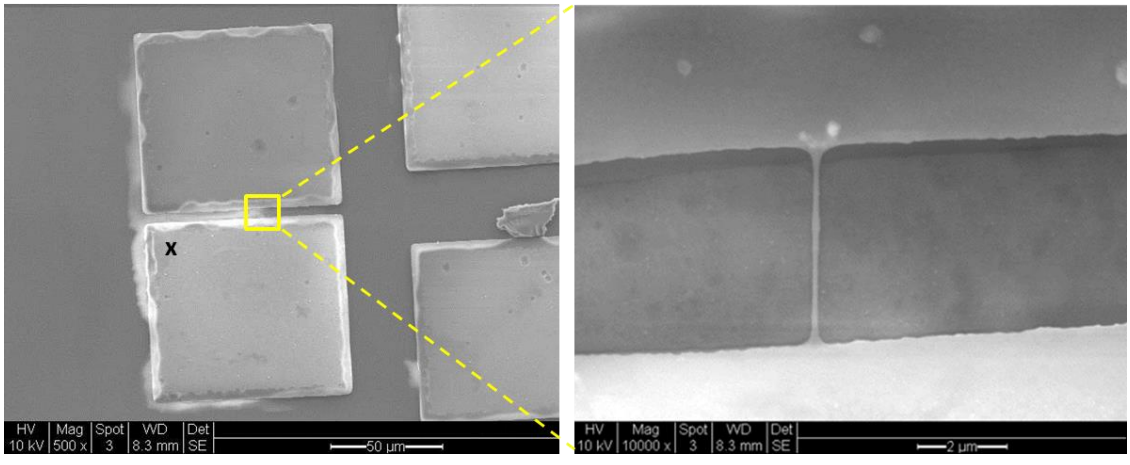

Figure 6.14: SEM images of electrode device consisting of a DNA-templated copper nanowire bridging across the trench etched into the SiO_2 substrate. The nanowire makes contact to both electrodes but importantly not the underlying surface

Energy-Dispersive X-ray (EDX) analysis was used to assess the elemental composition of the sample. The point of analysis is marked with an ‘x’ in figure 6.14. According to the EDX spectrum (figure 6.15, below), the sample contains the following elements: O, Cu, Al and Si. Both Si and O arise from the underlying SiO_2 substrate and the Al from the electrode. Cu is detected on the surface following its deposition.

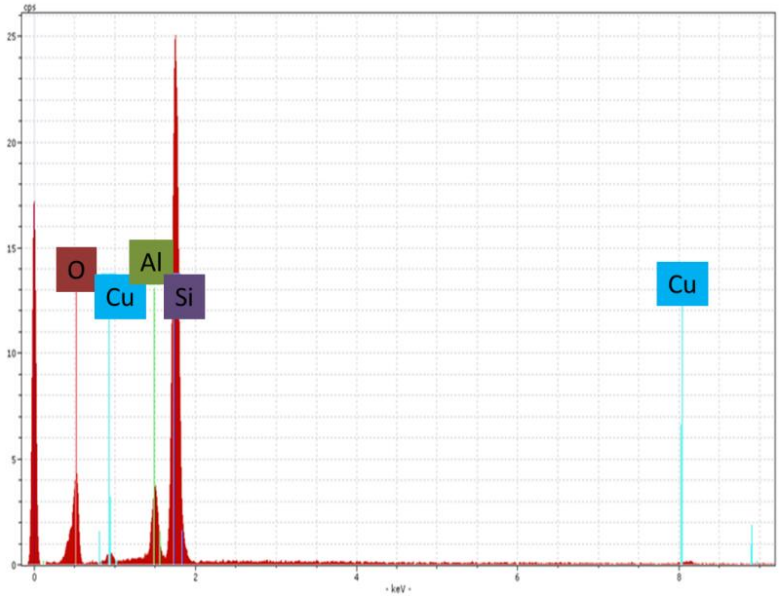

Figure 6.15: EDX spectrum of the sample surface. The ‘x-axis’ is in keV

As well as establishing that nanowires could be suspended between electrodes, SEM also revealed that nanowires were, in some cases, connected from electrodes to the substrate background. An SEM image in figure 6.16a shows an example of this. As observed, within the dotted black circle, a strand appears to stretch from one electrode to the adjacent electrode and then extends further onto the substrate surface. As stated earlier, conductive bridges connecting electrode to surface may short-circuit the device, which is unwanted. Figure 6.16b is a smaller scan size image of the device between this trench, where the same strand is located. The image shows that the strand is composed of several individual nanowires which are loosely bundled together. This observation may relate to what was observed under the optical microscope on the TEM substrate (see section 6.3.3, figure 6.11) where thick strands were seen to extend across the surface. Such features present a problem for fabrication of single nanowire devices. Namely, bundles of nanowires are formed and the presence of such, as has been shown here, acts to potentially short-circuit the device. Indeed, the strand appears to overhang

from the electrode interface and into the trench below, rather than suspending between the electrodes, providing further opportunity to short-circuit the device.

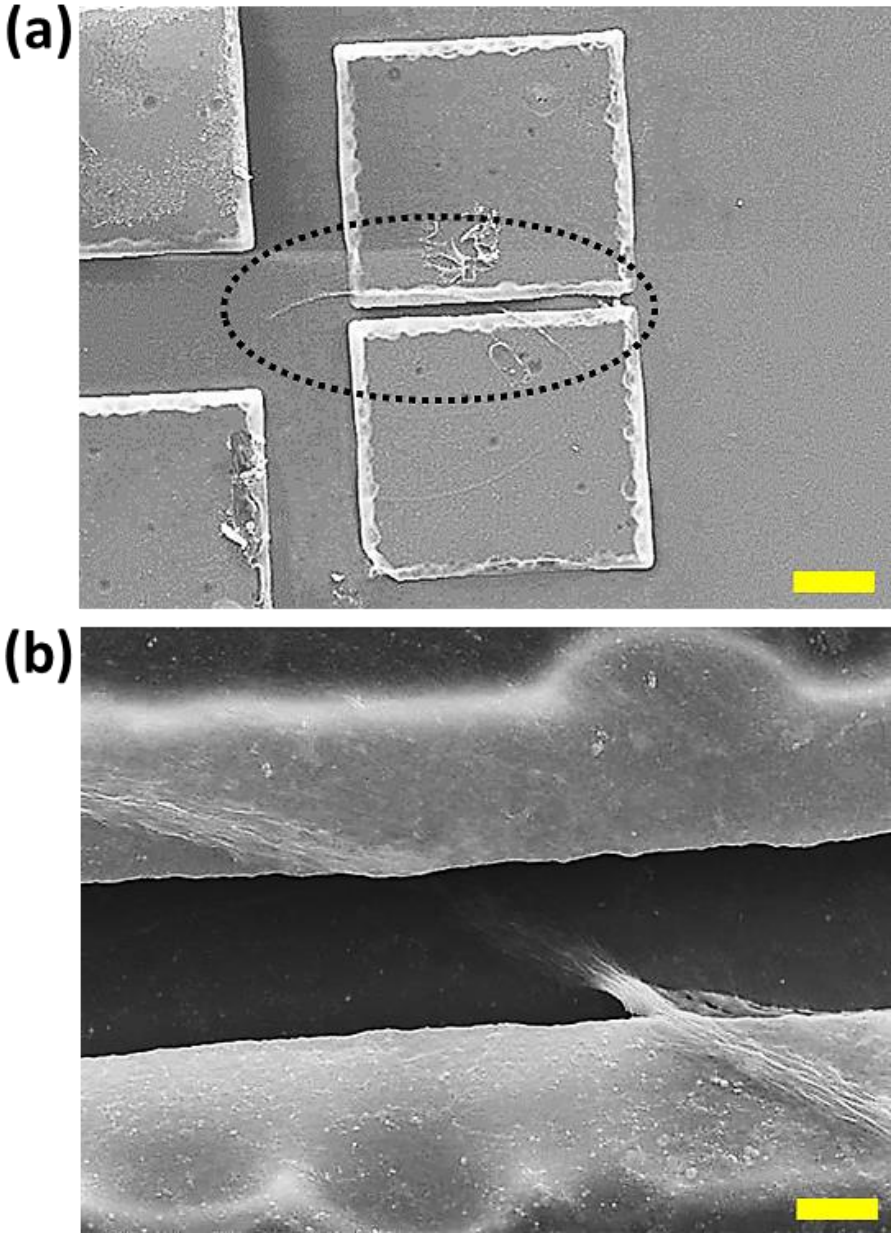

Figure 6.16: (a) SEM image showing a wire extending from one electrode, across the trench to the opposite electrode, and onto the conducting SiO_2/Cu substrate, (b) a smaller scan size image between the trench which indicates that the 'wire' is actually comprised of a 'loose' bundle of nanowires. The bundle appears to overhang down from the edge of the electrode into the trench below. Such features are likely to short-circuit the device. Images have been sharpened and the contrast adjusted using 'Microsoft Word 2010.' Scale bars= (top) 10 µm and (bottom) 2 µm

6.3.5. i-V Measurements

Based upon previously described observations (see section 6.3.4) that DNA nanowires can bridge across the trench and may also act to bridge between electrode and the conductive surface, potentially short connecting the device, we sought to examine the

electrical performance of the device. Figure 6.17 is a diagram detailing a proposed model of our DNA-templated device. Here, a nanowire is shown to bridge across the trench from electrode to electrode (point 1 to point 2) as in the real device shown in the SEM image below (figure 6.18). To illustrate the effect of a short circuit, nanowires are also shown to bridge from electrodes to the conductive surface (point 1 to point 3 and/or point 2 to point 3), thus bypassing the insulating enclosure surrounding the electrode perimeter.

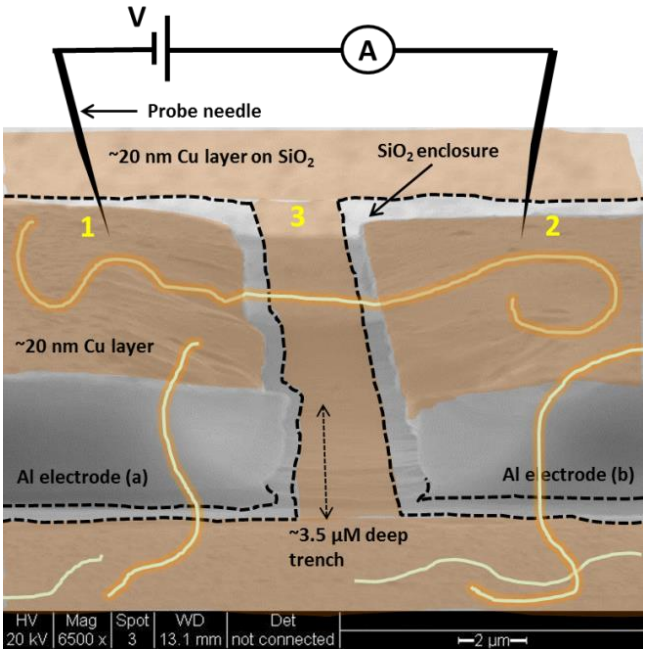

Figure 6.17: Proposed model of the DNA-templated copper nanowire electrode device. Nanowires may bridge the inter-electrode gap (between points 1 and 2) and also act to bridge between electrodes (1,2) to the conductive copper surface (3). Electrical measurements are made by placing the two probe needles onto the device (positions 1, 2 or 3) and recording a current-voltage (i-V) sweep

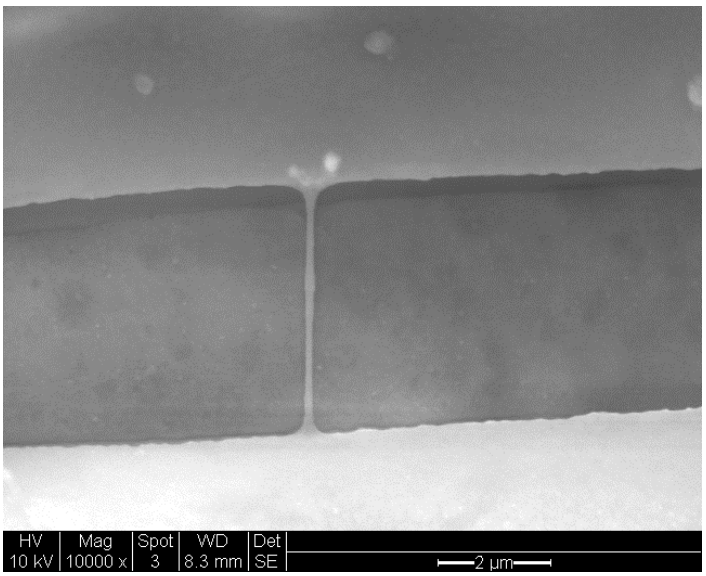

Figure 6.18: SEM image of a nanowire device. A DNA-templated copper nanowire is shown to bridge across the trench and between the two electrodes

Electrical measurements were carried out in order to test this proposed model. Current-voltage (i-V) sweeps were performed between points 1-1, 1-2, and 1-3 using tungsten probe needles (9 µm radius tips). If the model is indeed correct, one would expect to observe conductance for each set of points. The device to be tested has a nanowire bridging between the electrodes (points 1-2) and is shown in figure 6.18.

i-V curves are shown in figure 6.19 below. Conductance values were obtained from the slope of each graph (current/voltage, AV^{-1} or Siemens (S)). The highest conductance value, recorded when both probes were positioned onto the same electrode (points 1-1), was $5x10^{-3}$ S around zero bias with an ohmic current-voltage relationship. To measure the conductance of the nanowire bridging between the electrodes (as shown in figure 6.18 above) the probes were positioned at points 1-2 (refer to schematic, figure 6.17). The current-voltage relationship was ohmic, as expected for a conductive wire, and the zero bias conductance value was also high ($2x10^{-4}$ S). To test if the device is conductive between electrodes and surface (short-circuit) the probe needles were positioned at points 1-3 (or 2-3) and a further i-V sweep was recorded. The conductance value was high ($4x10^{-4}$ S), suggesting that the device is shorted. In fact, the conductance between the electrode and substrate is double that obtained for the bridging nanowire across the trench (between electrodes). These results may prove our proposed model to be correct.

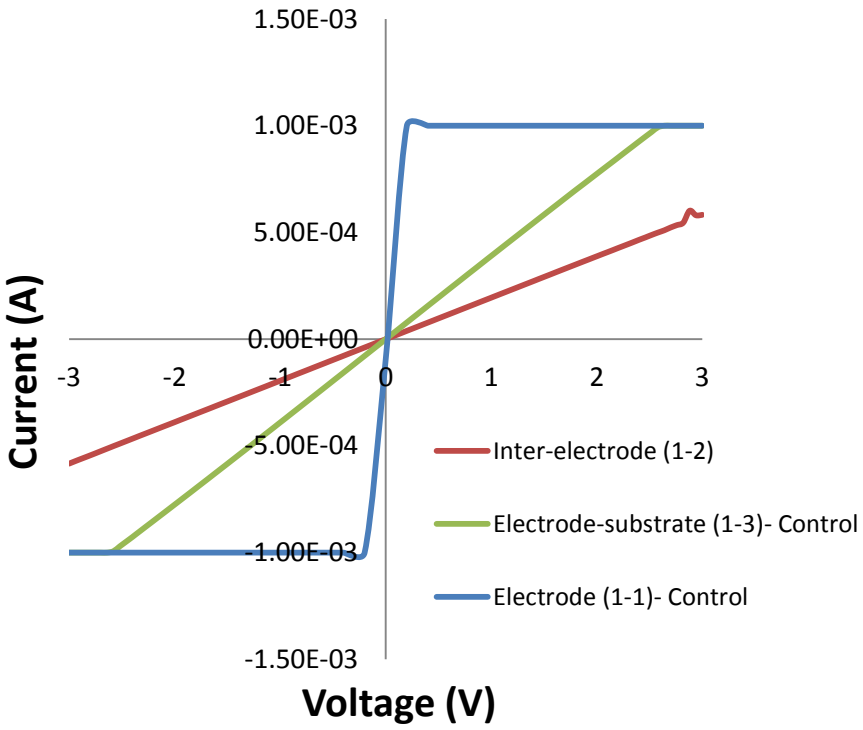

Figure 6.19: Current-voltage (i-V) plots obtained by placing the probe needles at different locations on the nanowire device. All plots exhibit an ohmic relationship and high conductance

However, in order to verify if the conductance of the device is indeed the result of metallised DNA bridges, connecting between electrodes (1-2) as well as electrode and surface (1-3), a further set of i-V measurements were carried out. Here, i-V sweeps are performed on a control sample which comprises a duplicate set of electrodes, as used in the previous set of experiments. This sample was metallised by evaporation of copper as before, but was importantly *not* DNA-templated.

Figure 6.20 shows the i-V curves obtained between points 1-1, 1-2 and 1-3 (refer to schematic in figure 6.17).

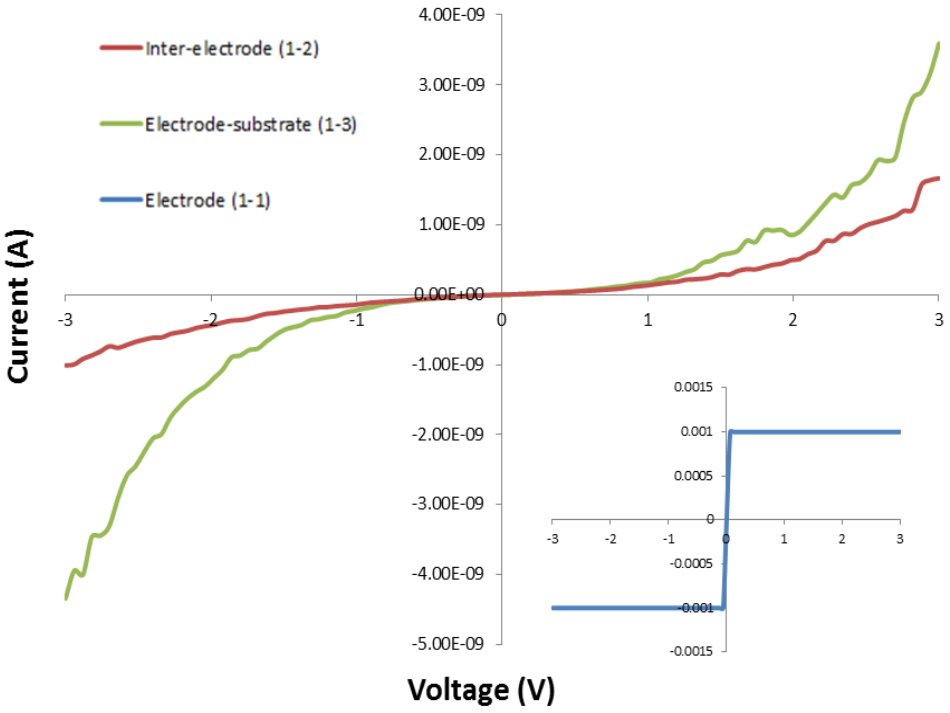

Figure 6.20: Current-voltage (i-V) plots obtained by placing the probe needles at different points on the non DNA-templated, metallised sample (control). Inset: i-V plot obtained when both probes are positioned onto the same electrode. Significantly low current values are obtained between the electrodes (1-2) and electrode-substrate (1-3) due to the absence of DNA bridges

As shown, in the absence of DNA to act as a template, there was no conductance between any two contact points on the surface, except when both probe needles are positioned onto the same electrode (see i-V plot, inset figure 6.20). These results demonstrate that the electrodes are functioning as desired. Importantly, the insulating enclosure around the perimeter of the electrodes has prevented short-circuiting which may have been expected to occur via the deposition of copper between the electrode and substrate surface interface (points 1-3 and 2-3). These results support our earlier claim that DNA bridges are responsible for the electrical performance of the device. In as much as, DNA must be present to act as a template in order to make the device conductive by bridging between insulating gaps (i.e. between electrode to electrode or electrode to surface).

6.4. Conclusions

Two-terminal nanowire devices have been fabricated by physical vapour deposition of copper onto suspended DNA templates. DNA strands act to bridge insulating gaps on the electrode substrate before being metallised in order to make the device conductive. Scanning Electron Microscopy (SEM) revealed that metallised DNA nanowires were freely suspended across trenches etched into the substrate surface between two electrodes. The conductivity of the resulting nanowire device was confirmed by i-V analysis. Nanowires were also shown to bridge between electrodes to the conductive surface. The latter effect results in a short-circuit connection to the device, as evidenced by i-V analysis. A further set of experiments on a metallised sample, which is non DNA-templated, indicated that the 'device' was non-conductive. This result further confirms that DNA is required to act as a template for deposition of copper in order to make 1-diemensional bridges across insulating gaps (i.e. the trench) and thus make the device conductive. This holds true regardless of whether DNA mediated short-circuits are present.

Individual nanowires were characterised by Transmission Electron Microscopy (TEM) in order to analyse their morphology. These were shown to possess highly continuous copper coatings and they were uniform in width along their entire lengths.

The methods presented in this chapter for fabrication of conductive single nanowire devices may be beneficial to the future manufacturing of interconnect technology. The ability to fix a template to the substrate, in a pre-determined orientation, is of huge advantage to the electronics industry. Templating methods could offer great control over both feature sizes and spatial orientation of device components. Given that that DNA is a versatile tool for construction of sophisticated nano-assemblies, the potential for fabrication of defined circuit designs on substrates, via DNA templating in one, two or even three dimensions makes this approach highly attractive. Thus, such physical-templating methods could be extended for fabrication of more sophisticated device elements. Moreover, the effort invested here for construction of copper-based nano devices may help to ease the transition from top-down fabrication of copper-based interconnects to the bottom-up assembly of copper interconnects and other electronic components.

6.5. References

1. K. Reichelt and X. Jiang, The preparation of thin films by physical vapour deposition methods. *Thin Solid Films*, 1990, **191**, 91-126.
2. K. Seshan, Elsevier, Editon edn.
3. A. Bezryadin, C. N. Lau and M. Tinkham, Quantum suppression of superconductivity in ultrathin nanowires. *Nature*, 2000, **404**, 971-974.
4. Y. Zhang and H. Dai, Formation of metal nanowires on suspended single-walled carbon nanotubes. *Applied Physics Letters*, 2000, **77**, 3015-3017.
5. A. Rogachev and A. Bezryadin, Superconducting properties of polycrystalline Nb nanowires templated by carbon nanotubes. *Applied Physics Letters*, 2003, **83**, 512-514.
6. M. Remeika and A. Bezryadin, Sub-10 nanometre fabrication: Molecular templating, electron-beam sculpting and crystallization of metallic nanowires. *Nanotechnology*, 2005, **16**, 1172-1176.
7. A. Bezryadin and P. M. Goldbart, Superconducting nanowires fabricated using molecular templates. *Advanced Materials*, 2010, **22**, 1111-1121.
8. D. S. Hopkins, D. Pekker, T. C. Wei, P. M. Goldbart and A. Bezryadin, Local superfluid densities probed via current-induced superconducting phase gradients. *Physical Review B - Condensed Matter and Materials Physics*, 2007, **76**.
9. D. S. Hopkins, D. Pekker, P. M. Goldbart and A. Bezryadin, Applied Physics: Quantum interference device made by DNA templating of superconducting nanowires. *Science*, 2005, **308**, 1762-1765.
10. T. Ghodselahi, M. A. Vesaghi, A. Shafiekhani, A. Baghizadeh and M. Lameii, XPS study of the Cu@Cu2O core-shell nanoparticles. *Applied Surface Science*, 2008, **255**, 2730-2734.
11. M. C. Biesinger, L. W. M. Lau, A. R. Gerson and R. S. C. Smart, Resolving surface chemical states in XPS analysis of first row transition metals, oxides and hydroxides: Sc, Ti, V, Cu and Zn. *Applied Surface Science*, 2010, **257**, 887-898.
12. G. Van Der Laan, C. Westra, C. Haas and G. A. Sawatzky, Satellite structure in photoelectron and Auger spectra of copper dihalides. *Physical Review B*, 1981, **23**, 4369-4380.
13. S. Buckhout-White, J. T. Robinson, N. D. Bassim, E. R. Goldman, I. L. Medintz and M. G. Ancona, TEM imaging of unstained DNA nanostructures using suspended graphene. *Soft Matter*, 2013, **9**, 1414-1417.

Chapter 7: Final Conclusions

Much of the work contained in this thesis is directed towards the realisation of a specific and challenging objective: to fabricate smooth, conductive DNA-templated copper nanowires at the low end nanometre scale (<10 nm). In this regard, our objectives have been achieved to some extent. Namely, the results contained in chapters 4 and 5, whereby nanowires were prepared in the solution phase, have demonstrated those three principal targets. These approaches resulted in continuous coatings of copper (7 nm) being deposited along DNA template strands in a uniform manner, and were proven to carry significant levels of current over micron length scales. What remains apparent, however, is that the wires produced by these chemical-based methods are not sufficiently conductive for the realistic application as components within integrated electronic devices. More specifically, these Cu-DNA nanowires cannot be currently considered as a candidate for the wholesale replacement of the existing interconnect technology, which although limited in potential for significant size reduction utilising the currently established top-down methods, exhibit conductivity many orders of magnitude higher than the bottom-up routes described here within. However, if the conductivity of the nanowires produced in this current work can be increased, then these DNA-based bottom-up routes hold much promise.

One of the more striking outcomes in this research was the insight gained into the growth processes of copper on DNA and how this can be substantially dependent on whether the metallisation reaction occurs on the surface or in a solution of DNA. Chapter 3 describes the two-step chemical templating approach on surface-immobilised DNA and chapter 4 describes a solution-phase DNA-templating approach. The surface-based route tended to afford 1-dimensional copper nanostructures, mostly continuous in coverage, but observably of a polycrystalline appearance, which was attributed to their high resistivity. Whereas, the solution-based approach afforded smoother looking wires and were indeed conductive. Based upon these comparisons it is reasoned that the surface-immobilisation of DNA may lead to the blocking of DNA-metal ion binding sites and thus inhibit the nucleation of copper along the template. This could in turn result in the formation of granular structures. On the other hand when DNA is in solution, DNA-metal ion binding may occur more efficiently along the template leading

to higher density nucleation and smoother wires. Detailed AFM studies in this thesis have supported this theory.

Despite the high resistivity encountered for the 1-D structures produced using the surface-based method in chapter 3, they were found to be noticeably smoother than other analogous surface based routes in the literature, where DNA was used as a template for the construction of copper nanowires (see section 1.5). The improvement in our studies was likely to result from the use of a Cu(I) coordination compound (the first method to utilise a Cu(I) precursor for metallisation of DNA), as opposed to Cu(II) which was used elsewhere in the literature and led to discontinuous nanostructures; so-called 'beads-on-a-string' assemblies (where DNA is the 'string' and the 'beads' are copper nanoclusters). The Cu(I) method is a non-aqueous approach whereby organo-based solvent were exploited during the metallisation step. The choice of solvent here is likely to be responsible for the morphological dissimilarities in nanostructures produced on surface-immobilised DNA using Cu(I) compared to those produced using Cu(II), where the latter is best solubilised in aqueous media. This is suggested to be attributable to the competitive binding of solvent molecules and DNA binding sites with copper ions. DNA-copper ion binding is expected to be enhanced in low polarity solvent (e.g. acetonitrile) and inhibited to an extent in high polarity solvent (e.g. water). Indeed, the results contained in this thesis have supported this claim.

Other factors were also found to be critical towards the formation of smooth DNA-Cu nanowires. One such factor was the Cu:DNA(P) ratio. This had a significant influence on the structural nature of the final product formed in solutions of DNA. At high Cu:DNA(P) ratio (e.g. 25) it was found that Cu^{2+} induced DNA condensation, as evidenced by a high degree of aggregation. At low Cu:DNA(P) ratio (e.g. 0.01) individual DNA strands were obtained, but contained only low levels of metal coverage. A Cu:DNA(P) ratio of 0.05 was found to be the most suitable for the preparation of smooth and conductive nanowires.

Having invested much effort into the development of wet-chemical based approaches towards the formation of conductive copper nanowires using DNA as a template, an alternative physical-based DNA-templating strategy was investigated. This was based on the evaporation of copper (although a wide range of metals and composite materials could be used in theory) upon suspended DNA templates stretched across raised electrodes. This resulted in highly conductive DNA-Cu nanowire devices. However, on

this occasion a conductivity measurement on a single nanowire could not be obtained. Optimisation of the electrode device layout could help to improve future measurements for single nanowire characterisation. This method holds much promise for the fabrication of future bottom-up constructed copper interconnects.

PostScript

During the final stages of writing this thesis, a report by Woolley *et.al.,* documenting the first breakthrough in conductive copper metallised DNA nanostructures was published.[1] In this work, small DNA origami structures were initially seeded with Pd particles before copper was deposited electrolessly. The resulting metallised DNA origami structures covered ~200 x 200 nm^2 in surface area, and the copper coating was ~40 nm in diameter. These structures were impressively shown to retain the shape of the folded DNA assembly following metallisation. Moreover the structures were found to be conductive, following measurements between two gold electrodes. The resistivity was found to be 3.6 X 10^{-4} Ω.m, which is 4 orders of magnitude greater than that of bulk copper. In relation to this work, this paper represents the first *published* example of conductivity on a copper metallised DNA structure, of any kind. However, the conduction is over small length scales (100s of nm's) in comparison to the conduction reported in this thesis for copper metallised DNA (see chapters 4 and 5), which is demonstrated to place over larger length scales (micrometres). Conductivity over such a length scale will be required for the future fabrication of high aspect ratio interconnect.

1. *Y. Geng, A. C. Pearson, E. P. Gates, B. Uprety, R. C. Davis, J. N. Harb and A. T. Woolley, Electrically conductive gold- and copper-metallized DNA origami nanostructures. Langmuir, 2013,* ***29****, 3482-3490.*

The End